HYDRODYNAMICS STUDY OF LIQUID-SOLID MICRO-CIRCULATING FLUIDISED BED

by

Orlando Lopes do Nascimento

A thesis presented for the degree of

Doctor of Philosophy

School of Engineering

Newcastle University, United Kingdom

September 2019

Abstract

Solid-liquid circulating fluidised beds possess many qualities which makes them useful for industrial operations where particle-liquid contact is vital, e.g. improved heat transfer performance, and consequent uniform temperature, limited back mixing, excellent solid-liquid contact, good control of reaction and regeneration of catalysts or bio-solids at the same time. All these characteristics make them suitable for various industrial processes, e.g. waste water treatment, food processing, and bioconversion of agricultural-waste into lactic acid, fermentation, linear alkyl benzene production, and photo-catalytic ozonation. Despite this, they have seen no application in the micro-technology context.

Solid-liquid micro circulating fluidised beds (μCFBs), which essentially involve fluidisation of micro-particles in sub-centimetre beds, hold promise of applications in the areas of microfluidics and micro-process technology. This is mostly due to fluidised particles providing enhancement of mixing, mass and heat transfer under the low Reynolds number flows that dominate in micro-devices.

Albeit there are few reports on liquid-solid micro-fluidised beds, this thesis presents the first experimental study of a solid-liquid circulating fluidised bed at the microscale. It is well known that particle handling in micro technology devices remains one of the big challenges in the field. Development of a micro circulating fluidised bed is providing one solution to the problem, e.g. for solid catalyst recovery, recycle and regeneration.

This thesis reports on the design and study the hydrodynamics of a liquid-solid micro-circulating fluidised (LS μCFB) systems for possible applications as novel micro (bio)-reactors and diagnostics device, high-throughput kinetics screening, high-heat flux cooling and others. In order to successfully implement this, it is very important to understand the hydrodynamic parameters such as the influence of surface forces and inevitable wall effect on minimum fluidisation velocity, and bed expansion dynamics as they play a crucial role in the hydrodynamic behaviour and determine the bed performances, as well as dictating the solid-liquid contacting.

The experimental research was performed in a novel micro-circulating fluidised bed which was made by micro-machining channels of $1mm^2$ cross section in Perspex. (Polymethylmethacrylate (PMMA) and soda lime glass microspheres particles were used as the fluidised particles and tap water and glycerol of different concentration (5, 10, and 15 vol. % aqueous glycerol) as the fluidising liquid to study the hydrodynamics of solid-liquid

fluidisation in micro-circulating fluidised bed channel. Furthermore, additive manufacturing technology, digital light processing (Miicraft+ printer) and stereolithography (Form2 printer) were also used to fabricate the novel micro-circulating fluidised bed. This allowed the rapid fabrication of a reliable micro-circulating fluidised bed using low cost material and most importantly, the bed geometry could easily be modified.

Two novel measurement techniques, the valve accumulation and digital particle image velocimetry (PIV) methods were developed to measure the particle velocity in the micro-circulating fluidised bed system, and the results looks relevant when compared with previous reported studies. As in a macroscopic circulating fluidised bed, the solid flux in a micro-circulating fluidised bed increases with liquid velocity in two distinct zones, increasing sharply first then levelling off at higher inlet fluid velocities.

The result indicates that fluidisation in a solid-liquid micro circulating fluidised bed system could be categorised in four operating regimes like in macroscopic case: fixed bed, conventional fluidisation, circulating fluidisation, and transport regime. However, the surface forces influence strongly the minimum fluidisation velocity which can be up to 20 times bigger for the smallest PMMA microparticles while the increase is only minor for glass particle (less than 2 times for the same size smallest glass microparticles). The determined critical transition velocity is comparable to the particle terminal velocity, i.e. the normalised transition velocity is approximately 1 in line with previous macroscopic studies. Yet, there was a weak increase in the normalized transition velocity with particle size which is probably due the wall effects (higher particle to bed ratio). In addition, the normalised velocity is slightly higher for PMMA particles due to stronger adhesion and cohesion forces, but influence is minimal in comparison with influence on the minimum fluidisation velocity. Finally, it seems that transition to the transport regime is influenced by cohesion so the relative transition velocity for PMMA particles is around 20 times particle terminal velocity while it is only 5 times for the glass beads. Consequently, the conventional regime is proportionally bigger for the glass beads in comparison with PMMA particles, whist the situation is opposite for circulating fluidisation regime as it is bigger for PMMA particles.

The study also confirms that fluidisation behaviour in a liquid-solid micro-circulating fluidised bed system is also influenced by bed geometry such as the size of solid feed pipe cross section and the angle between the riser and solid feed pipe.

The results also show that solid flux in a micro-circulating fluidised bed is influenced by the viscosity of the fluidised liquid. The minimum superficial liquid velocity at which particles fluidisation is achieve decreases with increasing liquid viscosity. The reduction in the minimum fluidisation velocity with an increase in the liquid viscosity is mostly due to the fact that viscous systems have a lower ratio of adhesion to drag force.

Keywords: Liquid-solid Fluidisation, Micro-Fluidised Bed, Circulating-Fluidised Bed, Chemical Micro-process Technology, Microfluidics, Additive Manufacturing Technology, Particle Image Velocimetry, Process Intensification.

Acknowledgements

I would like to express my deepest gratitude to my supervisors Vladimir Zivkovic and David Reay for their immense help, guidance, and support during the PhD programme. Their constructive ideas and encouragement helped me to complete this study. It would not be possible for me to finish this study without their invaluable help and kind advice.

I would also like to thank Jonathan McDonough for his invaluable support in the design and printing the Circulating Fluidised Bed.

Thanks, are also extended to Iain Strong, Iain Ditchburn, Brian Grover and all the workshop technicians from the School of Engineering at Newcastle University for their technical assistance in constructing the experimental equipment.

Many thanks to EPSRC for providing me the financial support to carry this research.

Most important, I would like to thank my family for all the endless love and support I received from them.

Table of Contents

Abstract i
Acknowledgements iv
Publications and conferences ix
List of figures x
List of Tables xix
Nomenclature: xx
Chapter 1. Introduction 1
1.1 Fluidisation 1
1.2 Industrial applications of fluidisation technology 2
1.3 Fluidisation regime 4
1.4 Fluidised bed shape 5
1.5 Micro-fluidised bed 5
1.6 Significance and innovation 6
1.7 Motivation 9
Chapter 2. Literature review 11
2.1 Circulating fluidised bed 11
2.1.1 Solid-gas circulating fluidised bed 11
2.1.2 Solid-liquid circulating fluidised bed (CFB) 16
2.1.3 Solid-liquid-gas circulating fluidised bed 26
2.2 Inverse fluidisation 28
2.3 Additive manufacturing technology 28
2.4 Novelty 34
2.5 Thesis structure 37
Chapter 3. Methodology 38
3.1 Consideration design 38
3.1.1 Perforated plate 39
3.1.2 Sparge or Pipe distributor 39
3.1.3 Bubble caps and Nozzles 40
3.1.4 Conical distributor 40
3.1.5 Porous plate distributor 41
3.2 Final bed design 42
3.3 3D printing technology in microfluidic 44
3.3.1 Distributor for the 3D printed bed 47
3.3.2 Printing test 49

3.3.3 Cure time 58
3.3.4 Optimum number of layers 59
3.3.5 Printing multiple channel at once 60
3.3.6 Printing problems 61
3.3.7 Final 3D printing CFB design 62
3.4 Minimum fluidisation velocity 63
3.4.1 Minimum fluidisation velocity measurement 63
3.4.2 Minimum fluidisation velocity measurement in the present study 64
3.4.3 Predicted minimum fluidisation velocity 65
3.4.4 Estimation of surface forces 66
3.5 Solid circulation rate 68
3.5.1 Ball valve measurement 68
3.5.2 Butterfly valve 69
3.5.3 Magnetic valve 69
3.5.4 Visual technique 70
3.5.5 Laser Doppler velocimetry 70
3.5.6 Impact technique 70
3.5.7 Radioactive technique 70
3.5.8 Particle image velocimetry 70
3.6 Solid circulation rate measurement 71
3.6.1 Image pre-processing 72
3.6.2 Image analysis 73
3.6.3 Post processing 77
3.6.4 Background movement 77
3.7 Critical transition velocity measurement 80
3.7.1 Solid circulation rate method: 80
3.7.2 Emptying bed time: 80
3.7.3 Pressure gradient method: 80
3.7.4 Critical transition velocity determination in the present study 81
Chapter 4. Influence of surface forces and wall effect on the minimum fluidisation velocity of liquid-solid micro-fluidised beds 83
4.1 Introduction 83
4.2 Experimental details 84
4.2.1 Experimental set up 84
4.2.2 Particle and liquid materials 85
4.2.3 Experimental methodology 85

4.3 Surface force and wall effect in the micro-fluidised bed experiment 86
4.4 Result and discussion 86
4.5 Minimum fluidisation velocity 89
4.5.1 Importance of surface force and wall effects 93
4.5.2 Hysteresis in micro-fluidization expansion behaviour 97
4.6 Conclusions 99
Chapter 5. Solid circulating velocity measurement in a liquid-solid micro-circulating fluidised bed system 101
5.1 Introduction 101
5.2 Experimental details 102
5.2.1 Experimental set up 102
5.2.2 Particles and liquid used in the present study 103
5.2.3 Experimental procedure 103
5.3 Results and discussion 105
5.3.1 Background movement 105
5.3.2 Effect of the liquid flow rate on solid flux 106
5.3.3 Effect of solid inventory in the system 108
5.3.4 Effect of particle size 108
5.4 Validation 110
5.4.1 Solid circulation rate using magnet 111
5.5 Conclusions 114
Chapter 6. Influence of circulating fluidised bed geometry on the hydrodynamics of liquid-solid flow in microchannel 115
6.1 Introduction 115
6.2 Experimental details 116
6.3 Results and discussion 118
6.4 Conclusion 126
Chapter 7. Influence of liquid viscosity in liquid-solid micro-fluidised beds 127
7.1 Introduction 127
7.2 Experimental procedure 129
7.3 Result discussion 134
7.3.1 Adhesion force prediction 134
7.3.2 Influence of liquid viscosity on the minimum fluidisation velocity 136
7.3.3 Influence of particle density on the on minimum fluidisation velocity 138
7.3.4 Surface force magnitude for glycerol mixtures 141
7.3.5 Influence of liquid viscosity on solid circulating velocity 145

7.3.6 Influence of liquid viscosity on the critical transition velocity 148
7.3.7 Influence of liquid viscosity on the transition velocity U_a, from circulating fluidised bed to transport regime 150
7.4 Conclusions 151
Chapter 8. Flow regime mapping of a liquid-solid micro-circulating fluidised bed 153
8.1 Introduction 153
8.2 Results and discussion 154
8.2.1 Observation 154
8.2.2 Transition from circulating fluidisation regime to transport regime 155
8.2.3 Flow regime map 157
8.2.4 Flow regime map for liquid-solid micro-circulating fluidised bed system with change in liquid viscosity 159
8.2.5 Flow regime map for liquid-solid micro-circulating fluidised bed system with change in solid feed pipe geometry 161
8.2.6 Flow regime map for liquid-solid micro-circulating fluidised bed system with change in the angle between riser and solid feed pipe 162
8.3 Conclusions 164
Chapter 9. Conclusions 165
Chapter 10. Future work 167
Chapter 11. Appendix 170
11.1 Calibration 170
11.2 Minimum fluidization experiments results 171
11.3 Solid circulation rate conversion to solid circulating velocity 177
11.4 Influence of fluidising liquid viscosity on the solid flux 178
Reference 184

Publications and conferences

Publications

- **Orlando L. do Nascimento**, David A. Reay, Vladimir Zivkovic. Study of Transitional Velocities of Solid–Liquid Micro-circulating Fluidized Beds by Visual. Journal of chemical engineering of Japan 51 (2018) 349-355
- **Orlando L. do Nascimento**, David A. Reay, Vladimir Zivkovic. Influence of surface forces and wall effects on the minimum fluidization velocity of liquid-solid micro-fluidized beds. Powder Technology 304 (2016) 55–62

Future publication

- **Orlando L. do Nascimento**, David A. Reay, Vladimir Zivkovic. Solid flux measurement in a solid-liquid micro-circulating fluidised bed. To be submitted to Powder Technology.
- **Orlando L. do Nascimento**, David A. Reay, Vladimir Zivkovic. Flow regime map of liquid-solid micro-circulating fluidised beds. To be submitted to Powder Technology.

Conference Presentations

- Vladimir Zivkovic**, Orlando L. do Nascimento**, David A. Reay. Solid flux measurement in a solid-liquid micro-circulating fluidised bed. Oral presented at the 12th International Conference on Fluidized Bed Technology, 2017, Krakow, Poland
- Vladimir Zivkovic, **Orlando L. do Nascimento**, David A. Reay. Flow regime map of liquid-solid micro-circulating fluidised beds. Oral presented at the Fluidization XV Conference, 2016, Quebec, Canada

Conference Posters

- **Orlando L. do Nascimento**, David A. Reay, Vladimir Zivkovic. Influence of Circulating Fluidised Bed geometry on the hydrodynamics of liquid-solid flow in micro-circulating fluidised bed. Poster presented at the 10th World Congress of Chemical Engineering, 2018, Barcelona, Spain.
- **Orlando L. do Nascimento**, David A. Reay, Vladimir Zivkovic. Flow regime map of liquid-solid micro-circulating fluidised beds. Poster presented at UK Particle Technology Forum, 2016, The University of Surrey, Surrey, United Kingdom
- **Orlando L. do Nascimento**, David A. Reay, Vladimir Zivkovic. Flow regime map of liquid-solid micro-circulating fluidised beds. Poster presented at the Process Intensification Network 24 Conference, 2016, Newcastle University, Newcastle upon Tyne, United Kingdom

List of figures

Figure 1: flow behaviour in liquid and gas fluidisation. ……..1
Figure 2. Flow regime in solid-gas fluidised bed……4
Figure 3: solid-gas circulating fluidised bed regime map……..12
Figure 4. Flow regime in solid-gas circulating fluidised bed……13
Figure 5. Previous measurement technique to determine the critical transition velocity…….15
Figure 6. Schematic illustration of solid-liquid circulating fluidised bed……17
Figure 7. Flow regime in solid-liquid circulating fluidised bed……21
Figure 8. Operation regime map for solid CFB, adapted from Liang……23
Figure 9. Solid-particles circulation rate vs. superficial liquid velocity……24
Figure 10. Onset velocity Ucf reported by Zheng and Zhu……25
Figure 11. Solid-liquid-gas circulating fluidised bed regime map……27
Figure 12. Fluidisation and inverse fluidisation process……...28
Figure 13. 3D microfluidic device……30
Figure 14. Perforated plate distributor model……39
Figure 15. Example of Sparge and pipe distributor……...39
Figure 16. Bubble cap distributor……..40
Figure 17. Conical distributor model……40
Figure 18. Porous plate distributor……41
Figure 19: Schematic of a simple micro-circulating fluidised bed design……43
Figure 20. Lithography technique vs 3D printing technology for microfluidic……45
Figure 21. 3D printing process……46
Figure 22. Decision rout for liquid distributor design……..47
Figure 23. Baffle distributor model……..49
Figure 24. Perforated & pillar distributor……50
Figure 25. Unsuccessfully prints……...50
Figure 26. Schematic of perforated and pillar distributor……51
Figure 27. Printed pillars……..52
Figure 28. Printed perforated plate distributor……52
Figure 29. Combined pillar……...53
Figure 30: warped pillar……54
Figure 31. Joined pillars……54

Figure 32. Successfully printed pillar of 100 μm diameter……55
Figure 33. Successfully printed pillar of 150 μm diameter……56
Figure 34a. Pillar distributor supporting the bed material……56
Figure 34b Particles suspension in the channel……56
Figure 35: schematic of cross-linked pillars distributor……57
Figure 36. Printed cross-linked distributor……58
Figure 37a. Successfully printed bed……59
Figure 37b. Unsuccessful print bed with blocked channel……59
Figure 38. Multiple layer pillar distributor……60
Figure 39. Schematic of multiple channel per print……..60
Figure 40. 3D bed design ……..62
Figure 41. Relative bed height as a function of superficial liquid velocity……..64
Figure 42. 3D printed micro-circulating fluidised bed with a magnet inside the system used to measure the solid circulation rate……... ……69
Figure 43. PIV principles……71
Figure 44. Fluidized bed for the 58 μm glass particles at flow rate inside 15% solid inventory bed showing area interest for the digital PIV analysis. ……73
Figure 45. Velocity map calculated using DCC vs FFT……....74
Figure 46a. PIV analysis of interrogation window……75
Figure 46b. PIV analysis of interrogation window……75
Figure 46c. PIV analysis of interrogation window……..……..75
Figure 46d. PIV analysis of interrogation window……...75
Figure 47. PIV setting use in the investigation ……76
Figure 48a. Velocity vector field in downcomer ……78
Figure 48bVelocity vector field in background……78
Figure 49a: Original particle velocity field ……..79
Figure 49b. Velocity field after subtracting background motion ……..79
Figure 50. Background motion during PIVlab analysis……79
Figure 51. Particle circulating speed as a function of superficial liquid flow rate for both PIV technique and accumulation method ……81
Figure 52. The photo of downcomer which was visually observed by stereo-microscope for detecting solid particle circulation……82
Figure 53a. Photograph of the experimental setup ……...85

Figure 53b. Photograph of micro-FB and micro-CFB……..85

Figure 54a. Adhesion of 35 μm glass particle……87

Figure 54b. Adhesion of 35 μm glass particle……...87

Figure 54c. Adhesion of 35 μm PMMA particle……..87

Figure 54d. Adhesion of 35 μm PMMA particle……..87

Figure 55a. Successfully fluidisation using 115 μm glass particle……88

Figure 55b. Successfully fluidisation using 26 μm glass particle……..88

Figure 55c. Successfully fluidisation using 115 μm PMMA particle……...88

Figure 55d. Successfully fluidisation using 23 μm PMMA particle……88

Figure 56. Relative bed height as a function of superficial liquid velocity, U, with increasing liquid velocity (Umf, u), and decreasing liquid velocity (Umf, d) for 26 μm glass microparticles in $1mm^2$ micro-bed……...91

Figure 57(a). U_{mf} as a function of particle size for glass particle inside a 1mm and 2mm bed and (b) PMMA particle inside a 1mm and 2mm bed……92

Figure 57(b). U_{mf} as a function of particle size for PMMA particles inside a 1mm and 2mm bed……92

Figure 58. Effect of Bed height on minimum fluidisation velocity……93

Figure 59. U_{mf} experimental/U_{mf} calculated vs. adhesion force/drag force for D = 1mm full square D = 2mm empty circle……...94

Figure 60. U_{mf} experimental/*Umf* calculated vs. adhesion force/drag force for D = 1mm full square and D = 2mm empty circle……95

Figure 61. Ratio of experimental and theoretical Umf versus product ratio for D = 1mm full square and D = 2mm empty circle……96

Figure 62. Ratio of experimental and theoretical Umf versus product ratio for D = 1mm in red and D = 2mm blue……97

Figure 63(a). The ratio of the experimental minimum fluidization velocity for increasing, *Umf,u,* and decreasing, Umf,d, flow rate experiments versus product of force and particle-to-bed diameter ratios for glass micro-particles……..98

Figure 63(b). The ratio of the experimental minimum fluidization velocity for increasing, Umf,u, and decreasing, Umf,d, flow rate experiments versus product of force and particle-to-bed diameter ratios for PMMA micro-particles……..99

Figure 64(a). Schematic of experimental set up for imaging and (b) micro-circulating fluidis……..103

Figure 64(b). Schematic of experimental micro-circulating fluidised bed……103

Figure 65. Example of solid inventory measurement……105

Figure 66(a). Velocity vector field in the downcomer determined by PIVlab analysis…….106

Figure 66(b). Velocity vector field in the background determined by PIVlab analysis…….106

Figure 67(a). Examples of Original particle velocity field for the 58 µm glass particle at 445 µl/min liquid flow rate with 15% solid inventory bed……106

Figure 67(b). Examples of the velocity field after subtraction of the background movement for the 58 µm glass particle at 445 µl/min liquid flow rate with 15% solid inventory bed……..106

Figure 68(a). Particle circulating speed as a function of normalised velocity (Ul/Ut) for PMMA particle. Errors are smaller than the symbols…….107

Figure 68(b). Particle circulating speed as a function of normalised velocity (Ul/Ut) for PMMA particle. Errors are smaller than the symbols…….107

Figure 69a. Effect of solid inventory on normalised transition velocity for 35µm glass particles……..108

Figure 69b.Effect of solid inventory on normalised transition velocity for 35µm PMMA particles……..108

Figure 70a. Normalised critical transition velocity as a function of particle size for Glass micro-particles with solid inventory in the range of 10 - 25%.....109

Figure 70b. Normalised critical transition velocity as a function of particle size for PMMA micro-particles with solid inventory in the range of 10 - 25%.....109

Figure 71a. Schematic of the micro-circulating fluidised bed used for PIV measurement…….....110

Figure 71b. Schematic of the micro-circulating fluidised bed used for magnet measurement technique……...110

Figure 72. Picture of 3D printed micro-circulating fluidised bed with a magnet inside the system used to measure the solid circulation rate……112

Figure 73. Particle circulating speed as a function of normalised velocity (Ul/Ut) for both PIV technique (blue) and accumulation method (red)……113

Figure 74. Normalised critical transition velocity as a function of particle size obtained from the PIV and accumulation measurement technique……114

Figure 75a. Schematic of the 2mm riser and 2mm solid feed pipe used to study the influence of solid feed pipe cross section on the flow behaviour of a liquid-solid micro-circulating fluidised bed system……117

Figure 75b. Schematic of the 2mm riser and 1.5mm solid feed pipe used to study the influence of solid feed pipe cross section on the flow behaviour of a liquid-solid micro-circulating fluidised bed system……117

Figure 75c. Schematic of the 2mm riser and 1mm solid feed pipe used to study the influence of solid feed pipe cross section on the flow behaviour of a liquid-solid micro-circulating fluidised bed system……117

Figure 76(a). Schematic of the CFB with a 60° between the riser and solid feed pipe system used to study the influence of the angle between the riser and solid feed pipe on the liquid-solid flow behaviour in a micro-circulating fluidised bed system……..118

Figure 76(b). Schematic of the CFB with a 50° between the riser and solid feed pipe system used to study the influence of the angle between the riser and solid feed pipe on the liquid-solid flow behaviour in a micro-circulating fluidised bed system……118

Figure 76(c). Schematic of the CFB with a 30° between the riser and solid feed pipe system used to study the influence of the angle between the riser and solid feed pipe on the liquid-solid flow behaviour in a micro-circulating fluidised bed system……118

Figure 77. Average particle velocity as a function of normalised velocity (Ul/Ut) for both 165µm glass particle in black and 196 µm glass particle in white colour……119

Figure 78. Importance of solid feed pipe on the normalised transition velocity for both 165 and 196 m glass particle……121

Figure 79. Importance of solid feed pipe on the transition velocity from circulating fluidised bed regime to transport regime for both 165 and 196 m glass particle. The angle between the riser and solid feed pipe was 60°……122

Figure 80: Influence of the angle between the riser and solid feed effect on the flow behaviour for both 165µm glass particle in black and 196 µm glass particle in white colour……123

Figure 81. Effect of angle between riser and solid feed pipe on the normalised transition velocity for both 165 and 196 m glass particle……124

Figure 82. Effect of angle between riser and solid feed pipe on the transition velocity from circulating fluidised bed regime to transport regime for both 165 and 196 m glass particle using a circulating fluidised bed with 2mm cross section feed pipe and riser……..125

Figure 83a. Relative bed height as a function of superficial liquid velocity, U, with increasing liquid velocity (Umf, u), and decreasing liquid velocity (Umf, d) for water as the fluidising liquid in 1 mm2 micro-fluidised bed using 26µm glass particles. Errors are not visible in the graph as they are smaller than the symbols……130

Figure 83b. Relative bed height as a function of superficial liquid velocity, U, with increasing liquid velocity (Umf, u), and decreasing liquid velocity (Umf, d) for 5% v/v glycerol solution as the fluidising liquid in 1 mm2 micro-fluidised bed using 26µm glass particles. Errors are not visible in the graph as they are smaller than the symbols……130

Figure 83c. Relative bed height as a function of superficial liquid velocity, U, with increasing liquid velocity (Umf, u), and decreasing liquid velocity (Umf, d) for 10% v/v glycerol solution as the fluidising liquid in 1 mm2 micro-fluidised bed using 26µm glass particles. Errors are not visible in the graph as they are smaller than the symbols……130

Figure 83d. Relative bed height as a function of superficial liquid velocity, U, with increasing liquid velocity (Umf, u), and decreasing liquid velocity (Umf, d) for 15% v/v glycerol solution as the fluidising liquid in 1 mm2 micro-fluidised bed using 26µm glass particles. Errors are not visible in the graph as they are smaller than the symbols……130

Figure 84. Experimentally determined minimum fluidisation velocity over the theoretical calculated values using the Ergun equation as a function of particle diameter four different liquid medium, tape water, 5% aqueous glycerol, 10% aqueous glycerol and 15% aqueous glycerol solution, with glass as the fluidised particle……..137

Figure 85. Experimentally determined minimum fluidisation velocity over the theoretical calculated values using the Ergun equation as a function of particle diameter four different liquid medium, tape water, 5% aqueous glycerol, 10% aqueous glycerol and 15% aqueous glycerol solution, with PMMA as the fluidised particle…….137

Figure 86. Experimental minimum fluidisation velocity as a function of particle size for glass particle with 5% v/v aqueous glycerol as the fluidising liquid……138

Figure 87. Experimental minimum fluidisation velocity as a function of particle size for PMMA particle with 5% v/v aqueous glycerol as the fluidising liquid……139

Figure 88. Optical Microscope illustrating adhesion of 35 µm PMMA particle inside 1 mm2 micro-fluidised bed…….140

Figure 89. Optical Microscope illustrating agglomeration of 35µm PMMA particle inside 1mm2 micro-fluidised bed…….140

Figure 90. Adhesion to drag forces ratio as a function of particle diameter for glass micro-particles with water and aqueous glycerol solution (5% v/v, 10% v/v, and 15% v/v) as the fluidising liquid in 1 mm2 micro-fluidised bed……..142

Figure 91. Adhesion to drag forces ratio as a function of particle diameter for glass micro-particles with water and aqueous glycerol solution (5% v/v, 10% v/v, and 15% v/v) as the fluidising liquid in 1mm2 micro-fluidised bed……142

Figure 92. Experimentally determined minimum fluidisation velocity over the theoretical calculated values using the Ergun equation as a function of adhesion/drag force ratios for four different liquid medium, tape water, 5% aqueous glycerol, 10% aqueous glycerol and 15% aqueous glycerol solution……...144

Figure 93. Experimentally determined minimum fluidisation velocity over the theoretical calculated values using the Ergun equation as a function of adhesion/drag force ratios for four different liquid medium, tape water, 5% aqueous glycerol, 10% aqueous glycerol and 15% aqueous glycerol solution…….144

Figure 94. Influence of fluidising liquid viscosity on the solid flux for 35µm glass particle……146

Figure 95. Influence of fluidising liquid viscosity on the solid flux for 115µm glass particle……146

Figure 96. Influence of fluidising liquid viscosity on the solid flux for 35µm PMMA particle……147

Figure 97. Influence of fluidising liquid viscosity on the solid flux for 115µm PMMA particle……..…..147

Figure 98. Influence of liquid viscosity on the critical transition velocity from conventional to circulating fluidised bed regime for glass particles……149

Figure 99. Influence of liquid viscosity on the critical transition velocity from conventional to circulating fluidised bed regime for glass particles…….149

Figure 100. Influence of liquid viscosity on the transport velocity from circulating fluidised bed regime to transport regime for glass particles…….150

Figure 101. Influence of liquid viscosity on the transport velocity from circulating fluidised bed regime to transport regime for PMMA particles……..151

Figure 102. The time sequenced images extracted from the movie of circulating fluidized bed using 38 µm soda lime glass microsphere particle at 1.5 mm/s. the arrows shows small downwards flow of particles close to the riser wall. The letters a, b and c shows three consecutive images of downwards flow of particles taken in a short time interval (0, 40, and 80 second respectively)……...155

Figure 103a. Transition velocity from circulating fluidised bed regime to transport regime for glass particle with solid inventory in the range of 10 – 25%.....156

Figure 103b. Transition velocity from circulating fluidised bed regime to transport regime for PMMA particle with solid inventory in the range of 10 – 25%.....156

Figure 104. Flow regime map of solid–liquid micro–circulating fluidised bed for glass (filled symbols) and PMMA (empty symbols) particles. The solid lines are the theoretical prediction for minimum fluidisation velocity and terminal velocity. The dashed (glass particles) and dotted (PMMA particles) lines connecting experimental points for the minimum fluidisation velocity (circles), the critical transitional velocity (triangles) and the transport transition velocity (squares) are a guide for the eye only. Three dotted lines labelled 1, 2 and 3 are Ucr of glass particles at solid inventories of 8%, 6% and 3% respectively……158

Figure 105a. Flow regime map of solid–liquid micro–circulating fluidised bed for Glass particles with water (empty circle), 5% volume aqueous glycerol (empty square), 10% volume aqueous glycerol solution (filled circle) and 15% volume aqueous glycerol solution (empty triangle) as fluidising liquid. The solid lines are experimental minimum fluidisation velocity, the dotted lines connecting experimental points for the critical transition velocity, and the dashed lines are the transport transition velocity……160

Figure 105b. Flow regime map of solid–liquid micro–circulating fluidised bed for PMMA particles with water (empty circle), 5% volume aqueous glycerol (empty square), 10% volume aqueous glycerol solution (filled circle) and 15% volume aqueous glycerol solution (empty triangle) as fluidising liquid. The solid lines are experimental minimum fluidisation velocity, the dotted lines connecting experimental points for the critical transition velocity, and the dashed lines are the transport transition velocity……160

Figure 106. Flow regime map of solid–liquid micro–circulating fluidised bed with change in the solid feed pipe cross section size. Three different solid feed pipe structure of 1mm, 1.5mm, and 2mm cross section were used construct the fluidisation regime map for 165 and 196µm glass particles with water as fluidising liquid. The angle between the riser and solid feed pipe was 60°. The solid lines are experimental minimum fluidisation velocity, the dotted lines connecting experimental points for the critical transition velocity, and the dashed lines are the transport transition velocity……162

Figure 107. Flow regime map of solid–liquid micro–circulating fluidised bed with change in the angle between the riser and the solid feed pipe. Three different angles of 30°, 50°, and 60°were used to construct the fluidisation regime map for 165 and 196µm glass particles with water as fluidising liquid. The micro-circulating fluidised bed employed for this experiment had a riser and solid feed pipe of 2mm square cross section. The solid lines are experimental minimum fluidisation velocity, the dotted lines connecting experimental points for the critical transition velocity, and the dashed lines are the transport transition velocity……163

Figure 108. Liquid calibration……170

Figure 109. Relative bed height as a function of liquid velocity for 30µm glass particle in 1mm micro-fluidised bed with water as the fluidised particles……171

Figure 110. Relative bed height as a function of liquid velocity for 35µm glass particle in 1mm micro-fluidised bed with water as the fluidised particles……171

Figure 111. Relative bed height as a function of liquid velocity for 58µm glass particle in 1mm micro-fluidised bed with water as the fluidised particles……172

Figure 112. Relative bed height as a function of liquid velocity for 82µm glass particle in 1mm micro-fluidised bed with water as the fluidised particles……172

Figure 113. Relative bed height as a function of liquid velocity for 98µm glass particle in 1mm micro-fluidised bed with water as the fluidised particles……173

Figure 114. Relative bed height as a function of liquid velocity for 115µm glass particle in 1mm micro-fluidised bed with water as the fluidised particles……173

Figure 115. Relative bed height as a function of liquid velocity for 165µm glass particle in 1mm micro-fluidised bed with water as the fluidised particles……174

Figure 116. Relative bed height as a function of liquid velocity for 196µm glass particle in 1mm micro-fluidised bed with water as the fluidised particles ……...174

Figure 117. Relative bed height as a function of liquid velocity for 23µm PMMA particle in 1mm micro-fluidised bed with water as the fluidised particles ……..175

Figure 118. Relative bed height as a function of liquid velocity for 35µm PMMA particle in 1mm micro-fluidised bed with water as the fluidised particles ……..175

Figure 119. Relative bed height as a function of liquid velocity for 41µm PMMA particle in 1mm micro-fluidised bed with water as the fluidised particles ……..176

Figure 120. Relative bed height as a function of liquid velocity for 58µm PMMA particle in 1mm micro-fluidised bed with water as the fluidised particles ……176

Figure 121. Relative bed height as a function of liquid velocity for 115µm PMMA particle in 1mm micro-fluidised bed with water as the fluidised particles ……177

Figure 122. Solid flux for 26µm glass particle as function of normalized liquid velocity for water and glycerol mixtures……178

Figure 123. Solid flux for 30µm glass particle as function of normalized liquid velocity for water and glycerol mixtures……178

Figure 124. Solid flux for 58µm glass particle as function of normalized liquid velocity for water and glycerol mixtures……179

Figure 125. Solid flux for 82µm glass particle as function of normalized liquid velocity for water and glycerol mixtures……179

Figure 126. Solid flux for 98µm glass particle as function of normalized liquid velocity for water and glycerol mixtures……180

Figure 127. Solid flux for 165µm glass particle as function of normalized liquid velocity for water and glycerol mixtures……180

Figure 128. Solid flux for 196µm glass particle as function of normalized liquid velocity for water and glycerol mixtures……181

Figure 129. Solid flux for 23µm PMMA particle as function of normalized liquid velocity for water and glycerol mixtures……181

Figure 130. Solid flux for 35µm PMMA particle as function of normalized liquid velocity for water and glycerol mixtures……182

Figure 131. Solid flux for 41µm PMMA particle as function of normalized liquid velocity for water and glycerol mixtures……182

Figure 132. Solid flux for 58µm PMMA particle as function of normalized liquid velocity for water and glycerol mixtures……183

List of Tables

Table 1. Solid-liquid circulating fluidised bed vs solid-gas circulating fluidised beds……..19

Table 2. Critical transition velocity and terminal particle velocity for various particle reported…….24

Table 3. Critical velocity and onset liquid velocity suggested by Zheng……..25

Table 4: Current 3D printing technology used for microfluidic devices fabrication……33

Table 5. 3D Printer description…….45

Table 6: Printing troubleshooting……61

Table 7. The calculated terminal particle velocity for Glass Particle……....65

Table 8. The calculated terminal particle velocity for PMMA Particle…….65

Table 9. Liquid and solid surface tension components…….67

Table 10. PIV settings……...77

Table 11. Glass and PMMA particle Free energy of Interaction ΔG1w2 (mJ/m2)……..87

Table 12. Experimental and theoretical Umf results for Glass particle…….89

Table 13. Experimental and theoretical Umf results for PMMA particle……....90

Table 14: Density and viscosity of fluidising liquid……129

Table 15. The theoretical minimum fluidisation velocity for PMMA particle using Ergun equation from chapter 3……..131

Table 16. The theoretical minimum fluidisation velocity for glass particle using Ergun equation mentioned in chapter 3……131

Table 17. The Experimental minimum fluidisation velocity for PMMA particles obtained from the plot of bed height expansion as a function of superficial liquid velocity……..131

Table 18. The Experimental minimum fluidisation velocity for glass particles obtained from the plot of bed height expansion as a function of superficial liquid velocity……132

Table 19. Liquid and solid surface tension components……..133

Table 20. Free energy of interaction (mJ/m2) acting between glass particles and PMMA walls with water, and glycerol (5% v/v, 10% v/v, and 15% v/v) solution as the fluidising liquid……...135

Table 21. Free energy of interaction (mJ/m2) acting between PMMA particles and PMMA walls with water, and glycerol (5% v/v, 10% v/v, and 15% v/v) solution as the fluidising liquid……..135

Nomenclature:

ADC = Analog to Digital Converter
A_d =downcomer cross sectional area (m)
A_r = riser cross-sectional are (m)
Ar = Archimedes number
CFB = Circulating fluidised bed
D = bed diameter (m)
dp = particle diameter (m)
d_p* = dimensionless particle diameter
F_{adh} = adhesion force (N)
F_d =drag force (N)
F_b =buoyancy force (N)
g = acceleration due to gravity (m/s^2)
G_s = solid circulation rate ($kgm^2.s$)
H = bed height (m)
L-S μCFB = Liquid-solid Micro-circulating fluidised bed
SLCFB = solid-liquid circulating fluidised bed
GSCFB = solid-gas circulating fluidised bed
Re_p = particle Reynolds number
U_a = transition liquid velocity from circulating fluidisation regime to transport regime (m/s)
U_c = superficial gas velocity where standard deviation of the pressure fluctuation reaches a maximum as the onset of turbulent regime (m/s)
U_{cf} = onset velocity (m/s)
U_{cr} = critical transition velocity of the circulating fluidisation in solid-liquid system (m/s)
U_{cr}/U_t = normalised transition velocity (m/s)
U_g = gas velocity (m/s)
U_l = superficial liquid velocity (m/s)
U_l* = dimensionless superficial liquid velocity (m/s)
U_{mb} = minimum bubbling velocity (m/s)
U_{mf} = minimum fluidisation velocity (m/s)
U_{ms} = minimum slugging velocity (m/s)
U_{tr} = critical transition velocity from turbulent to circulating fluidised bed regime (m/s)
U_t = particle terminal velocity (m/s)
Us = particle circulating velocity (m/s)
U_{se} = blowout velocity (m/s)
ε = volume fraction
ε_l = bed volume fraction
ε_s = solid volume fraction
$\partial\varepsilon/\partial h$ = voidage gradient
ΔG_{1w2} = free energy of interaction (mJ/m^2)
ΔP = pressure drop (Pa)
ΔP/ΔZ = pressure gradient
μ = dynamic viscosity (Pa.s)
ρ_f = fluid density (kg/m^3)
ρ_g = density of gas(kg/m^3)
ρ_p = particle density (kg/m^3)
γ = surface energy (mJ/m^2)
γ^{AB} = polar Lewis acid-base (mJ/m^2)
γ^{LW} = a polar Lifshitz-Van der Walls (mJ/m^2)

γ^+ = Lewis acid (mJ/m^2)
γ^- = Lewis base (mJ/m^2)
σ = standard deviation
µCFB = Micro-circulating fluidised bed
L-S µCFB = Micro-circulating fluidised bed

Chapter 1. Introduction

1.1 Fluidisation

Fluidisation refers to the process by which a bed of solid particles starts to behave like a fluid through contact with liquid or gas [1, 2] . The fluidisation process starts when liquid or gas is introduced into a bed of granular material at such a flowrate that the particle (buoyant) weight is equal to the drag force of the fluid [3]. Consequently, the bed is transformed from a solid state to a dynamic fluid-like state where particles can move freely. [3]. 'Fluidised bed' is the term used for beds in which fluidisation of particulate solids takes place [4].

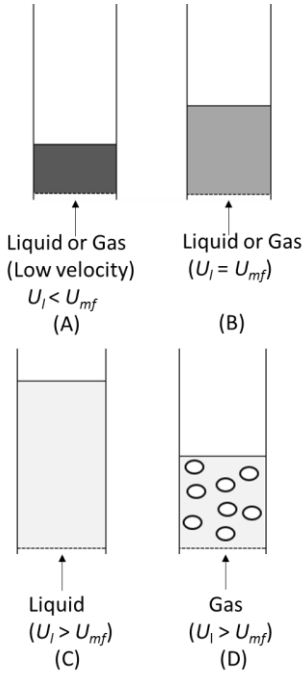

Figure 1: flow behaviour in liquid and gas fluidisation. A: packed bed, B: minimum fluidisation velocity, C: liquid fluidisation, B: gas fluidisation

The fluidisation process could be achieved by utilising gas, liquid, or by combining gas and liquid to speed up chemical reactions and mixing in a bed of solid particles [5]. In solid-liquid fluidisation the flow characteristics are generally homogenous and stable, when superficial liquid velocity is higher than the minimum fluidisation velocity (U_{mf}) the bed expands smoothly and progressively as shown in Figure 1 [6, 7]. In normal circumstance large amount of heterogeneity or bubbles is not observed and flow instabilities are small [8, 9]. The expansion behaviour of these types of system are well described by the Richardson and Zaki

$$\frac{U}{U_t} = \varepsilon^n \qquad (1)$$

where U_t the particle terminal velocity, U is the liquid velocity, ε the voidage and n an exponent with a value of 4.66 for laminar regime represents an empirical correlation index. In general n depends on Re number. In solid-gas fluidisation the flow characteristics are heterogeneous, as the gas velocity is increased above the minimum fluidisation velocity, the flow becomes unstable and large amount of bubbles and channelling can be spotted.

The dynamics of fluidisation is closely linked to the solid particle properties (i.e. size of particle, density, distribution size, particle cohesion and characteristic of surface), fluid properties, and bed design (i.e. cross sectional area, shape and bed height) [1, 3] . This is the favoured solid-fluid processing technique when solid and fluids (liquid or gas) need to be in contact for chemical or physical processes due to its efficiency mixing particles and fluids (liquid or gas) [10].

1.2 Industrial applications of fluidisation technology

Fluidisation is an important solid-fluid contacting process and it is recognised as one of the most important technologies in many industrial processes. As a technology, fluidisation has been developed over a long period. The first fluidised bed which was used for coal gasification applications was developed by Fritz Winker in Germany in 1922 for the production of synthesis fuel from coal [11]. With the threat of the Second World War all over Europe and the Far East in the late 1930s, the USA predicted a need for an immense amount of high octane gasoline. Hence it recommended that the American engineering society should discover a new method to convert gas oil and kerosene into essential fuel. In the early 1940s, a fluidised bed technology for oil feedstock catalytic cracking was developed by the US petroleum industry [12]. The technology began with gas fluidised beds, and then moved to liquid fluidised beds. Fluid catalyst cracking is still recognised as the principal conversion unit technology in most petroleum refineries worldwide to produce diesel fuel, gasoline, and heating oil from crude oil [13, 14]. Fluidisation applications in industry could be classified in two type groups [15, 16]:

1. Physical processes: mixing particle, transport, absorption, heating, drying, coating, and sizing
2. Chemical processes: solid-gas reactions, solid-liquid reactions, or solid-liquid-gas reaction.

Some application of the fluidised bed are polymerisation, calcination, combustion, ore roasting, mineral processing, coking, catalytic oxidation, and gasification for the production of pharmaceuticals, essential fuel, food, and various essential chemical products [17-20].

Fluidisation technology finds also application in the nuclear industry for processes such as nuclear fuel fabrication, uranium extraction and waste disposal [11].

Research investigations have demonstrate that fluidisation offer many benefits to the processes, for example: reduced pressure drop, uniform temperature, elimination of diffusion limitations, and increase of heat and mass transfer rates [21, 22]. These important qualities have made fluidisation one of the most important units of operation in many industrial processes [23, 24]. Even though particle fluidisation could be achieved either by liquid or gas as fluidising medium, solid-liquid fluidised beds have not received much attention in the fluidisation literature compared to gas-solid fluidised beds [25], because they are less applicable in process industries due to the insufficient knowledge on scaling up procedure from the small scale (laboratory units) to a larger commercial engineering scale device [11, 26]. Lots of significant processing characteristics such as hydrodynamics, transport mechanism, heat and mass transfer in solid-liquid fluidised beds are sensitive and vary with unit size [27, 28]. For example, flow regime characteristics could vary between small and large fluidised beds even when the same liquid velocity and particles are used. For industrial applications, in depth understanding of hydrodynamics, heat and mass transfer mechanisms which are extremely important in order to improve the design and scale up of solid-liquid fluidised beds and to enhance process intensification are not completely understood [29, 30]. The major disappointing issue is the reduction in the solid-liquid fluidised beds performance when scaled up to an engineering scale equipment [11]. Nonetheless, new applications in bio-chemical and hydro-metallurgy technology such as backwashing filters, adsorption, protein recovery, crystallisation, reduction of ore, ion exchange, and substrate enzyme reaction processes have generated much scientific interest in liquid fluidisation [31, 32]. Liquid fluidised beds have found application in mineral, chemical and biochemical processes as reactors, heat exchangers, bioreactors, and crystallizers. They are particularly suitable for operations where bed temperature-uniformity is necessary [33]. Liquid fluidised bed heat exchangers are amongst the most effective processing technology in limiting fouling [34]. Liquid fluidised bed bio-reactors are one of the most effective processing equipment for biological wastewater treatment [35]. Some examples of fluidised beds include bio-reactors for the production of penicillin, degradation of phenol, and wastewater treatment in general [36]. Due to the lack of hydrodynamic stability in gas-fluidised beds compared to liquid-fluidised beds, gas fluidised beds are not suitable for biochemical operations [37]. For biochemical processes involving large volumes of fine and small catalyst or bio solid particles that are expensive and deactivate very fast and needs to be continuously

regenerated, liquid-solid circulating fluidised beds (LSCFB) are the preferred solid-liquid contactors [11]. The liquid-solid circulating fluidised beds have the capability to accommodate a wide-ranging of particles with high liquid throughputs. As well the LSCFB, facilitates the regeneration of catalysts, or biosolid particles, resulting in enhanced mass transfer between phases and high product throughputs can be achieved [16, 38].

1.3 Fluidisation regime

Generally solid-gas fluidisation can be categorise into six fluidisation regimes: fixed bed, minimum fluidisation velocity, bubbling bed, slugging bed, turbulent bed, and pneumatic transport regime when gas flow rates are varied as shown in figure 2 [39, 40].

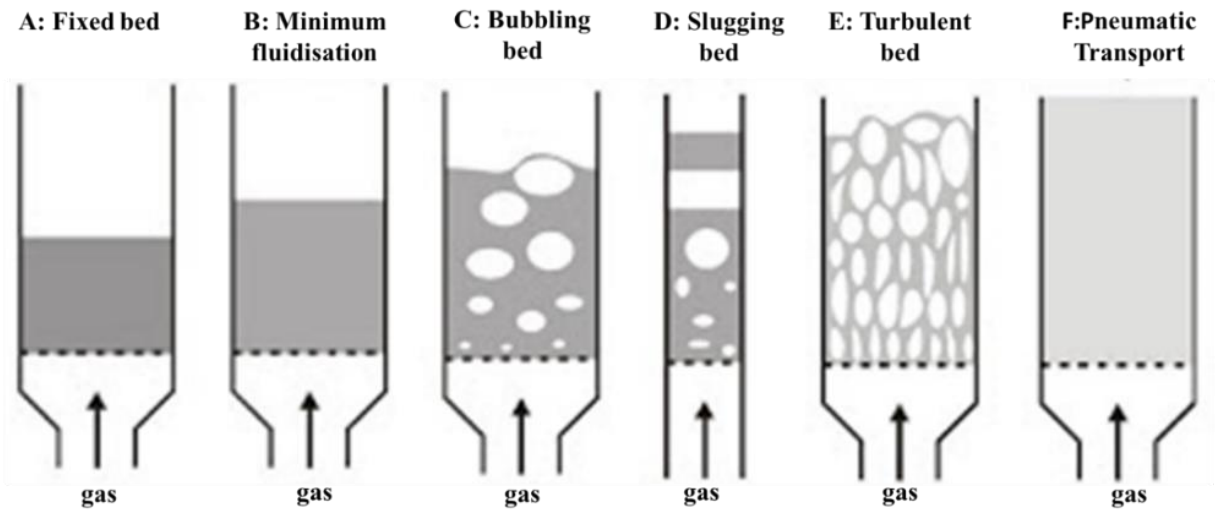

Figure 2. Flow regime in solid-gas fluidised bed [39, 40].

When the gas flow rate is below the minimum fluidisation velocity, particles in the bed remain static, and this regime is called ‘fixed bed’. As the gas flow rate in is increased to a point where the particle weight is equated by the drag force of the fluid, and bed voidage increases, the bed is operating at minimum fluidisation velocity regime. Increasing the gas flow rate beyond the minimum fluidisation velocity causes bubbles formation in the system indicating that the bed is operating at the bubbling regime. In the bubbling regime when gas flow rate is increased, the bubbles grown in size and its diameter almost equates the bed width, this regime is slugging. When gas flow rate is increased beyond critical transition velocity, the bubbles in the system disappear and turbulent particle flow cluster are observed, this indicate that the system is operating in the turbulent regime. If gas flow rate is significantly increased within the turbulent regime, large amounts of particles are transported out of the system indicating pneumatic

transport regime [41, 42]. The shape and size of air bubbles in slugging and bubbling regime have different characteristics. Generally, in the bubbling regime bubbles are small and have a spherical structure. In the slug regime bubbles are usually in form of square nosed shape or in form of round nosed shape with bubble size approaching the bed inner diameter. Some smaller bubbles can also be spotted in the slug regime [43]. Solid-liquid fluidised beds normally only have a single operating flow regime, the conventional fluidised bed regime, at which fluidisation is homogeneous and solids are distributed uniformly in the system, nonetheless flow instabilities can still occur in some cases. [44, 45].

1.4 Fluidised bed shape

Based on bed shape, fluidised beds could be categorised into conical, cylindrical, and rectangular beds [46]. Cylindrical shaped beds are the most popular type of fluidised bed found in industry and laboratory applications when compared to conical shaped beds due to the fact that little is known about the conical shaped beds [47]. Conical shaped beds have some advantages when compared to cylindrical beds. For immobilised wastewater treatment bio-reactors, the fluid velocity and drag acting on the bio-particles in the top section of the conical bed bio-reactor are less than in the cylindrical shaped bed, and this significant advantage prevents bio-particles entrainment and allows a broad range of operating fluid velocities [48]. Conical shaped beds finds many applications in processes such as waste water treatment, granulation, coating, micro-organism, and drying processes [49]. However, rectangle fluidised beds provides a better flow visualisation as a result of their flat faced shaped channel [50-54]

1.5 Micro-fluidised bed

Micro fluidised beds are a new concept in chemical engineering and find potential applications in a micro process and micro fluidics context [55, 56]. Micro-fluidised beds refer to those with the bed cross-section or inner diameter at millimetre scale [57, 58]. These types of bed are considered to be a promising way of achieving high quality fluid and solid mixing and process intensification of heat and mass transfer under a laminar flow regime and could potentially offer novel process windows [57, 58]. Studies on fluidisation in the liquid-gas or liquid-solid micro-fluidised beds are still very limited [58, 59]. The main reason is that micro fluidised beds hydrodynamics such as solid flux and voidage are extremely hard to be accurately measured using current measurement technology such as valves, X-ray tomography, electrical capacitance tomography, and magnetic resonance imaging as they are expensive, but more importantly it is very difficult to scale down for application in a microfluidics context [60]. The

major difference between micro-fluidised bed and macro-fluidised bed flows is the importance of surface forces and the effect of walls caused by the small-scale bed size [61]. Like other miniaturised technologies, micro-fluidised beds combine the advantages of fluidised beds and micro technology systems such as reduced pollution, waste and by products, less energy and resources consumption, less operational and capital cost, increased safety, intensive heat and mass transfer, and increases chemical reaction conversion rates, good mixing, temperature uniformity. They are considered to be ideal for performing reactions in circumstances which would normally be limited by heat and mass transfer and unsafe operations [57, 62]. All these important qualities make micro-fluidised beds more efficient and sustainable fluid-solid processing equipment. The main drawback of microfluidised beds is simply the low scale of production, unless there are thousands in parallel. The current applications are mainly in high throughput screening and testing of catalyst as it enables fast and reliable measuring of solid catalysed reaction kinetics. Micro-fluidised beds are being employed to study particle segregation and drying of pharmaceutical materials in the pharmaceutical industry, as active pharmaceutical ingredients are costly and extremely hard to acquire during the early phase of formulation development [63, 64]. Recently the solid-gas micro-fluidised bed developed by the Institute of Process Engineering and the Chinese Academic of Science was successfully applied for analysing fast solid-gas reactions such as pyrolysis of biomass and coal, CO2 capture by Ca(OH)2, reduction of iron oxides and CuO, steam gasification of char, and combustion of graphite [65]. Micro fluidised bed applications includes thermogravimetric analysis of coal combustion and gasification, high throughput screening of catalysts, and catalytic oxidation processing of volatile organic compounds [65, 66]. The solid-gas micro-fluidised bed is already applied for thermogravimetric analysis of coal gasification and combustion, and catalytic oxidation processing of volatile organic compounds (VOCs) [67, 68]. For some applications continues circulation of particles would be required such as continuous regeneration of catalyst or bio-solid particles for which circulating fluidised beds are an excellent technology, in particular by improving solid-fluid contacting and reducing back mixing.

1.6 Significance and innovation

Whilst there have been many studies on the hydrodynamics of macro-fluidised bed, there is limited research on fluidisation at the micro-scale. The first research experiments on fluidised beds at the micro-scale were reported by Potic *et al.* [57]. They experimentally investigated liquid-solids fluidisation hydrodynamics using a 1mm inner diameter capillary. They reported that the minimum fluidisation velocity predicted using the Ergun equation was in accordance

with the minimum fluidisation velocity obtained in the experiment. Zivkovic *et al.* [61] experimentally studied the importance of surface force in a micro-fluidised bed with a cross section of 400 x175 μm. They found that the major difference between the micro-fluidised bed and their macroscale counterparts was the importance of surface forces which can even prevent fluidisation due to particle adhesion to the walls. Doroodchi *et al.* [69] experimentally investigated fluidised beds hydrodynamics with regards to expansion of the bed, minimum fluidisation velocity and pressure drop using tubes of 17.1, 1.2 and 0.8 mm inner diameter size. They found when the inner diameter of the tube was reduced, the voidage of the bed increased causing an increase in the minimum fluidisation velocity. Liu and co-workers [70] studied minimum bubbling velocity and minimum fluidisation velocities of silica sand particles using micro fluidised beds of 12, 20, and 32 mm inner diameter. They found that the minimum fluidisation velocities and minimum bubbling velocities increase when the fluidised bed inner diameter is reduced. Xu and Yue [66] investigated the hydrodynamics of micro fluidised bed using beds with column diameter of 4, 5, 10, 15, 20, and 25 mm. In their studies they investigated the influence of fluidised bed height, column diameter, fluid and solid properties on the minimum fluidisation velocity and pressure drop. They found that minimum fluidisation velocity is a function of fluidised particle and fluid, bed voidage and size distribution. The minimum fluidisation velocity of particles reduces with an increase in bed column diameter and increases with an increase in bed height. They also reported that the predicted pressure drop of micro fluidised beds by the Ergun equation is more than the experimental pressure drop value. The difference between the predicted and experimental pressure drop value was attributed to the increased bed voidage under reduced bed diameters. A reduction in the bed diameter increased the bed voidage resulting in a decrease in the experimental pressure drop across the bed. Nonetheless, the difference in pressure drop reduced with an increase in the bed diameter. When the bed diameter was close or larger than 15 mm, the experimental pressured drop of micro fluidised beds equated to the predicted pressure drop obtained by Ergun equation. Rao et al. [71] experimentally investigated the influence of fluidised bed height and diameter on the minimum fluidisation velocity. They reported that the minimum fluidisation velocity increases with bed height or when the column diameter of fluidised bed is reduced. Fei and Liang [60] studied the influence of wall in the solid-gas micro fluidised beds using FCC particles in beds ranging from 0.7 – 5 mm. They reported that the wall friction, minimum fluidisation velocity and bubbling in solid-gas micro-fluidised beds increases with reduction in bed size. Wall friction, minimum fluidisation velocity and bubbling velocity is greater for micro-channels compared to larger channels. Tang et al. [59] experimentally investigated the

characteristics of solid-liquid fluidisation in micro-fluidised beds using visual measurements. They found that the theoretical minimum fluidisation velocity by Ergun equation is 5 times less than the experimental minimum fluidisation velocity, and the increase in the measured minimum fluidisation velocity is associated to the wall effect, which becomes sufficiently great with decreasing bed column diameter. Li et al. [72] investigated the hydrodynamics characteristics of liquid-gas-solid fluidisation in a micro-fluidised bed system. They found that wall effect (higher particle to bed ratio) significantly influences the fluidisation behaviour and flow regime transition in micro-fluidised bed system causing flow regime transition at reduced solid holdup. Yanjun et al.[73] also studied the liquid-gas-solid fluidisation characteristics in micro-fluidised bed system experimentally. They found that minimum fluidisation liquid velocity and transition velocity increases with wall effect. Jia et al. [74] investigated the influence of oblique angle on the pressure drop and fluidisation characteristics in micro-fluidised beds using computational particle fluid dynamics (CPFD) software to simulate the fluidisation behaviour. They found that the bed oblique angle significantly influences the fluid, pressure and solids distribution in the bed due to effect of walls caused by the small scale bed size. The bigger the bed oblique angle is, the more uniformly the particle are distributed in the micro-fluidised bed, which indicates that micro-fluidised beds with oblique angle of 0° provides better fluid-particle contact when compared with inclined bed. The pressure drop in micro-fluidised bed does decreases with an increase in oblique angle of the bed. Zhongguo and co-workers[75] studied methylene blue photocatalytic degradation in a micro-fluidised bed system, and they reported an increase in mass transfer coefficient of about 11-13 times and an increase in apparent reaction rate constant of 5 times for coated inner fluidised bed wall when compared with non-coated inner bed wall. They found when the particles inside the bed and the bed wall were coated with catalyst, the ratio of degradation are 5 – 35% greater when compared with non-coating particle and bed wall. Xiangnan et al.[76] studied the bed expansion behaviour of a solid-liquid fluidisation in micro-fluidised bed channel. They found that in solid-liquid micro-fluidised bed system wall effect at higher particle to bed ratio leads to an increase in the expansion ration and larger local voidage. Pereiro et al.[77, 78] investigated the influence of magnetic field profile, and the interaction of magnetic bead dipolar on the flow regime of a micro-fluidised bed. They reported that their system shares lots of characteristics similar to gravity based fluidised bed system such as the existence of fixed bed and minimum fluidisation velocity regime, bubbling bed, slugging bed, turbulent bed, and pneumatic transport regime.

Albeit there are few studies of solid-liquid micro-fluidised beds as outline above, the proposed research will be the first experimental study of liquid-solid circulating fluidised beds at the micro-scale. It is well known that solid particle handling in micro-technology devices remains one of the big challenges in the field [55, 79]. Development of a circulating micro-fluidised bed is providing one solution to the problem, e.g. for catalyst recovery, recycle and recovery. The study will provide new fundamental knowledge (hydrodynamics of solid-liquid micro circulating fluidised bed) but also develop a new measurement technique (e.g. micro-valves for solid flow measurement). This can be a new platform for solids metering and dosing techniques as another solid handling issue in the micro-technology field.

1.7 Motivation

The long term goal of my research project is to design and study the hydrodynamics of a solid-liquid micro-circulating fluidised bed (µ-CFB) system for possible application as novel micro (bio)-reactors, as well as for diagnostics high-throughput kinetics screening, high-heat flux cooling and other applications. In order to successfully implement this, it is very important to understand the hydrodynamic parameters such as the influence of surface forces, wall effect, minimum fluidisation velocity, and solid flux as they play a crucial role in the hydrodynamic behaviour and determine the bed performances, as well as dictating the solid-liquid contacting. Even though solid-liquid flow is simpler and stable than solid-gas flow in micro-fluidised bed system, there is very limited research on the effect of parameters such as liquid viscosity, bed geometry, solid circulation rate, surface forces and wall effect on solid-liquid flow in micro-fluidised bed. Thus, it is essential to study the solid-liquid micro-circulating fluidised bed hydrodynamics. Therefore, in the present research investigation an attempt will be made to study the effect of these important parameters in the solid-liquid micro-circulating fluidised bed hydrodynamics.

The overall aim of the research project was to investigate the hydrodynamics of a solid-liquid Micro-Circulating Fluidised Bed (µCFB). The specific objectives of the study were:

1. Design and build a novel micro-circulating fluidised bed.
2. Study the influence of surface forces and wall effect on the Hydrodynamics of liquid-solid micro-circulating fluidised bed (LS µCFB)
3. Solid flux measurement in a micro-circulating fluidised bed.
4. Examine the effect of liquid viscosity on the hydrodynamics of LS µCFB
5. Study the influence of CFB geometry on the hydrodynamics of LS µCFB

6. Carry out flow regime mapping of a liquid-solid micro-circulating fluidised bed (LS μCFB)

Chapter 2. Literature review

2.1 Circulating fluidised bed

The circulating fluidised bed is a type of fluidised bed which was developed in the late 1960s by Reh for alumina calciners application [38]. Various different names has been adopted to describe the circulating fluidised bed like: line reactor, fast fluidised bed, and recirculating bed riser [80]. Circulating fluidised bed technology was invented to enable particles entrained in high velocity fluidisation system to be recycled back to the system to increase the production rate in comparison to others fluid-solid contacts equipment such as fluidised bed combustors [38]. The word circulating means that in circulating fluidised beds, solids are separated from the fluid and recirculate back to the bed, which is a fundamental and vital part of the bed configuration [38]. There has been a strong academic and industrial interest in circulating fluidised bed technology in the past 30 years due to the need to improve important processes in industry such as fluid catalytic cracking units (conversion of crude oil into essential products) and circulating fluidised bed combustors [38]. The majority of circulating fluidised beds are run in the fast fluidisation regime and there is no recognisable upper bed surface [16]. Circulating fluidised beds offer lots of advantages when compared to other types of fluid-solid contacting technique such as the packed bed and bubbling bed, as circulating fluidised beds remove several problems found in other beds. For example, in circulating fluidised beds particle back mixing is significantly reduced, solid-fluid contact is improved while solid and gas axial dispersion is limited, solid residency time is longer and controllable, solid cooling and regeneration of catalyst and it is much simpler to have staged processes [81]. Base on solid-fluid system, circulating fluidised beds could be categorised into solid-gas, solid-liquid and solid-liquid-gas circulating fluidised beds [38].

2.1.1 Solid-gas circulating fluidised bed

Solid-gas circulating fluidised beds (SGCFB) are widely used processing technology in various chemical process industry, predominantly in energy, petrochemicals, and environmental sectors for solid-gas catalytic reactions, solid-gas reactions, and physical process such as volatile organic compound or drying due to their advantage already mentioned above such as reduced back mixing, enhance carbon conversion rate, good solid-gas contact, improved heat transfer and possess excellent capability to manage particle agglomeration [38, 82, 83]. They have recently been applied in solar energy capture and storage systems and waste recovery to replace thermal fluids and molten salt as transfer and storage medium [84, 85].

Numerous research investigation has been done to map the solid-gas circulating fluidised bed flow regime. Zenz [86] experimentally investigated the solid-gas flow characteristics and suggested a flow diagram where the concurrent pneumatic and dense fluidisation flow regime were indicated, however the turbulent zone was not depicted. Yerushalmi and co-worker [87] also suggested a solid-gas circulating fluidisation flow regime map. In their experimental study they plotted the bed voidage as a function of gas flow rate to delineate the regime of solid-gas circulating fluidised beds. Li and co-workers [88] also proposed a similar regime map by plotting the bed voidage as a function of gas flow rate. Squires *et al.* [89] proposed a solid-gas circulating flow regime, however in their report they extended the regime map to incorporate the transport regime. Later on Bi and Grace [43] proposed a flow regime map for solid-gas circulating fluidised beds which includes fixed bed, bubbling, slugging, turbulent, circulating fluidisation and transport regimes depending on the particle motion as shown in figure 3 by plotting the non-dimensional superficial gas velocity (U^*) against non-dimensional the diameter of particles (d_p^*).

$$U^* = \frac{Re}{Ar^{1/3}} \tag{2}$$

$$d_p^* = Ar^{1/3} \tag{3}$$

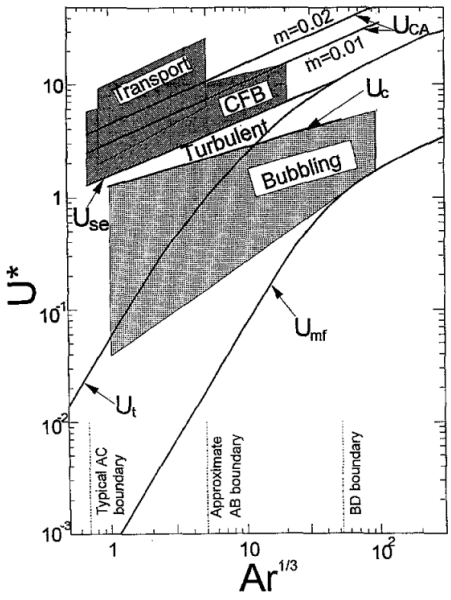

Figure 3: solid-gas circulating fluidised bed regime map [38].

Initially as the gas flow rate is below the minimum fluidisation velocity, (U_{mf}), granular material in the bed remains static (fixed bed) as show in in figure 4.

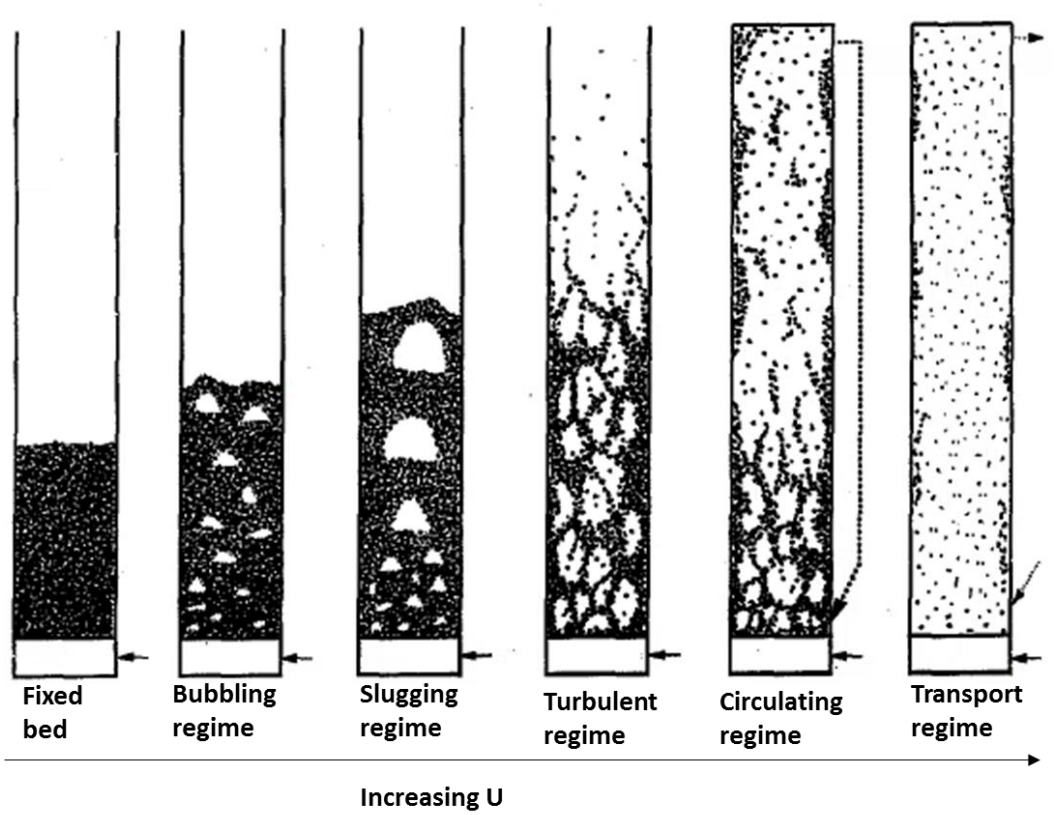

Figure 4. Flow regime in solid-gas circulating fluidised bed [38].

The passage from the fixed bed regime to fluidisation is indicated by the minimum fluidisation velocity, which is the minimum superficial gas flow rate where particles are fluidised. U_{mf}^{*} can be predicted using various available equations, such as the Grace Equation revised from the Wen and Yu equation [90]

$$Re_{mf} = \sqrt{27.2^2 + 0.0408Ar} - 27.2 \qquad (4)$$

Where *Re* is Reynolds number and *Ar* is Archimedes number.

With increasing gas flow rate beyond the minimum bubbling velocity (U_{mb}), bubble formation in the system is caused, indicating that the bed is operating at bubbling regime. Minimum bubbling velocity could be defined as the minimum gas flow rate where air bubbles first appears in the system and it is a function of solid properties. Minimum bubbling velocity is larger than minimum fluidisation velocity for group A particles of Geldard powder

classification and equal to minimum fluidisation velocity for group B and D particles [91]. Minimum bubbling velocity could be predicted using e.g. Abrahamsen and Geldart dimensional correlation [92]

$$U_{mb} = 33 d_p \left(\frac{\rho_g}{\mu_g}\right)^{0.1} \qquad (5)$$

where ρ_g and μ_g are density and viscosity of gas respectively

In the bubbling regime when gas flow rate is increased, the bubbles becomes larger and its diameter almost equates the bed diameter, this regime is slugging. The minimum slugging flow rate (U_{ms}), could be predicted using e.g. Stewart and Davidson equation [93]:

$$U_{ms} = U_{mf} + 0.07\sqrt{gD} \qquad (6)$$

When gas flow rate (U_g) is increased beyond (U_c) the velocity where pressure fluctuation standard deviation reaches maximum, the system enters the turbulent regime which could be estimated using the Grace and Bi equation [43]

$$Re_c = 1.24 Ar^{0.45} \quad (2 < Ar < 1 \times 10^8) \qquad (7)$$

Within the turbulent regime when gas flow rate is increased above the critical transition velocity (U_{tr}), the system enters the circulating fluidised bed regime where particles are transported to the top of the column and recirculated back to the system. Bi and co-worker [43] suggested a better way to predict the transition velocity from turbulent to circulating fluidised bed based on the critical velocity (U_{se}). U_{tr} depends on the location and distance between the two taps which measures the pressure drop across the system. U_{se} behave likes U_{tr} and it is more reliable. U_{se} can be predicted using Bi *et al.* equation

$$Re_{se} = 1.53 Ar^{0.50} \quad (2 < Ar < 4 \times 10^6) \qquad (8)$$

If gas flow rate is increased with a great extent within circulating fluidised bed regime, the system will enter the transport regime where lots of particles are carried out of the system.

2.1.1.1 Critical transition velocity in solid-gas circulating fluidised bed system

A number of experimental studies has been done to determine the critical transition velocity (U_{tr}), which demarcates the transition from turbulent fluidisation to circulating fluidisation regime as shown in figure 5.

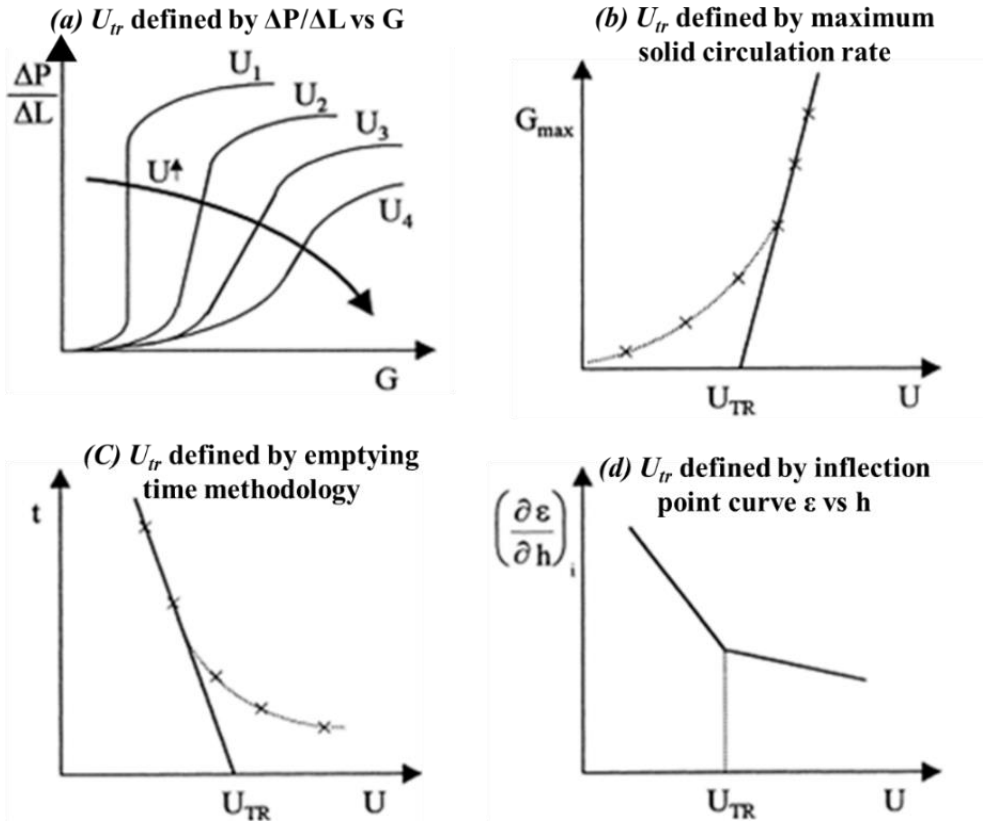

Figure 5. Previous measurement technique to determine the critical transition velocity (a) Yerushalmi, (b) Schnitzlein (c) Perales, (d) Horio [94-97].

Yerushalmi *et al.* [94] suggested a method to determine the U_{tr} by plotting the pressure gradient as a function of particle circulation rate. The particle circulation rate was measure with help of a butterfly valve. By closing the valve at a given time, particle accumulation above the valve was measured giving the particle circulation rate. The pressure drop was measure with aid of a pressure transducer installed across the column riser and linked to a PC through an Analog to Digital Converter (ADC). The critical transition velocity in their experiment was defined as the critical velocity at which the sharp change in the pressure gradient disappears as particles circulation rate increases. Schnitzlein *et el.* [95] determined the U_{tr} by a linear extrapolation method, the maximum particle circulation rate was plotted as a function of gas velocity. U_{tr} was given by a tangent curve as seen in figure 5b. Perales [96] determined U_{tr} by the emptying bed methodology, which was done by measuring the time needed to emptying all the particles

in the bed against gas velocity when no fresh particles were introduced into the system. The U_{tr} was defined as the inflection point in the emptying time plot as a function of gas velocity. Horio *et al.* [97] also determined the U_{tr} by plotting the voidage gradient $(\partial\varepsilon/\partial h)$ as a function of gas velocity (U). The voidage were obtained by the pressure gradient at different locations across the column riser. The pressure drop was measured by ten pressure transducers which were installed across the column riser. They defined U_{tr} as the velocity at which the voidage gradient at inflection point stops decreasing with gas velocity.

Although fluidisation can be achieved either by liquid or gas as fluidising medium, solid-liquid-circulating fluidised beds did not receive much attention in the fluidisation literature compared to gas-solid circulating fluidised beds. However, experimental knowledge on solid-gas circulating fluidised beds can eventually be applied to study solid-liquid circulating fluidised bed hydrodynamics [98, 99].

2.1.2 Solid-liquid circulating fluidised bed (CFB)

Solid-liquid fluidisation has been viewed as a completely academic matter by most researchers. But, new processes in various chemical sectors such as hydrometallurgy, water treatment, food processing, and biochemistry have prompted the urgency for new type of particle-fluid contact device which could control reaction and regeneration at the same time and reduce small and light particle entrainment [100]. The solid-liquid circulating fluidised bed is one of these excellent solid-fluid contacting devices. It possesses many advantages over the conventional solid-liquid fluidised bed which makes it useful for industrial operations where particle-liquid contact is vital, e.g. improved heat transfer performance, and consequent uniform temperature, limited back mixing, and excellent solid-liquid contact [101]. The component of a solid-liquid CFB include two columns the storage vessel or down comer and the riser with continuous particle circulation between the two columns, solid return pipe, and solid feeding pipe or return leg as shown in figure 6. Under normal conditions the column riser operates in the circulating fluidised bed regime (liquid superficial velocities are above the particle terminal velocity) and the storage vessel is a slower column and operates in the fixed mode regime or in the expanded mode regime [102]. The circulating fluidised bed system takes place when solids are transported up the riser by upward motion. Entrained solids are collected at the top by a solid-liquid separator and recirculated back to the system by downwards motion. In the solid-liquid circulating fluidised bed system the contacting time between the particle and liquid depends on the solid inventory (solid amount in the volume of the whole CFB system) in addition to the fluid velocity [103].

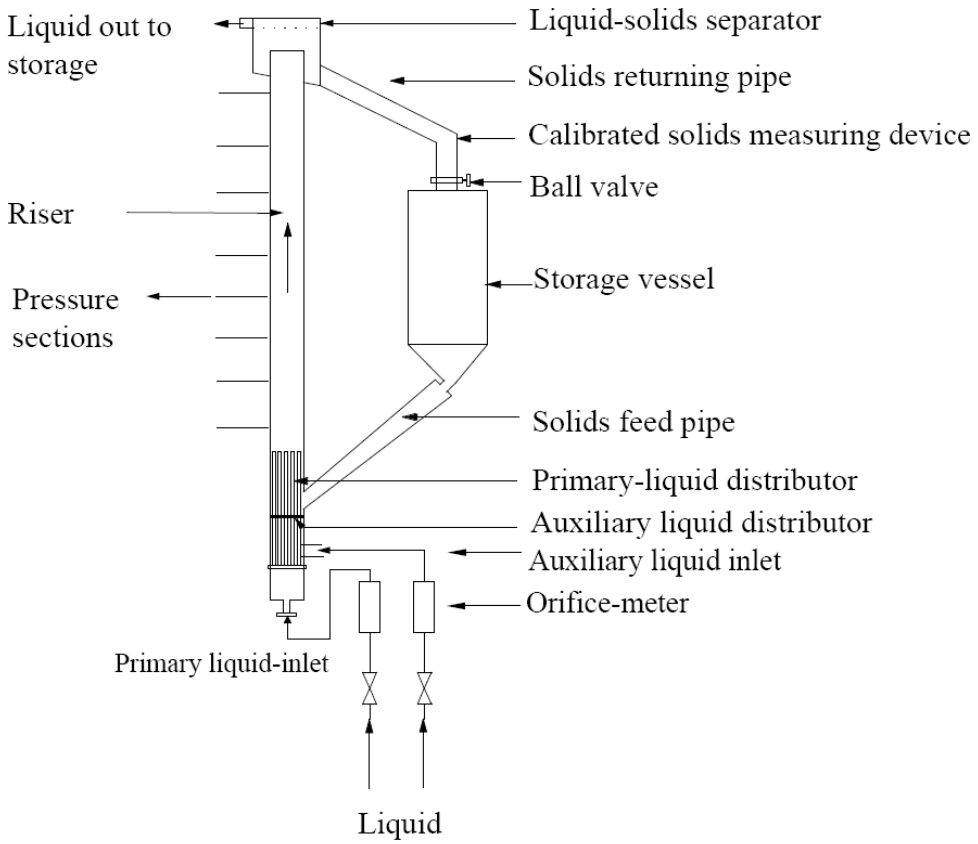

Figure 6. Schematic illustration of solid-liquid circulating fluidised bed [104].

Many research studies on the solid-liquid circulating fluidised bed hydrodynamics and its application in the processes industries have been carried out in the last decades [33, 36]. Most investigators studied the solid-liquid fluidised bed axial particle volume fraction distribution. They observed axial uniform but radial non-uniform solid distribution in the circulating fluidised bed regime flow structure while the flow structure in the conventional and transport regime was uniformly distributed in both radial and axial direction. This is different to the non-uniform behaviour of solid-gas CFB in both directions.

Lan *et al*. [105] experimentally studied the effect of solid volume fraction on the hydrodynamics of a solid-liquid circulating fluidised bed by predicting the solid volume fraction from the pressure gradient in the system. The pressure gradient was measured by a manometer.

$$\frac{\Delta P}{\Delta z} = \left(1 + \frac{h}{\Delta z}\right)\rho_l g \qquad (9)$$

$\Delta P/\Delta z$ is the pressure gradient, ρ_l the liquid density, g the gravity, h, riser height, Δz average distance from the bottom of the column

By ignoring the pressure drop as the superficial liquid velocity in the riser and downcomer was very low (9 and 1.9 mm/s respectively). The voidage, solid volume fraction and pressure could be linked as shown in equation 10

$$\frac{\Delta P}{\Delta z} = (\varepsilon_s \rho_s + \varepsilon_l \rho_l) g \qquad (10)$$

ε_s is the solid volume fraction and ε_l the bed voidage, $\varepsilon_s + \varepsilon_l = 1$, the solid volume fraction and pressure gradient relation is expressed as shown in equation 11

$$\varepsilon_s = \frac{(\rho_s - \rho_l)}{\rho_s} \frac{h}{\Delta z} \qquad (11)$$

In their report based on the solid volume fraction, they suggested that the downcomer can be divided in three regions, the dense region, diluted region, and free board region. Liang and co-workers [106] experimentally measured the solid volume fraction radial distribution using electrical conductivity and observed the distribution was non uniform. They reported a radial non uniform flow structure in the circulating fluidised bed regime which differs from the uniform flow structure in the axial and radial direction in the conventional and transport regime. The bed non uniformity radially was directly proportional to the solid circulation rate and liquid velocity. When the solid circulation rate and liquid velocity were increased the bed non uniformity radially also increased. Zheng and co-workers [107] also reported the radially non uniform flow distribution found in circulating fluidised bed regime using a fibre optic probe. They found that the properties of solids and operating conditions plays an important role in the radially flow distribution. The non-uniform radially flow structure increases when the particle circulation rate is higher. System with lower solids density tend to have less radially non uniformity flow distribution for the same cross section average bed voidage. Fluidisation in solid-liquid circulating fluidised beds is homogeneous and solid particles are distributed uniformly in the system, with limited radial non-uniform distribution found in the circulating fluidised bed regime. But the radial non uniform distribution found in solid-liquid fluidised beds is smaller compared to the non-uniform distribution in solid-gas fluidised bed [106, 107].

Table 1. Solid-liquid circulating fluidised bed vs solid-gas circulating fluidised beds [106, 107]

	SLCFB	SGCFB
Voidage distribution in axial direction	uniform	Non uniform
Voidage distribution in radial direction	Non uniform	Non uniform
Fluid velocity in radial direction	Non uniform	Non uniform
Slid velocity in radial direction	Non uniform	Non uniform
Non uniformity	significant	Even more significant
cluster	Not seen	Clearly seen
Transition velocity	$U_{cr} < U_t$	$U_{tr} \gg U_t$

Vidyasagar *et al.* [108] experimentally investigated the solid inventory and viscosity of the liquid effect on the critical transition velocity and solid hold up and found that the critical transition velocity from the conventional fluidised bed to the circulating fluidised bed is inversely proportional to the solid inventory and auxiliary liquid velocity, i.e. it decreased when the solid inventory and auxiliary liquid velocity are increased. On the other hand they found that the average solid volume fraction was proportional to the solid inventory and the liquid superficial velocity, it increased with increasing solid inventory and liquid superficial velocity. Natarajan and co-worker [36, 98] investigated solid-liquid circulating fluidised bed behaviour by analysing solid volume fraction and circulation rate variation. They found that there are two regions in the circulating fluidisation regime. The first region is where solid flux increases rapidly with increasing superficial liquid velocity and the second region is where solid flux insignificantly varies with increasing superficial liquid velocity. Sang and Zhu [109] investigated how particle size and density affects the solid volume fraction in the SLCFB system by analysing the normalised velocity, excess velocity ($U_l - U_t$), and liquid velocity. They found that excess velocity was the best parameter to analyse the effect of solid sizes and densities on solid volume fraction.

Hashizume et *al.* [110] studied the pressure drop in a solid-liquid circulating fluidised bed riser. In their experimental investigation the pressure drop was obtained using an inverted U tube manometer located in the centre of the column riser. From their experimental results their suggested a pressure drop method with a predicting accuracy of ± 20%. Grbavcic *et al.* [111] have investigated the pressure drop in the SLCFB riser using a water manometer. Based on their experimental investigation they suggested a one dimensional steady state solid-liquid flow model which can predicted the pressure drop based on the momentum and continuity equations for solid-fluid phases of Nakamura and Capes [112]. Liang *et al.* [113] also conducted an experimental studied of pressure drop in the SLCFB riser using a manometer. Based on their

experimental results they developed a theoretical model to predict the pressure drop in the solid-liquid system.

Geometry design can greatly influence the flow characteristics in a solid-liquid circulating fluidised bed system. Zheng and Zhu [107] experimentally investigated particle velocity in a solid-liquid circulating fluidised bed by varying particle density, solid inventory and solid feed pipe diameter. They reported that solids feed pipe diameter and solid inventory greatly influence the operating range and particle velocity of liquid-solid circulating fluidised bed system. Natarajan [104] investigated flow characteristic of SLCFB by varying the solid feed pipe diameter and reported that the solid circulation rate increases with increase solid feed pipe diameter. Feng *et al.* [114] report that bed geometry such as location of the riser outlet and solid feed pipe strongly influence the hydrodynamics of solid-liquid circulating fluidised bed. In their report they found that the higher the column riser exit, the less the particle circulation rate is, and the solid feed pipe diameter has more influence on the solid circulation rate than the length of solid feed pipe does.

2.1.2.1 Solid-liquid circulating fluidised bed industrial applications

The solid-liquid circulating fluidised bed is finding application in many industrial processes, for example: waste water treatment, bioconversion of agricultural-waste into lactic acid, fermentation, linear alkyl benzene production, photo-catalytic ozonation [99, 115]. A common characteristics of these processes is that they include a solid catalyst and liquid reactant and major reactions, desorption, or anoxic processes takes place in the column riser and catalysts regeneration, aerobic process, or adsorption takes place in the storage vessel (also known as the down comer) [102, 103].

2.1.2.2 Solid-liquid circulating fluidisation regime map

A hydrodynamics investigation is fundamental in order to develop and design a solid-liquid fluidised bed as a contact equipment or reactor for future industrial application because it dictates the bed performance and solid–liquid contacting [38]. Generally, the solid-liquid fluidised bed can be classified into four operating regimes [106, 116]: fixed or packed bed, conventional particulate fluidisation, circulating fluidisation, and transport regimes as a result of changing the superficial liquid velocity and consequent change in solid-particle motion. At the beginning when the superficial liquid velocity is below the minimum fluidisation velocity, solids in the bed remain stationary (fixed bed regime), figure 7(a). When the superficial liquid velocity is increased beyond the minimum fluidisation velocity, the solid-liquid system enters the conventional particulate fluidisation regime, as shown schematically in figure 7(b). In

general the minimum fluidisation velocity can be easily calculated using the Ergun equation [117] and equating it to the buoyant weight of the bed [118, 119].

$$\frac{\Delta P}{H} = 150\frac{\mu_f U_{mf}(1-\varepsilon)^2}{d_p^2 \varepsilon^3} + 1.75\frac{(1-\varepsilon)}{\varepsilon^3}\frac{\rho_f U_{mf}^2}{d_p} \quad (12)$$

where μ_f and ρ_f are fluid viscosity and density respectively, d_p represent the diameter of solid-particle, ΔP is the pressure drop, g is the gravitational acceleration, ε is voidage and H is bed height. The pressure drop required for minimum fluidisation is given by:

$$\Delta P = (1-\varepsilon)\left(\rho_p - \rho_f\right)gH \quad (13)$$

where ρ_p and g are particle density and gravitational acceleration respectively.

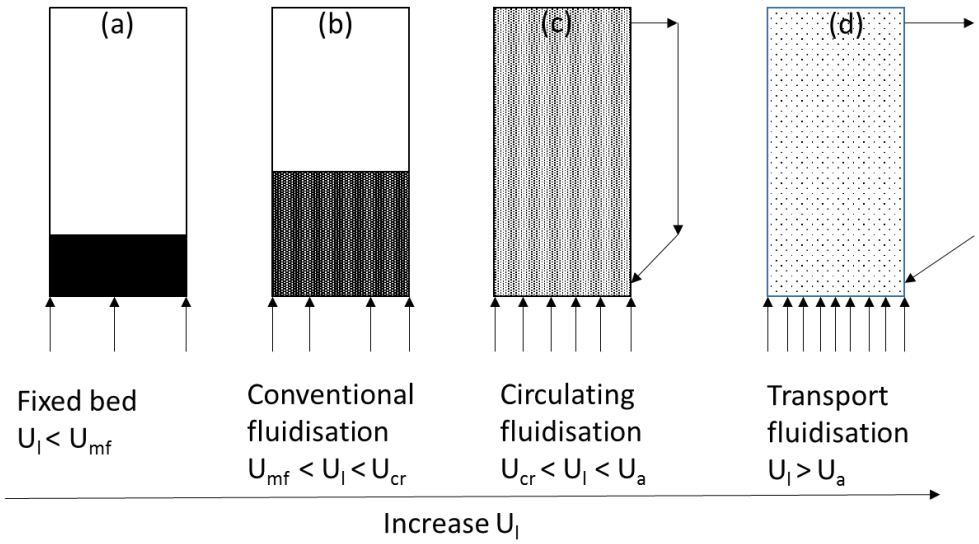

Figure 7. Flow regimes in solid-liquid circulating fluidised bed [106, 107].

In the conventional particulate fluidisation operation regime, there is a clear borderline separating the lower dense zone of the bed and the higher freeboard zone. When the superficial liquid velocity is increased above the critical transition velocity, the solid-liquid system enters the circulating fluidised bed regime where a number of particles are moved out of the system and it is important to re-introduce particles to retain the bed [106, 107], figure 7(c). If the superficial liquid velocity is increased to a great extent within the circulating fluidised bed regime, the solid-liquid system will enter the transport regime where lots of particles will be carried out of the system. The transition velocity from circulating fluidised bed regime to transport regime varies with solid circulation rate. A big solid circulation rate postpones the passage from the circulating fluidised bed to transport regime, due to the fact that bigger solid circulation rate causes an increase in the solid volume fraction, and this results in an increased

non-uniform radially flow distribution. The superficial liquid flow rate must be high enough to achieve uniform radial flow distribution and entering the transport regime [106, 107]. The critical transition velocity could be defined as the transition or passage from the conventional particulate fluidised bed regime to a circulating fluidised bed regime [106, 116]. The critical transition velocity in the system is reached when the solid velocity becomes zero with a reduction in superficial liquid velocity [106]. Solid-liquid circulating fluidised beds systems also have a transition phase from conventional particulate fluidised bed regime to circulating fluidised bed regime where the borderline separating the two zones is not clearly defined and the dense zone expands and a number of particles are carried out of the bed [106].

Liang and co-workers [106] experimentally investigated the characteristics of the solid-liquid circulating fluidised bed flow and reported a solid-liquid fluidisation regime map as shown in figure 8 by plotting non-dimensional solid-particle diameter (d_p^*) against non-dimensional superficial liquid velocity (U_l^*) as given by Equations 14-17.

$$d_p^* = Ar^{1/3} \quad (14)$$

$$Ar = \frac{g d_p^3 (\rho_p - \rho_f)\rho_f}{\mu^2} \quad (15)$$

$$U_l^* = \frac{Re_p}{Ar^{1/3}} \quad (16)$$

$$Re_p = \frac{\rho_l d_p U}{\mu} \quad (17)$$

The operation regime map for solid-liquid fluidised beds suggested by Liang and co-workers was identical to the operation map suggested by Grace [38] for solid-gas circulating fluidised beds. In figure 8, the U_{cr} is the critical transition velocity which indicates the transition from conventional particulate fluidised bed to circulating fluidised bed occurs at approximately 60% of the particle terminal velocity (U_t). U_a is the velocity at which transition from the circulating fluidised bed to the transport regime occurs. The Stokes particle terminal velocity for laminar flow, where Re < 1, which is applicable to the research project is:

$$U_t = \frac{(\rho_p - \rho_f) g d_p^2}{18\mu} \quad (18)$$

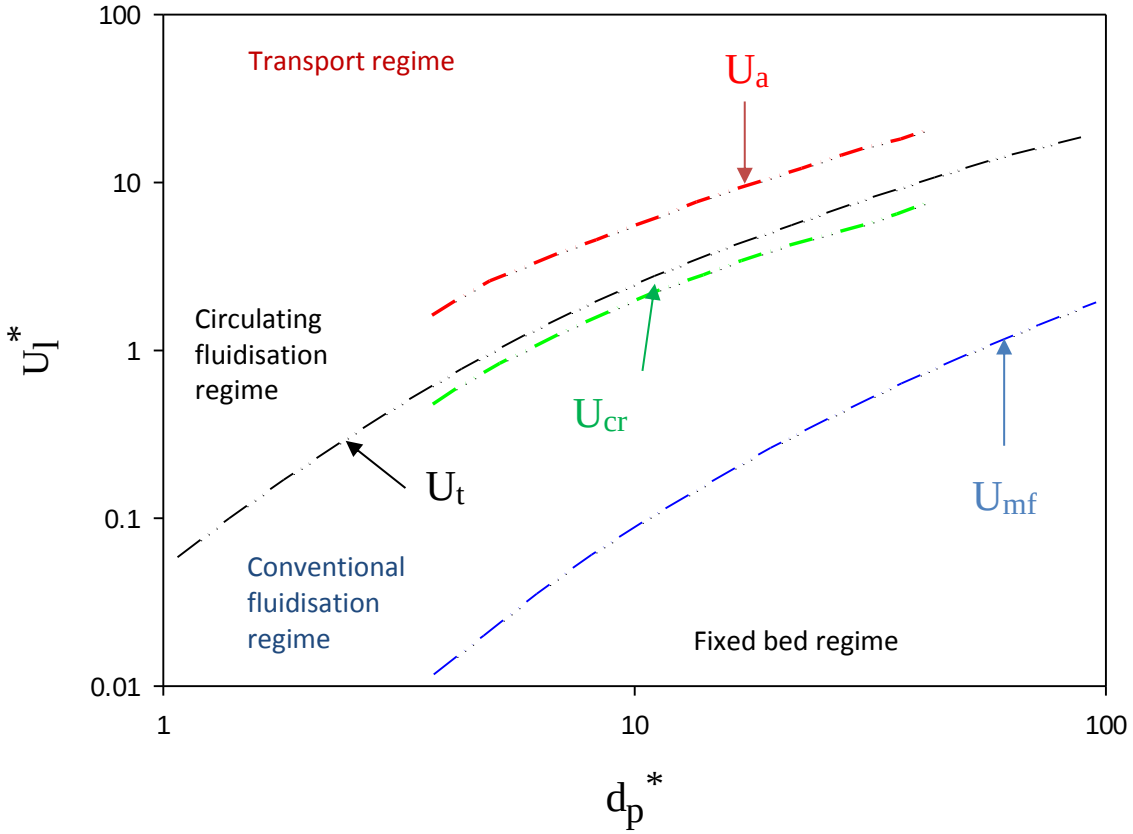

Figure 8. Operation regime map for solid CFB, adapted from Liang [106].

2.1.2.3 Transition from conventional fluidisation to circulating fluidisation regime

Liang and co-workers [106] suggested a method to find the critical transition velocity (U_{cr}), the transition from conventional particulate fluidised bed to circulating fluidised bed by plotting the solid circulation rate as a function of the liquid velocity as shown in figure 9. In their method the critical transition from conventional fluidised bed to circulating fluidised beds occurs at the point where the solid circulation rate becomes zero when superficial liquid velocity is reduced. The U_{cr} was found to be around 50 to 60% of the particle terminal velocity (U_t) and was dependent on the bed design, solid inventory, and operational conditions [99]. Liang and co-workers' circulating fluidised bed device had a third liquid stream close to the downcomer which was sufficiently high to fluidise particles in the downcomer. This third stream carries particles from the downcomer to the bottom of the column riser and joins the other two streams (primary liquid flow rate and auxiliary liquid flow rate) to fluidise particles at the column riser. However, they did not take into account this third stream when reporting the total liquid flow rate and this could explain why their reported critical transition velocity (U_{cr}) was lower than the calculated terminal velocity (U_t) [116].

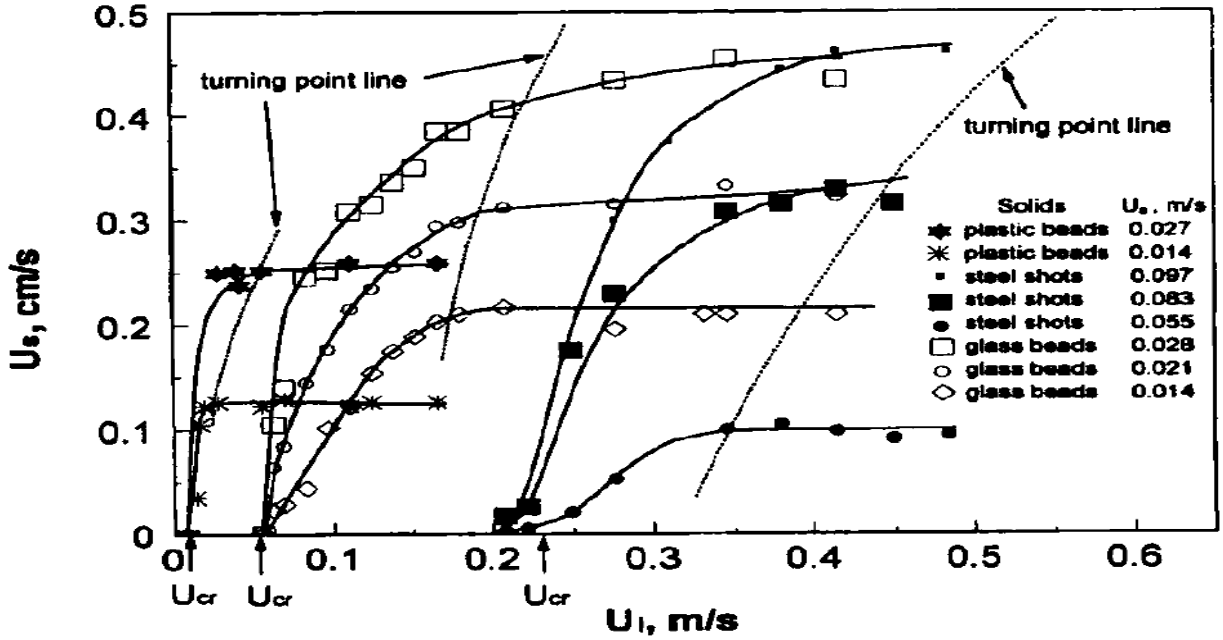

Figure 9. Solid-particles circulation rate vs. Superficial liquid velocity for determination of critical transition velocity U_{cr} reported by Liang [106].

Table 2. Critical transition velocity and terminal particle velocity for various particle reported Liang[106] .

Particle	ρ_s (kg/m^3)	d_p (mm)	U_{cr} (cm/s)	U_t (cm/s)	U_{cr}/U_t
Silica gel A	1363	0.385	1	1.85	0.54
Silica gel B	1375	0.57	1.9	3.32	0.57
Glass beads A	2460	0.405	3.1	5.29	0.59
Glass beads B	2440	0.777	6.3	11.1	0.57

Zheng and co-workers [116] in the other hand experimentally investigated the critical transition velocity from the conventional particulate fluidised bed to the circulating fluidised bed regime. They suggested an onset velocity (U_{cf}) which gives the lowest critical transition velocity from the conventional fluidised bed to the circulating fluidised bed regime and is independent of the solid inventory, equipment design and operating conditions. The U_{cf} was found by the 'emptying bed methodology' which was done by measuring the time needed to empty the solid-particles in the bed using different superficial liquid velocities as shown in figure 10. The U_{cf} is defined as the inflection point in the emptying time plot as a function of the liquid velocities. It was found to be approximately equal to the particle terminal velocity. They suggested that U_{cr} is the actual transition from the conventional to circulating fluidised bed regime and U_{cf} represents the lowest transition from the conventional to circulating fluidised be regime [107, 116].

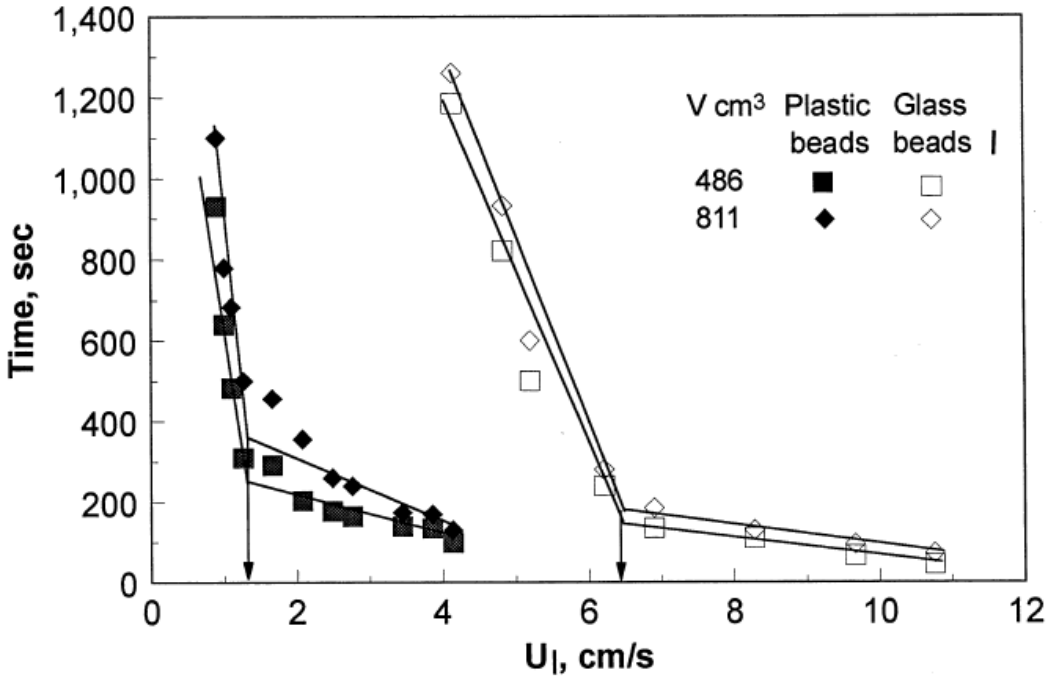

Figure 10. Time needed to empty all the solid particles in the bed vs. superficial liquid velocity for determination of onset velocity U_{cf} reported by Zheng and co-workers [116]

Table 3. Critical velocity and onset liquid velocity suggested by Zheng [116].

Particle	ρ_s (kg/m^3)	d_p (mm)	U_{cr}	U_{cf} (cm/s)	U_t (cm/s)	U_{cr}/U_t	U_{cf}/U_t
Plastic Beads	1100	0.53	1.17	1.15	1	1.17	1.15
Glass beads I	2490	0.51	6.47	6.45	5.9	1.1	1.1
Glass Beads II	2541	1	-	16.30	14.4	-	1.13
Steel shot	7000	0.58	24.84	23.7	21.6	1.15	1.1

Nirmala and co-worker [99] also determined the critical transition velocity, U_{cr} by plotting the solid circulation rate as a function of the liquid velocity. The solid circulation rate was measured using a ball valve. When the valve was closed in the downcomer, the accumulation of particles above the valve at given time could be measured, giving the particle circulation rate. The critical transition velocity was taken as the point where the solid circulation rate becomes zero when reducing superficial liquid velocity. The U_{cr} was found to be 1.33 times the particle terminal velocity (U_t).

2.1.3 Solid-liquid-gas circulating fluidised bed

Solid-liquid-gas fluidisation could be defined as the fluidisation of particles by liquid and gas as the fluidising media where liquid could act as the continuous phase and gas as the dispersed phase or vice versa [120, 121]. Solid-liquid-gas circulating fluidised beds (SLGFB) finds applications in various environmental, petroleum, chemical and biochemical applications for processes such as sewage sludge pyrolysis, hydrogenation, petroleum hydro-treating, production of methanol, ethanol fermentation, biological waste water treatment and catalysis reaction where contacting of particles with both liquid and gas are required [122, 123]. They are extremely important processing technology for biochemical and chemical applications in which independent control of solid, liquid, gas phases holdup and continuous regeneration of catalyst is required to guarantee an undisturbed operation mode [124, 125]. In these types of bed, the adsorbents or deactivated catalyst are continuously regenerated by particle circulation between the riser where reaction takes place and the downcomer where regenerations are performed [126]. Solid-liquid-gas circulating fluidised bed have a number of advantages such as uniform and fine bubbles, better mass and heat transfer rate, higher liquid and gas flow rate, excellent solid-liquid and gas contacting when comparing to conventional solid-liquid-gas fluidised beds [121, 122]. The higher shear stress differences between the riser and downcomer in SLGCFB could be exploited to promote biofilm renewal in circulating fluidised bed bio-reactors, where micro-organisms can be immobilised on the inert particle surface creating an active micro-organism layer [125, 127].

Solid-liquid-gas circulating fluidised bed has been the subject of numerous research publications in the past 20 years. Liang *et al.* [122] experimentally investigated the solid-liquid-gas circulating fluidised bed hydrodynamics by using a conductive probe. They observed a uniform gas and particle hold ups distribution in the riser column, and a non-uniform radially distribution. Yang *et al.* [128] investigated the liquid flow structure in SLGCFB using an electrolyte tracer method. They reported a non-uniform radially liquid velocity distribution. The non-uniform radial liquid velocity in the SLGCFB are more uniform compare to solid-liquid gas fluidised beds (SLGFB). Jin *et el.* [129] has studied the flow characteristics in the solid-liquid-gas circulating fluidised bed, and proposed a flow regime map as shown in figure 11 which includes, coalesced bubble, dispersed bubble, slugging, recirculation and transport regime when liquid flow rate is increase. At the start the system operates at the coalesced bubble regime which is characterised by lower liquid flow rate and intermediate gas flow rate. Bubbles at this regime are larger with wide distribution size as a result of increasing coalescence bubble. Increasing liquid flow rate within coalesced regime causes a reduction in

bubbles size indicating that the system is operating at dispersed bubble regime where bubbles are small and also much uniformly distributed. The transition from coalesced bubble regime to dispersed bubble regime takes place when gas hold up increases with increasing liquid flow rate. When the liquid flow rate is increased above the dispersed bubble regime, the system enters the recirculation regime where a number of particles are carried out of the riser column and recirculated back to the system via the solid feed pipe, and it is important to re-introduce particles to retain the bed. Within the recirculating fluidisation regime if liquid flow rate is further increased, the system will enter the transport regime. Liang and co-worker [130] reported that it could potentially be possible to map the circulating fluidisation regime of the solid-liquid circulating fluidised bed and the transport regime of the solid-gas circulating fluidised bed within the recirculation regime in the solid-liquid-gas circulating fluidised bed.

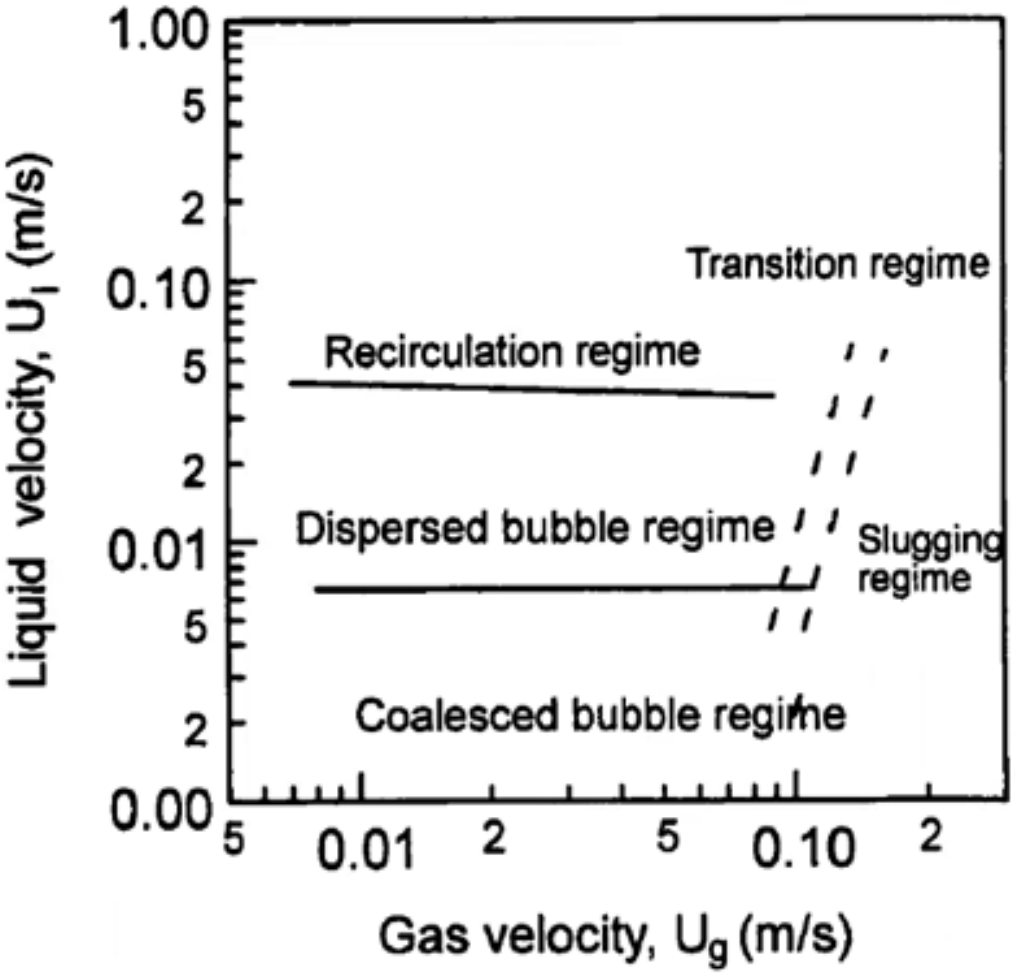

Figure 11. Solid-liquid-gas circulating fluidised bed regime map [11, 38]

2.2 Inverse fluidisation

Inverse fluidisation is a process by which particles with a density smaller than the continuous liquid, are fluidised by a downwards flow of the continuous liquid [131, 132]. Inverse fluidised beds are very effective solid-liquid contact devices for biological waste water treatment compared to other types of fluidised beds, i.e. bio-film thickness could effectively be controlled to prevent intra-biofilm diffusional limitations[133, 134]. Figure 12 shows the schematic fluidised bed and inverse fluidised beds. The inverse fluidisation process has several advantages such as high transfer rates, particle attrition is very limited, bio-film thickness are effectively controlled and it can easily be re-fluidised if power outage occurs [132, 133]. Inverse fluidised beds find numerus applications in many industrial applications such as in aerobic waste-water treatment, food processing, biotechnology and environmental engineering. Inverse fluidised beds have been important tools in the treatment of waste water from wine, sugar and distillery industries [132, 133].

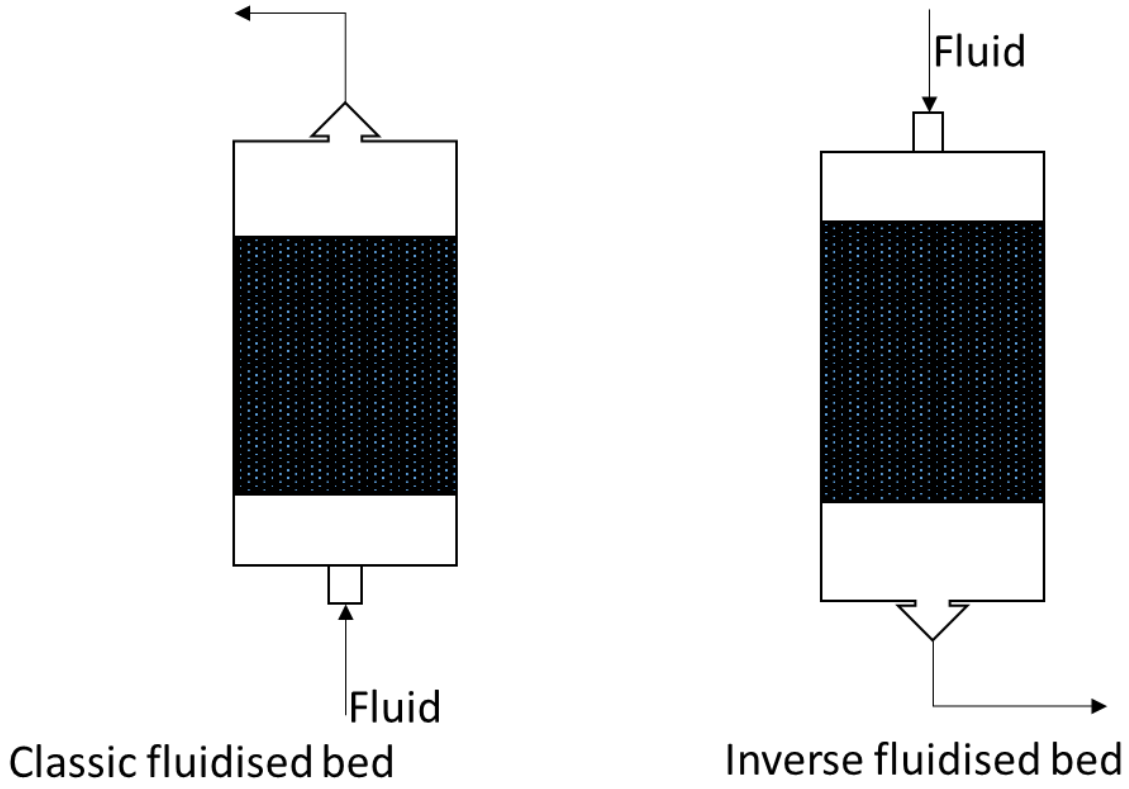

Figure 12. Fluidisation and inverse fluidisation process [131].

2.3 Additive manufacturing technology

The controlled manipulation of small volumes of fluids at micrometres length scales provides important advantages for chemical and biological applications, including inkjet printers, waste

water treatment, cell biology research, chemical micro-reactor, medical diagnostics, drug screening, micro-processor cooling, protein crystallization, genetic analysis, electro-chromatography, fuel processing and power generation [135, 136]. Historically, the scaling of fluidic systems has primarily relied on micromachining technologies that were developed for semiconductor and microelectromechanical systems industries [137]. Notably, soft lithography techniques for micro-moulding and bonding elastomeric materials, such as polydimethylsiloxane (PDMS), have served as the basis for most of current microfluidic systems [137]. However, these techniques have many known limitations, such as the complicated commercial translation of academic research, because of difficulties in large volume manufacturing [138]. These techniques require much space to hold multiple pieces of equipment, are labour intensive, cause time wastage when making a change in design, and requires highly specialized skills [139]. For scientific research, however, it is often more important to minimize the technological and temporal effort for device fabrication to quickly and easily adopt microfluidic devices to new demands and developments [140]. Fortunately, the rapid development of additive manufacturing technology in terms of resolution and speed is providing a solution to the problem [140, 141].

Additive manufacturing is the process which fabricates three dimensional structures by adding layer upon layer under computer control [140, 141]. In the field of microfluidics, additive manufacturing technology, also known as 3D printing, offers the capability to directly print complex 3D microfluidic devices with low-cost desktop printers, changing the way in which such devices are designed, and manufactured [142]. Compared with other microfabrication techniques, 3D printing requires little training outside of the ability to use computer-aided drafting software [142]. Fabrication can be accomplished in relatively short amounts of time, with a build time of approximately 4 hours for a structure of ~2 mm x 2 mm dimensions [143]. Perhaps more importantly, 3D printing does not require dedicated microfabrication facilities and is lower overall in cost than the instrumentation required for lithography approaches [144]. There are several other notable advantages associated with 3D printing for the fabrication of microfluidic devices over conventional methods, including the embedding of a tissue scaffold with high porosity, high resolution and defined pore structure into the device, using a range of different materials [144]. Thus, issues normally associated with microfluidics, such as blockages are significantly reduced [144]. This could possibly aid the field of microfluidics in finding the killer application that will lead to its acceptance by researchers, especially in the chemical and biomedical field. Finally, 3D printing design files can be shared easily, which

should facilitate collaboration and enable broad use. For those reasons additive manufacturing technology is well suited for microfluidic applications [145]. Example of 3D microfluidic device is shown in figure 13.

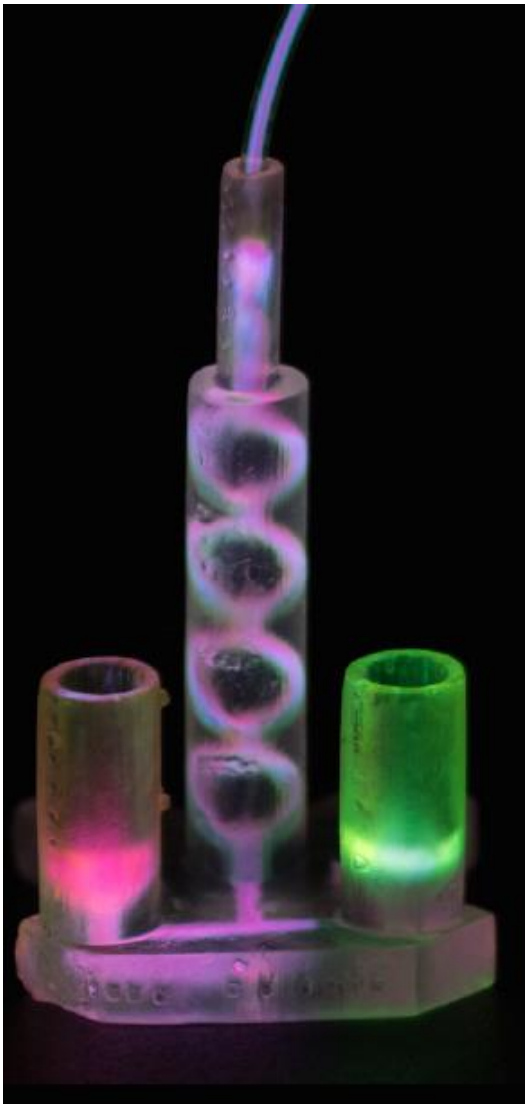

Figure 13. 3D micro-mixer with 1500 micron circular channel printed using Formlabs Form1+[146]

In spite of the mentioned advantages offered by additive manufacturing technology over soft lithography, most microfluidic researchers have been reluctant in adopting 3D printing techniques because of concerns regarding material availability, biocompatibility of the resin, optical transparency, surface quality, shape conformity and dimensional fidelity [145]. Additive manufacturing technology for microfluidic was pioneered by McDonald *et al*.[147] who reported the used of additive manufacturing technology to produce templates for poly (dimethyl siloxane) (PDSM) casting. The first successfully printed microfluidics device was

achieved by Moore et al [148] involving disk-based microfluidics. Anderson et al[149] created a microfluidic channel to investigate drug transport and cells effect. The micro channel was printed via Fuse deposition modelling comprising 8 parallel 3 x 1.5 mm channels to enable integration with commercial polycarbonate membrane. Lee *et al.* [150] proposed an additive manufacturing technique to produce integrated microfluidic devices. They managed to print a microfluidic channel comprising of different configurations such as T-Junction, straight sections, and separate unit to mix the flows for detection of alpha fetoprotein (AFP) biomarker. Munshi *et al.* [151] used additive manufacture to create a microfluidic wall-jet electrochemical detector and demonstrate that additive manufacturing technology could be a powerful tool to create microfluidic devices. Their result design shows an improved sensitivity and limit detection when compared with soft lithographic design. Saggiomo and velders [152] presented a simple and cheap scaffold removal technique to produce complex 3D microfluidic channels. They also demonstrate how externa components, such electronic, heating element and circuitry could be directly incorporate into the microfluidic device using the scaffold removal manufacturing technique. Gowers et al.[153] reported a 3D printed microfluidic system that integrates the commercially available micro-dialysis probes for online analysis of lactate and glucose in humans. He et al [154] produced a 3D printed microfluidic chips from a simple and cheaper 3D sugar printer to investigate cell culture and their result shows that this simple and cheaper method to produce 3D microfluidics chips could potentially be used in biomedical researches. Rogers et al. [155] presented a novel 3D printed microfluidic channel with integrated valves. The microfluidic channel was fabricated using a stereolithographic (SLA) modelling 3D printer. They demonstrated that their fabricated 3D printed microfluidic device is less prone to non-specific protein adsorption than polydimethylsiloxane (PDSM) and showed lots of attributes which are attractive for microfluidic applications. Shallan et al. [156] presented a transparent 3D printed microchips device to study the effect of nitrate in tape water. The printed microchips were fabricated using commercial stereolithographic 3D printer (MiiCraft). Their experimental result demonstrates the potential of the MiiCraft 3D printer to produce cheaper and reliable microfluidic device compared to others published design using traditional manufacturing technique. They stated that it would be extremely hard to produce a similar microfluidic device for a similar price and similar time using soft lithography fabrication technique. Recently Gaal et al.[157] use additive manufacturing technique to produce integrated microchannel using polylactic acid (PLA), a low-priced alternative material to Polydimethylsiloxane (PDSM). The microchannel was printed via Fuse deposition modelling (FDM). To illustrate the capability of the additive manufacturing technique in

produce a microfluidic device, a 3D printed microfluidic electronic tongue capable to differentiate basic tastes was fabricated. The electronic tongue was produced in less than 1 hour, which could hardly be achieved by PDSM process. Additive manufacturing for microfluidic include stereolithography (SLA), fused deposition modelling (FDM), electronic beam melting (EBM), multi jet modelling (MJM), selective laser sintering (SLS), laminated object manufacturing (LOM), and digital light processing (DLP) [140, 141]. The above mentioned additive manufacturing technique finds application in the fabrication of microfluidic devices, and their advantages and current limitations is summarized in table 4. One of the challenge facing the microfluidic industry is the absence of a standards for fluidic interface and components [140, 141]. Additive manufacturing technology could provide a solution to this problem by offering standard fabrication which could be adopted by the microfluidic community.

Table 4: Current 3D printing technology used for microfluidic devices fabrication.

Printing Technology	Applications	Advantages	Disadvantages
Stereolithography (SLA)	Microfluidics interface [158] Modular microfluidic [139] Microfluidics chips [155] Master mould fabrication [159].	High resolution & High accuracy transparent microfluidic chip easy to operate Fast and cheaper process	Post treatment is required Material availability is limited Limited operating temperature
Fuse deposition modelling (FDM)	Master mould fabrication [159]. Micro-fluidic reactionware [160] 3D sugar printing of microfluidic chip [154]	Low cost material Easy to remove support material Highly accessible and reconfigurable format	Poor resolution & rough surfaces restricted accuracy Slow fabrication time Material availability is limited
Multi-jet modelling (MJM)	Fabrication of vertical microfluidic channel [161]. Design of complex microfluidics molds[162]	High resolution Multi material printing capability Rapid printing speed High accuracy and quality	Post treatment is required Material availability is limited Hard to remove support structure Expensive
Digital light processing (DLP)	Mold casting [156]	High accuracy Fast building speed Consistent building time Cheaper equipment	Non-bio-compatibility Material availability is limited Limited operating temperature Post treatment is required
Selective laser sintering (SLS)	Integrated micro-valves & pump Triple helix fabrication [163]	High accuracy, High strength Rapid fabrication	Poor resolution Post treatment is required Very costly
Selective laser melting (SLM)	Metal electrode supports fabrication [164]	High accuracy High strength Wide material adaptation Rapid fabrication	Very costly Rough surface Lower resolution Hard to remove support structure
Laminated object manufacturing (LOM)	Paper based microfluidic analytical with different agents [165]	Cheaper Easy to fabricate large parts	Low material availability Time consuming

2.4 Novelty

Chapter 1 & 2: Review of micro-fluidised bed

A general background and review of solid-liquid circulating fluidised beds at micro-scale is presented for the first time. In this chapter, a detailed review of published literature on the circulating fluidised bed, liquid-solid fluidisation, micro-fluidised beds, flow regime transition, inverse fluidisation, and estimation of surface forces identifies the vital characteristics of the micro-circulating fluidised bed that are applicable to the current research study and different measurement technique employed by previous researchers. It is well known that solid particle handling in micro-technology devices remains one of the big challenges in the field. Development of a circulating micro-fluidised bed is providing one solution to the problem, e.g. for catalyst recovery, recycle and recovery. The study provided new fundamental knowledge (hydrodynamics of solid-liquid micro circulating fluidised bed) but also developed a new measurement technique (e.g. micro-valves for solid flow measurement). This can be a new platform for solids metering and dosing techniques as another solid handling issue in the micro-technology field

Chapter 3 Methodology

Additive manufacturing was used for the first time for design and fabrication of a novel micro-circulating fluidised bed (μCFB) to investigate the hydrodynamics of solid-liquid fluidisation in micro channels. This allowed us to rapidly create micro-channels of any shape while providing high micro resolution of 10s of microns in the x, y and z directions. The method also provided fast and simple solutions to manufacturing reliable micro-structures such as micro-circulating fluidised beds and the distributor using low-cost materials. Thus, issues normally associated with micro-fluidics, such as blockages was significantly reduced.

For the first time particle image velocimetry (PIV) software PIVlab was used to measure the solid flux in a liquid-solid micro-circulating fluidised bed. This technique is non-invasive and easy to implement in microfluidics setup which is not trivial for other conventional techniques such as the valve technique. In addition of PIV software, a novel measurement technique (e.g. magnet valve for solid circulation rate measurement) was developed to measure the Solid circulation rate in the micro-circulating fluidised bed. A magnet was installed inside the micro-circulating fluidised bed in the downcomer, and an external magnet was used to move and control the magnet inside the bed as a magnetic measuring valve. By closing the downcomer with the magnet valve which was installed in the bed, the accumulation of particles above the

valve at any given time interval could be measured, giving the particle circulating speed, and the results were compared with those obtained using PIV methodology.

Chapter 4 Influence of surface force and wall effect

In general, the major difference between micro and macro-scale flows is the importance of surface forces which can prevent fluidisation, and inevitably the wall effects due to small bed size. Therefore, for the first time an attempt was made to investigate the influence of surface force and wall effect in liquid-solid micro-circulating fluidised bed system. The experimental results showed that the acid-base model of van Oss, Chaudhury and Good combined with the Derjaguin approximation can successfully predict the propensity of micro-particles to adhere to the walls of micro-fluidised beds using common liquid fluidizing media.

Chapter 5 Solid flux measurement

In this chapter, solid flux in a liquid-solid micro circulating fluidised bed was successfully studied for the first time. The experimental research was performed in a micro-CFB which was made by micro-machining channels of $1mm^2$ cross section in Perspex. PMMA and soda lime glass micro-particles were used as the fluidised particles and tap water as the fluidising liquid. The experimental results look relevant when compared with their macroscopic counterparts.

Chapter 6 Effect of liquid viscosity

For the first time, the influence of liquid viscosity on the hydrodynamics of liquid-solid micro-circulating fluidised bed is presented. In most industrial processes where SLCFB are employed as a solid-liquid processing equipment, viscous liquid is required as a processing fluid. Hence, it is crucial to understand the effect of liquid viscosity on the hydrodynamics, particularly on the solid circulation rate and minimum fluidisation velocity of a liquid-solid circulating fluidised bed.

Chapter 7 Influence of circulating fluidised bed geometry

Here, it was presented the first study on the effect of bed geometry (solids feed pipe-riser ratio, and angle between solid feed pipe and riser) on the hydrodynamics of liquid-solid circulating fluidised beds (LSCFB) at the micro-scale. The circulating fluidised bed (CFB) geometry can have a significant effect on the internal recycling of solids in a riser, and subsequently on the riser hydrodynamics and particle residence time distribution. Hence, effort were made to understand their influence on the hydrodynamics of SLCFB at micro scale.

Chapter 8 Flow regime map

A new fluidisation regime, the solid-liquid micro-circulating fluidisation regime, was mapped for the solid-liquid fluidisation systems of different particles size and materials

(Polymethylmethacrylate (PMMA) and soda lime glass microspheres). The operation regime map is a function of liquid velocity inherently related with particle terminal velocity (function of solid-particle density and size, liquid density and viscosity).

2.5 Thesis structure

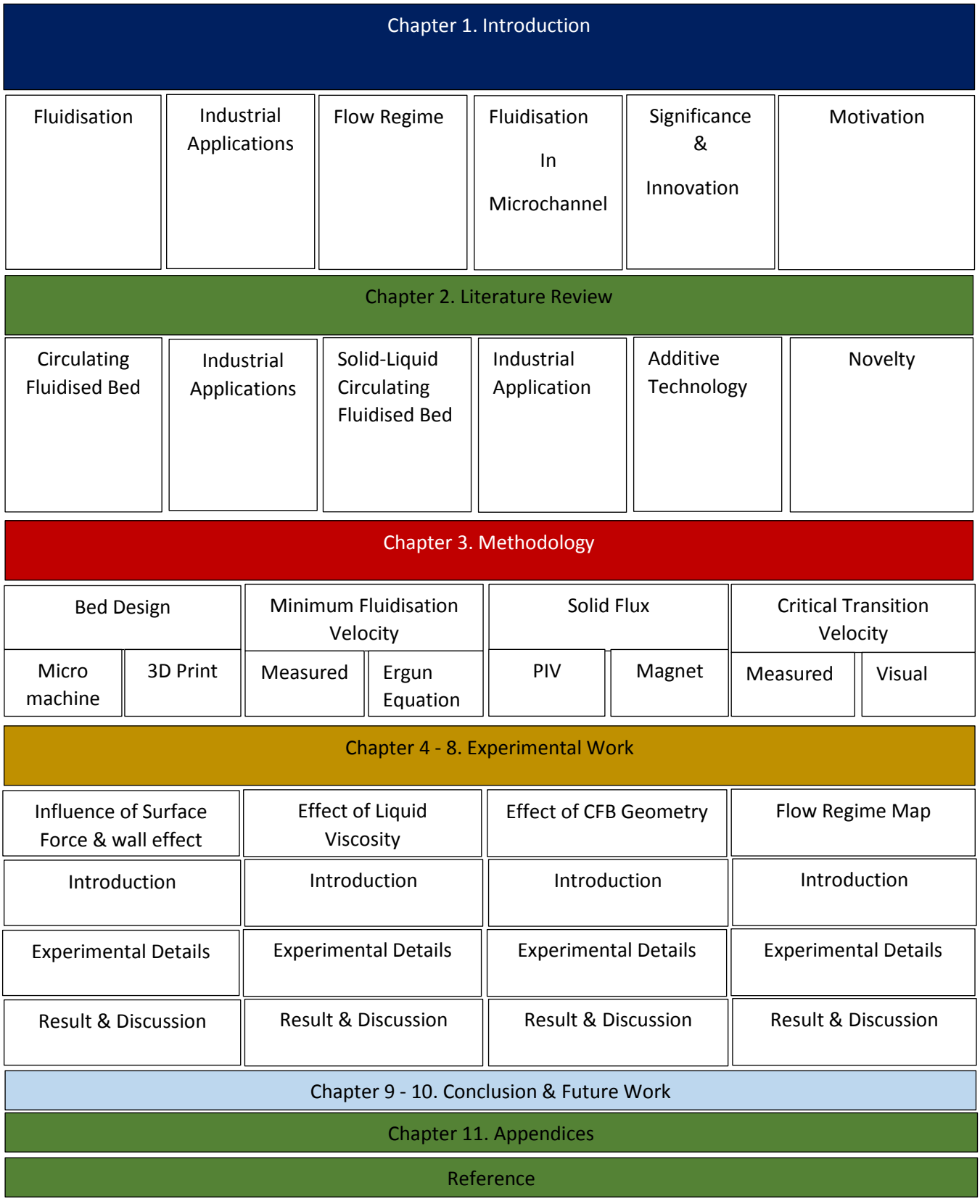

Chapter 3. Methodology

This chapter outlines the design fabrication of the Micro-circulating fluidised bed and procedure to investigate the hydrodynamics characteristics of liquid-solid fluidisation in micro and mini channel. At the beginning, different types of distributor were analysed and the most suitable distributor design which would provide stable and uniform flow distribution across the micro-circulating fluidised bed was chosen. A soft lithography technique and additive manufacturing technology were used to fabricate the micro-circulating fluidised bed channel to be used in the present investigation. Different measurement technique capable of measuring the minimum fluidisation velocity and the solid circulation rate in the micro-circulating fluidised bed channel are outlined.

3.1 Consideration design

The design of micro-circulating fluidised bed influences the bed performance as a solid-liquid processing equipment including the hydrodynamics such as minimum fluidisation velocity, solid circulation rate and flow regime map. The liquid distributor represents the most important part of a circulating fluidised bed system. The liquid distributor dictates the performance of a circulating fluidised bed as a solid–liquid contact equipment. The main function of the liquid distributor is to provide stable and uniform fluidisation across the bed cross-section while reducing particles back mixing and to prevent particles leaving the bed at the bottom [11]. Therefore, liquid distributor design generally dictates the success or failure of a circulating fluidised bed as they play a major influence on the hydrodynamics characteristics of a circulating fluidised bed. Currently there are various different distributor models, some more applicable than others depending on the cost, mechanical feasibility and process conditions. Those distributor design with their applications, advantages and limitations are discussed in this section. The nature of the distributor model strongly dictates the number and size of bubbles formed in a fluidised bed. The important characteristics of a good distributor plate should include:

- Provide uniform and stable fluidisation
- Prevent formation of dead zones on the grid
- Prevent particle back mixing
- Reduce particles attrition
- Reduce particles erosion

3.1.1 Perforated plate

Perforated plates are the most commonly used distributor model in many industry where fluidised bed is employed as solid-liquid processing equipment because of its low price, simple fabrication, easy to scale up and down [166]. Possible drawback of this type of distributor is the lack of rigidity and formation of dead zone. In perforated plate distributor the fluidising fluid is introduced into the bed in upwards direction. Perforated plate distributor finds application in powder agglomeration, coating of particle and tablets, and also spray granulation of liquid granulation [167]. The perforated plate distributor is made of arranged triangular or square holes of varying size and shape in various patterns as displayed in figure 14.

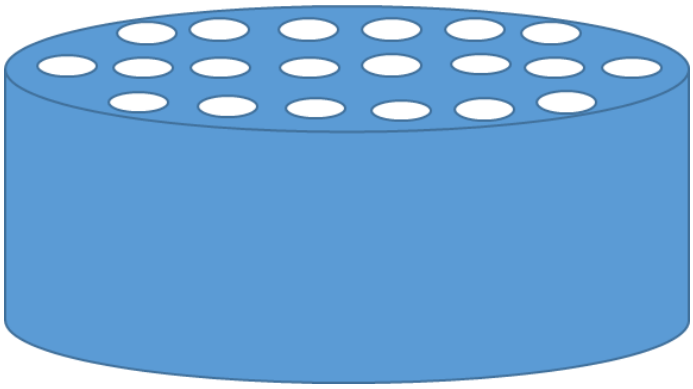

Figure 14. Perforated plate distributor model

3.1.2 Sparge or Pipe distributor

Sparge or pipe grid are tubes with holes drilled in them as illustrated in figure 15. In sparge and pipe distributors the fluidising fluid is introduced into the bed in a downwards or lateral direction. The advantages of this type of distributor is that reduces weeping, low pressure drop, and it is easy to fabricate and to install in the circulating fluidised bed system. The main drawback is that with Sparge distributor it is difficult to prevent dead zone formation. Sparge and Pipe distributor finds application in the Sohio acrylonitrile process [168, 169].

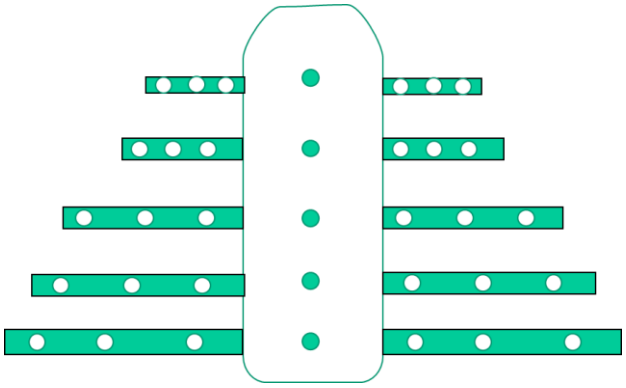

Figure 15. Example of Sparge and pipe distributor

3.1.3 Bubble caps and Nozzles

In bubble cap and nozzles distributors the fluidising fluid is introduced into the system in lateral direction. The main advantage of those type of distributor is that reduces particles back mixing and weeping. However, the major disadvantage includes that it is hard to avoid the formation of dead particles regions, they are expensive to design, hard to clean and to modify. Bubble cap and nozzles distributor finds application in energy and food industry [170, 171]. An illustration of a bubble cap distributor is shown in figure 16.

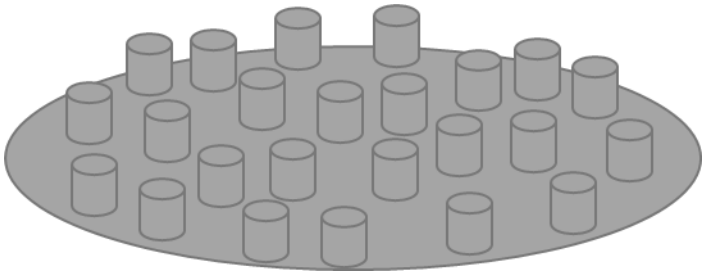

Figure 16. Bubble cap distributor

3.1.4 Conical distributor

In this type of distributor, the fluid motions are conical as displayed in figure 17, this distributes the fluidised fluid uniformly, promotes mixing of particle, eliminates the formation of dead zone, minimises pressure drop and segregation of particles. However conical distributors are hard to fabricate, and carefully fabrication design is required to guarantee good fluid distribution across the bed cross-section. Conical distributor finds application in industrial drying of foods [11, 172].

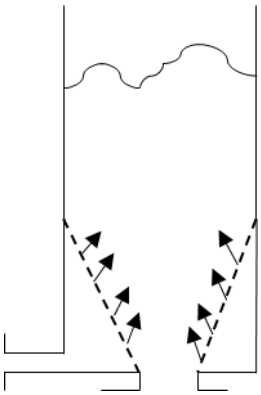

Figure 17. Conical distributor model

3.1.5 Porous plate distributor

Porous plate distributors are fabricated from either synthetic, ceramic or sponge metal. These type of distributor are popular in the research laboratory to investigate fluidisation characteristics at small scale but are unsuitable for industrial scale fluidised bed due to high pressure drop [40]. Porous plate distributor provides high pressure drop compared to other distributor design, the pressure drop is directly proportional to the fluid velocity through the hole. Hence porous plate distributor does not suffer from the misdistribution of fluid as the other type of distributor design. Porous plate distributor promotes mixing of particles, prevent dead zone formation and they are the best type of distributor design in terms of fluidisation quality according to Richardson [173]. The main drawback of porous plate distributor is the high pressure drop across the plate which leads to an increase in power consumption and processing costs, plate blockage by fine particles and thermal stresses sensitivity [1]. An illustration of porous plate distributor is given in figure 18.

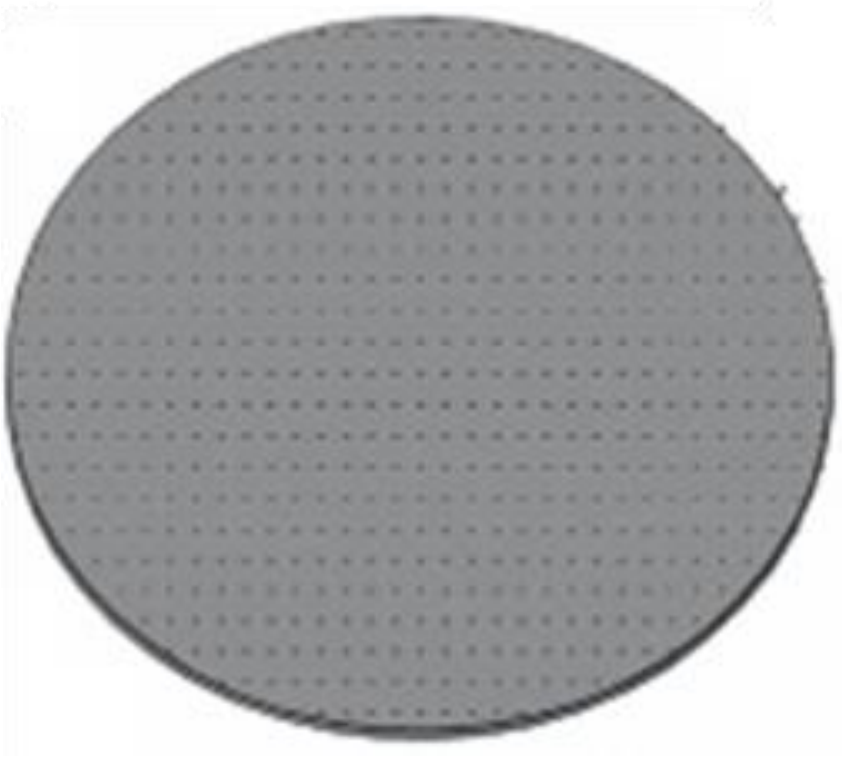

Figure 18. Porous plate distributor

3.2 Final bed design

Micro-fluidised beds channel could be of any geometrical shape, circular and square shaped bed channel are the most popular type of micro-fluidised found in industry and laboratories applications. Circular shaped channels provide a better axial uniform solid distribution because of their circular shape. However, square shaped channels provide a better flow visualisation as a result of their flat faced shaped channel. Square shaped channel was chosen for the present studies as it will enable a better visualisation of fluidisation behaviour in micro-circulating fluidised bed without distortion. The major difference between micro-scale and macro-scale flow is the importance of surface forces relative to volumetric forces. Base on this principle the boundary between the micro and macro-scale flow is considered to be 1 mm in the micro-fluidic field in general [174]. When the channel diameter is bellow 1mm the system is a micro-fluidised bed system, and if the channel diameter is above 1mm it is considered to be mini-fluidised bed system. Hence, this was the general reason for the choice of the bed dimension. In addition, this is also of practical nature as the workshop could provide us this as upper limit for fabrication. Our recent study has shown that adhesion and cohesive forces strongly influences the fluidisation characteristic in the micro-fluidised bed as they can postpone or even prevent fluidisation [175]. The design of the micro-circulating fluidised will evolve throughout the research project.

The first micro-circulating fluidised bed design was made by milling 1mm x 1mm cross-section channels into Perspex in the workshop to investigate the hydrodynamics of liquid-solid fluidisation at micro-scale. The bed was made of Perspex to enable to visualise the fluidisation behaviour and record them for offline analysis. The labelled photo of fabricated micro-circulating fluidised bed is shown in figure 19.

To make the face of the 1mm square cross-section channel milled into a methacrylate plate optically clear, first a very fine emery paper (a type of abrasive or sandpaper) was used to smooth the surface faces of the 1mm channel. This was done by moving the emery paper with light pressure against the bed surface to remove any marks from the surface. Then buffing wheel was used to polish the bed surface to get a clear finish (glass-like finish).

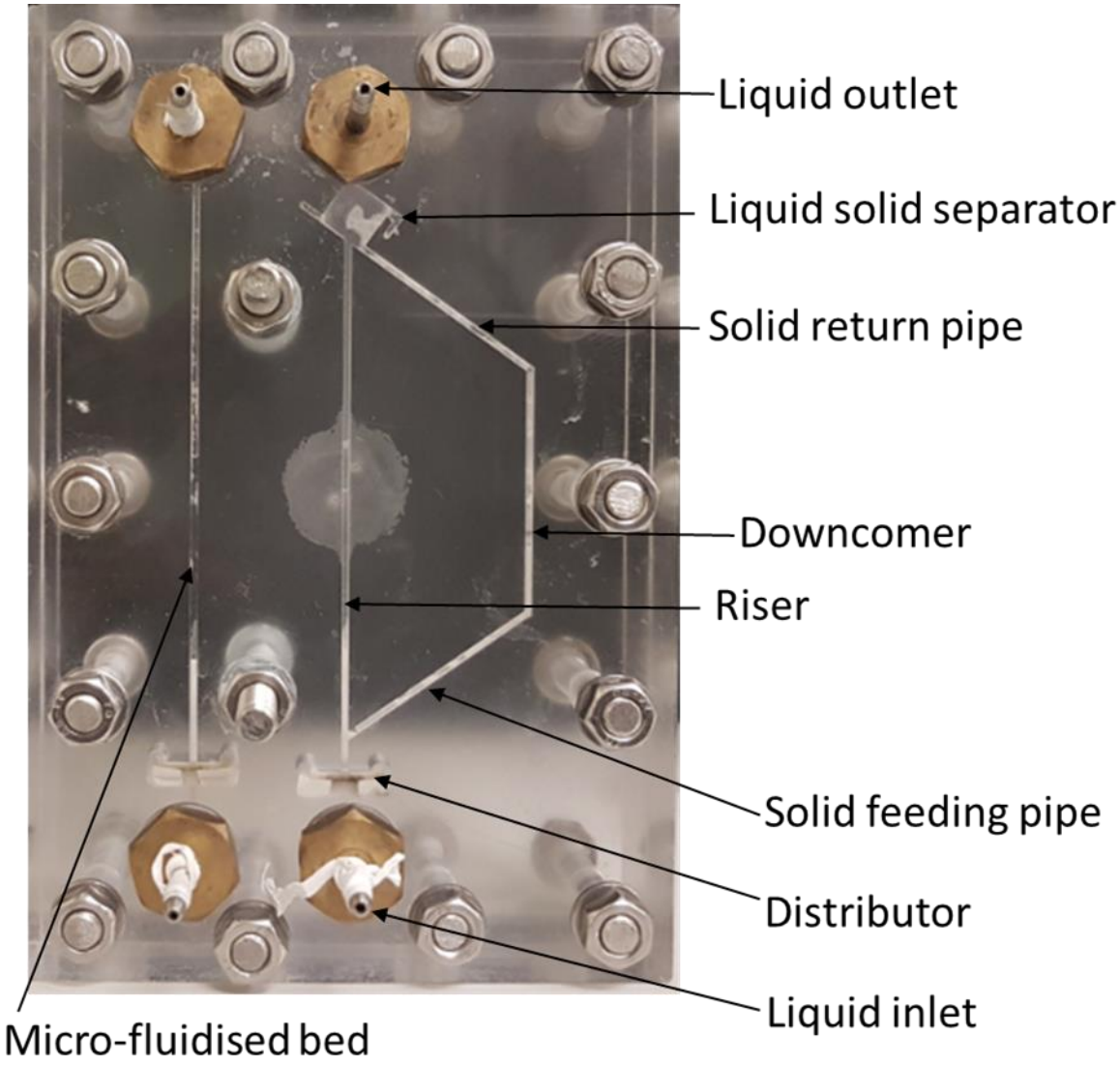

Figure 19: Schematic of a simple micro-circulating fluidised bed design

The micro-circulating fluidised bed consist of a riser column of 1mm square cross-section and 100 mm in height, a solid-liquid separator, a down comer acting as a particle reservoir, a solid return pipe, and a solid feeding pipe. At the base of the riser is the distributor (a 1.5 mm thick porous plate distributor with mean pore size of 21 μm) which prevents particles leaving the bed at the bottom and provides uniform flow distribution and stable fluidisation. The porous plate distributor are cheaper, simple to fabricate, easy to modify, promotes particle mixing, and provides enough pressure drop to ensure that the flow is not disturbed by the pressure fluctuation [11]. The liquid separator is a simple diamond-shaped expansion that enables the particles to be separated from the outflowing liquid.

3.3 3D printing technology in microfluidic

As previously mentioned microfluidic devices offer many benefits over conventionally reactors such as reduces dramatically the resources consumption, short time for analysis, significantly reduces waste and by products, low operational and capital costs, enhancing the percentage conversion and selectivity of chemical reaction, and intensification of heat and mass transfer which results in a more efficient and sustainable operation processes and helps protecting the environment [135, 136]. However, current fabrication methods such as soft lithography techniques for micro-moulding and bonding elastomeric materials, such as polydimethylsiloxane (PDMS) require much space to hold multiple pieces of equipment, are labour intensive, cause time wastage when making a change in design, and requires highly specialized skills [139, 176]. For scientific research, however, it is often more important to minimize the technological and temporal effort for device fabrication to quickly and easily adopt microfluidic devices to new demands and developments [140]. Fortunately, the rapid development of additive manufacturing technology in terms of resolution and speed is providing a solution to the problem [140, 141].

Additive manufacturing also referred as 3D printing is the process which fabricates three dimensional structures by adding layer upon layer under computer control [140, 141]. Compared with other microfabrication techniques, 3D printing requires little training outside of the ability to use computer-aided drafting software [142]. Fabrication of a simple microchip can be accomplished in 20-30 min, while a more complex microchip device of 2 mm sided and 120 mm in height could be printed in 5 hours [143]. Perhaps more importantly, 3D printing does not require dedicated microfabrication facilities and is cheaper than the instrumentation required for lithography approaches [144]. Figure 20 shows the fabrication process of microfluidic device using both additive manufacturing technology and conventional lithography technique.

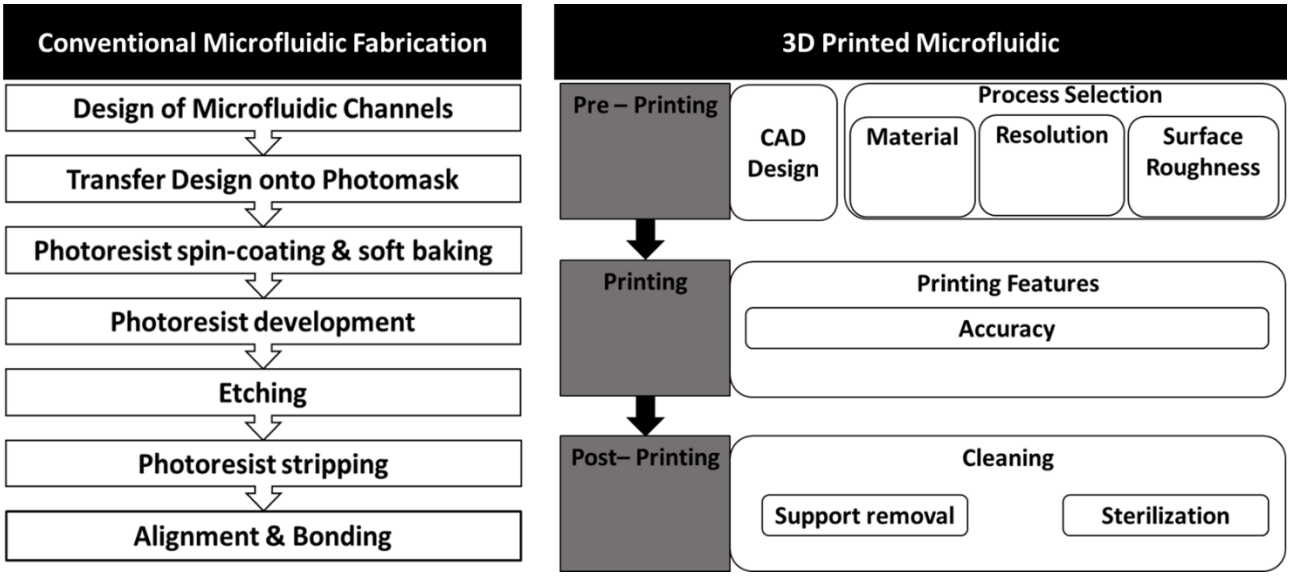

Figure 20. Comparison between Microfluidic fabrication using conventional lithography technique and 3D printing technology.

At the present investigation study additive manufacturing technology, digital light processing (Miicraft+ printer) and stereolithography (Form2 printer) were used to fabricate the micro-circulating fluidised bed to study the influence of bed geometry on the hydrodynamics of liquid-solid fluidisation in micro-channel. In digital light processing (DLP) and stereolithography (SLA) technique, 3D solid objects are created by joining material in a layer upon layer fashion using a liquid photopolymer resin by applying an ultraviolet (UV) laser or digital light projector until the physical part is complete. Form2 printer employs a UV light (155 µm size and 120 mW) to obtain each layer. For this printer, the printing time dependents on the layer size. While the Miicraft+ printer employs a digital micromirror device to project the entire layer geometry at once, and the printing time per layer is independent from the layer size, and the printing time per layer is constant irrespective the model size. The detailed 3D printer specifications are summarized in table 5.

Table 5. 3D Printer description

Printer name	Printing type	Maker	XYZ resolution	Build size (mm)
Form2	SLA	FormLabs	155 µm (xy), 25-200 µm (z)	125 x 125 x 165
Miicraft+	DLP	Miicraft	56 µm (xy), 30-100 µm(z)	43 x 27 x 180

3D printing fabrication design consist of four major steps: image design, image post processing, 3D printing, and post processing as shown in figure 21. First, 3D modelling computer program SketchUp is used to create a digital image of the structure to be made, which is then converted into stereolithography (STL) file format and transferred to the 3D printer apparatus, which

creates the 3D solid structure layer by layer until the desired solid object is completed. Finally support material are removed from the printed circulating fluidised bed and isopropyl alcohol or methanol was used to remove the excessive resin in the bed channels. Post processing is an important step as it enhances the printed CFB mechanical properties.

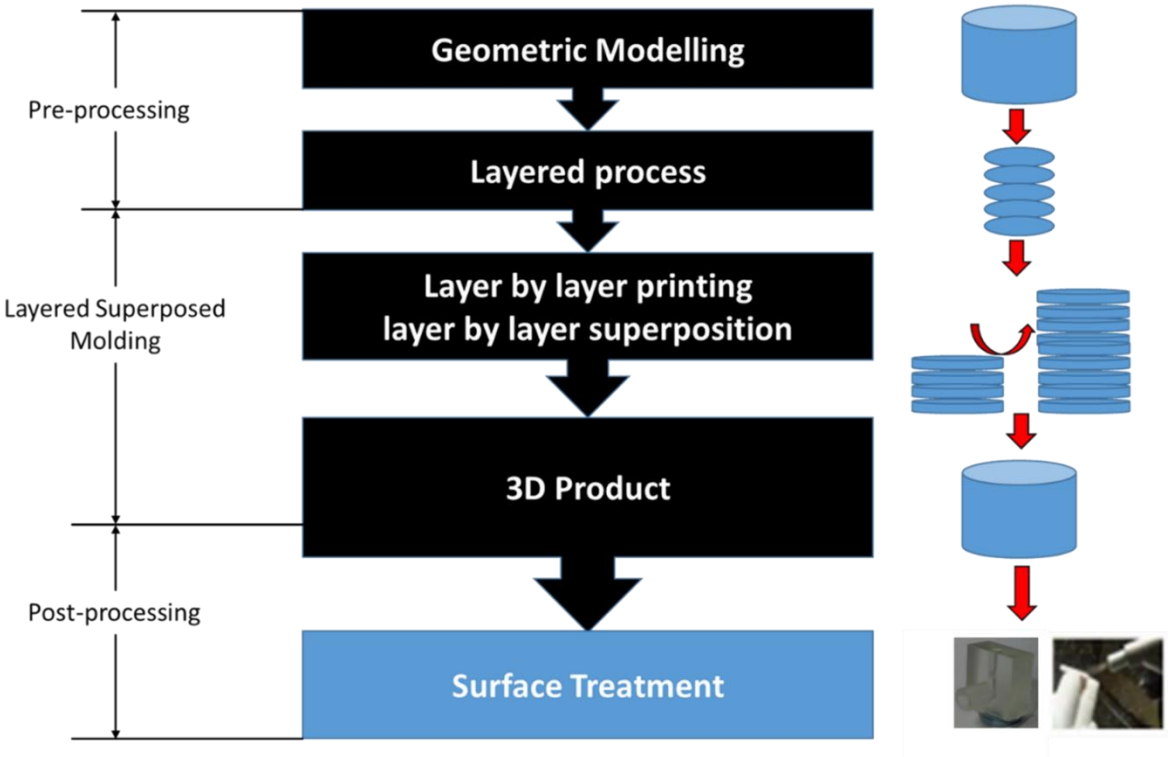

Figure 21. 3D printing process

The Miicraft+ printer was able to produce the micro-circulating fluidised bed within 6 hours. The Form2 printer was faster and allowed the production of up to four micro-circulating fluidised bed at the same time within just 8 hours. Miicraft+ prints had the most visible layers while Form2 prints had the smoother surface finish. The Miicraft+ and Form2 printer used very similar clear photopolymer resin. The clear resins are a mixture of methacrylic acid esters and photoinitiator. The Miicraft+ resin was purchased from Young Optics Europe GmbH, while the Form2 resin was purchased from FormLabs. After printing process, Form Wash was employed to clean the circulating fluidised bed. Form Wash uses isopropyl alcohol to remove the liquid resin from the bed channel and surface, the cleaning process was approximately 20 minutes. Once washing was completed Form Cure was used to cure the bed for at least 40 minutes. This was done to improve prints strength and performance. Once the bed was completely cured, flush cutter was used to remove supporting material from the printed circulating fluidised bed.

3.3.1 Distributor for the 3D printed bed

As previous mentioned, the liquid distributor is one of the most important components of a circulating fluidised bed. Hence, one major task was to decide which type of distributor model can provide stable and uniform liquid distribution and support the particles in a 3D printed micro-circulating fluidised bed. There are several types of distributor models which are able to provide those important qualities, however, both the Form2 and Miicraft + printer are not capable to printing some of these distributors due to ultra-fine resolution. Hence, it was important to analyse each potential distributor model to see which of them could be printed using the Form2 and Miicraft+ printer. After completing these analysis, the potential distributor models were tested to choose which one would best support the bed of particles and provide uniform fluidisation into the bed. Figure 22 illustrates the type of questions considered in order to choose the suitable distributor model to be implement in the micro-circulating fluidised bed.

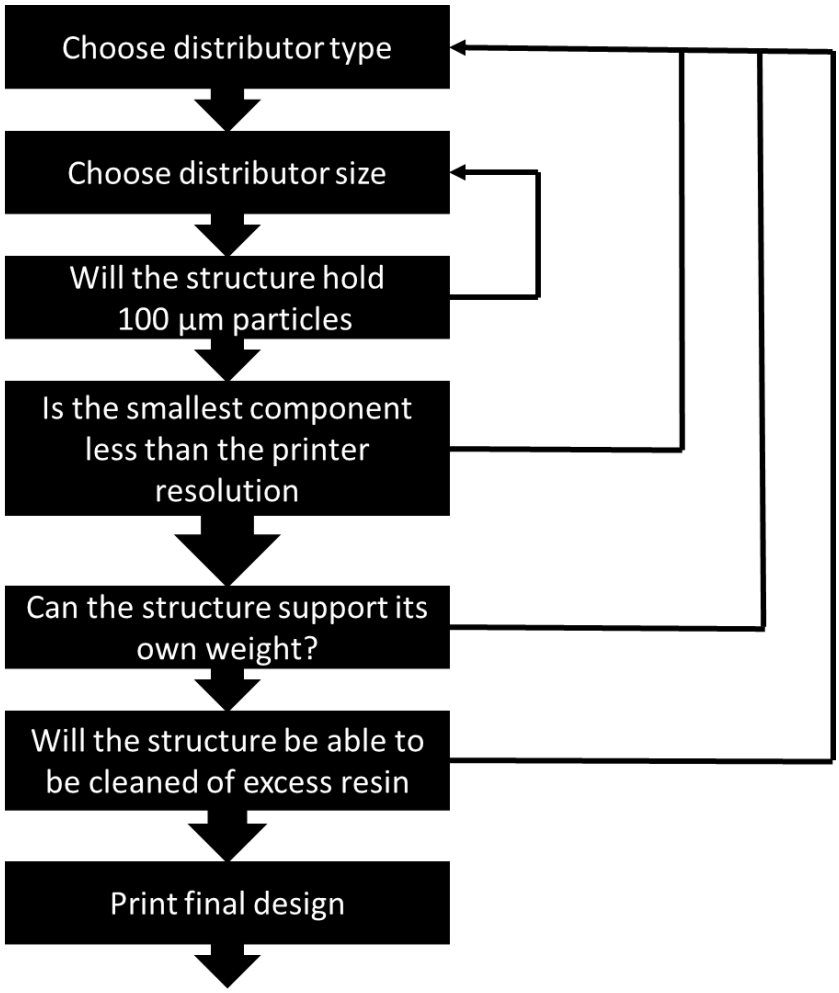

Figure 22. Decision rout for liquid distributor design

3.3.1.1 Perforated plate distributor

This type of distributor could be suitable for the 3D printing micro-circulating fluidised bed as it provides a good balance between liquid distribution and structural integrity. The distributor hole size can easily be modified, and they are easy to fabricate compared to others type of distributor. Possible disadvantage may be the lack of structure to support the bed material

3.3.1.2 Mesh

A wire mesh could potentially be suitable distributor model for the micro-circulating fluidised bed as it possesses a very fine orifices capable of support particles and prevent them leaving the bed at the bottom. However, as the wire mesh distributor comprises of very fine components for a 2 mm conduit the distributor components would be beneath the printer resolution. For that reason, the wire mesh was dismissed.

3.3.1.3 Pillars distributor

The pillars within the channel could be arranged in horizontal or vertical direction. Horizontal arranged pillars could be of different sizes and with different space between the pillars. The main drawback with horizontal pillars is that very fine pillars can be subjected to breakage, as they may not be able to support the weight of the particles. Vertical pillars distributor generate gaping holes between the pillars, which could be blocked in case of excess resin, making this type of distributor unsuitable for this study. Horizontal pillars distributor of different dimension will be tested to see if they could be viable option.

3.3.1.4 Ring baffles distributor

The baffles distributor could be a good candidate for the micro-circulating fluidised bed as it has a very good liquid distribution performance characteristics especially at low flowrate. However, a baffles ring is not able to serve as a distributor on its own as it is incapable of supporting the solid particles before fluidisation, because of their thinner strands when compared to the micro-channel diameter. For a 2 mm conduit, the components of the distributor will be too small to support the particles in the bed. An example on a baffle distributor is shown in figure 23.

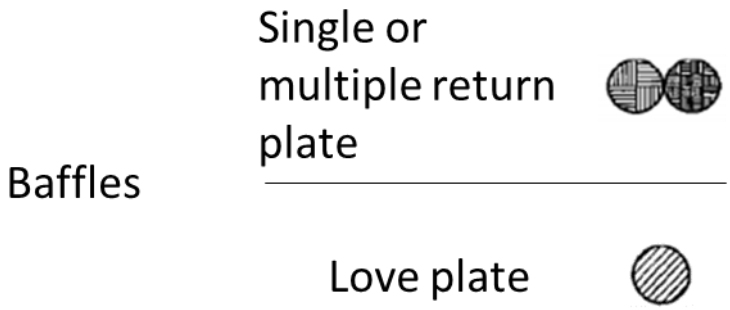

Figure 23. Baffle distributor model [177]

3.3.2 Printing test

Printing tests were performed to help determine the best suitable distributor model to the solid-liquid micro circulating fluidised bed. Here two types of distributor model, the perforated plate and the horizontal pillar distributor were studied. As the resolution is one of the key factors which indicates the printing quality, tests were done in order to find if it was possible to print objects at the exact quoted resolution, and to determine if the printed distributor could support the weight of the bed material. Additional tests were also carried out to determine the optimal curing time to print the micro-circulating fluidised bed, and the optimum layer thickness.

3.3.2.1 Printing resolution

The Miicraft printer resolution is quoted to be 56 µm in the x and y direction by its maker [178]. So as to confirm if this quoted resolution could be achievable several printing tests was performed. Here, two types of distributor model, the perforate plate distributor of 1 mm in perforation depth and horizontal pillar distributor of 1 mm in height were printed. For both prints the layer thickness was 100 µm. The perforations and the pillars diameters for the test were chosen to be 200, 150, 100, 70, and 60 µm as shown in figure 24 in order to confirm if it is possible to achieve the quoted resolution.

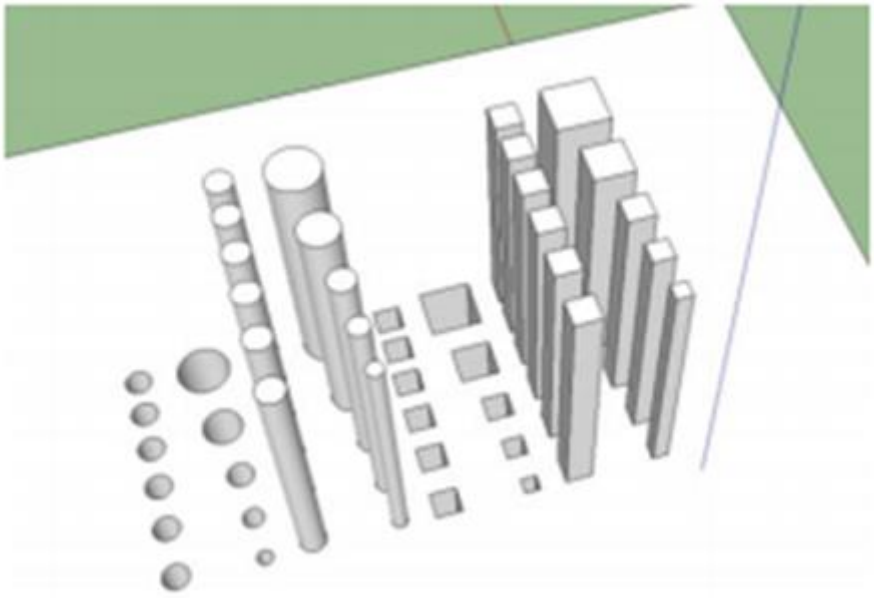

Figure 24. Perforated & pillar distributor

The investigation results are displayed in figure 25. From the results it can clearly been seen that both the pillars and perforate plate distributor have not been successfully printed. It can be observed that there is not clear perforation visible and some pillars are distorted. These observation are similar to that reported by Shallan and co-workers [156], which found that only perforate plate distributor of 300µm could be successfully printed without imperfections and that only pillars distributor above 250 µm could be printed without warping.

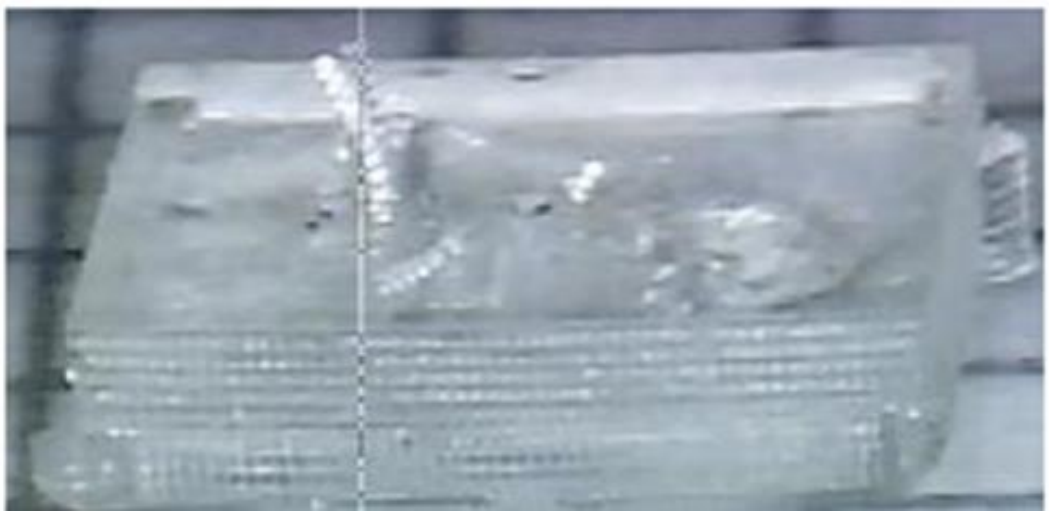

Figure 25. Unsuccessfully prints: perforated plate and pillar distributor with 100 µm layer thickness, and 1 mm pillar height and perforation depth.

As is well known in the 3D printing research community, one simple method of improving the printing resolution is by reducing the layer thickness of the material to be printed. Hence, here a number of printing tests were carried out with 30µm layer thickness in order to increase the printing quality. However, the test was not successful, as the layer was too thin and fail to attach properly to the build plate. So, additional tests were carried out at layer thickness of 50 µm to find the optimal layer thickness as displayed in figure 26. In these tests, pillars of 60, 80, 100, 150, 200, and 250 µm diameter with perforation of 60, 80, 100, 150, 200, and 250 µm diameter were printed and the results is shown in figure 27 and 28. In this test, the optimal resolution between the pillars were also evaluated. The space between the pillars were 50, 60, 70, 80, 90, and 100 µm.

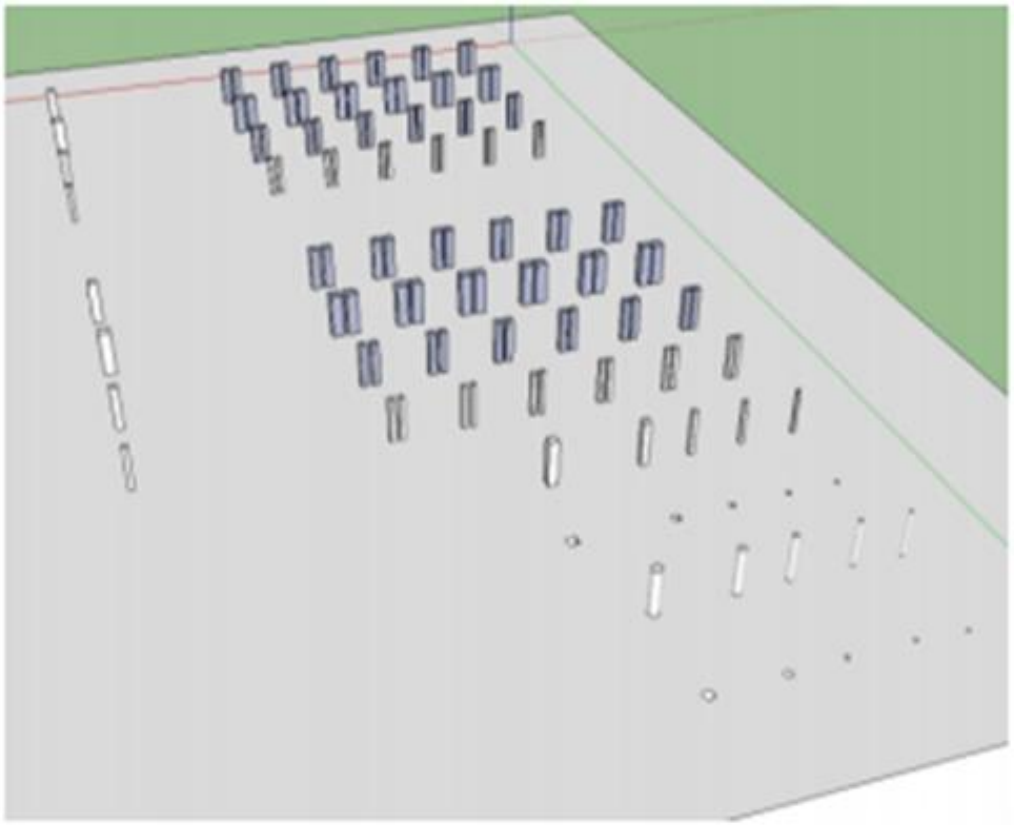

Figure 26. Schematic of perforated and pillar distributor

From figure 27, it can be notice that the test was successful as most pillars were printed without warping. This confirms that the printing resolution improves when the layer thickness is reduced from 100µm to 50µm. The Miicraft+ printer also managed to print the perforated distributor as shown in figure 28, but these were not as perfectly printed as the pillars in figure 14. So, the optimal layer thickness for the 3D printing experiment was chosen to be 50 µm.

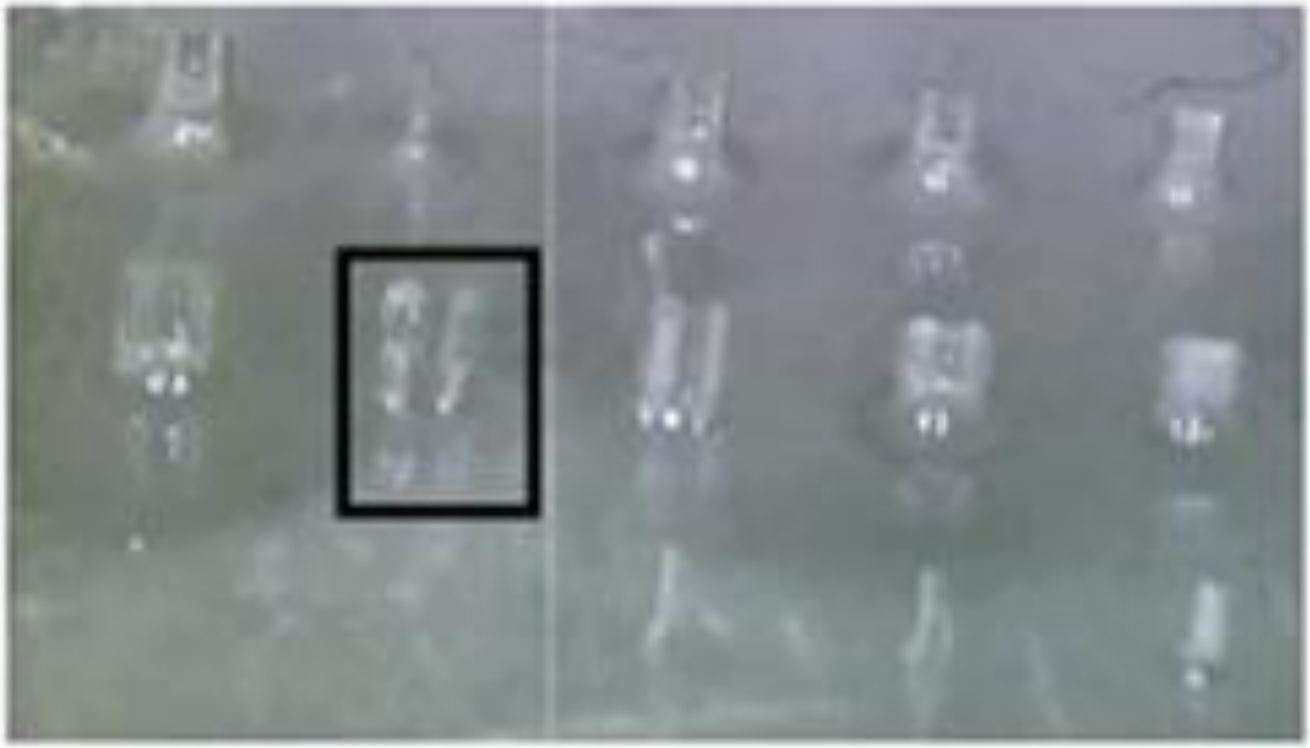

Figure 27. Printed pillars of 60, 80, 100, 150, 200, and 250 µm diameters with 50 µm thickness layer

Figure 28. Printed perforated plate distributor of 60, 80, 100, 150, 200, and 250 µm diameters with 50 µm thickness layer

3.3.2.2 Pillar distributor

Two types of pillar distributor combine pillar and cross-linked pillar were tested in this investigation. These two types of pillar distributor were investigated as it was thought they can potentially provide stable and uniform flow distribution in the system and support the bed material.

3.3.2.3 Combined pillars

Several numbers of tests were carried out to find the most suited pillar design for this study. The diameters of the tested pillars were 50, 100, 150, 200, and 250µm with layer thickness of

50µm, as it was found to be the optimal layer thickness during the printing resolution test. A schematic of combined pillar is displayed in figure 29. The space between the tested pillars were 60, 80, 100, and 150 µm.

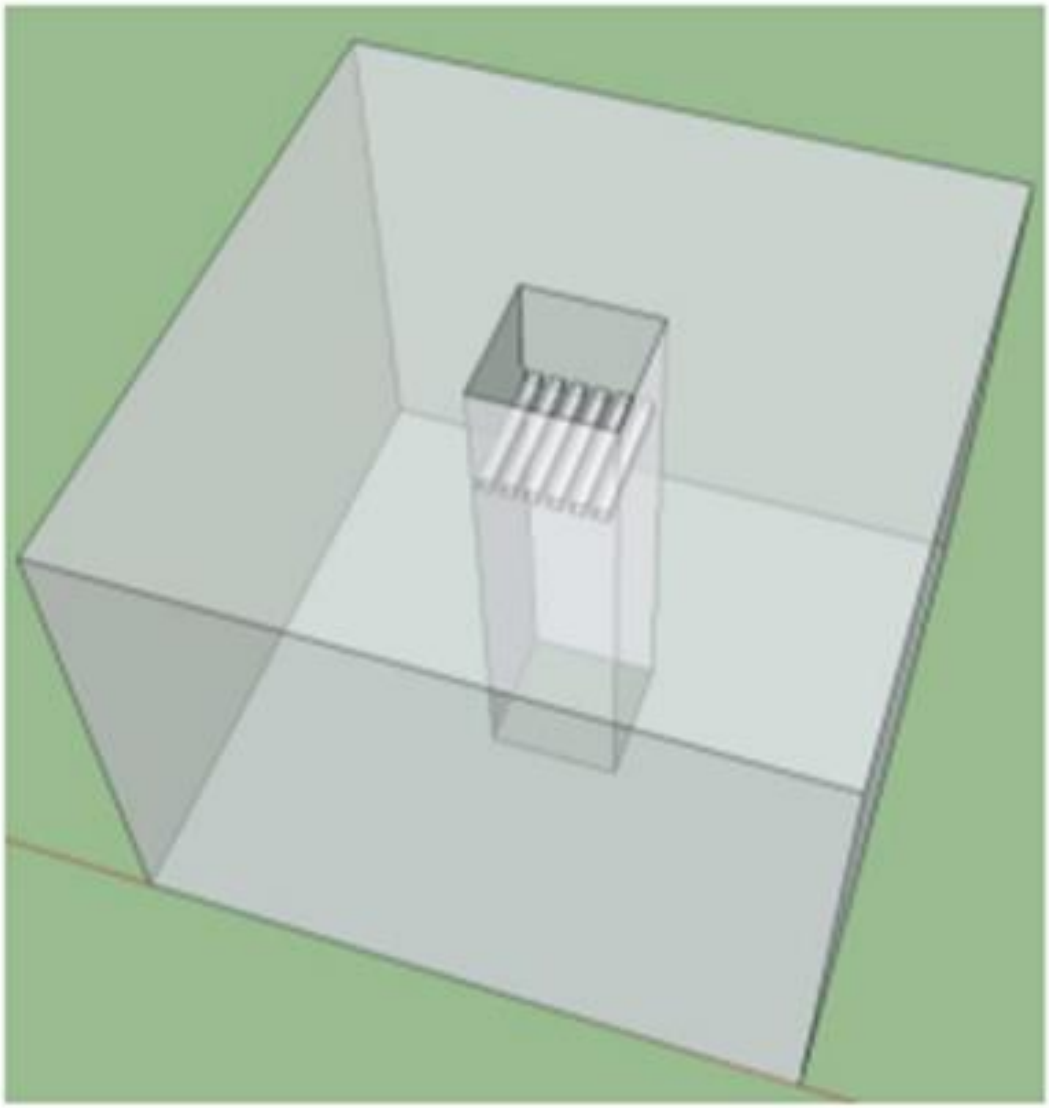

Figure 29. Combined pillar

Figure 30 -33 shows the printed combined pillars. From figure 30, it can be notice that the printed pillars are warped, and this made them unusable. This warping problem occurred as the pillars were too close to each other with 60 µm spacing between them.

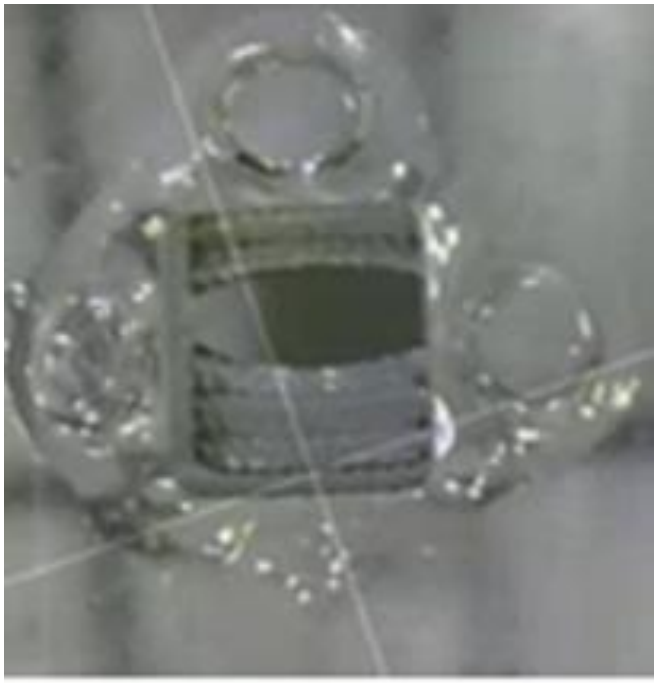

Figure 30: warped pillar of 50 µm diameter with layer thickness of 50 µm, and 60 µm space between pillars.

Figure 31 displays a printed joined pillar. Joined pillars could potentially provide even liquid distribution into the bed and support the fluidised particles as there are additional pillars in the channel. However, the Miicfraft+ printer fail to reproduce this type of pillar design after several attempts. It was extremely difficult to replicate this design consistently. Thus, it was concluded that this type of pillar is not suitable for this project.

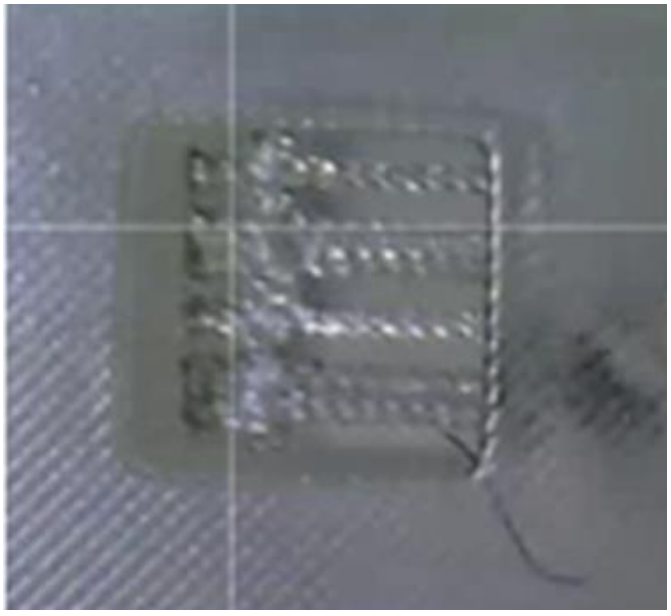

Figure 31. Joined pillars of 100µm diameter with layer thickness of 50 µm and 80 µm gapping between pillars

Figure 32 displays a successfully printed pillar of 100 µm in diameter with 100 µm spacing. However, it was also hard to replicate this printing design after several attempts as the pillar diameter were too thin resulting in warped pillars for most test, making them also not suitable for this study.

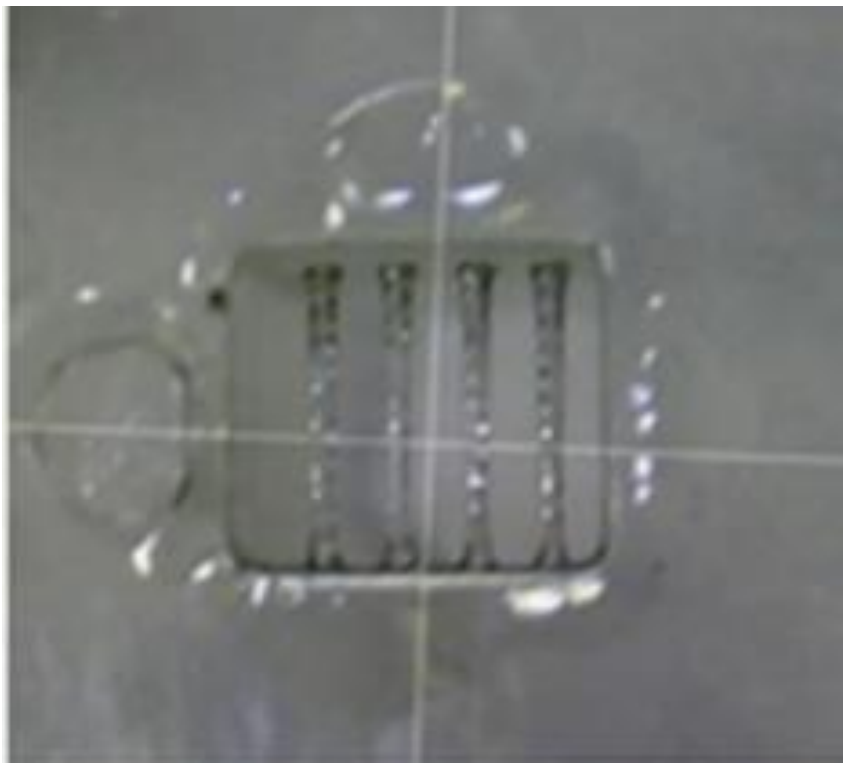

Figure 32. Successfully printed pillar of 100 µm diameter with layer thickness of 50 µm and 100 µm gapping between pillars. This design could not be replicate

Figure 33 illustrates the successfully printed pillar of 150 µm in diameter with 150µm gaping between pillars. From the printed distributor in figure 33 it can be observed that one of the pillars is attached to the wall of bed, nevertheless, this problem can be solved by employing multiple layers of pillars. From figure 33, it is also observed a small volume of resin on top of the printed channel which can easily be removed with isopropyl alcohol or acetone during post processing stage. Overall this printing design meet all the requirement for this study as it produced the better pillar distributor, and was easy to replicate without deformation, and more important was able to support the particles as shown in figure 34a and the 150 µm space between pillars will enable particle suspension (165 and 196 µm glass particles) as shown in figure 34b.

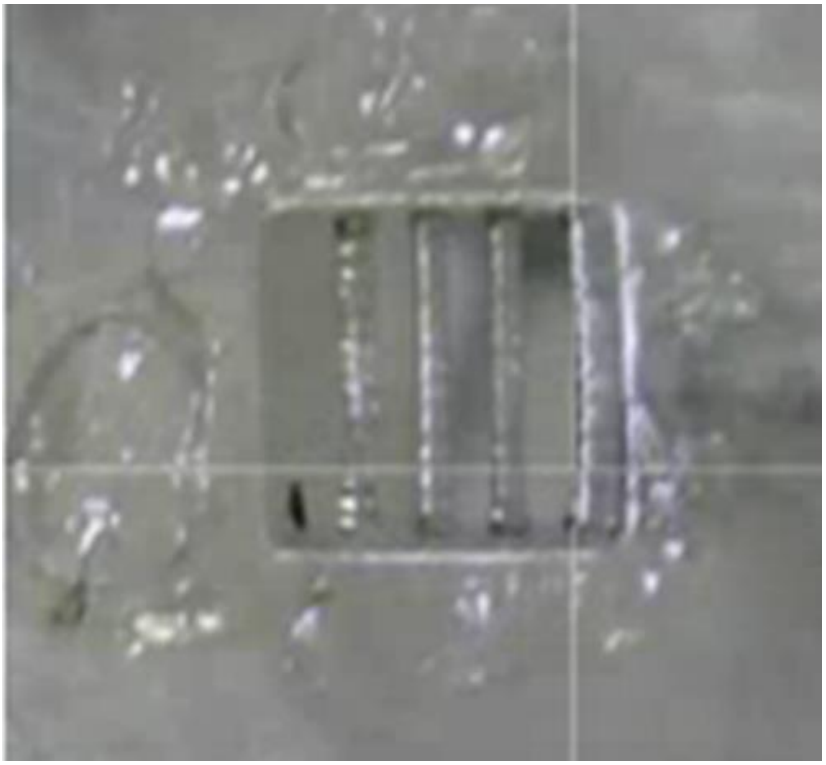

Figure 33. Successfully printed pillar of 150 μm diameter with layer thickness of 50 μm and 150 μm gapping between pillars. The design was easily replicated without warping

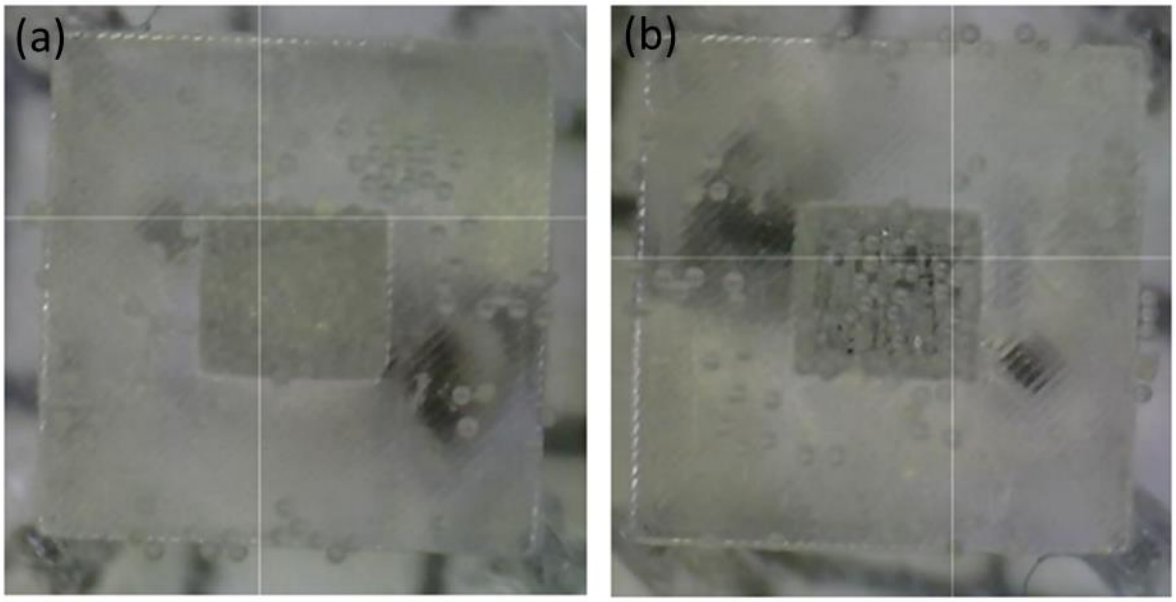

Figure 34: (a) Pillar distributor supporting the bed material. (b) Particles suspension in the channel.

3.3.2.4 Cross linked pillars

Crossed linked pillars were also tested in this study. This type of distributor design could potentially offer more support to the bed material as there is an increase in the number of pillars in the channel and more importantly the space between pillars in the channel is very much reduced as shown in figure 35.

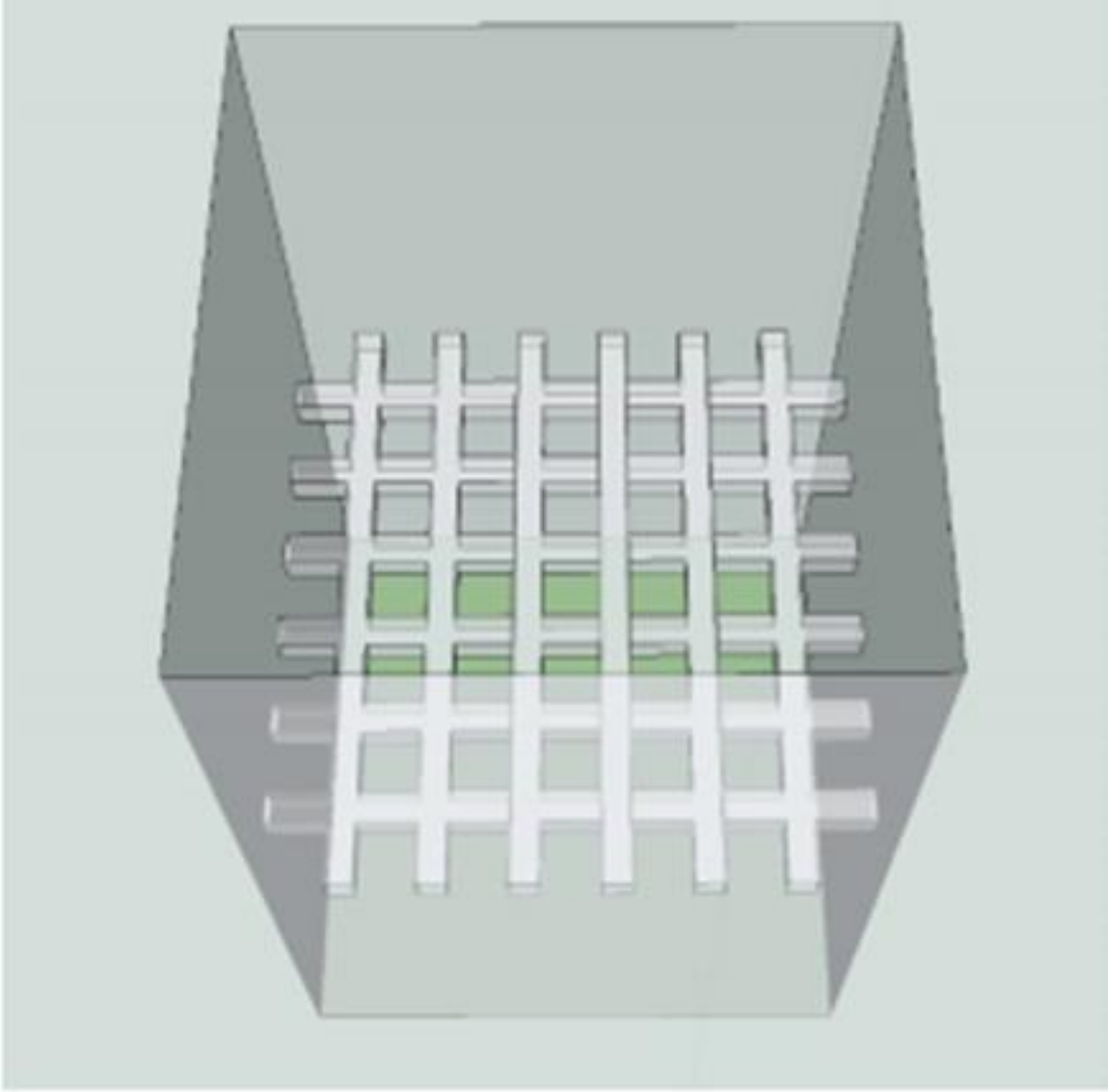

Figure 35: schematic of cross-linked pillars distributor of 150 μm dimeter with 50 μm layer thickness

Figure 36 illustrates the printed cross linked distributor. The distributor appears to be completely blocked by the cured resin preventing liquid passing through it. This problem happened because the gapping between the pillars distributor were too small, causing resin to

pool inside the channel, this resin became trapped in the channel as there were no holes to allow the resin to drip out, so the resin cured and blocked the channel making this type of distributor design unsuitable for this study.

Figure 36. Printed cross-linked distributor of 150 µm dimeter with 50 µm layer thickness

3.3.3 Cure time

One of the key parameters which influences the printing quality is the curing time per layer. Incorrect curing time will result in warped and blocked print. Therefore, preliminary test was conducted to find the optimal curing time to print the micro-circulating fluidised bed. The tested cure time were 6, 7, 8, 9, 11, 14 seconds. The layer thickness was 50 µm in all the experimental test. The successfully printed bed was achieved with curing time of 8 seconds. In those tests it was found, when the curing time per layer was shorter than 8 seconds the bed suffered from under cure problems and the bed was printed smaller than expected, in some cases the printed bed fell and damaged the resin tray. In the other hand a curing time per layer longer than 8 seconds resulted in loss of details and blocked print as shown in figure 37b

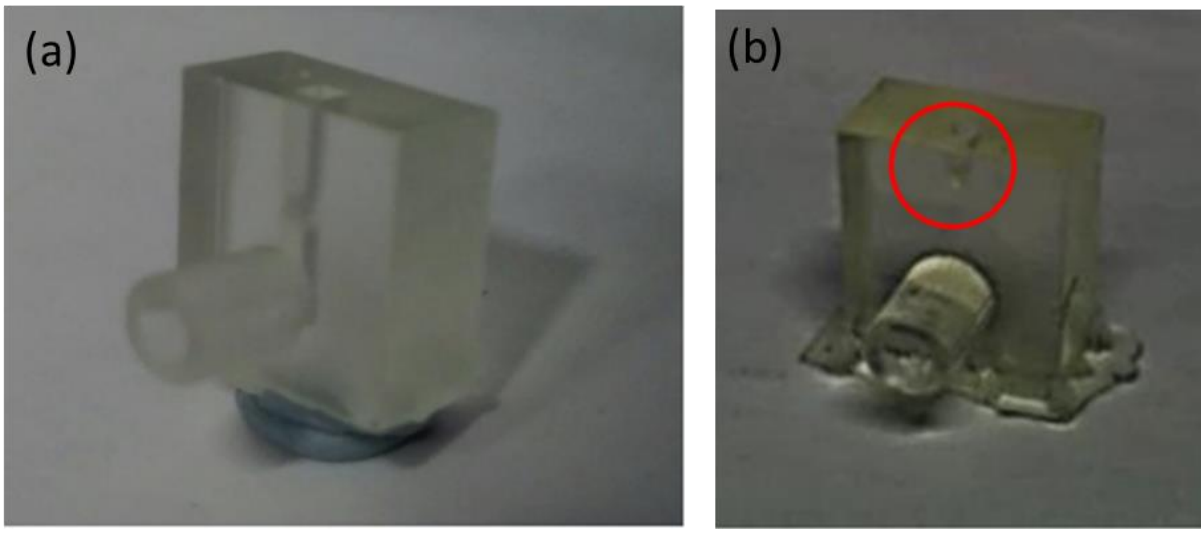

Figure 37: (a) successfully printed bed, curing time per layer was 8 seconds. (b) Unsuccessful print with blocked channel. Curing time per layer was 11 seconds

3.3.4 Optimum number of layers

Preliminary tests were conducted to determine the optimum number of layers for the circulating fluidised bed. From these tests it was discovered that a single layer pillar distributor was not enough in order to achieve even fluidisation across the bed, as some parts of the bed became defluidised during the experiment and blocked part of the channel. Hence, a multiple layer plate distributor was employed in this study as shown in figure 38. This type of distributor design was found to promote equal fluidisation across the bed over the range of operating conditions. Furthermore, the double layer pillar was able to support the bed material, and prevented particles leaving the bed at the bottom. Excessive loss of particles decreases the solid inventory in the system, and this may postpone the critical transition velocity from conventional to circulating fluidised bed regime. It was surprising to note that additional layer (three and four layer) delivered the same result. So, there was no need to employ three- or four-layer pillar distributor in this study in order to save printing time.

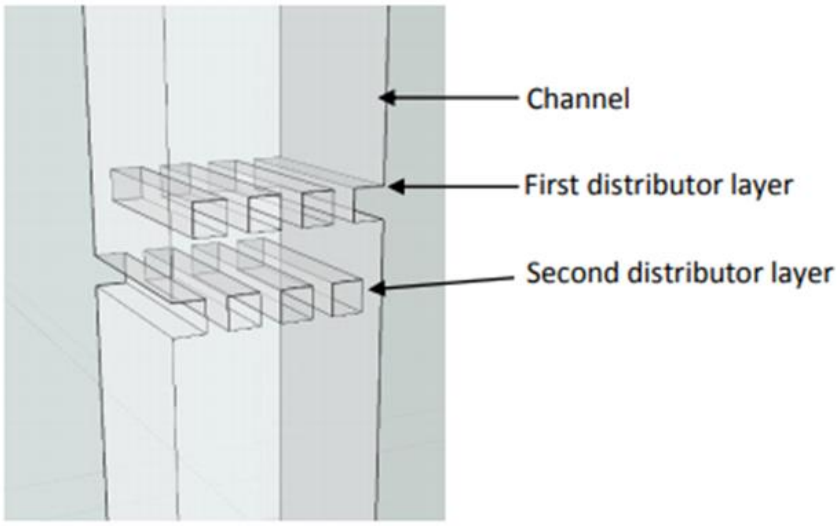

Figure 38. Multiple layer pillar distributor

3.3.5 Printing multiple channel at once

In this experimental research, multiple channels were printed simultaneously instead of printing them one by one. Printing multiple channels in a single print was more convenient as it was found to accelerate printing production. The Miicraft+ printer was able to produce 12 channels within 3-4 hours and that saved significant amount of time as it was possible to conduct multiple test per day. A schematic of multiple test which were printed simultaneously is given in figure 39.

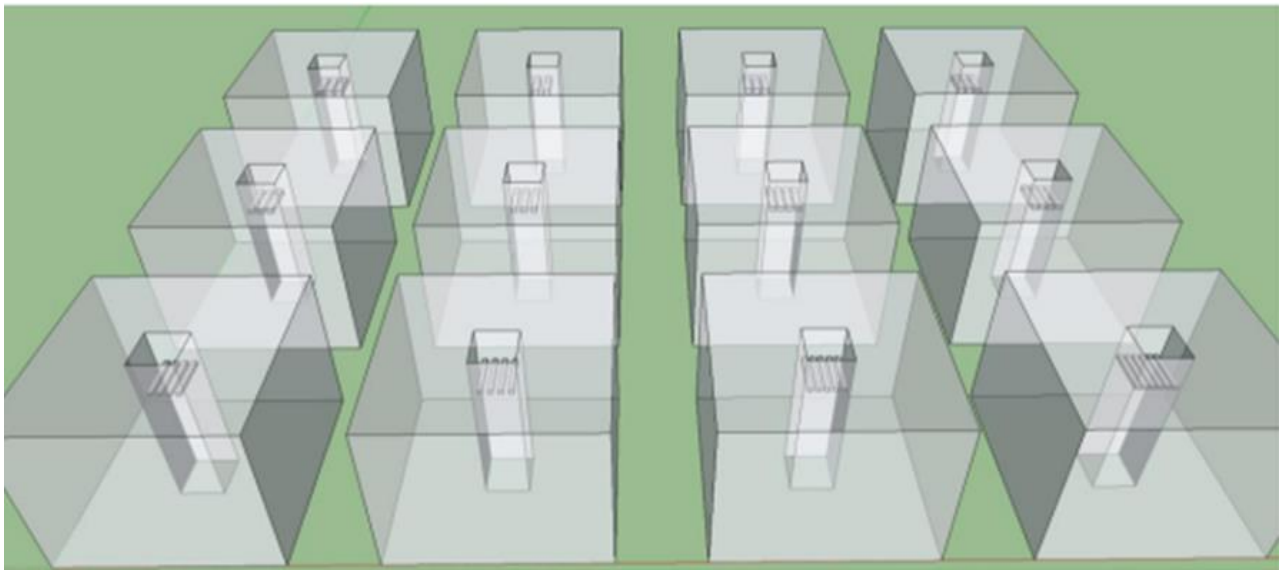

Figure 39. Schematic of multiple channel per print

All the above printing studies were also done for form2 lab, and the results were approximately the same.

3.3.6 Printing problems

Table 6: Printing troubleshooting

Problems	Problem details	How to fix
Prints not adhering to the build plate	During printing process, the 3D printer software generates supporting material to ensure prints sticks properly to the build plate preventing sagging due to gravity. In some cases, this supporting material fails to adhere to the build plate due to speed, uneven build surface, or cooling problems resulting in print falling damaging the resin tray.	• Clean the build platform • Level the build platform • decrease printing speed • Decrease height of first layer • Replace the film module • Pre-heating resin before printing • Roughen bed and build plate surface
Warped prints	In some printing experiments, printing object warped due to thermal deformation and lack of support making them dysfunctional.	• Make sure printing object is well supported • heat build plate • heat enclosure • clean build surface & degrease substrates
Small features fail to print	On some occasion the printer fails to print smaller part of the circulating fluidised bed correctly due to wrong set up	• Have a look at the slicer setting • Redesign the part • Save model as single body
Resin blocking problem	The pillar distributor was blocked by cured resin as the gap between the pillar was too small making them not fit to be used	• Increase the gap between pillars • Use more suitable resin • Lower printing speed
Poor Surface quality	The surface of printed bed shows a wavy pattern. This issue mainly appeared due to incorrect setting	• Check the settings • Lower the printing speed • Decrease the layer height
Hard to remove supporting structure	In few occasions it was hard to remove the supporting structure from prints after the post-process due to fused support structure	• Reduce the percentage of supporting material • Reduce the supporting structure diameter • Increase the space pattern
delamination	Parts of cured prints suspended in the resin tank due to dirty surface, issues with support structure	• Clean dirty surface • Get rid of cured resin and failed prints in the tank

3.3.7 Final 3D printing CFB design

The final design chosen to study the influence of bed geometry on the hydrodynamics of liquid-solid micro-circulating fluidised bed is shown in figure 40. The micro-circulating fluidised bed consist of a riser column of 2 mm square cross-section and 100 mm in height, a solid-liquid separator, a down comer acting as a particle reservoir, a solid return pipe, and a solid feeding pipe. At the base of the riser is a 2-layers pillar distributor (150 μm pillars diameter with 150 μm gaping between them) which prevent particles leaving the bed at the bottom and provided uniform liquid distribution. This design was easy to replicate without warping, prevents particles leaving the bed at the bottom, and most important provides uniform liquid distribution across the bed.

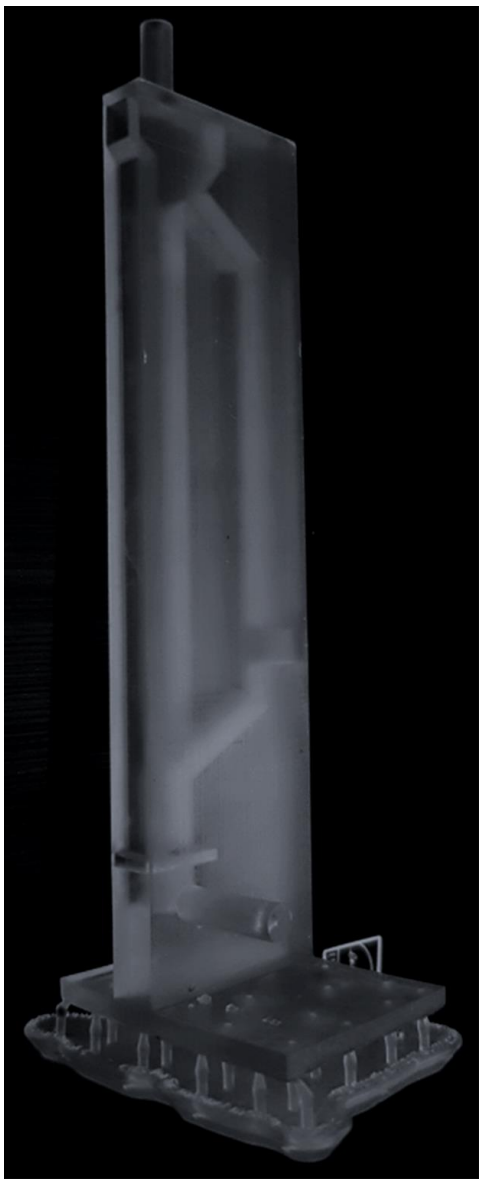

Figure 40. 3D printed Circulating Fluidised Bed

3.4 Minimum fluidisation velocity

The minimum fluidisation velocity (U_{mf}) and the terminal particle velocity (U_t) are important parameters of fluidisation phenomenon for understanding the hydrodynamics characteristics of fluidisation of solid-particles and are essential for fluidised bed operation and design [90, 179]. Minimum fluidisation is the minimum superficial liquid velocity where solid fluidisation is achieved or could also be described as the velocity where the overall fluidised bed pressure drop equates to the bed weight [180]. The minimum fluidisation velocity phenomenon happens as a consequence of the force of the liquid on the solid particles. U_{mf} depends on factors such as size, density and polydispersity of the particles. I.e. the density directly alters the net force of gravity acting on the particle, and hence the minimum velocity needed to lift a particle. When the bed is fluidised solids move in a disorganised way and the distance between solids gets bigger with increases in superficial liquid velocity resulting in the bed height to increase.

3.4.1 Minimum fluidisation velocity measurement

During fluidisation phenomena the minimum fluidisation velocity could be found by observing visually the bed height variation against the superficial liquid velocity or by measuring the pressure drop difference in the fluidised bed.

3.4.1.1 Pressure drop

A pressure transducer, which is installed on the bed wall at inlet and outlet, could provide the overall pressure drop along the micro-circulating fluidised bed between the two pressure transducer taps [22]. The plotting of pressure drop across the system versus the liquid velocity, shows two linear zones whose intersection indicates the minimum fluidisation velocity (U_{mf}) 20]. However, the pressure drop across the micro fluidised bed was not measured in this study, because it was hard due to very fine resolution required, the pressure drop across the bed is only of the order of few pascal.

3.4.1.2 Visual observation

One method to determine the minimum fluidisation velocity is to observe visually the flow across a transparent bed wall. Minimum fluidisation velocity is determined as the liquid velocity where the bed first starts to expand.

3.4.1.3 Extrapolation

In extrapolation technique minimum fluidisation velocity is obtained by extrapolation of linear relationship between the superficial liquid velocity and ratio of bed expansion. Minimum fluidisation velocity values were obtained from the plot of bed height expansion vs superficial

liquid velocity. The point of intersection of the expansion line with vertical line for packed bed height was taken as minimum fluidisation velocity [59, 76].

3.4.2 Minimum fluidisation velocity measurement in the present study

In the present experimental study the minimum fluidisation velocity required to achieve fluidisation was by obtained by observing visually the bed height expansion and also by extrapolation of linear relationship between the superficial liquid velocity and ratio of bed expansion as measuring pressure drop is difficult due to very fine resolution required (the pressure drop is only of the order of several Pa). The height of the expanded bed was obtained by using a Euromex Nexius trinocular microscope to take pictures. ImageJ [23], an image processing and analysis computer programme was used for off-line analysis to determine the bed height as a function of superficial liquid velocity. Minimum fluidisation velocity values were obtained from the plot of bed height expansion vs superficial liquid velocity. The point of intersection of the expansion line with vertical line for packed bed height was taken as minimum fluidisation velocity. Typical plots of relative bed height as a function of superficial fluid velocity are given in figure 41 (additional figures 109 to 121 are given in appendix).

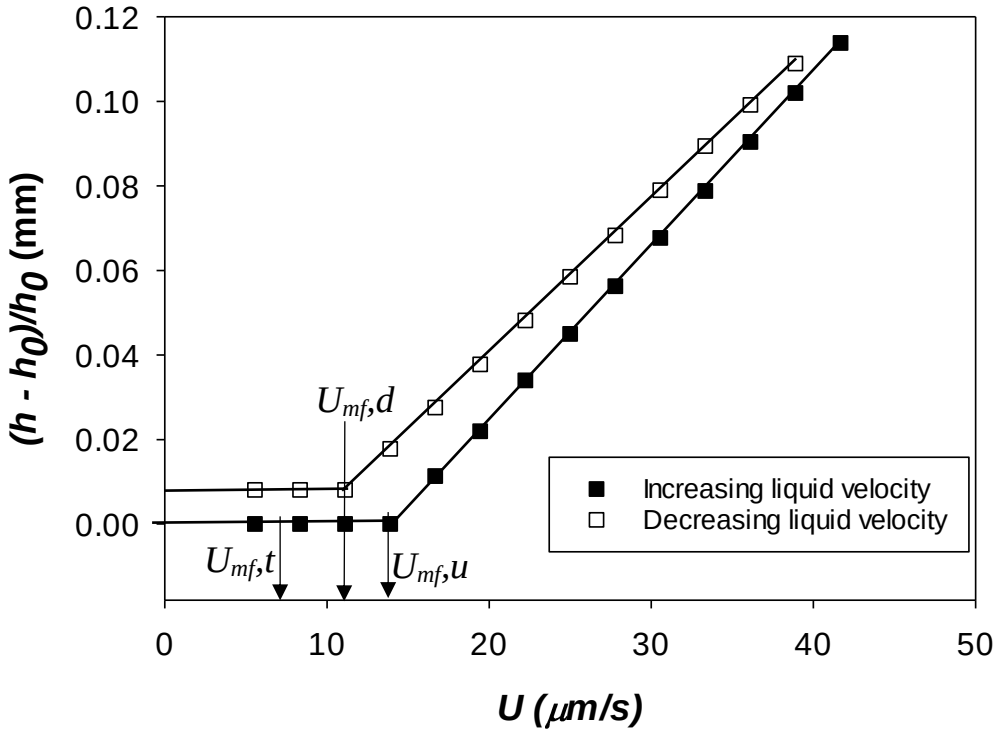

Figure 41. Relative bed height as a function of superficial liquid velocity, U, with increasing liquid velocity ($U_{mf,\,u}$), and decreasing liquid velocity ($U_{mf,\,d}$) for 26 μm glass microparticles in 1mm^2 micro-bed. Error are not visible in the graph as they are smaller than the symbols.

Step change in bed height on fluidisation was not observed in figure 41, this could be due to the extrapolation technique used to determine the minimum fluidisation velocity, instead to more reliable pressure drop measurement technique, as measuring the pressure drop in the micro fluidised bed system was difficult due to very fine resolution required (pressure drop across the bed was only of the order of few pascal).

3.4.3 Predicted minimum fluidisation velocity

Prior to the start of each experimental set, it was important to predict the minimum fluidisation velocity and terminal particle velocity, to determine the experiment starting point and the maximum liquid velocity at which particles remain in the fluidized bed. The predicted particle terminal velocity and minimum fluidisation velocity were used as the experimental starting point. The Ergun Equation and pressure drop equation, equations 12 and 13, were used to predict the minimum fluidisation velocity, as it has been shown to be accurate experimentally [90, 181]. The voidage was estimated to be 0.40 ± 0.01. The Stokes particle terminal velocity for the laminar regime (Equation 18), was used to predict the particle terminal velocity prior to the start of each experiment set to determine the range of velocities which was used in each experiment. The calculated particle terminal velocity was converted into a volumetric flow rate and this was done by multiplying by the bed cross sectional area. The calculated particle terminal velocity and corresponding volumetric flow rate for the current research investigation are shown in table 7 and 8.

Table 7. The calculated terminal particle velocity for Glass Particle

Particle Diameter (μm)	U_t (μm/s)	Volumetric Flow rate (μl/min)
26	580	34.73
30	741.7	44.46
35	1000	60
58	2770	166
82	5542	332.5
98	7915	475
115	11000	660
165	22438	1346
196	31661	1900

Table 8. The calculated terminal particle velocity for PMMA Particle

Particle Diameter (μm)	U_t (μm/s)	Volumetric flow rate (μm/min)
23	60.7	3.6
35	100	6
41	189.3	12
58	370	24
115	1466	900

3.4.4 Estimation of surface forces

The major difference between micro-fluidised beds and macro-fluidised beds flows is the importance of surface forces relative to the volumetric forces, i.e. gravity [61, 182]. Equation 19, the acid-based theory developed by Oss, Chaudhury and Good [183] can successfully predict particle adhesion to the walls of micro-fluidised beds and its absence as a function of fluidising liquid-solids materials involved. The free interaction energy when two different solid surfaces are submerged in a liquid could be expressed as:

$$\Delta G_{1w2} = \left(\sqrt{\gamma_1^{LW}} - \sqrt{\gamma_2^{LW}}\right)^2 - \left(\sqrt{\gamma_1^{LW}} - \sqrt{\gamma_w^{LW}}\right)^2 - \left(\sqrt{\gamma_2^{LW}} - \sqrt{\gamma_w^{LW}}\right)^2 + 2\left[\begin{array}{c}\sqrt{\gamma_w^+}\left(\sqrt{\gamma_1^-} + \sqrt{\gamma_2^-} - \sqrt{\gamma_w^-}\right) + \sqrt{\gamma_w^-}\left(\sqrt{\gamma_1^+} + \sqrt{\gamma_2^+} - \sqrt{\gamma_w^+}\right) \\ -\sqrt{\gamma_1^+\gamma_2^-} - \sqrt{\gamma_1^-\gamma_2^+}\end{array}\right] \quad (19)$$

Where γ^{LW} is the apolar Lifshitz Van der Waals, γ^{AB} is the polar Lewis acid base, γ^+ the Lewis acid (electron acceptor parameter), γ^- the Lewis base (electron donor parameter), the subscripts 1 and 2 are the two solid surfaces (particle and wall respectively), and subscripts w the liquid surface. The solid-liquid surface tension γ, is expressed as sum of the apolar Lifshitz Van der Waals γ^{LW}, and the polar Lewis acid base γ^{AB}, which was in turn expressed as a product of a Lewis-base γ^+, and a Lewis-acid γ^-, giving [61]

$$\gamma = \gamma^{LW} + \gamma^{AB} = \gamma^{Lw} + 2\sqrt{\gamma^+\gamma^-} \quad (20)$$

The Lifshitz van der Walls component γ^{LW}represents a single surface property, while the γ^{AB} represents both the polar Lewis acid, and polar Lewis base properties of the material.

The apolar component of ΔG_{1w2}, the Lifshitz Van der Waals component $\Delta G_{1w2}{}^{LW}$ between two different solid surfaces submerged in water is negative (attractive). The polar component of ΔG_{1w2}, the Lewis acid base component $\Delta G_{1w2}{}^{AB}$ between two different solid surfaces submerged in water can be positive or negative and is quantitatively the most important component dictating whether the free energy of interaction between two different solid surfaces 1 and 2, submerged in water is attractive or repulsive.

For any material the values of γ^- and γ^+, are unknown. For various liquids and solid surfaces in order to measure and express γ^+ and γ^-, it is presumed that the ratio γ^+/γ^-, is unity for water, at 20ºC, example: $\gamma^- = \gamma^+ = 25.5$ mJ/m^2 [183]. Given the free energy obtained from the acid base approach, the Derjaguin approximation could be helpful to determine the adhesion force [183], assuming the bed wall and particles can be approximated by a flat plate and spheres respectively. This leads to [183, 184]

$$F_{adh} = \pi \Delta G_{1w2} d_p \tag{21}$$

The hydrodynamics force experienced by the particle can be equated to the drag force, F_d, which in turn can be equated through a force balance to the difference between particle weight and buoyance force, F_b

$$F_d = W - F_b \tag{22}$$

where F_b, the buoyancy force, is expressed as:

$$F_b = V_p \rho_f g \tag{23}$$

where Vp is volume of particle.

Using equation 22 and 23, the drag force could be expressed as [185]:

$$F_d = \left(\frac{\pi d_p^3}{6}\right)(\rho_p - \rho_f) g \tag{24}$$

Table 9. Liquid and solid surface tension components

Material	γ (mJ/m^2)	γ^{LW} (mJ/m^2)	γ^{AB} (mJ/m^2)	γ^+ (mJ/m^2)	γ^- (mJ/m^2)	Reference
water	72.8	21.8	51	25.5	25.5	Van Oss [183]
Glass	59.8	42	17.8	1.97	40.22	Freitas & Sharma [186]
	64.37	42.3	22.07	2.9	42	Clint & Wicks [185]
	51.7	33.7	18	1.3	62.2	Van Oss [183]
PMMA	44.65	42	2.65	0.55	3.2	Della Volpe *et al.* [187]
	44.58	41.2	3.38	0.38	7.5	Clint & Wicks [185]
	40.6	40.6	0	0	12	Van Oss [183]
	39.21	36.68	2.53	0.16	10.02	Zdziennicka [188]

In the present research study the Dupree equation using acid-base theory developed by Oss, Chaudhury and Good [183] (equation 19) was used to predict the free interaction energy, ΔG_{1w2}, between two different solid surfaces submerged in a liquid. The surface tension parameters for the fluid (water), glass, PMMA particles and PMMA walls used in the micro-fluidised bed study are shown in table 9. The free interaction energy between glass, PMMA particles and PMMA walls in water were obtained using all combinations of values in table 9. Given the surface energy obtained from acid and base approach using surface tension components for liquid-solids given in table 8, the adhesion force was found using the Derjaguin approximation (equation 21), and the drag force was found from the buoyant weight of particles (equation 24). When ΔG_{1w2} value is negative, particle has the propensity to adhere to the walls of the micro-fluidised bed in presence of water, and when ΔG_{1w2} value is positive, the interaction between the particle and bed wall is repulsive.

3.5 Solid circulation rate

In order to successfully design a solid-liquid micro circulating fluidised bed system for micro-technology applications, it is essential to understand their hydrodynamics such as solid flux as it determines the bed performance as processing equipment, controlling heat and mass transfer, and dictating mixing in the system.

One of the fundamental parameters needed to in order to successfully design a solid-liquid micro circulating fluidised bed system for micro-technology applications, is the solid circulation rate, as it determines the bed performance as processing equipment, controlling heat and mass transfer, and dictating mixing in the system. Therefore, an attempt will be made to determine the solid circulation rate in the micro-circulating fluidised bed system. The solid circulation rate could be determined by various different methodology such as Ball valve, Butterfly valve, Magnet, Laser Doppler velocimetry, Particle image velocimetry (PIV), visual and impact technique.

3.5.1 Ball valve measurement

In this technique a solid circulation rate is measured by using a valve and a simple procedure. When the valve is closed in the downcomer, the accumulation of particles above the valve at given time interval could be measured, giving the particle circulation rate.

The overall solid flux is expressed

$$G_s = \frac{A_d}{A_r}\frac{\Delta H \rho_P}{\Delta t} \quad (25)$$

where A_r and A_d are the downcomer and riser cross-sectional areas respectively, ΔH the recorded bed height, and Δt time of particle accumulation above the valve.

3.5.2 Butterfly valve

By installed a butterfly valve in the downcomer of a circulating fluidised bed system, the solid circulation rate can be measured. When the two butterfly valves are flipped from one side to another, solid circulating through the bed could be accumulated in one side of the section being measured for a given time interval to provide the solid circulation rate [116].

3.5.3 Magnetic valve

In the case of small scale fluidized bed as used here, there are not available butterfly valves at micro scale and a magnet is installed inside the bed (downcomer) as shown in figure 42, and an external magnet is used to move and control the magnet inside the bed as a magnetic measuring valve. The solid circulation rate is measured by closing the downcomer with a magnet which is installed in the circulating fluidised bed system, and noting the time required to accumulate a defined height of solids above the magnet and the equation 25 was used to calculate the solid circulation rate.

Figure 42. Displaying the 3D printed micro-circulating fluidised bed with a magnet inside the system used to measure the solid circulation rate

3.5.4 Visual technique

This includes high speed videos and images, which can be important in dilute system for the analysis of the tracers of periodically excited fluorescent particles and for particle imaging velocimetry. But, the analysis of the results requires a high speed computation system and can be very time consuming [189].

3.5.5 Laser Doppler velocimetry

Solid velocities are measured by laser light. LDA Applies the Doppler Effect to determine the particle velocity in the bed. The advantage of Laser Doppler Velocimetry is that it is a non contacting technique, calibration is not needed and it can also be used to measure solid velocity in an inverse fluidisation system. On the other hand, Laser Doppler Velocimetry equipment is very expensive [190, 191].

3.5.6 Impact technique

This uses the force of re-circulating particles in the system to measure the solid circulation rate. In this technique forces of re-circulating solids dropping onto an inclined pan near the particles returning pipe are measured by a loaded beam. Wu, Gerhart [192] employed an impact plate flow meter to determine the solid circulation rate by measuring the torque on a hinged plate from falling particles impacts. The disadvantage of this type of solid flux measurement device is that calibration is very complex [193] .

3.5.7 Radioactive technique

Roy et al. used a radioactive technique to measure the solid circulation rate [194]. The basic theory was to determine the particles volumetric flow rate by measuring the particles velocity and volume fraction in the downcomer. Particle volume fraction was obtained by densitometry measurement, while particle velocity was obtained by measuring the falling time of a single radio-active tracer particle between two detectors installed in the downcomer.

3.5.8 Particle image velocimetry

Particle Image velocimetry (PIV) is a common experimental technique in the field of fluid mechanics used to measure the flow velocity profiles in fluids (using tracer particles) and for general granular flow [195, 196]. The particle displacement is determined by calculating the cross correlation of two consecutive image captured by a camera with a short time delay Δt. In PIV programme each image is divided into small sub images (interrogation region). Cross correlation function shown in equation 26 is then used to determine the most likely displacement of particles between each region as shown in figure 43 [197, 198]. The advantage

of this technique over other conventional techniques such as the valve technique is that it is non-invasive and easy to implement in microfluidics setup which is not trivial for the valve.

$$\max_{d} = \int_{w} A(r)\, B(r+d) dA \qquad (26)$$

where W is the correlation domain, A and B represents the interrogation area from image A and B, r is the position vector and d represent the displacement vector between interrogation area.

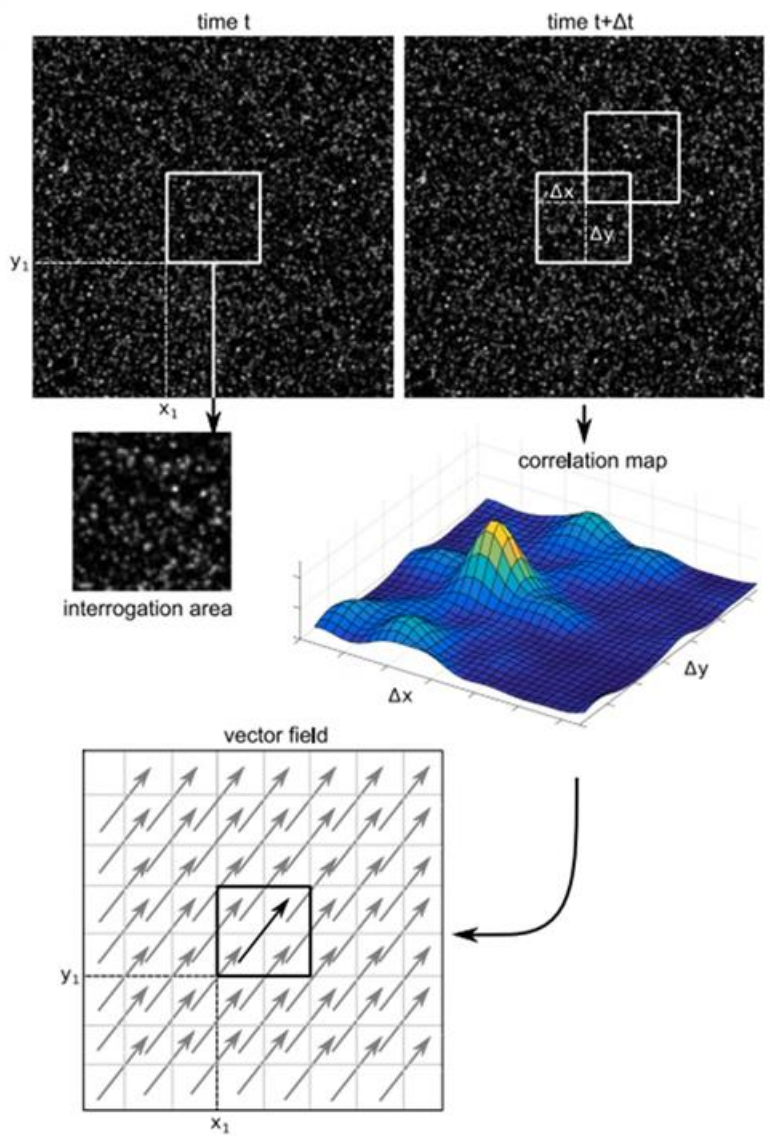

Figure 43. PIV principles [199]

3.6 Solid circulation rate measurement

In the current research investigation, particle imaging velocimetry (PIV) software PIVlab [200], was used to determine the solid flux in the micro-circulating fluidised bed. A digital PIV technique has been employed previously by researchers for measuring the flow velocity

profiles in granular flow [201, 202]. The advantage of this technique over other conventional techniques such as the valve technique is that it is non-invasive and easy to implement in microfluidics setup which is not trivial for the valve. In addition, PIVlab does not need any information regarding light intensity or the time between successive frames that some other forms of PIV need. PIVlab is able to calculate the velocity field of a material or fluid based only off of sequential images that are loaded into it. The effects of operating parameters such as solids inventory, particle size and density on solid flux has been carefully studied using PIVlab and MatLab.

Digital movies of granular flow were captured by a Basler aCA 1300-200uc digital camera which as a resolution of 1.3 MP. Basler Pylon viewer software was used to monitor the recording process. Flexible fibre optic illuminator was used to illuminate the granular flow in the circulating fluidised bed and produce high quality image. The camera capture rate was set to 25 fps with a shutter time of 100 μs after preliminary test revealed that it provided high quality videos without motion blur and the optimal PIV results. Each video has a recording time of 20 seconds.

Digital movies of liquid-solid fluidisation behaviour were recorded and stored on a PC for off-line analysis. The off-line examination comprised of movies conversion into successive frame sequences by VLC media player, and particle displacement calculation from successive frames using PIVlab, a Matlab code, which determines the velocity of particles by cross correlation PIV algorithm of multiple small sub-images. Determination of particle displacement using the PIVlab code in the current research investigation is composed of three major stages:

- Image Pre-processing to increase the analyse quality
- Image analysis to calculate the particle displacement in the area of interest
- Post processing of PIVlab analysis to eliminate erroneous data

3.6.1 Image pre-processing

Firstly, the solid feed pipe was chosen as the region of interest and a mask was applied to exclude the outside regions from the analysis as shown in figure 44. That is important as it decreases the computational time. The region of interest was about 3 x 1 mm.

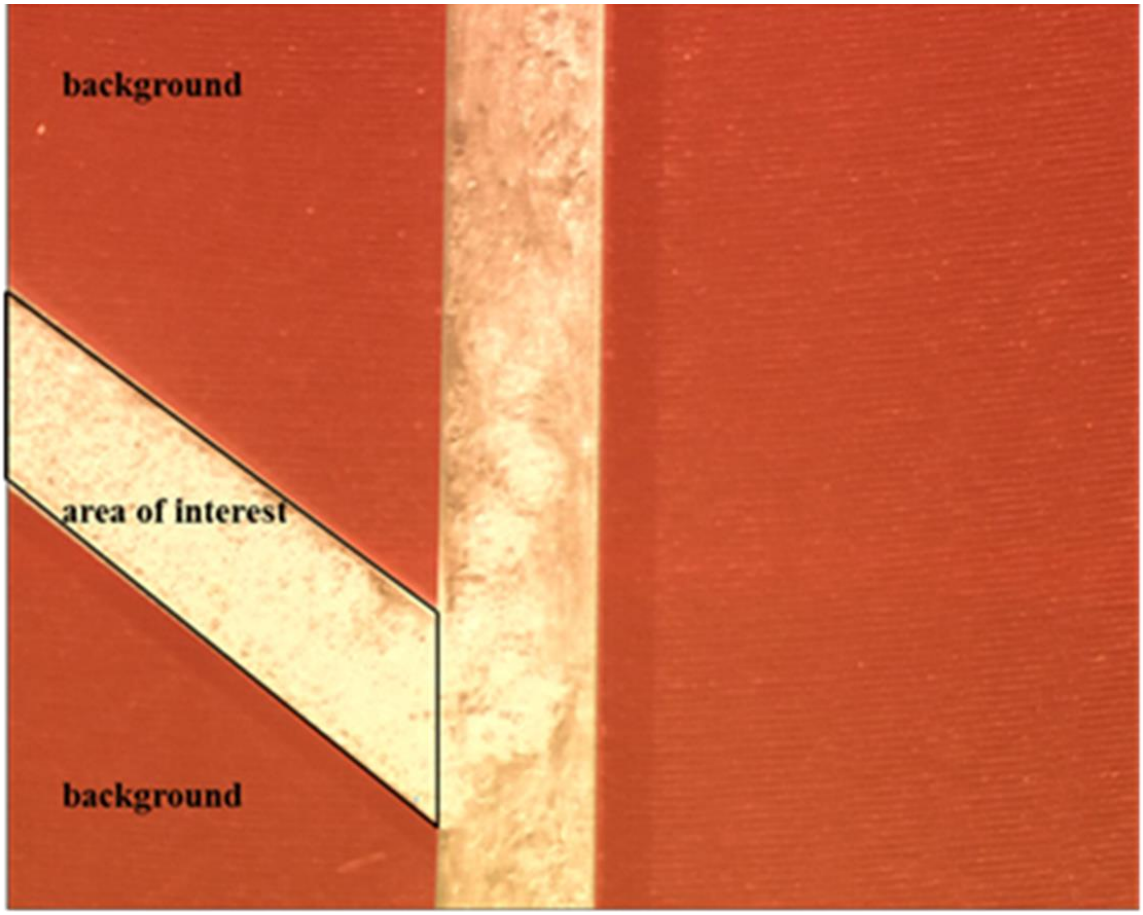

Figure 44. Fluidized bed for the 58 µm glass particles at flow rate inside 15% solid inventory bed showing area interest for the digital PIV analysis.

Before the image analysis takes place, it is very important to reduce or eliminate the faulty data which contributes to erroneous PIV analysis. Thus, image pre-processing was done to raw data to enhance the PIV analysis quality. Here, several image pre-processing techniques such as image pre-processing contrast limited adaptive histogram equalisation (CLAHE), high pass filtering, intensity capping filter were tested, so as to evaluate their effect on the PIV performance. It was preliminary concluded that the only image pre-processing technique need for the PIV analysis is the CLAHE filter, and the optimal performance was obtained with CLAHE filter of 20-pixel size. Hence, prior to PIV analysis, CLAHE filter was applied to all frames to enhance the image contrast and the probability of detecting valid vectors.

3.6.2 Image analysis

Image calibration was performed by specifying the bed cross sectional area (1 mm) and the time step between images of one frame (25 frames per second), this was done as to establish the correlation between the particle displacement in the image and the displacement of particles

in the flow. Image calibration converts pixel values to standard values that represent measurements in the real world.

Each image was divided into small sub images (interrogation region), and cross-correlation of successive frames was applied to determine the most likely displacement of particles in these regions. Particle displacement was determined using FFT (fast Fourier transform correlation with multiple pass and deforming windows algorithm). The PIVlab analysis shows that particle displacement calculation using DCC (single pass direct cross correlation) suffers from more missing correlations under the same conditions as FFT as shown in figure 45. Therefore, FFT was the preferable correlation algorithms for the PIV calculations, as it is much more robust, reduces erroneous correlations and provided the more accurate results.

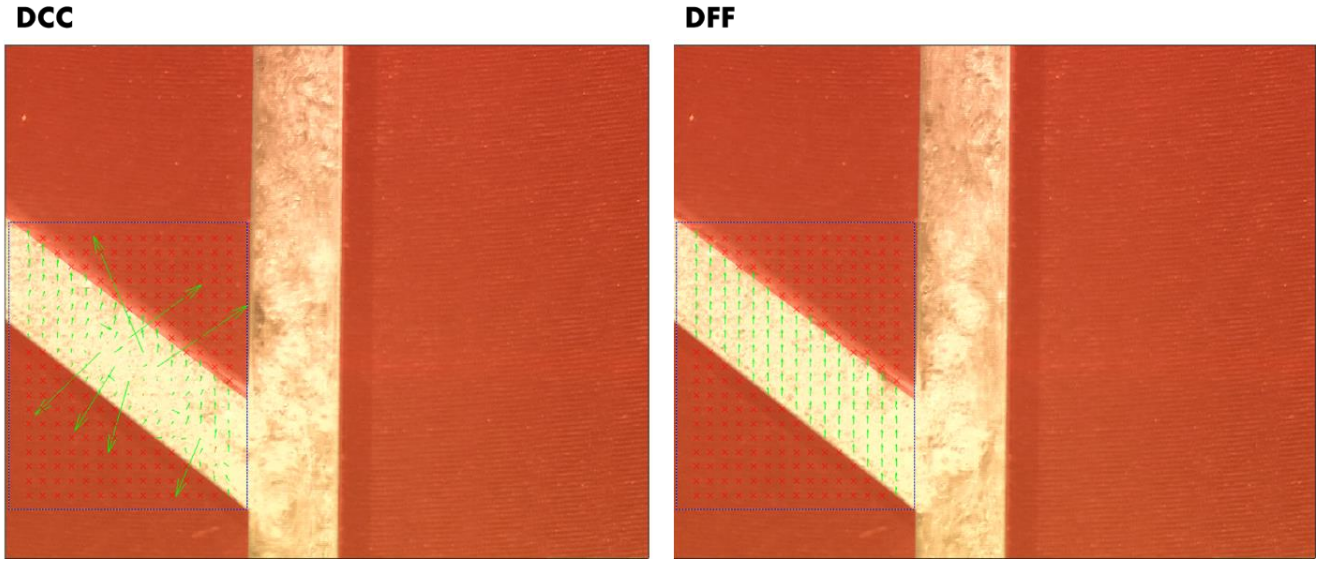

Figure 45. Comparison of the velocity map calculated using DCC (left) and window deformation (right) under the same experimental conditions. Large vectors are outliers. The window deformation technique FFT reduces the amount of erroneous correlations

As is well known, the quality of particle image velocimetry measurement is linked to the size of the interrogation area[201]. Several researchers suggested that to maximize the PIV analysis accuracy, the interrogation area size in the first pass should at least be four times bigger than the maximum particle displacement [203, 204]. If the size of the interrogation area is smaller, the cross correlation analysis will be incorrect, due to particle pair loss, as a number of particle pairs leave the interrogation area as shown in figure 47(c & d) [205]. However, a very large interrogation area causes a massive reduction in the measurement resolution leading to poor results as shown in figure 46a & 46b [206, 207].

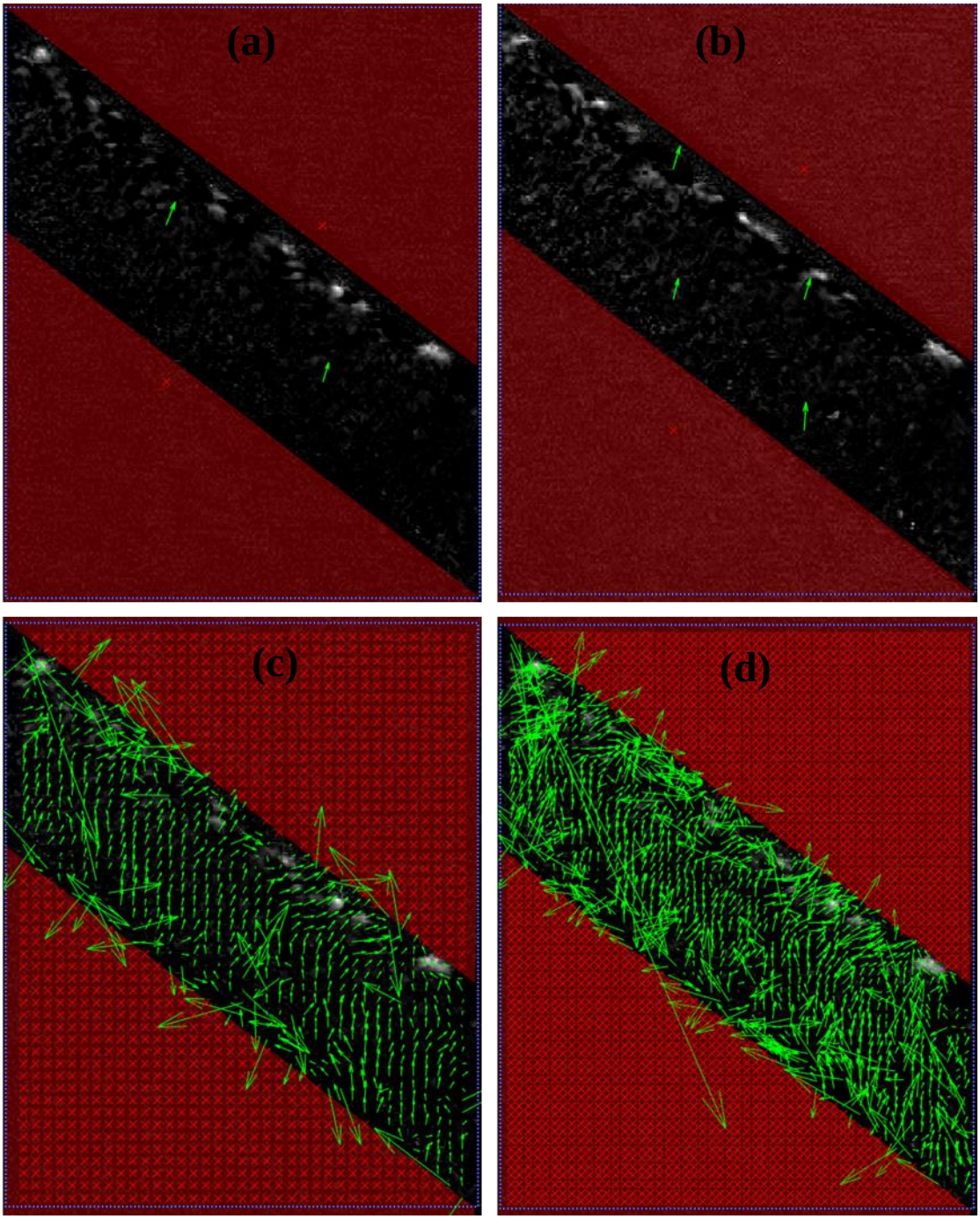

Figure 46. PIV analysis results of several interrogation area sizes. (a) 140-120-100 pixel, (b) 120-100-80 pixel, (c) 32-16-8 pixel, (d) 16-8-4 pixel

A preliminary test was conducted to determine the optimal size of the interrogation area and the number of PIV passes. A three step cross correlation analysis with an interrogation area of 64 pixel in the first pass, 32 pixel in the second pass, and 16 pixel in the third pass (corresponding to 0.64, 0.32, and 0.16 mm in real scale respectively) was chosen as the optimal PIV setting to determine the particle displacement of the image data. These PIV setting was found to produce excellent resolution with minimal noise and satisfy Keane and Adrian

recommended guideline [203]. Each interrogation area was overlapped by 50% as shown in figure 47.

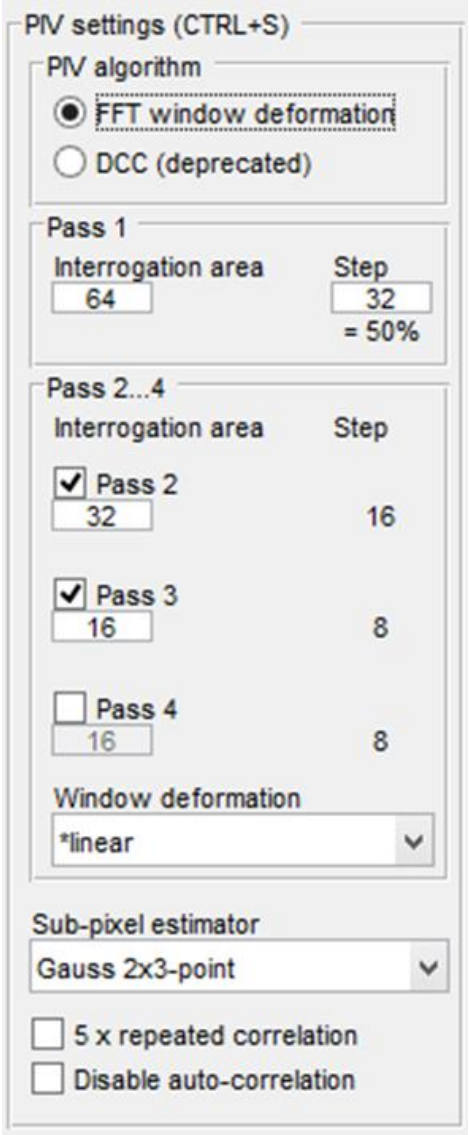

Figure 47. PIV setting use to calculate the particle motion inside the micro-circulating fluidised bed

The displacement information obtained in each pass is used to shift the interrogation windows in the next pass to increase the resolution of vector map, signal to noise ratio without sacrificing robustness. Gaussian function 2x3-point was used to estimate the sub-pixel displacement as shown in figure 48. All the particle image velocimetry calculations were conducted on partially overlapping frame pairs (i.e. 1-2, 2-3, 3-4 etc). The maximum particle image displacement was found to be approximately 5 pixel in all experimental investigation (less than 2 particle diameter). The particle image density was estimated to be 10-15 particles per interrogation area

which satisfy Thielicke recommended guideline [208] with the particle image diameter was approximately 3 pixel. All the PIV setting used for this experiment is shown in table 10.

Table 10. PIV settings.

Parameter	value	unit
Interrogation area	64-32-16	pixel
Particle image density	10 - 15	pixel
Particle image diameter	3	pixel
CLAHE Filter	20	pixel
High pass	off	n/a
Intensity capping	off	n/a
Wiener2 denoise filter	off	n/a

3.6.3 Post processing

Generally, the velocity field obtained from the PIV calculation is never error-free as it may contains some erroneous vector due to noise [209]. Therefore, the vector field were smoothed and validated using a number of filters (local median filter, and standard deviation filter) while missing data were interpolated using the boundary value solver interpolation technique to increase the accuracy of the velocity calculation this was required in order to eliminate erroneous vector (outliers) and to improve the results. The above procedure was repeated to calculate the velocity (horizontal u and vertical v component) for each frame for all the PMMA and glass particles at various liquid flowrates.

The results obtained using PIVlab code was exported as a consecutive Mat-file into Matlab workspace for further processing. Matlab was then employed for adjusting velocity field due to background movement and for time averaging of velocity field for each particle at different liquid flow rate by averaging the instantaneous velocity obtained using the PIVlab code.

3.6.4 Background movement

Initial PIVlab image analysis shows that particles move downwards and upwards as shown in Figure 48(a) instead of downwards along the solid feed pipe as expected and visually observed. Further analysis showed considerable background movement, so it was necessary to calculate the background movement velocity field using PIVlab as shown in Figure 48(b). The background movement could be the result of imperfect illumination due to shadow and light

reflection which was observed during the recording process. Under ideal conditions, image for PIV analysis comprises of bright particles on an entirely dark background. However, this ideal scenario is not always possible because the fluidised bed was fastened by screws and bolts as shown in figure 19, and those screws and bolts produced light reflections and shadow during the experiment process which influenced the PIV analysis and consequently created the background motion.

The imported vector field of particles in the solid feed pipe in Matlab is shown in figure 49(a) with the erroneous upward motion of particles. The velocities were then correctly adjusted by subtracting the background motion (Figure 48(b)) in Matlab to obtain the correct particle velocity field with downward motion as shown in Figure 49(b). From figure 50, it can be seen that the downwards and upwards background motion cancel each other

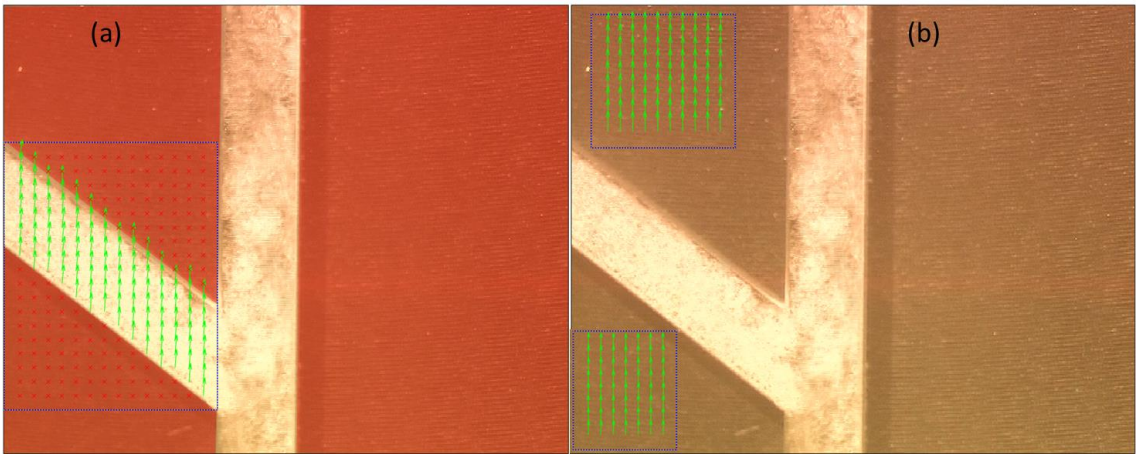

Figure 48. Velocity vector field in (a) the solid feed pipe and (b) in background determined by PIVlab analysis.

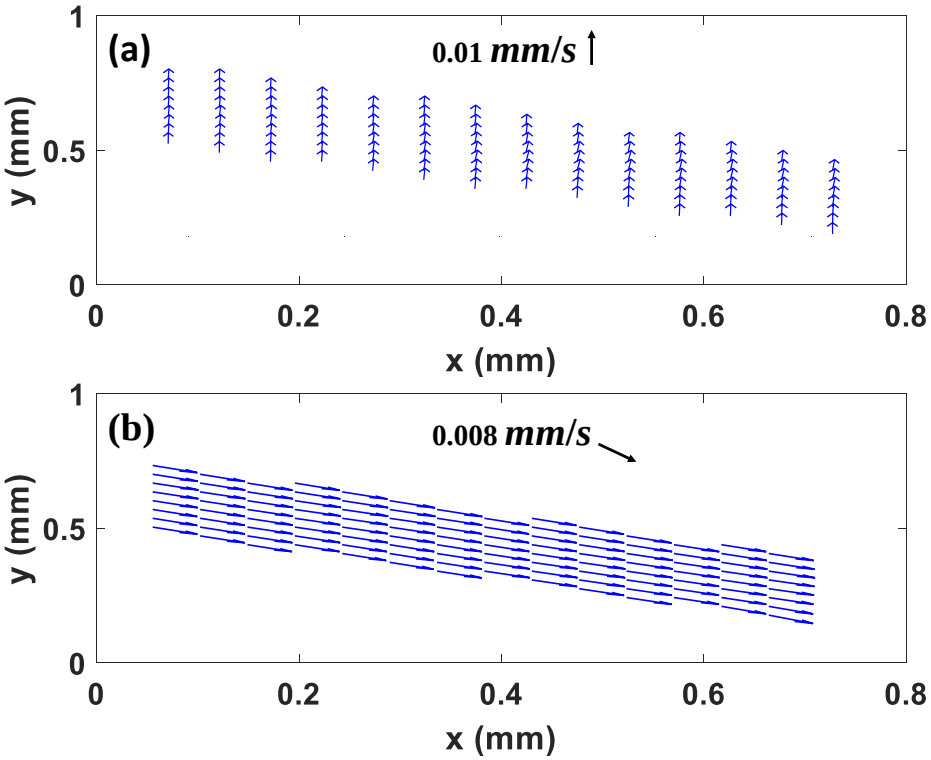

Figure 49. Examples of Original particle velocity field (a) and the velocity field after subtraction of the background movement (b) for the 58 µm glass particle at 445 µl/min liquid flow rate with 15% solid inventory bed.

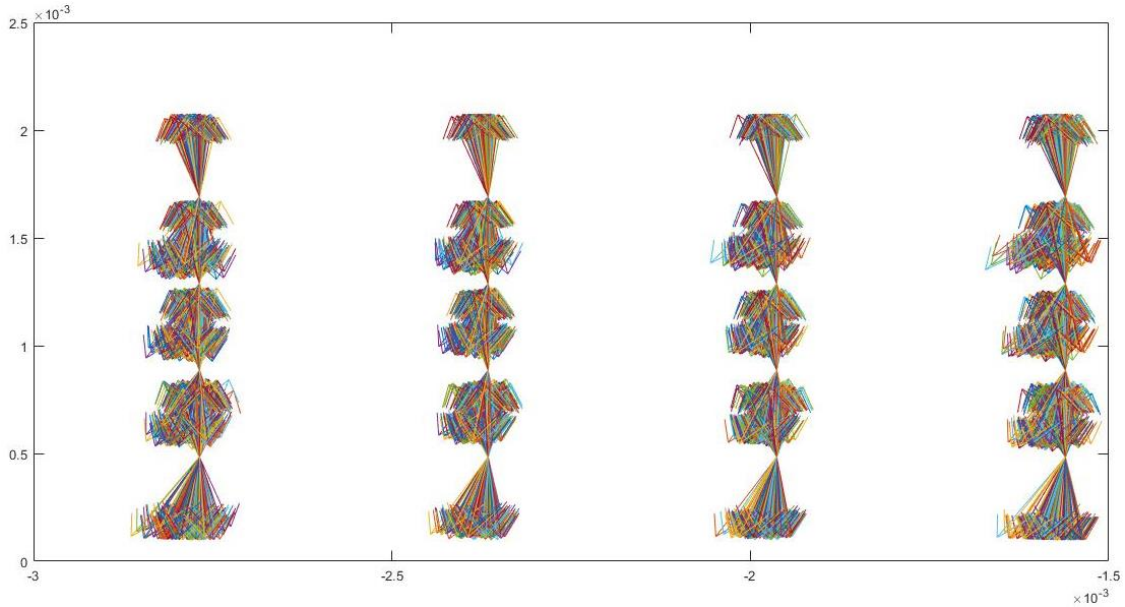

Figure 50. Example of downwards and upwards background motion as given by 2000 vectors over 20 seconds.

Figure 50 displays a MATLAB analysis involving the downwards and upwards background motion as given by 2000 vectors over 20 second. From figure 50, it can be noticed that the vector velocity field associated with the downwards and upwards background motion cancels each other in this analysis.

3.7 Critical transition velocity measurement

As previously mentioned, solid-liquid circulating fluidised beds system have different operating regimes as a function of liquid velocity. In order to understand their hydrodynamics characteristics it is crucial to identify the transition from one regime to another such as the critical transition velocity which delineates the transition from conventional to circulating fluidised bed regime [102, 210]. The critical transition velocity could be determined by three different methodology, solid circulation rate, bed emptying time, and pressure gradient method as given in

3.7.1 Solid circulation rate method:

Liang and co-workers [106] determined the critical transition velocity, U_{cr} by plotting the solid circulation rate as a function of the liquid velocity as shown in figure 9. The critical transition velocity was taken as the point where the solid circulation rate becomes zero when reducing superficial liquid velocity.

3.7.2 Emptying bed time:

Zheng and co-workers [116] determined the critical transition velocity using the emptying bed time. This was done by measuring the time needed for all the particles to be transported out of the bed by the outflowing liquid at various liquid velocities when no particles were introduced from the downcomer into the riser. At lower liquid flow rates, solids are not significantly entrained, so that the time needed for all the solid-particles to be carried out of the bed is longer. When the liquid flow rate is increased, there is a rapid increase in solid entrainment, and if no solid-particles are introduced into the riser column, the system becomes empty in a short time. Hence two different lines could be spotted by plotting the superficial liquid velocity against particle empty time in the column riser: at lower velocity and higher velocity. The critical velocity which indicates the transition from conventional fluidisation to circulating fluidisation regime could be found at the intersection between these two lines.

3.7.3 Pressure gradient method:

Pressure gradient method as previously been applied by Vatanakul *et al* [211], Vidyasagar *et al* [210]. In this method the critical transition velocity is obtained by plotting the pressure gradient at two locations (above the distributor and on top of the riser) as function of superficial liquid velocity. Vidyasagar measured the pressure drop using a pressure taps connected to a manometer. Vatanakul measure the pressure gradient with aid of a pressure transducer and wall electrical conductivity probes which was linked to a PC through an ADC. The critical transition

velocity was defined by all these researchers as the superficial liquid velocity at the peak of pressure gradient line.

3.7.4 Critical transition velocity determination in the present study

In the current research the critical transition velocity from conventional to circulating fluidisation regime was determined by plotting the average particle velocity from PIV measurement as a function of the liquid velocity. This PIV method was chosen over magnetic valve due to its simplicity and easy of the experiment. The critical transition velocity *Ucr,* was taken as the point where the particle velocity becomes zero when reducing superficial liquid velocity as shown in figure 51. In addition, the critical transition velocity was also determined by visualising the circulating flow across the transparent bed wall. The critical transition velocity was taken as the maximum liquid velocity where no fresh particles were reintroduced back to the riser from the downcomer by decreasing the superficial liquid velocity as shown in figure 52, i.e. Solid flux of particles is essentially zero.

The transition velocity U_a, which demarcates the transition from circulating fluidised bed regime to transport regime, was also determined by plotting the average particle velocity as a function of the liquid velocity. The critical transition velocity U_a, was taken as the point where the particle velocity becomes constant when increasing superficial liquid velocity as shown in figure 51 [106, 107].

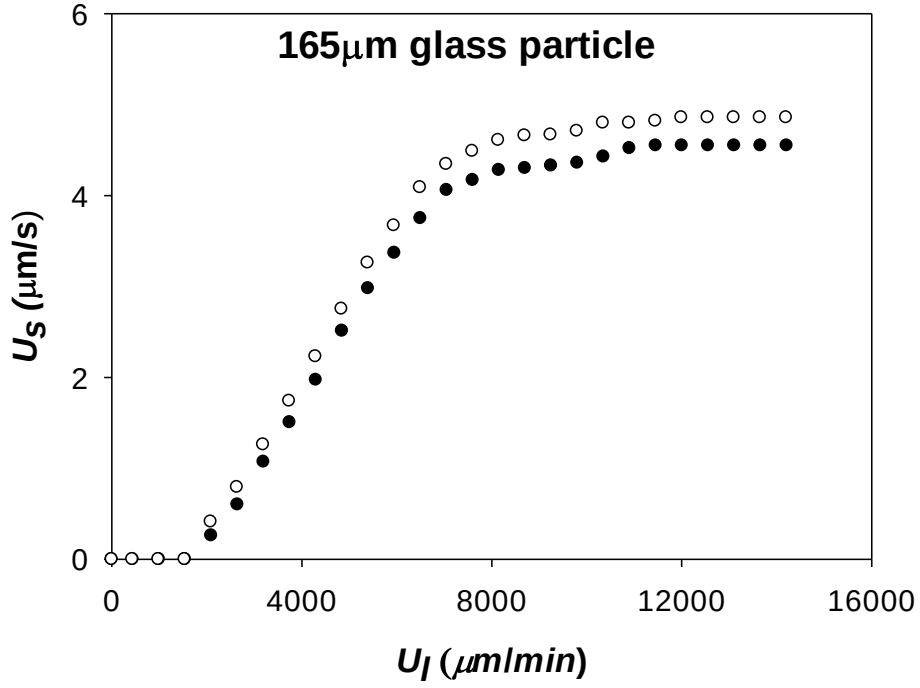

Figure 51. Particle circulating speed as a function of superficial liquid flow rate for both PIV technique (empty circle) and accumulation method (filled square)

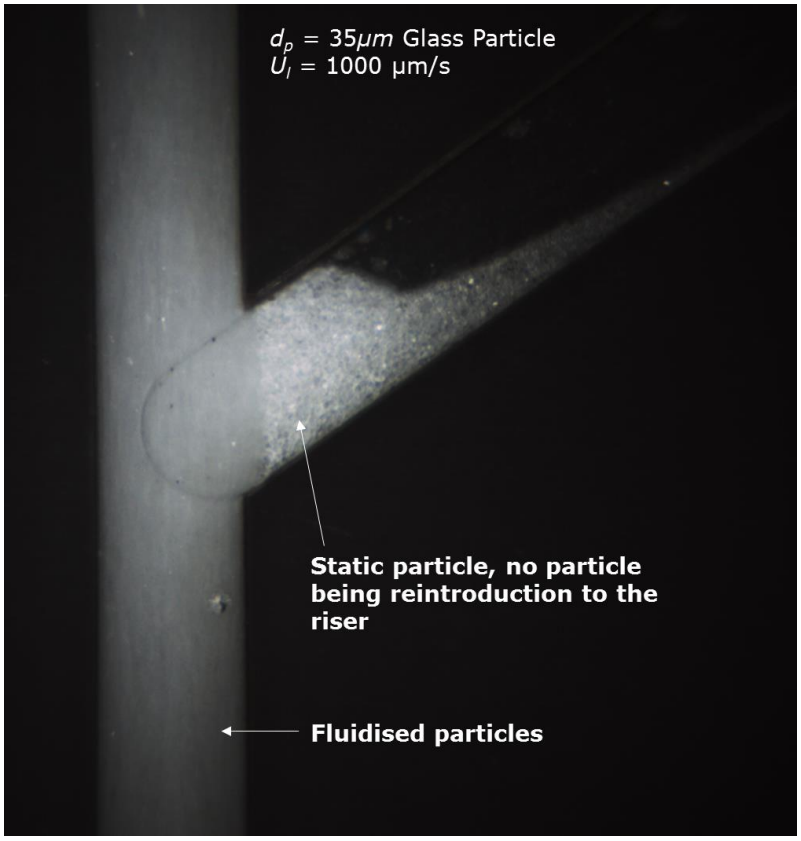

Figure 52. The photo of downcomer which was visually observed by stereo-microscope for detecting solid particle circulation.

Chapter 4. Influence of surface forces and wall effect on the minimum fluidisation velocity of liquid-solid micro-fluidised beds

4.1 Introduction

Microfluidics is the science and technology of processing of small volumes of fluids in conduits having dimensions of the order of tens to hundreds of micrometres [212-214]. This fascinating technology holds broad application areas, including medical diagnostics [215], power generation [216], materials synthesis [217], chemical and biochemical research [218, 219] due to their advantages such as the dramatic reduction in the amount of required sample, chemicals and reagents reducing the global fees of applications, less energy consumption, short times for analysis, improved safety, and less pollution [220-226]. However, transport process in microfluidic systems are dominated by molecular diffusion that comes with the inevitable laminar flow found in micron-sized conduits[174]. Fluidized beds have long been used at the macro-scale to enhance mixing and, thereby, heat and mass transport. Recent experimental work [227, 228] has demonstrated that liquid-solid micro-fluidized beds are feasible, offering the potential to not only overcome diffusion-limited fluid mixing, heat and mass transport in simple micron-sized channels, but also to provide higher sensitivity and multi-modal detection in the diagnostic context by virtue of the large surface area per unit volume that comes from use of micro-particles [229, 230].

In general, the major difference between micro and macro-scale flows is the importance of surface forces which can prevent fluidisation, and inevitably the wall effects due to small bed size. Base on this principle the boundary between the micro and macro-scale flow is considered to be 1mm in the micro-fluidic field in general [231-233]. As expected, our previous experimental study confirmed that surface forces play a vital role in the micro-fluidised bed and can even prevent fluidisation in many cases [174, 234]. We showed that the acid-base model of van Oss, Chaudhury and Good combined with the Derjaguin approximation [235] can successfully predict the propensity of micro-particles to adhere to the walls of μFBs using common liquid fluidizing media [174, 227]. Furthermore, we used a comparison of surface and hydrodynamic driving forces to estimate the boundary between micro- and macro-scale fluidization at 1 cm with stricter limits at 1 mm, the same as for microfluidics [174].

A second major issue in μFBs is the high potential for the particle-to-bed diameter ratios to be greater than 0.1, leading to significant influence of the bed walls on the packing of the particles

in the bed and subsequently fluidization behaviour [58, 227]. The bed voidage in the μFB (micro-packed beds as the starting fluidization point) is indeed substantially higher compared to macroscale beds, leading to a significant increase in the minimum fluidization velocity [58, 227]. The bed expansion behaviour also varies with the particle-to-bed ratio confirming strong wall effects as in the original Richardson-Zaki correlation for viscous flow [236]. Previous experiments indicate that the Richardson-Zaki exponent, *n*, increases significantly in a linear manner with the particle-to-bed diameter ratio only when the ratio exceeds 0.1 [227]. Subsequently, Tang *et al.* [228] confirmed our findings if only for narrow particle size distributions, while the trend is opposite for particles with wider distribution. Their study shows that wall effects are still influencing minimum fluidization behaviour for very high bed to particle ratios of up to 30, i.e. particle-to-bed diameter ratios greater than 0.03 [228]. In gas-solid miniaturized beds experiments, the influence of the wall effects on the minimum fluidization velocity was observed for even lower particle-to-bed diameter ratios of 0.02 [70, 71]. We performed new experiments with glass micro-particles and water as a fluidizing medium at a boundary of a micro-fluidization according to our previous mentioned study. Specifically, we used micro-machined Perspex fluidized bed of 1 mm^2 and 2 mm^2 square cross sections in this study.

4.2 Experimental details

4.2.1 Experimental set up

The system used in the present experimental investigation was made by micro machining channels in Perspex. Two micro-bed units were used in experiments with a cross section of 1 mm x 1mm and 2 mm x 2 mm. Figure 53 (a & b) illustrates a schematic of the research experimental set up which consist of syringe pump (AL-4000, WPI INC., US) to pump water as a fluidising medium at the desired flow rate using a 5 ml B-D Plastipak syringe, and Euromex Nexius trinocular digital microscope fitted with a USB digital camera (JB Microscopes Ltd, UK) to record the micro fluidisation behaviour. The images and movies were saved on a computer for offline investigation studies. The equipment was connected using Deluxe Luer Fitting kit and flexible plastic tubing.

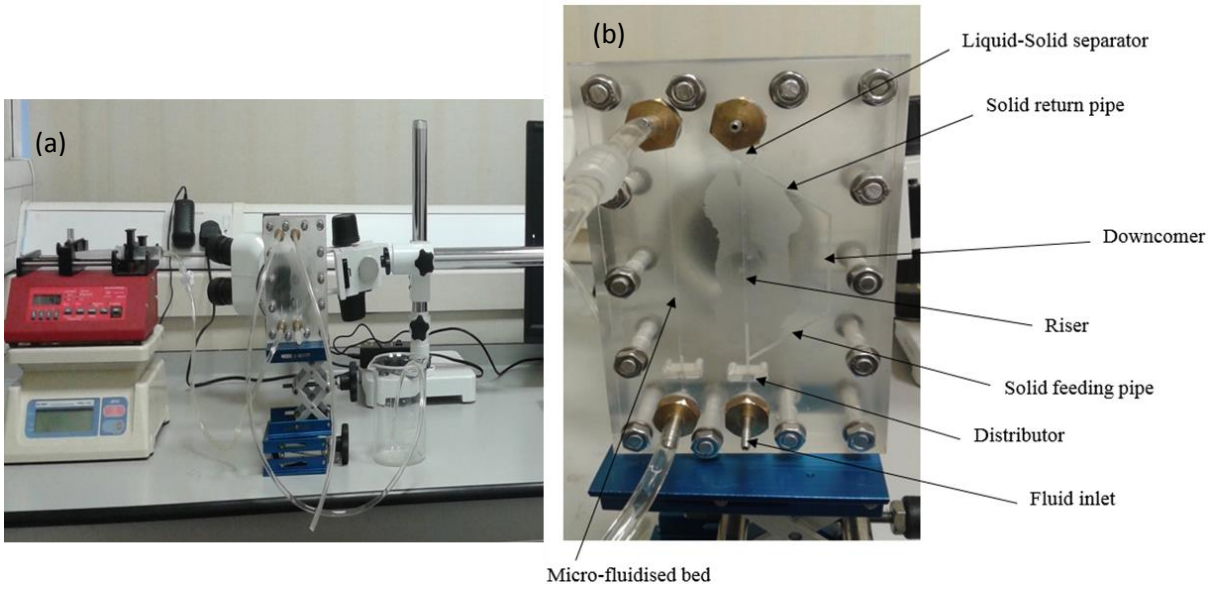

Figure 53. Photograph of (a) the experimental setup used in the research studies and (b) the micro-machined μ-FB and μ-CFB

4.2.2 Particle and liquid materials

Two different groups of particles were used as fluidised solid: (1) soda lime glass microspheres of five different diameters, d = 26 ± 1.5 μm, 30 ± 1.5 μm, 35 ± 3 μm, 58 ± 5 μm, 82 ± 6 μm, 98 ± 8 μm, 115 ± 9 μm, *165 ± 15 μm*, *196 ± 16 μm* μm whose density is ρ_p = 2500 kg/m^3 and (2) PMMA particles of five different diameters, d = 23 ± 3.5 μm, 35 ± 3 μm, 41 ± 3.5 μm, 58 ± 5 μm, and 115 ± 9 μm whose density is ρ_p = 1200kg/m^3. Tap water (with average density of 998 kg/m^3) was used as the fluidising liquid. All experiments were performed at room temperature of average 18 ± 2 ºC.

4.2.3 Experimental methodology

The minimum fluidisation velocity required to achieve fluidisation was determined by observing visually the bed height expansion and also by extrapolation of linear relationship between the superficial liquid velocity and ratio of bed expansion. Flowrates were calibrated in the range of fluidization velocities with and without particles inside the bed as in some cases a high pressure drop across the porous distributor caused a considerable but linear discrepancy from syringe pump readings. All experiments were started with the bed totally filled with tap water and solids up to a known height. For a desired liquid system and particle size, the liquid flow rate was slowly increased every 10 minutes and the corresponding bed height was noted. The height of the expanded bed was obtained by using a Euromex Nexius trinocular digital microscope to take pictures. ImageJ [237], an image processing and analysis computer

programme was used for off-line analysis to determine the bed height as a function of superficial liquid velocity. Minimum fluidisation velocity values were obtained from the plot of bed height expansion vs superficial liquid velocity. The point of intersection of the expansion line with vertical line for packed bed height was taken as minimum fluidisation velocity.

4.3 Surface force and wall effect in the micro-fluidised bed experiment

The importance of surface force and wall effect in micro-fluidised beds were investigated experimentally. As previously mentioned, the major difference between micro-fluidised beds and macro-fluidised beds flows is the importance of surface forces which can prevent fluidisation [61]. In the present research study the Dupree equation using acid-base theory developed by Oss, Chaudhury and Good (equation 19, chapter 3) [183] was used to predict the free interaction energy, ΔG_{1w2}, between two different solid surfaces submerged in a liquid. The surface tension parameters for the fluid (water), glass, PMMA particles and PMMA walls used in the micro-fluidised bed study are shown in table 9 in chapter 3. The free interaction energy between glass, PMMA particles and PMMA walls in water were obtained using all combinations of values in table 9. Given the surface energy obtained from acid and base approach using surface tension components for liquid-solids given in table 9, the adhesion force was found using the Derjaguin approximation (equation 21, chapter 3), and the drag force was found from the buoyant weight of particles (equation 24, chapter 3). When free interaction energy, ΔG_{1w2} value is negative (i.e. $\Delta G_{1w2} < 0$), particle has the propensity to adhere to the walls of the micro-fluidised bed in presence of water, and when ΔG_{1w2} value is positive (i.e. $\Delta G_{1w2} > 0$), the interaction between the particle and bed wall is repulsive.

4.4 Result and discussion

In the first experimental investigation involving glass particles and PMMA wall using water as the fluidised medium, the free energy of interaction, $\Delta G1w2$ obtained using most of the combination of values in table 9 from chapter 3 estimated that the interfacial energy acting between the PMMA walls of micro-fluidised bed and glass particles in the presence of water is attractive. However, when van Oss glass surface tension components were used with PMMA components excluding Della Volpe a positive free interaction energy was obtained (3/12 combinations). The average predicted free interaction energy obtained using these three combinations indicates glass particles does not have the tendency to adhere to PMMA walls in the presence of water (ΔG_{1w2} = 8 mJ/m^2 and $\sigma(\Delta G)$ = 3.8 mJ/m^2). The ΔG_{1w2} of only estimated adhesion values (9/12 combinations) was -8.87 mJ/m^2 and $\sigma(\Delta G)$ = 5.77 mJ/m^2.

As displayed in table 11, the average free interaction energy, ΔG_{1w2} obtained using the 12 parameter combinations between glass particle and PMMA walls when using water as the fluidised medium was negative (-4.63 mJ/m^2) and standard deviation of 9.29 mJ/m^2. This indicates that the glass micro-particles have a small propensity to adhere to a PMMA walls surface in the presence of water. The interfacial energy acting between the PMMA micro fluidised bed walls and the glass particles is attractive. These observation are proximately identical to that described by Zivkovic and Biggs [61]. It was observed during the experimental investigation that some glass particles were sticking to the bed walls when there was no liquid flowing (packed bed) and it was also observed that particles were sticking to the top of the fluidised bed during the de-fluidisation experiments as shown in figure 54 (a & b).

Table 11. Glass and PMMA particle Free energy of Interaction ΔG_{1w2} (mJ/m^2)

Surface 1	Surface 2	Liquid	ΔG1w2	σ(ΔG)	$(\Delta G)_{min}$	$(\Delta G)_{max}$	Interaction
Glass	PMMA	Water	-4.63	9.29	-19.22	12.38	attractive
PMMA	PMMA	Water	-47.22	7.49	-62.79	-37.83	attractive

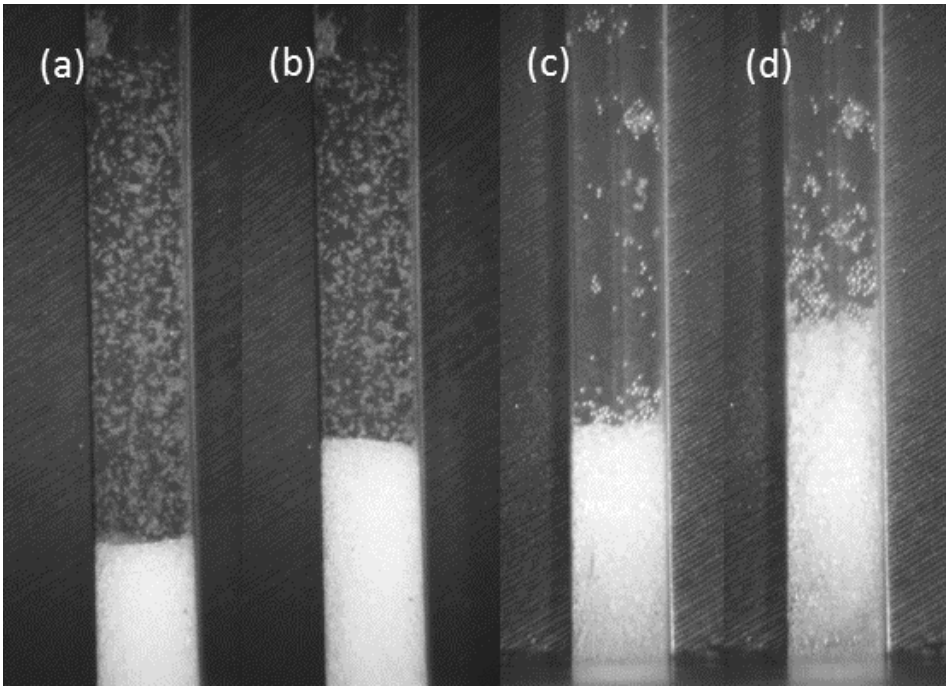

Figure 54. Adhesion of 35 μm glass particle (a) and (b) and PMMA particle(c) and (d) in the walls of the micro-fluidised bed. Adhesion can be seen at the top of the packed bed (a) and (c) and also at the top of the fluidised bed during defluidisation (b) and (d).

In the second experimental studies involving PMMA particles and PMMA walls using water as the fluidising medium, the free energies of interaction, ΔG_{1w2} obtained using the 16 surface tension components combination of PMMA were less than zero, with average free energy of interaction, ΔG_{1w2} = -47.22 mJ/m^2 and standard deviation of 7.49 mJ/m^2. This indicates that PMMA particles have a significant tendency to adhere to PMMA micro-fluidised bed surface when submerged in water as displayed in figure 54 (c) an (d). The free interaction energy, ΔG_{1w2} obtained using similar surfaces (4/16 combinations) were a little different with a mean of -46.66 mJ/m^2 and standard deviation of 9.98 mJ/m^2, which indicates a significant cohesion of PMMA particles when submerged in water unlike glass particle which are hydrophilic and its interaction is repulsive with mean free energy of 22.17 mJ/m^2

In the present experimental study smooth fluidisation was achieved for all glass particles as displayed in figure 55(a) and (b). Smooth fluidisation surprisingly was also obtained for each PMMA particle as shown in figure 3 (c & d).

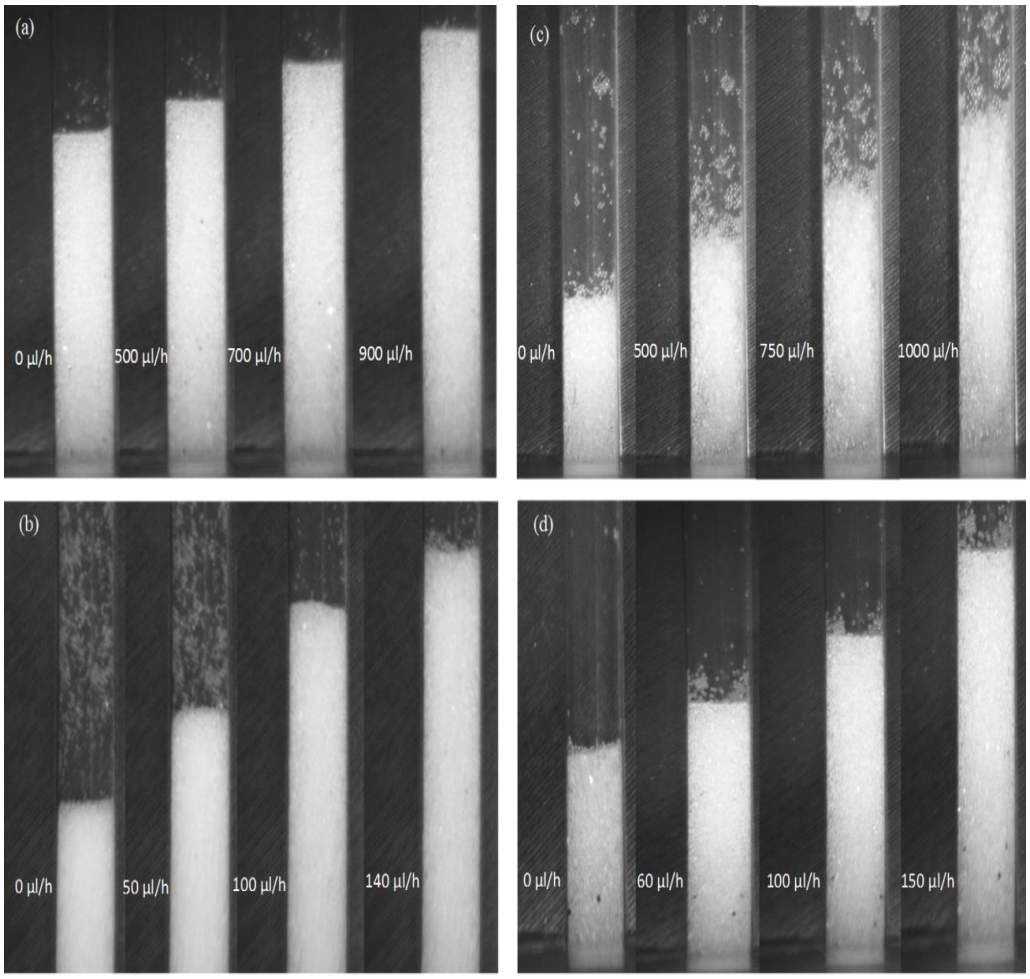

Figure 55. Successfully fluidisation using (a &b) 115 and 26 µm glass particle, (c & d) 115 and 23 µm PMMA particle

In the experiments even though the free energy permits the identification of the propensity for solid particle adhesion to the bed surface, the adhesion and drag forces ratio experienced by solid particles in the bed is required if adhesion to the micro-fluidised bed wall will in fact occur. In the present research study, for both the PMMA and glass particles, the adhesion forces were 3-5 orders of magnitude bigger than the calculated drag forces, indicating that particle adhesion to the micro-fluidised bed walls is highly likely in these cases. This was observed in the efforts to fluidise the solid-particles in the bed, which proved difficult due to the solid-particles adhering to the bed walls as displayed in figure 54.

4.5 Minimum fluidisation velocity

ImageJ was used to analyse videos and images to determine the bed height as a function of liquid superficial liquid velocity, which is displayed in figure 55. In the experiments the minimum fluidisation velocity was the point of transition between the packed bed regime and the conventional fluidisation regime in a fluidised bed. The experimental and theoretical minimum fluidisation velocity for glass and PMMA in the present experimental investigation are shown in table 12 and 13 respectively.

Table 12. Experimental and theoretical U_{mf} results for Glass particle

bed size D (mm)	d_p	U_{mf} Theory	U_{mf} Exp.	U_{mf} Exp. / U_{mf} Theory
1	26	7.01	13.81	1.97
	30	9.05	16.74	1.85
	35	12.10	19.97	1.65
	58	33.97	48.58	1.43
	82	68.15	89.96	1.32
	98	97.34	120.70	1.24
	115	134.70	157.60	1.17
	165	275.75	303.32	1.10
	196	388.87	396.65	1.02
2	26	7.01	9.46	1.35
	35	12.10	14.76	1.22
	58	33.97	35.33	1.04
	115	134.70	125.27	0.93

Table 13. Experimental and theoretical U_{mf} results for PMMA particle

bed size D (mm)	d_p	U_{mf} Theory	Umf Exp.	U_{mf} Exp./ Theory
1	23	0.75	16.79	22.39
	35	1.66	25.25	15.21
	41	2.33	30.80	13.22
	58	4.55	46.62	10.25
	115	18.03	139.73	7.75
2	23	0.75	7.61	10.14
	35	1.66	12.02	7.24
	41	2.33	14.33	6.15
	58	4.55	22.80	5.01
	115	18.03	83.12	4.61

In an ideal fluidised bed system, the U_{mf} is the minimum superficial liquid velocity where a bed of granular material is transformed from packed state to a fluidised state. In the present experimental investigation for 115 µm glass particle using the 2mm bed, a partially fluidised bed was observed at a superficial liquid velocity bellow the predicted minimum fluidisation velocity as shown in table 2. As the superficial liquid velocity was increased in a small range, the majority of particles in the bed became fluidised, however, it was also observed small amount of un-fluidised particles at superficial liquid velocity significantly higher than those where the system appeared to be fluidised. For PMMA particles the transitional region from fixed state to fluidised state was considerable extensive as the cohesive forces present on them are by far higher than the gravitational force, and the fluid drag and buoyancy forces acting on them are not sufficiently high and that made difficult to determine the minimum fluidisation velocity. As there was observed fluidised and un-fluidised regions at the same time in the system, it was important to standardise an approach to determine de minimum fluidisation velocity to enable comparison of different bed characteristic. This was done by plotting the bed height expansion as a function of superficial liquid velocity as shown in figure 56. Extrapolation of a linear relationship between the superficial liquid velocity and ratio of bed expansion was used to determine the experimental minimum fluidisation velocity. The point of intersection of the expansion line with vertical line for packed bed height was taken as the minimum fluidisation velocity.

Figure 56 displays the bed height against liquid velocity obtained from the experimental results. This is shown on the plot for both the forward and reverse cases. U_{mf}, U indicates the minimum fluidisation velocity obtained by increasing the liquid velocities, and U_{mf}, d indicates the minimum fluidisation velocity obtained by decreasing the liquid velocity, U_{mf}, T is the

theoretical minimum fluidisation velocity. The Bars are the standard error of the height obtained from image analysis in ImageJ.

From figure 56 it can be observed that the height of the bed stays the same until it reaches the minimum fluidisation velocity after which it begins to increase. Before the minimum fluidisation velocity is reached, the fluid force on the fixed bed is not enough to cause it to change as it is less than the weight of the fixed bed. When U_{mf} is reached, the fluid force acting in the upwards direction upon the fixed bed is greater and for this reason the packed bed increases in height. Hence solid particles become suspended. At this point fluidisation takes place. From the experimental results, it can be identified that the minimum fluidisation velocity is directly proportional with solid particle size. The minimum fluidisation velocity rises with increasing particle diameter.

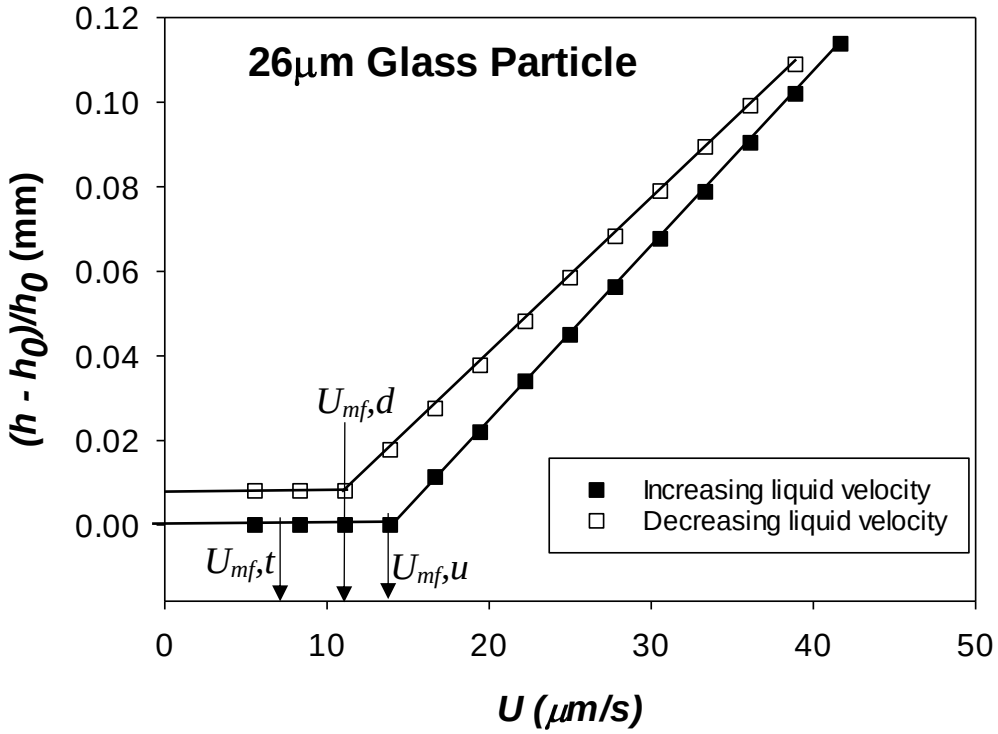

Figure 56. Relative bed height as a function of superficial liquid velocity, U, with increasing liquid velocity ($U_{mf,\,u}$), and decreasing liquid velocity ($U_{mf,\,d}$) for 26 μm glass microparticles in 1mm^2 micro-bed. Error are not visible in the graph as they are smaller than the symbols.

Figure 57 displays the minimum fluidisation velocity values obtained from the experimental investigation for 1mm and 2mm bed as a function of particle size. It can be observed that minimum fluidisation velocity is inverse proportional to bed size. For particles with same size and density U_{mf} increases with decreasing in bed size, and it can also be seen that the bed size becomes more significant with increase particle size special for PMMA particles.

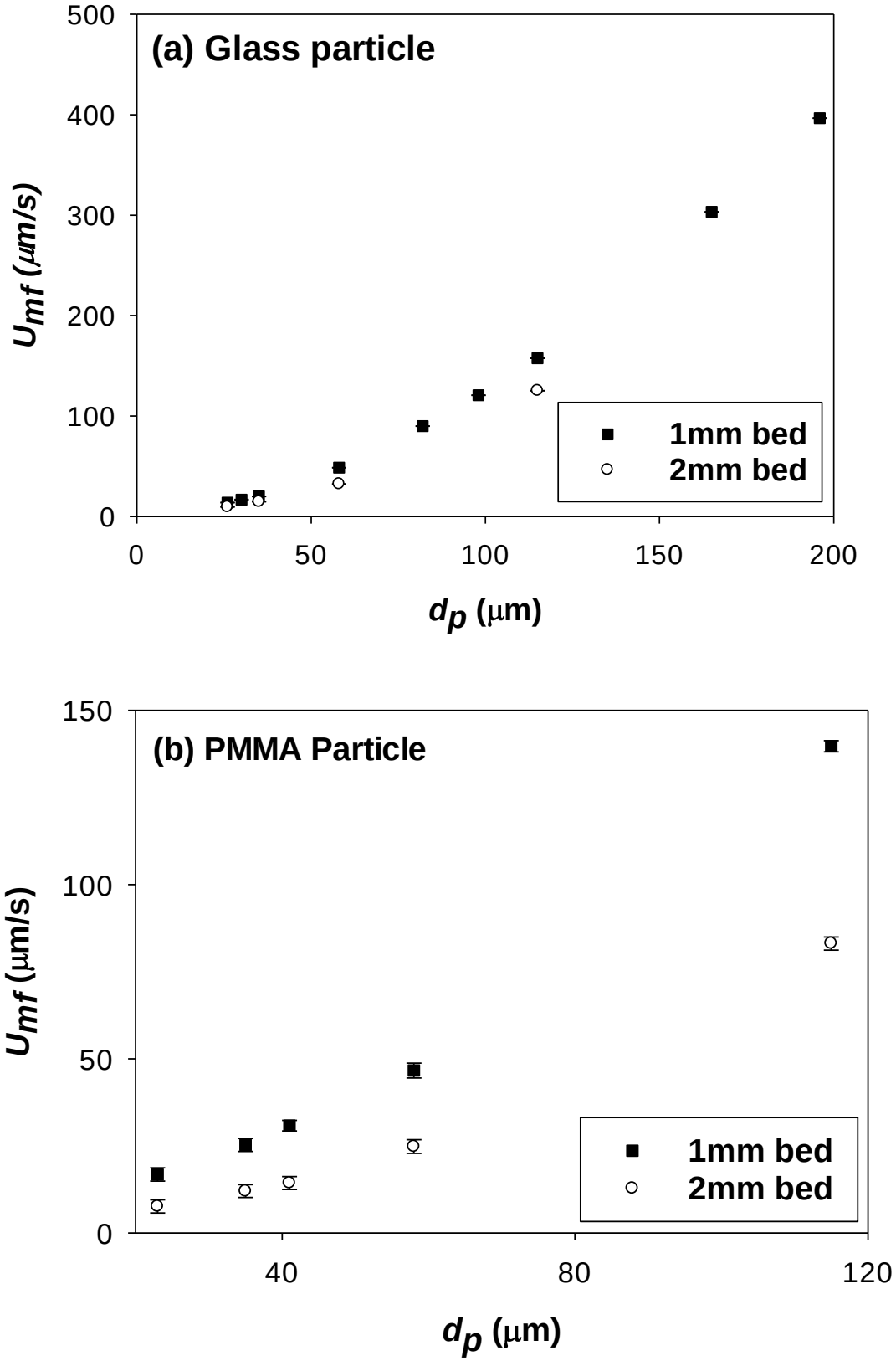

Figure 57. U_{mf} as a function of particle size for (a) glass and (b) PMMA particles inside a 1mm and 2mm bed

From figure 58 it can be observed that minimum fluidisation velocity is independent of bed height. For various bed heights used in the experimental study, the minimum fluidisation velocity required to achieve fluidisation was the same. The U_{mf} did not show changes when the initial bed height or solid inventory was increased. In other words the bed height did not have a significant effect on the minimum fluidisation velocity.

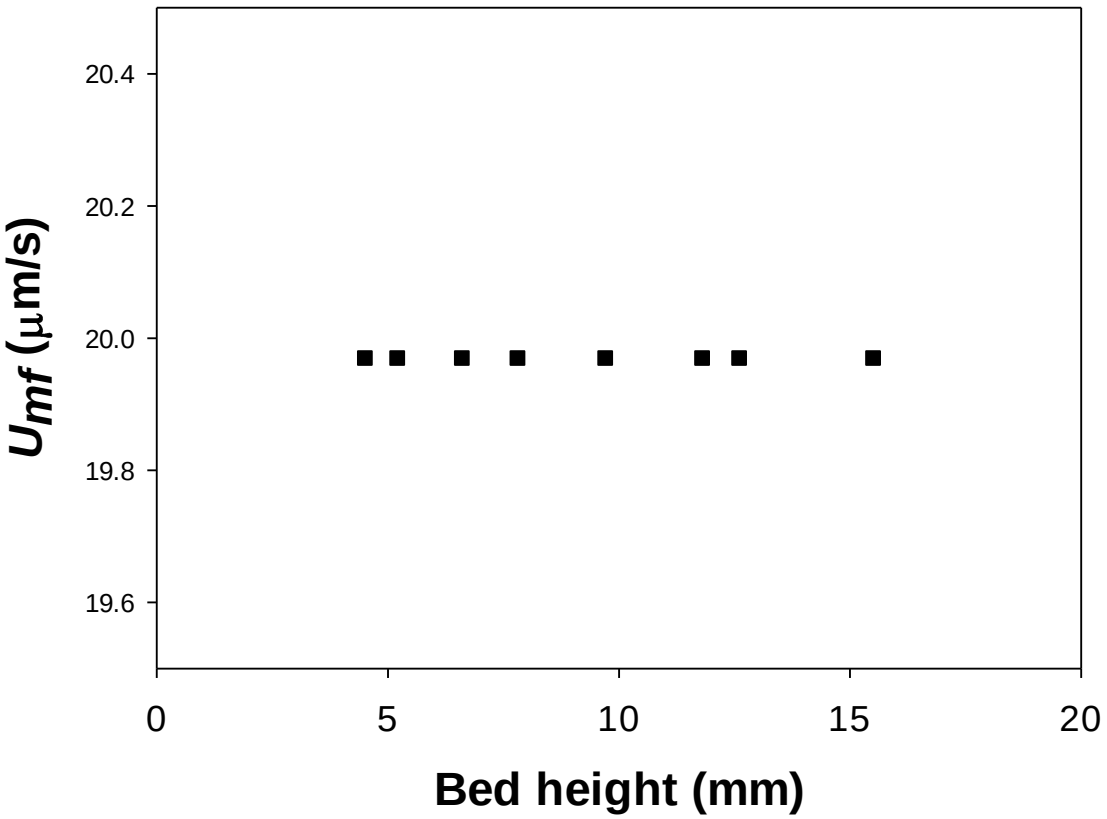

Figure 58. Effect of Bed height on minimum fluidisation velocity

4.5.1 Importance of surface force and wall effects

We plotted ratios of experimentally determined fluidization velocity over the theoretical calculated values using the Ergun equation as a function of adhesion/drag force ratios as shown in Figure 59 and 60. In the case of glass micro-particles, Figure 59, the velocity ratio goes below unity which is a consequence of underestimation of experimental minimum fluidization velocity by the extrapolation of expansion lines, a technique applied here as discussed in the previous sub-section. Yet, it seems that the velocity ratios level off at around 0.9 at lower fluid

velocities in the case of 2 mm^2 (empty circle) micro-fluidized bed indicating probably a 20-30% underestimation in the determination of the U_{mf} in our experiments. Regardless of these systematic underestimations, the figure undoubtedly shows that the increase in experimental minimum fluidization velocity is linearly scaling with the force ratio both for glass and PMMA micro-particles fluidization. However, it is noticeable that two distinct lines represent results in 1 mm^2 (full square) and 2 mm^2 (empty circle) micro-fluidized beds in both glass and PMMA particle fluidization experiments. This clearly indicates that wall effects, i.e. the particle-to-bed diameter ratio, influence the postponement of incipient fluidization in addition to the adhesion/drag force ratio.

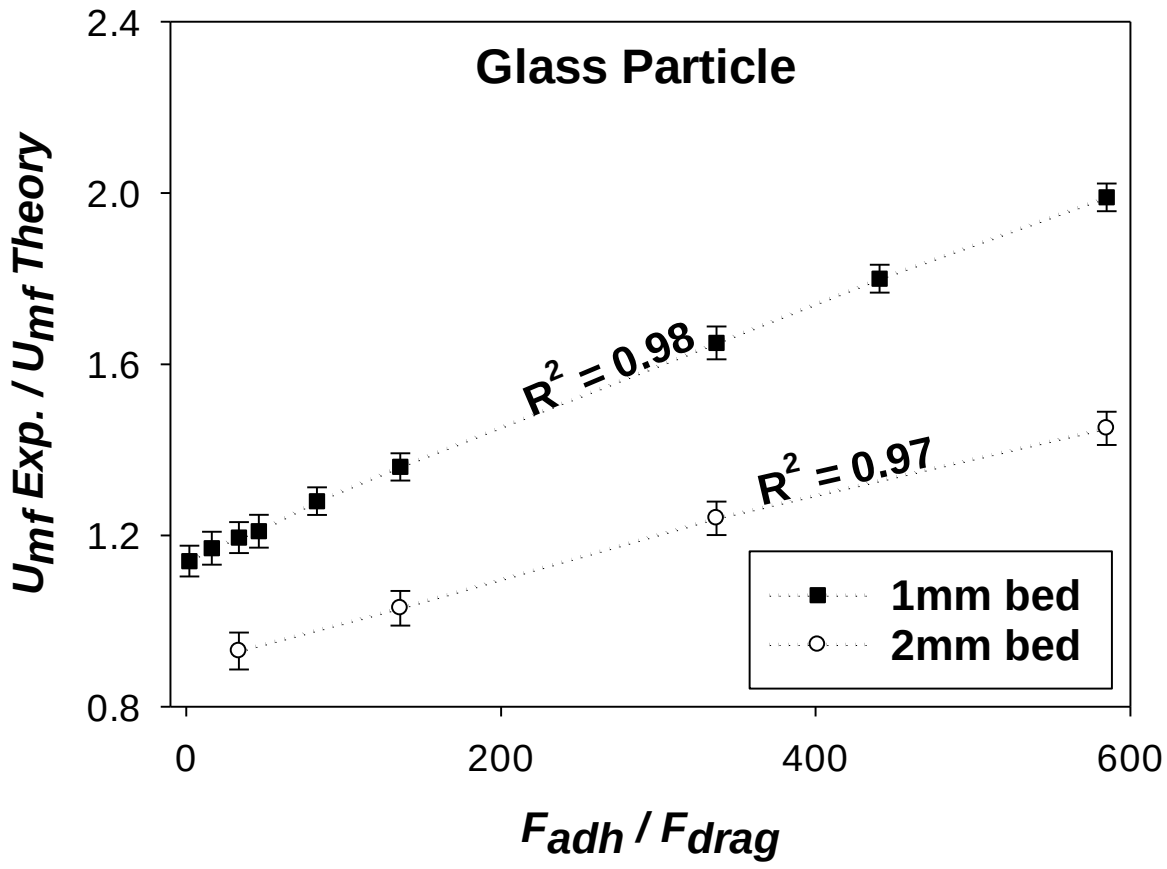

Figure 59. U_{mf} experimental/U_{mf} calculated vs. adhesion force/drag force for D = 1mm full square D = 2mm empty circle.

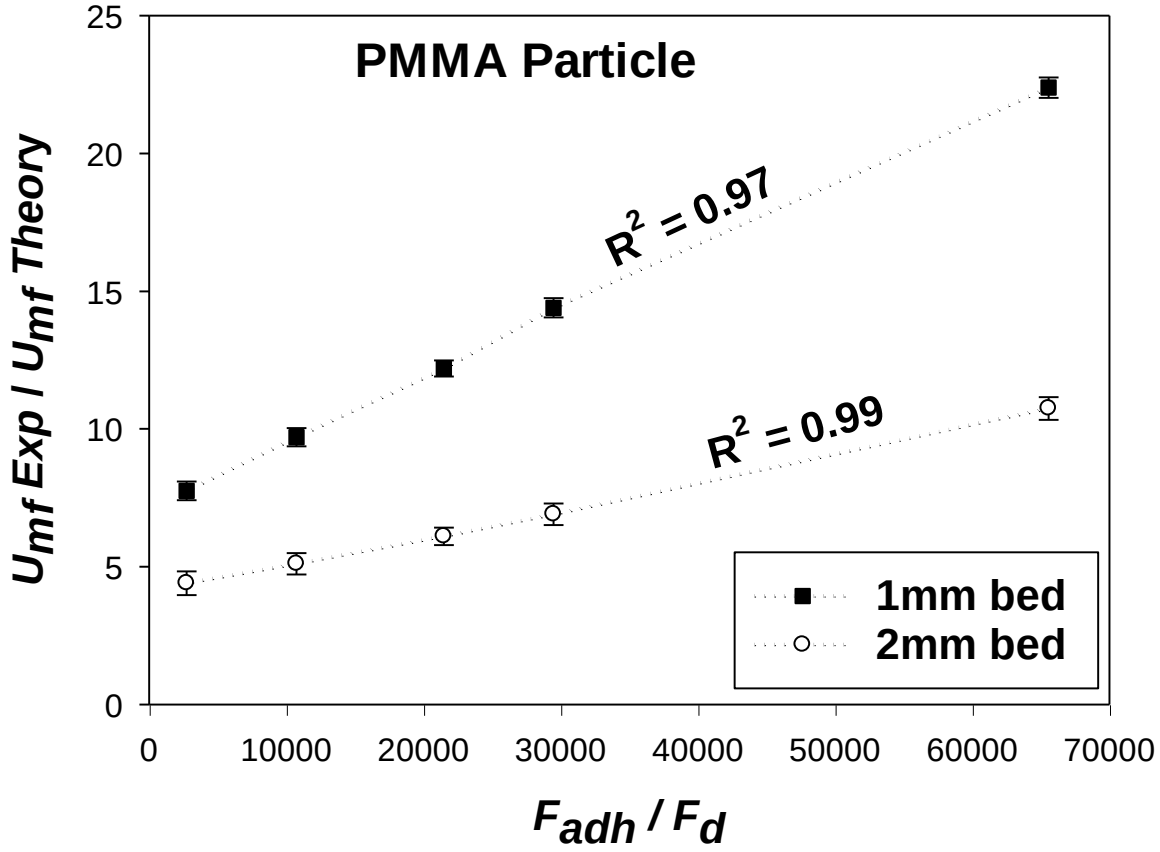

Figure 60. U_{mf} experimental/U_{mf} calculated vs. adhesion force/drag force for $D = 1mm$ full square and $D = 2mm$ empty circle.

In order to take wall effects into account, we replotted the data from Figure 59 and 60 as a function of the simple product of two ratios: adhesion/drag force ratio and particle-to-bed hydraulic diameter ratio. In both particles cases, the data fall on one master line showing good linear trend of increase of the minimum fluidization velocity as a function of the introduced ratios product. The linear fitting to the glass micro-particles fluidization data gives a line of slope 0.077 ± 0.0025 as shown in Figure 61 (adjusted $R^2 = 0.996$) while for the PMMA beads slope of linear fitting line is 0.027 ± 0.0009 (adjusted $R^2 = 0.996$), Figure 62. The difference in the slope of the lines for glass and PMMA particles could be caused by the cohesion of particles that is present in PMMA particles and not in glass particles when submerged in water. Cohesion increases particle size as a result of agglomeration and that reduces the significance of surface force and decreases the line of slope. In general cohesion will increase the particle size due to agglomeration which will reduce the importance of surface forces as the major factor and therefore reduce the slope of the line.

In the study of PMMA particles, experimental U_{mf} is approximately 4-23 times higher than the predicted $U_{mf.}$ The ratio between experimental U_{mf} and theoretical U_{mf} increases with decreasing particle size, for 23µm PMMA particle the ratio is almost 23 times higher. Although this corresponds to the level of surfaces importance, it is not completely proportional to surface and adhesion forces ratios, but rather scale with the product of force ratio and the particle to bed diameter ratio as can be seen in figures 60 and 62. Hence, both wall effect and surface forces influence fluidisation behaviour of micro-fluidised beds at the boundary of micro fluidisation.

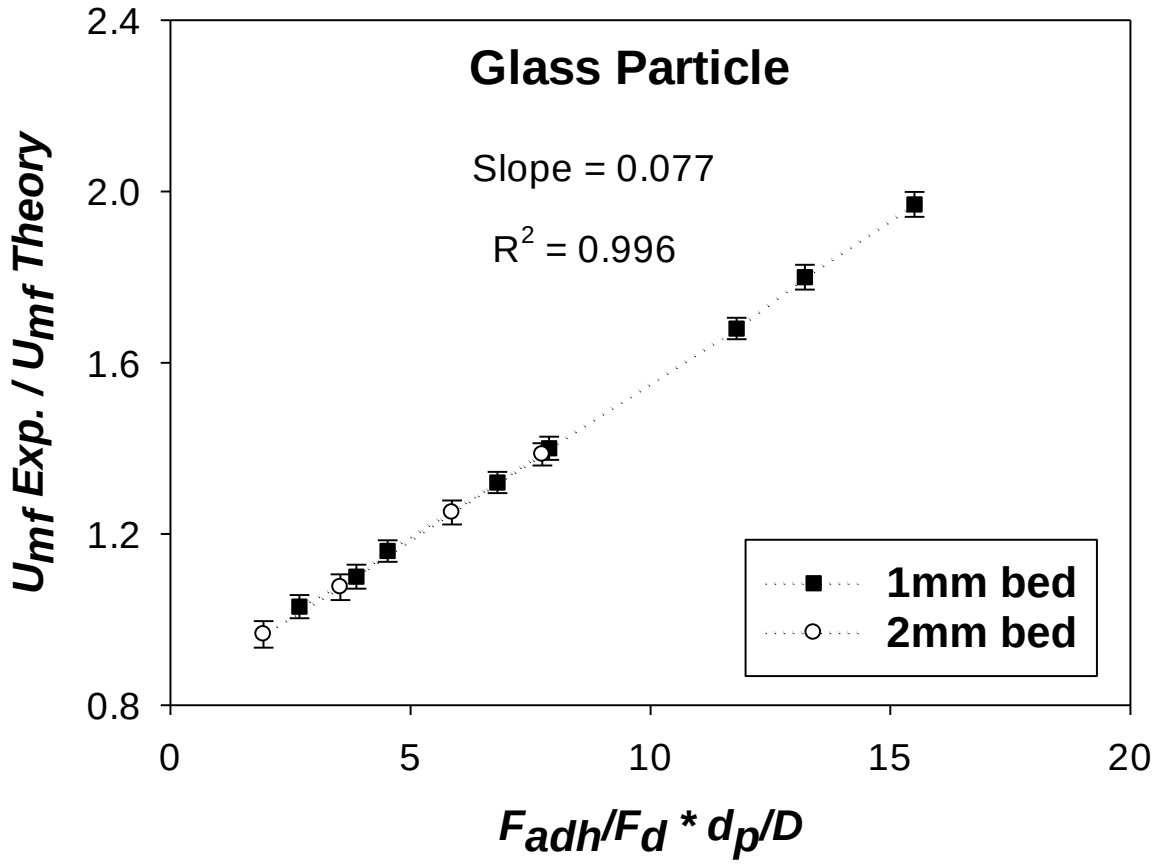

Figure 61. Ratio of experimental and theoretical U_{mf} versus product ratio for D = 1mm (full squares) and D = 2mm (empty circles).

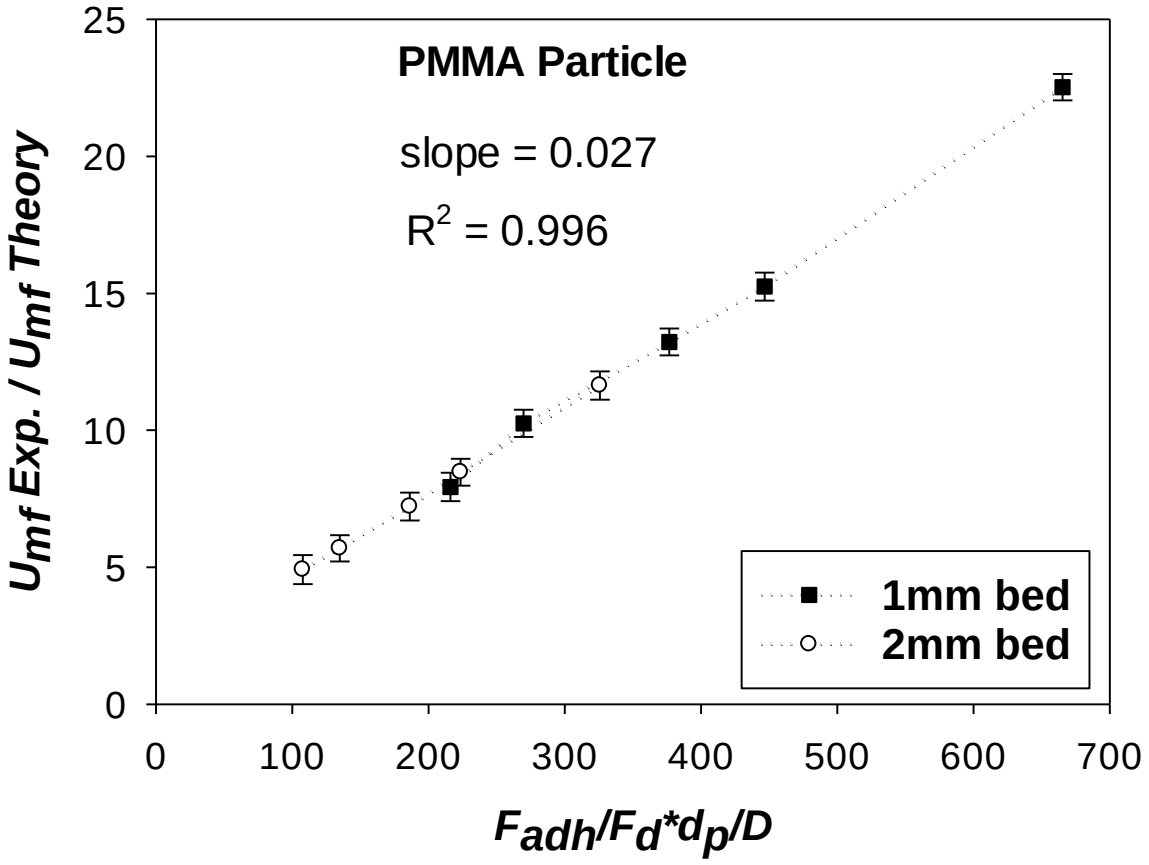

Figure 62. Ratio of experimental and theoretical U_{mf} versus product ratio for D = 1mm (full squares) and D = 2mm (empty circles).

In the study of PMMA particles, experimental U_{mf} is approximately 4-23 times higher than the predicted $U_{mf.}$ The ratio between experimental U_{mf} and theoretical U_{mf} increases with decreasing particle size, for 23μm PMMA particle the ratio is almost 23 times higher. Although this corresponds to the level of surfaces importance, it is not completely proportional to surface and adhesion forces ratios, but rather scale with the product of force ratio and the particle to bed diameter ratio as can be seen in figures 60 and 62. Hence, both wall effect and surface forces influence fluidisation behaviour of micro-fluidised beds at the boundary of micro fluidisation.

4.5.2 Hysteresis in micro-fluidization expansion behaviour

The expansion plots, Figure 56, shows obvious and quite large hysteresis effects in expansion lines for both glass and PMMA particles, probably due to considerable pressure overshoot for fluidization cycle experiments as already measured in the micro-fluidized bed [69]. This may also be an indication of jamming transition as demonstrated by the careful experimentation of

Goldman and Swinney [238]. We quantify the degree of hysteresis as the ratio of $U_{mf,u}$ and $U_{mf,d}$ for each size of particles. The velocity ratios were the order of 1.2-1.3 and 1.15-1.25 for PMMA and glass particles fluidization indicating larger hysteresis for more adhesive PMMA beads. The plot of glass particles fluidization results shows good trend of increase of hysteresis with the product of force and particle-to-bed diameter ratios as shown in Figure 63 (b). On the other hand, this trend is not present in results of PMMA particles fluidization with no obvious trend with either force ratio or particle-to-bed diameter ratio alone.

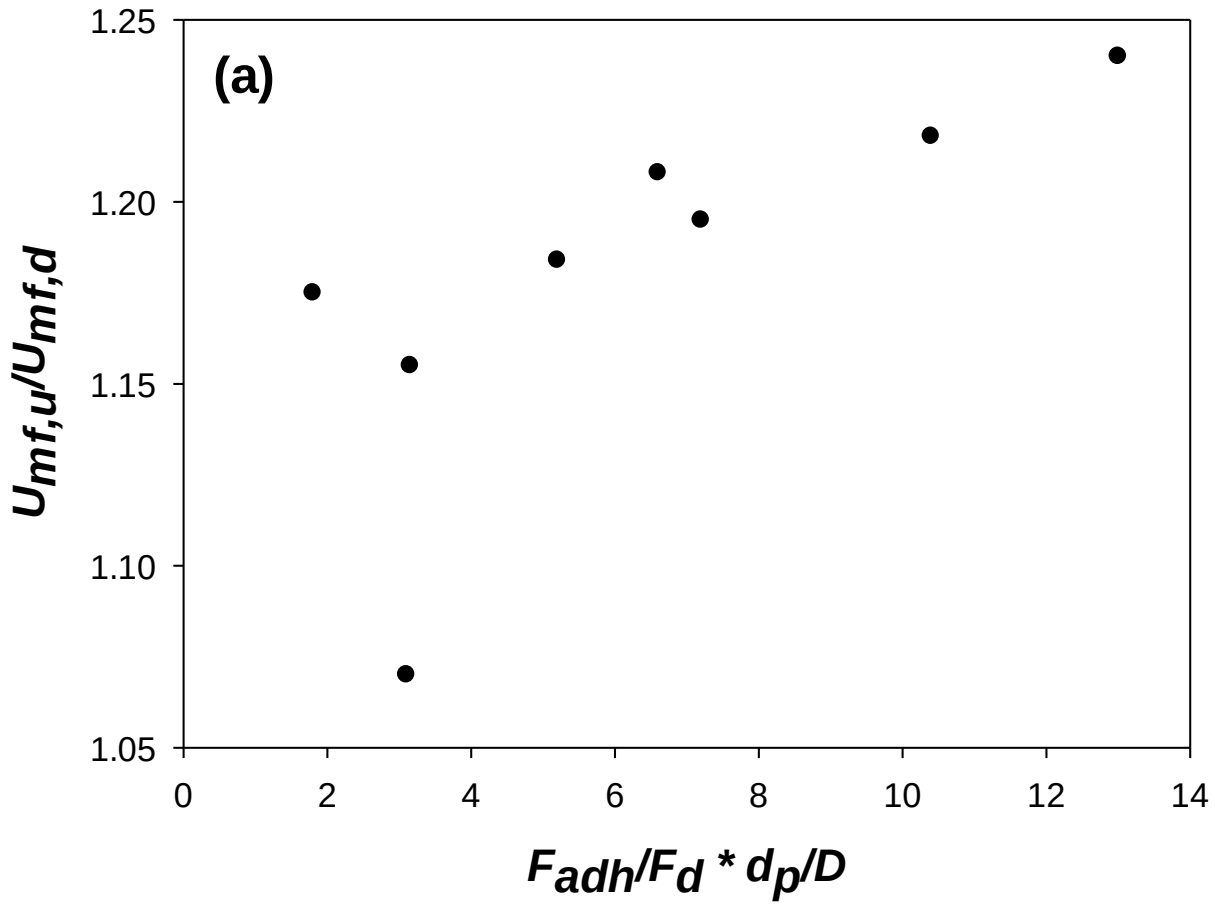

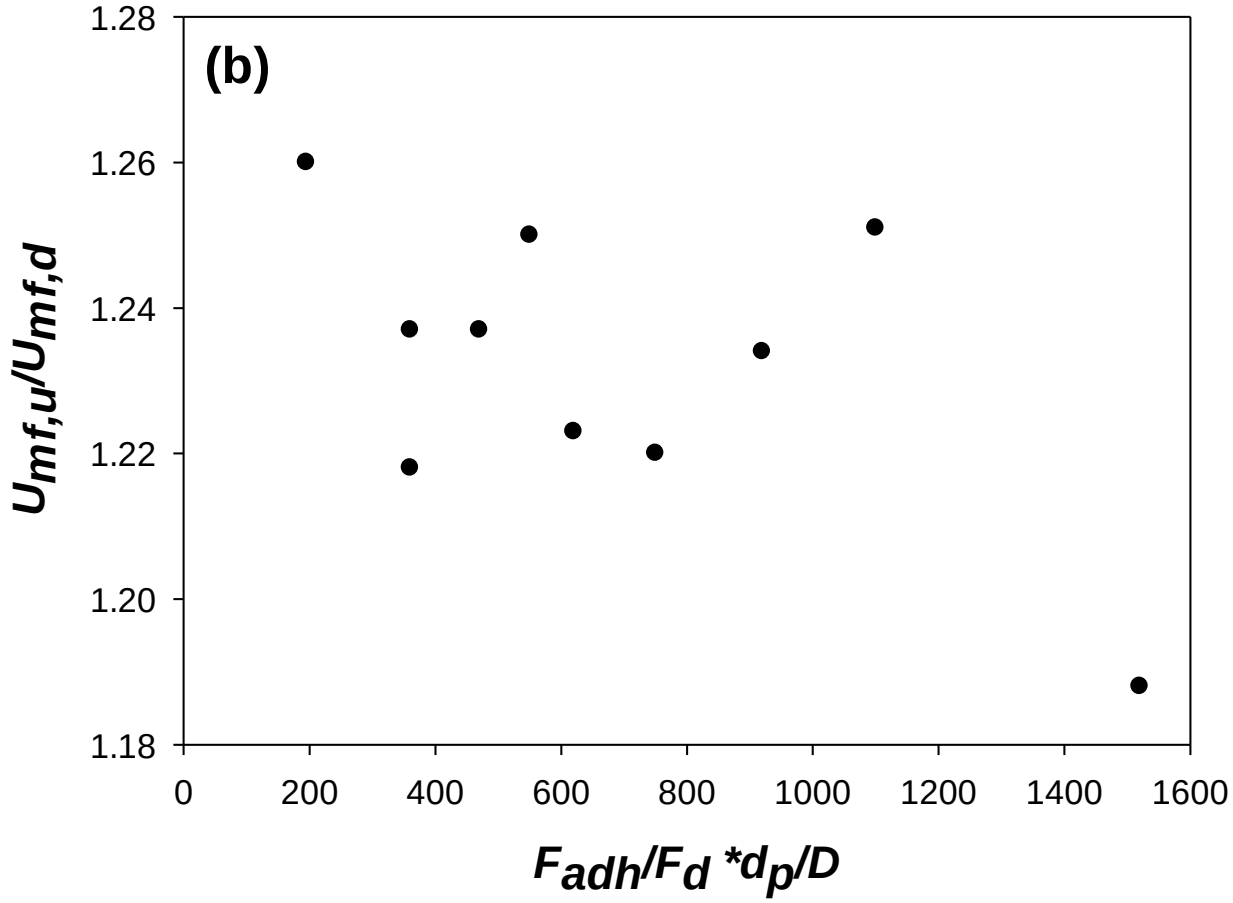

Figure 63. The ratio of the experimental minimum fluidization velocity for increasing, $U_{mf,u}$, and decreasing, $U_{mf,d}$, flow rate experiments versus product of force and particle-to-bed diameter ratios for (a) glass and (b) PMMA micro-particles.

4.6 Conclusions

We studied fluidization of glass and PMMA micro-particles in 1 mm^2 and 4 mm^2 square micro-fluidized beds made of Perspex (PMMA). As predicted by the acid-base theory of van Oss, Chaudhury and Good there was noticeable adhesion to the bed walls for both particle materials. The Derjaguin approximation was used to estimate adhesion forces between micro-particles and bed walls for comparison with drag forces approximated by the buoyant weight of the particles. The observed incipient fluidization in the micro-fluidized bed was postponed in comparison with theoretical predictions based on macroscopic experiments. This was influenced both by adhesion strength and wall effects. The increase in the minimum fluidization velocity scales linearly with the simple product of adhesion/drag force and particle-to-bed diameter ratios. Particle cohesion and bed walls/particle materials properties like

elasticity influence the scaling relationship but further investigation is needed on this point. The hysteresis is proportional to the product of force and particle-to-bed diameter ratios in the case of glass particles but not for PMMA particles' results- further investigation is needed to elucidate this further.

Chapter 5. Solid circulating velocity measurement in a liquid-solid micro-circulating fluidised bed system

5.1 Introduction

One of the major tasks in liquid-solid circulating fluidised bed is to use the reliable technique to measure the solid circulating velocity in the system. An accurate solid circulating velocity measurement is desirable as it reduces operational and capital cost, increases safety and provides process stability [239, 240]. As previous mentioned one of the fundamental parameters needed to quantify mass and heat transportation and one that dictates the fluidised bed capability as a reactor, is the solid circulating velocity in the bed, which controls the time of contact between solid and liquid. Solid circulating velocities are important as they affect heat and mass transfer, erosion, and mixing in circulating fluidised beds. Measurement of solid circulating velocity in a micro circulating fluidised bed is extremely hard to be implement using current measurement technology such as butterfly valve, X-ray tomography, electrical capacitance tomography, magnetic resonance imaging, as they are expensive, as it is very difficult to scale down these techniques for application in a microfluidics context [60].

The solid circulation rate measurement in a solid-liquid circulating fluidised bed has been reported previously by various researchers. Several research groups [36, 106, 107, 210] measured the solid circulation rate by using a simple procedure with a measuring valve in the downcomer. The accumulation of particles above the ball valve at a given time interval could be measured by closing the valve in the downcomer, thus giving the particle circulation rate. They reported that the solid circulation rate increases with liquid flow rate and solid feed pipe diameter but decreases with increasing particle density and size. Roy, Kemoun [194] used a radioactive technique to measure the solid circulation rate. The basic idea was to determine the particles volumetric flow rate by measuring the particles velocity and volume fraction in the downcomer. Particle volume fraction was obtained by densitometry measurement, while particle velocity was obtained by measuring the falling time of a single radio-active tracer particle between two detectors installed in the downcomer. This type of measurement technique is costly and requires considerable safety measures. Wu *et al*. [192] and Masuda and Linoya [241] measured the solid circulation rate based on the impact technique. In this technique an impact plate flow meter installed in the downcomer is employed to determine the solid circulation rate by measuring the force of re-circulating particles falling onto an inclined plate.

The disadvantage of this type of solid flux measurement device technique is the issues with its breadth measurement range and calibration is very complex. Hensler, Firsching [242] employed X-ray tomography to determine the solid circulation rate. They found that the solid circulation rate increases with liquid velocity. Wang, Dyakowski [243] used electrical capacitance tomography to measure the solid circulation rate in a circulating fluidised bed. Patience et al. [194, 244] used an approximate technique to estimate the solid circulation rate in a gas-solid circulating fluidised bed system based on differential pressure drop measurement. Lech [245] predicted the solid circulation rate based on parallel measurement of pressure drop and particles velocity. They also reported an increase in the solid flux with an increase in the liquid velocity. Kuramoto et al.[246] measured the solid circulation rate by using a tracer micro-spherical particles coated with fluorescent dyes. The tracer particles motion was detected by a fiber optic sensor installed in the storage vessel.

In the current research investigation, particle imaging velocimetry (PIV) software PIVlab [200], was used to determine the solid circulating velocity in the micro-circulating fluidised bed. A digital PIV technique has been employed previously by researchers for measuring the flow velocity profiles in granular flow [201, 202]. The advantage of this technique over other conventional techniques such as the butterfly and ball valve technique are that it is non-invasive and easy to implement in microfluidics setup which is not trivial for the valve. The effects of operating parameters such as solids inventory, particle size and density on solid circulating velocity has been carefully studied using PIVlab and Matlab.

5.2 Experimental details

5.2.1 Experimental set up

The schematic representation of the experimental set up is illustrated in Figure 64(a). The system consists of a syringe pump (AL-4000, WPI INC., US) to pump the water as a fluidising medium at the desired flow rate using a 5ml B-D Plastipak syringe, and Basler aCA1300-200uc digital camera to record the micro fluidisation behaviour. The system used in the present experimental investigation was made by micro machining channels in Perspex as schematically shown in Figure 64(b). The micro-circulating fluidised bed consist of a riser column of 1 mm square cross-section and 100 mm in height, a solid-liquid separator, a down comer acting as a particle reservoir, a solid return pipe, and a solid feeding pipe. At the base of the riser is the distributor (a 1.5 mm thick porous plate distributor with mean pore size of 21 μm) which prevents particles leaving the bed at the bottom and provides uniform flow distribution and stable fluidisation. The solid-liquid separator is a simple diamond shaped expansion that

enables the particles to be separated from the outflowing liquid as the reduced liquid superficial velocities is not sufficient for liquid to carry over particles.

5.2.2 Particles and liquid used in the present study

Two different groups of particles were used as fluidised solid: (1) soda lime glass microspheres of five different diameters, d = 26 ± 1.5 μm, 30 ± 1.5 μm, 35 ± 3 μm, 58 ± 5 μm, 82 ± 6 μm, 98 ± 8 μm, 115 ± 9 μm, *165 ± 15 μm*, *196 ± 16 μm* µm whose density is ρ_p = 2500 kg/m^3 and (2) PMMA particles of five different diameters, d = 23 ± 3.5 μm, 35 ± 3 μm, 41 ± 3.5 μm, 58 ± 5 μm, and 115 ± 9 μm whose density is ρ_p = 1200kg/m^3. Tap water (density ρ_f = 998 kg/m^3 and viscosity μ_f = 0.001 Pa.s) was used as the fluidising liquid. All experiments were performed at room temperature of average 18 ± 2 ºC.

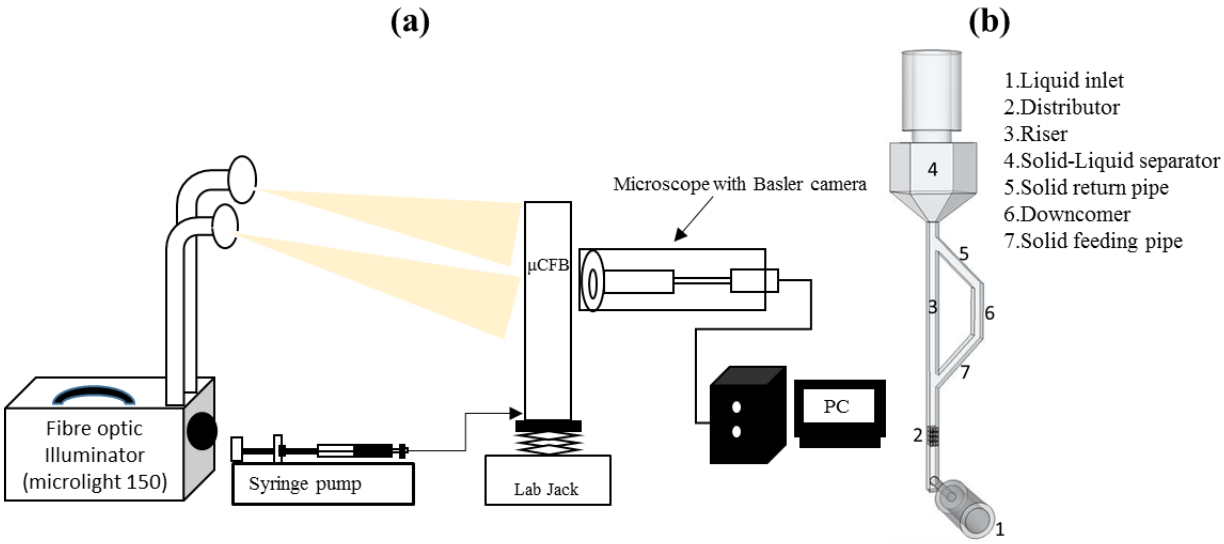

Figure 64. Schematic of (a) experimental set up for imaging and (b) micro-circulating fluidised bed.

5.2.3 Experimental procedure

Prior to loading the particles into the micro-circulating fluidised bed, the bed was cleaned several times with tap water to make sure that no particles and air bubbles was left within the system. The bed was filled with liquid (water) using a syringe pump, taking care to ensure no air bubbles entered the fluidised bed system. This was done because any trapped air bubbles within the system could affect the experimental results. Once the CFB was flooded with water, PMMA and glass particles (23-196 µm) were loaded into the top of the CFB and left to fall down on to the top of the distributor by gravity. The solid particles were left to settle for 24 hours, to ensure they properly settled in the bed. Calibration was performed with and without particles to determine the flowrate at which liquid moves through the system and showed a

good linear relationship from the pump reading. The solid inventory was measured with the aid of ImageJ [237]. This was done by measuring the initial static bed height using ImageJ and expressed in terms of surface percentage occupied by the particles out of the whole system surface (in this case this is the same as volume percentage as the depth is constant) as shown in figure 65. Liquid at varying velocity was pumped by a syringe pump from the syringe to the bed inlet to produce the fluidisation liquid at the required velocity in the bed. Particles at the bottom of the riser were kept in motion by the upward liquid flow. When the liquid flow rate was high enough, particles were carried out of the riser and separated from the outflowing liquid by the solid-liquid separator and recirculated back to the riser through the solid feed pipe. The experimental procedure was performed with both decreasing and increasing superficial liquid velocities. For each particle, this procedure was repeated at least three times to ensure repeatability and the measurement of experimental errors. Digital movies of granular flow were captured by a Basler aCA 1300-200uc digital camera which as a resolution of 1.3 MP. Basler Pylon viewer software was used to monitor the recording process. Flexible fiber optic illuminator was used to illuminate the granular flow in the circulating fluidised bed and produce high quality image. The camera capture rate was set to 25 fps with a shutter time of 100 μs after preliminary test revealed that it provided high quality videos without motion blur and the optimal PIV results. Each video has a recording time of 20 seconds. The images and movies were saved on a computer for offline study. The off-line examination comprised of movies converted into successive frame sequences by VLC media player, and the particle displacement calculation was made from successive frames using PIVlab, a Matlab code, which determines the velocity of particles by cross correlating a PIV algorithm of multiple small sub-images.

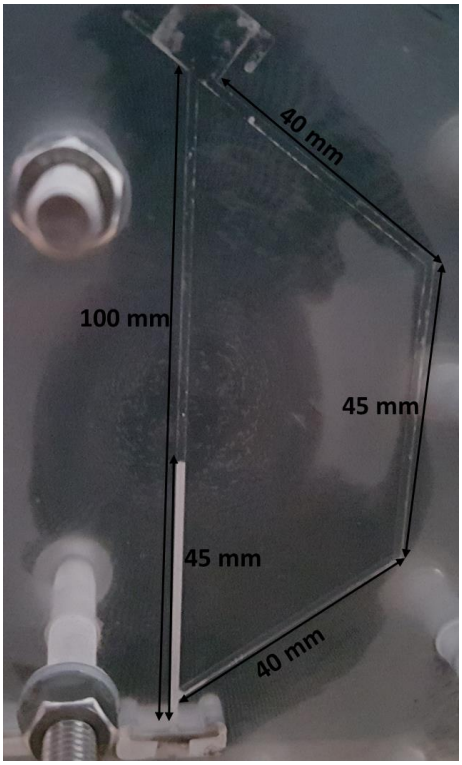

Figure 65. Example of solid inventory measurement with static bed height of 45mm as determined by ImageJ. In this case 45mm static bed height corresponds to 20% of surface percentage occupied by the particles out of the whole system surface. Therefore, the solid inventory in the system was estimated to be 20%

5.3 Results and discussion

5.3.1 Background movement

Initial PIVlab image analysis shows that particles move upwards as shown in Figure 66(a) instead of downwards along the solid feed pipe as expected and visually observed. Further analysis showed considerable background movement, so it was necessary to calculate the background movement velocity field using PIVlab as shown in Figure 66(b). The imported vector field of particles in the solid feed pipe in Matlab is shown in Figure 67(a) with the erroneous upward motion of particles. The velocities were then correctly adjusted by subtracting the background motion, Figure 66(b), in Matlab to obtain the correct particle velocity field with downward motion as shown in Figure 67(b).

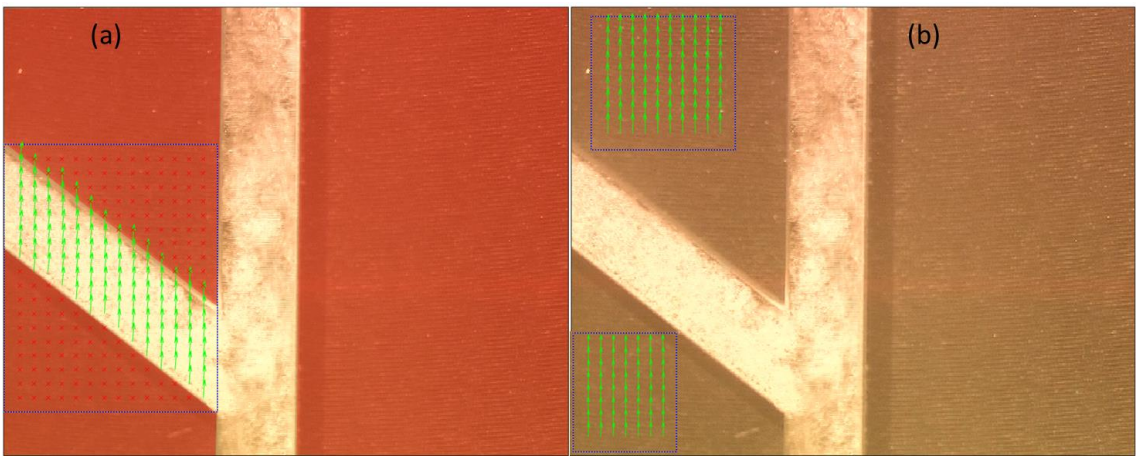

Figure 66. Velocity vector field in (a) the solid feed pipe and (b) in background determined by PIVlab analysis.

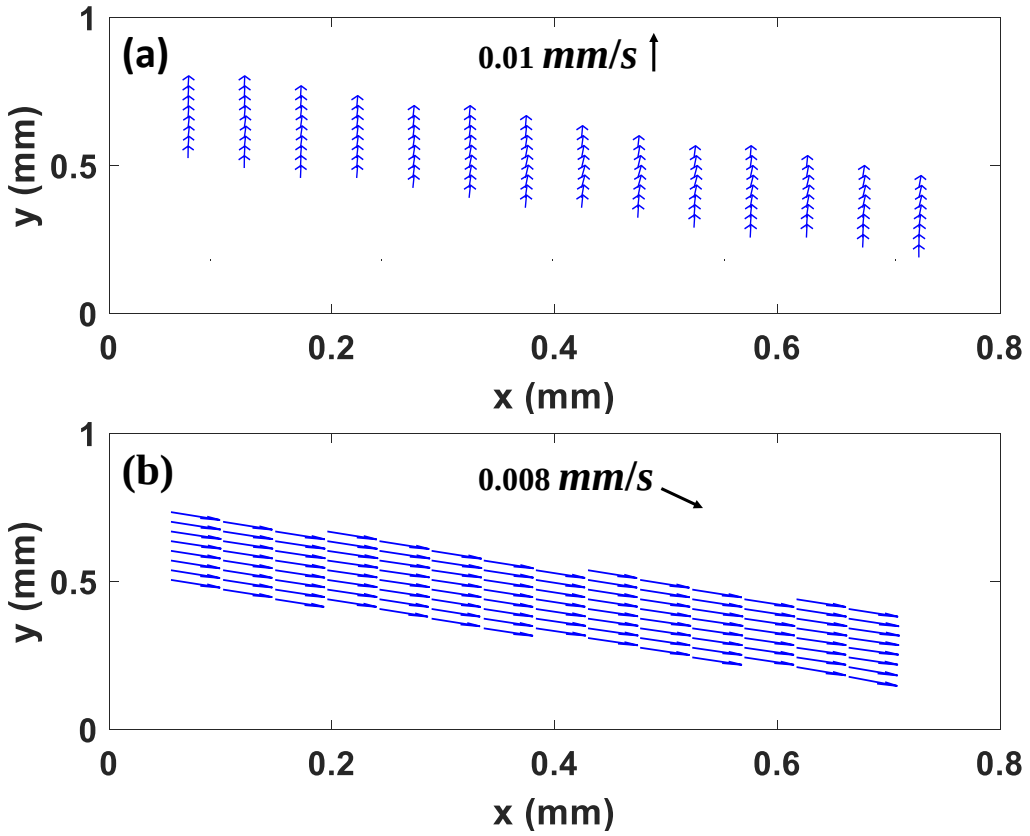

Figure 67. Examples of Original particle velocity field (a) and the velocity field after subtraction of the background movement (b) for the 58 µm glass particle at 445 µl/min liquid flow rate with 15% solid inventory bed.

5.3.2 Effect of the liquid flow rate on solid flux

In solid-liquid circulating fluidised beds, particle motion is controlled by changing the inlet superficial liquid flow rate. Figure 68 displays the effect of liquid velocity on the solid circulating velocity for glass and PMMA particles as determined by digital PIV analysis described in the previous section. The experimental results indicate that by increasing the superficial liquid flow rate, the solid circulating velocity in the system is close to zero (no solid

movement) then increases sharply at some critical superficial liquid velocity and then plateaus at higher superficial liquid flow rate. The change in solid circulating velocity with superficial liquid flow rate indicates two zones. The first zone (initial circulating fluidisation zone) where solid circulating velocity increases rapidly with increasing superficial liquid flow rate and the second zone (fully developed zone) where solid circulating velocity insignificantly varies with increasing superficial liquid velocity as reported by Zheng [107]. The critical transition velocity from a conventional fluidised bed to circulating fluidised beds occurs at the point where the solid circulating velocity becomes zero with reducing superficial liquid velocity. Thus, the critical transition velocities are determined as the intercept of no particle flow (nearly zero) and initial circulating zone line as shown in the plots. These plots clearly also show that the critical transition velocity, U_{cr}, is approximately equal to the particle terminal velocity, U_t in all consider cases.

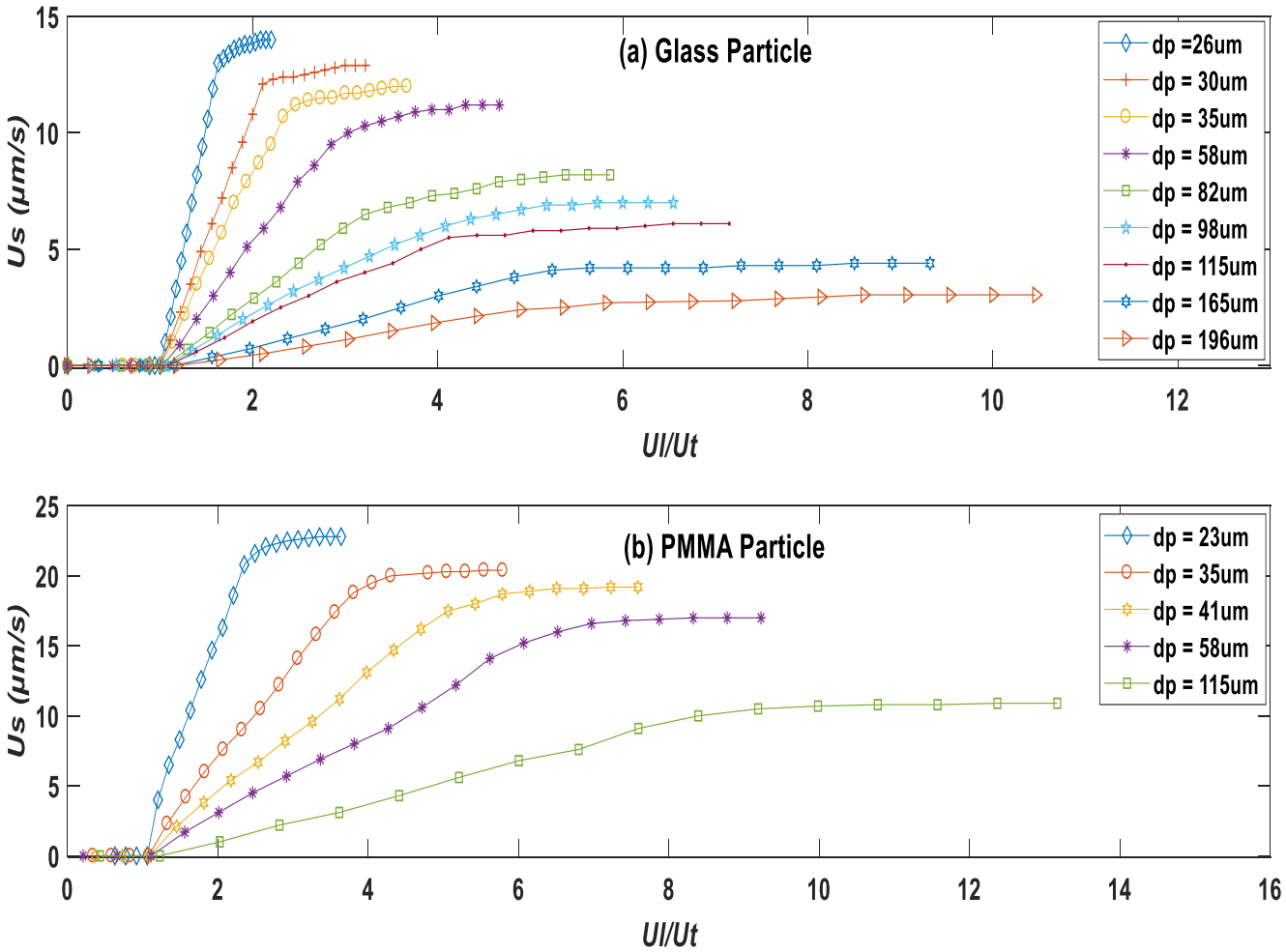

Figure 68. Particle circulating speed as a function of normalised velocity (U_l/U_t) for (a) glass and (b) PMMA particle. Errors are smaller than the symbols.

5.3.3 Effect of solid inventory in the system

Figure 69 shows the normalised critical transition velocity as a function of solid inventory, indicating that in the solid-liquid micro circulating fluidised bed the critical transition velocity is strongly influenced by solid inventory. For beds with a solid inventory lower than 10 %, a higher superficial liquid velocity is required to achieve a circulating fluidised bed, and the transition from conventional to circulating fluidised bed is greater than the particle terminal velocity (U_{cr}/U_t = 1.5 to 4.7). However, for systems with a solid inventory higher than 10%, the critical transition velocity from conventional to circulating fluidised bed regime occurs close to the particle terminal velocity, and the normalised transition velocity is approximately 1. These observations are similar to those reported by Liang et al. [106], the critical transition velocity decreases with solid inventory and finally becomes stable when the solid inventory is high enough. This is slightly different from the observation reported by Zheng and Zhu as their reported onset velocity (U_{cf}) which gives the lowest critical transition velocity from the conventional to circulating fluidised bed regime was found to be independent of the bed geometry, operating conditions and solid inventory, probably due to the method applied.

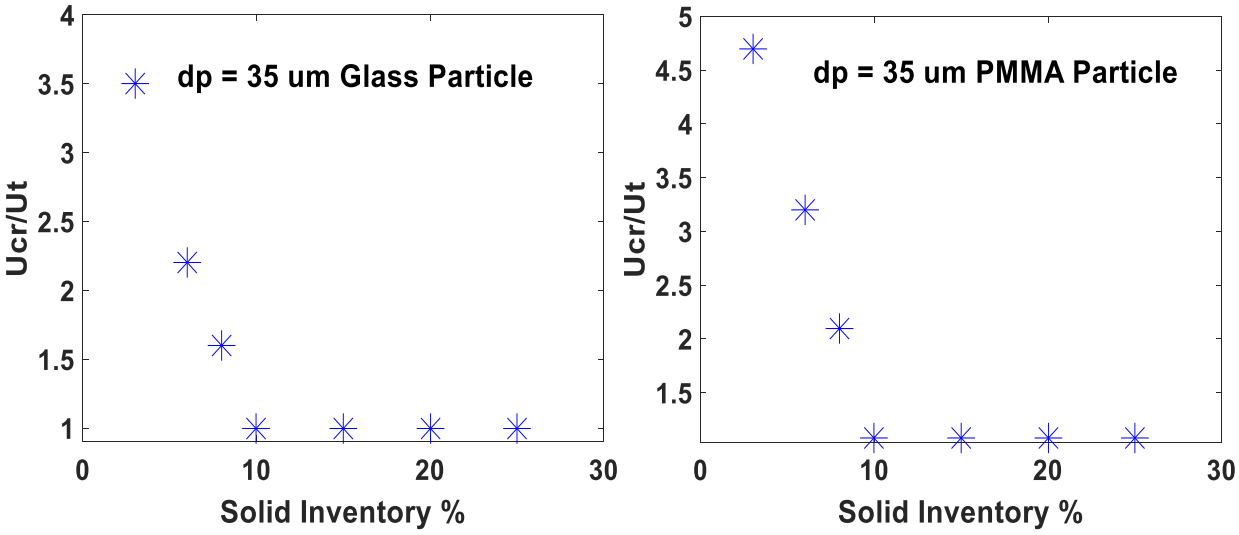

Figure 69. Effect of solid inventory on normalised transition velocity for 35µm (a) glass and (b) PMMA particles.

5.3.4 Effect of particle size

Figure 70 shows that the transition from conventional to circulating fluidised bed regime in a solid-liquid micro circulating fluidised bed is influenced by particle properties such as size and surface properties beyond the influence on the particle terminal velocity. First there is a trend of increased normalised critical transition velocity with an increase in particle size which is probably because of increased wall effects which are not usually present in large circulating fluidised beds. It can also be observed that the normalised transition velocity (U_{cr}/U_t) is

considerably higher for PMMA particles compared to glass particles of the same size. This is probably due to the difference in surface properties with PMMA particles being hydrophobic while glass particles are hydrophilic. Particle agglomeration due to cohesion was visually observed for PMMA as was some particle adhesion to the walls. Cohesion increases particle size as a result of agglomeration and that may postpone the critical transition velocity (U_{cr}) from conventional to circulating fluidised bed regime and the wall adhesion present in the downcomer will also contribute to postponing transition.

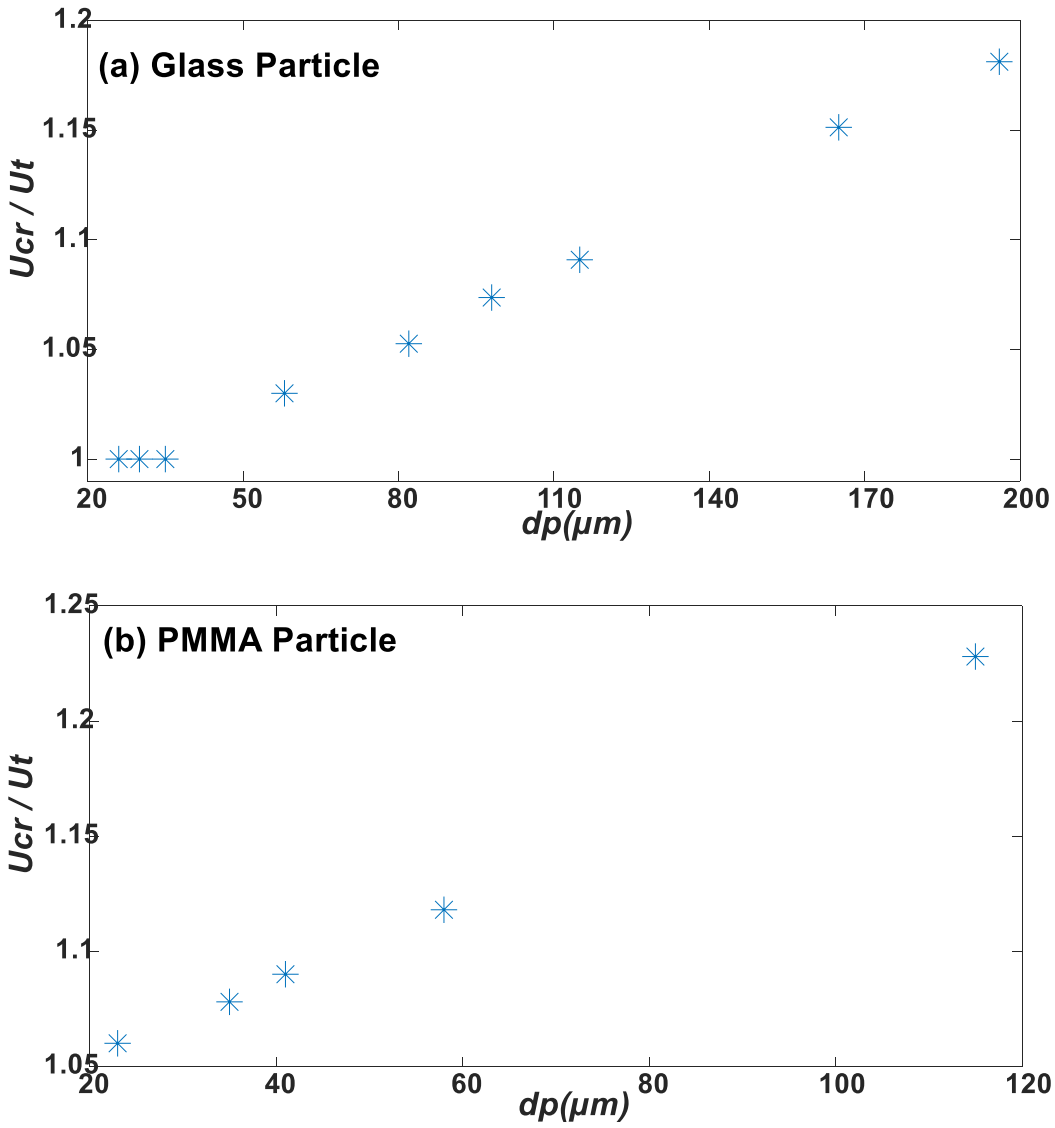

Figure 70. Normalised critical transition velocity as a function of particle size for (a) Glass and (b) PMMA micro-particles with solid inventory in the range of 10 - 25%.

5.4 Validation

A second experimental study was carried out to measure the solid flux in a liquid-solid micro-circulating fluidised bed. In this experimental investigation a novel measurement technique, the magnet for solid flux measurement was developed to measure the solid flux in the micro-circulating fluidised bed and the results was compared with those obtained using PIV software.

In order to validate the PIV measurement in micro-circulating fluidised bed, two experimental investigation was carried out, the first experiment was the solid flux measurement by PIV technique and the second experimental investigation was the solid flux measurement by a magnet valve (accumulation method). For the solid flux measurement by PIV methodology all the procedures used in the previous PIV study were employed.

Additive manufacturing was used for design and fabrication of a novel micro-circulating fluidised bed (μCFB). With 3D printing it is easy to implement the magnet valve to measure the solid flux which would be extremely difficult to implement using the present traditional design technique.

The micro-circulating fluidised bed used for both experimental investigations is shown in figure 71.

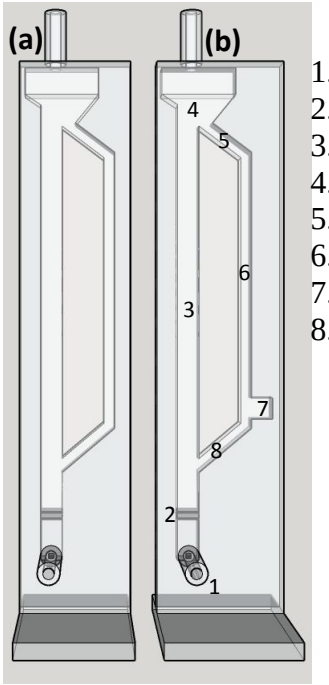

1.Liquid inlet
2. Distributor
3. Riser
4. Solid-liquid separator
5. Solid return pipe
6. Downcomer
7. T-piece
8. Solid feeding pipe

Figure 71. Schematic of the two micro-circulating fluidised bed used for the research experiment: (a) shows the bed used for the PIV measurement technique and (b) shows the bed used for the magnet measurement technique (accumulation method).

The micro-circulating fluidised bed consist of a riser column of 2mm square cross-section and 100 mm in height, a solid-liquid separator, a down comer acting as a particle reservoir, a solid return pipe, and a solid feeding pipe. At the base of the riser is the distributor (a two layer of parallel array pillars of 150 µm diameter and 100 µm spacing which prevents particles leaving the bed at the bottom and provides uniform flow distribution and stable fluidisation. In this experimental investigation lime glass micro-particles of two different diameters, d = 165µm ± 15 and d = 196 ± 16 µm whose density is ρ_p = 2500 kg/m^3 were used as the fluidised solid and tap water as the fluidising liquid. The above microsphere glass particles were chosen for this experimental study because the liquid distributor was not able to support any particle of diameter below 150 µm.

5.4.1 Solid circulation rate using magnet

A magnet was installed inside the micro-circulating fluidised bed (downcomer) as shown in figure72, and an external magnet was used to move and control the magnet inside the bed. The solid circulation rate was measured by closing the downcomer with a magnet which was installed in the circulating fluidised bed system, and noting the time required to accumulate a defined height of solids above the magnet and the equation 25 from chapter 3 was used to calculate the solid circulation rate. Since the bed was transparent, it was possible to observe visually the accumulation of solids after closing the valve, and ImageJ was used to determine the bed height from images as shown in Figure 72.

Figure 72. Picture of 3D printed micro-circulating fluidised bed with a magnet inside the system used to measure the solid circulation rate

Figure 73 presents the experimental results obtained from both, the solid circulating velocity measurement by PIV technique and with magnet valve technique. We plotted the particle circulation velocity as a function of normalised velocity for both 165 µm and 196 µm glass microsphere particle.

To facilitate comparison between the PIV technique and accumulation method, the solid circulation rate obtained from the accumulation method was converted to circulating solid velocity using equation 27 [99, 107].

$$U_s = \frac{G_s}{\rho_s} \qquad (27)$$

Where ρ_s is the solid density, U_s solid circulating velocity, and G_s solid circulation rate. (Example of solid circulation rate conversion to solid velocity are given in appendix)

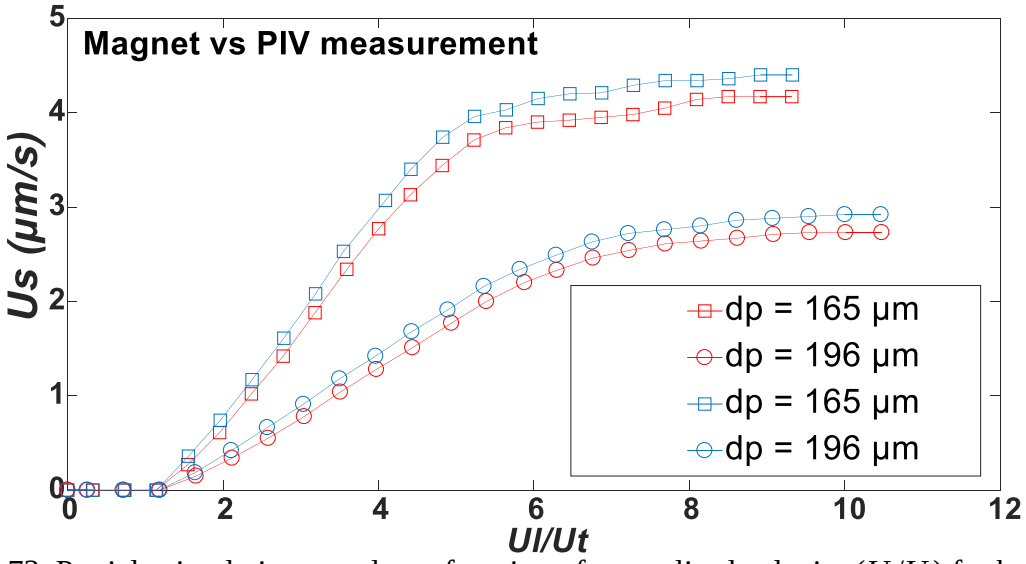

Figure 73. Particle circulating speed as a function of normalised velocity (U_l/U_t) for both PIV technique (blue) and accumulation method (red)

In general, the solid circulating velocity based on the accumulation method (magnet) was found to be 5-10% lower to the PIV technique measurements for all liquid velocities as shown in figure 73. However, for both measurement technique the critical transition velocity from conventional to circulating fluidised bed regime are almost identical as shown in figure 74. The critical transition velocity is just slightly higher for the accumulation technique for both 165 and 196 µm particle. Albeit the accumulation technique is simple to perform, and the solid flux in system can directly be determined, the measurement is not continuous. The interference caused by closing the downcomer with the magnet valve disturb the steady state operation of the system. Particle accumulation in the circulating fluidised bed downcomer imply reduction of particles in other part of the system and this introduce changes to fluidisation characteristics in the riser during the measurement. The larger the volume of particle accumulated in the downcomer, albeit increasing resolution of the results, the more unreliable is the experimental result as it influences dynamics in other part of the system. Overall the results obtained from these techniques agreed well with each other, and this agreement provided a strong basis for the development of a novel Particle image velocimetry (PIV) software PIVlab method and accumulation technique to measure the solid flux in a micro-circulating fluidised bed.

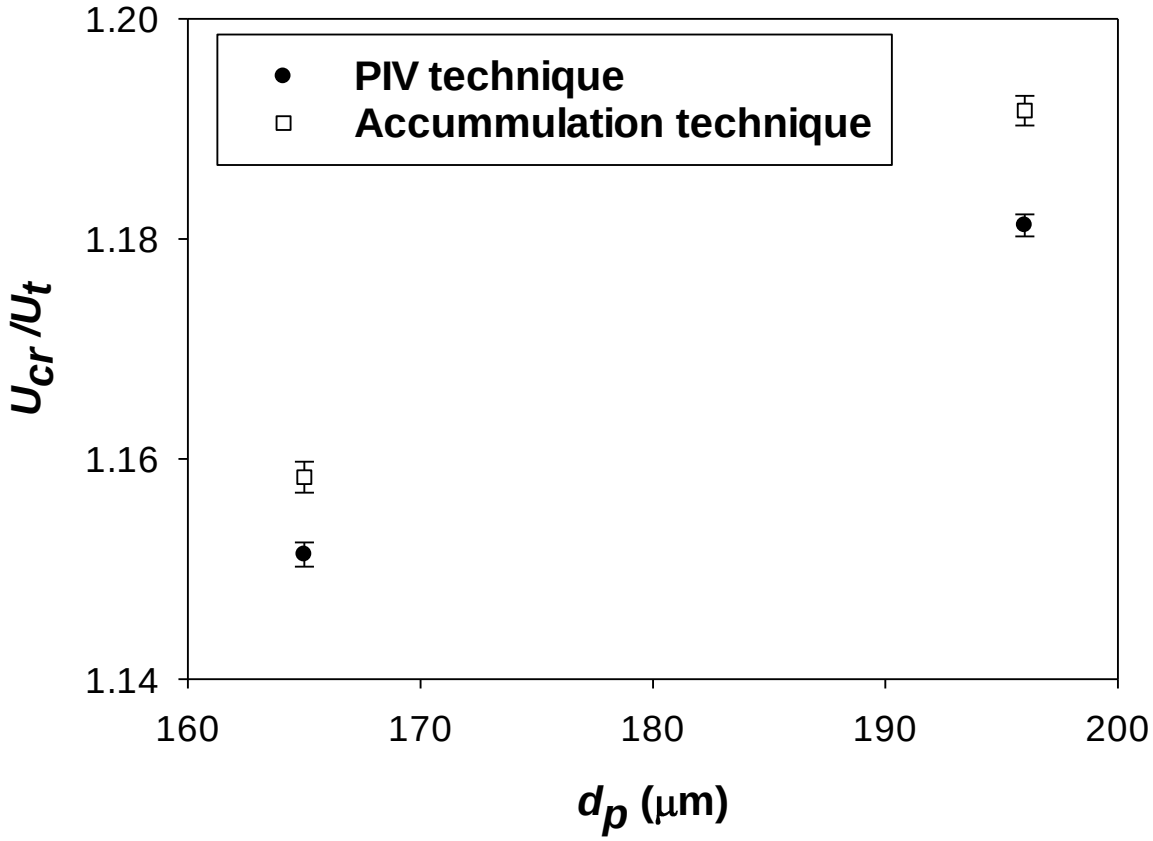

Figure 74. Normalised critical transition velocity as a function of particle size obtained from the PIV and accumulation measurement technique.

5.5 Conclusions

The digital PIV analysis using PIVlab and MATLAB was used to determine the solid circulating velocity in a micro-circulating fluidised bed. The use of PIVlab and Matlab codes to estimate the solid circulating velocity seems promising, and the results looks relevant when compared with previous reported studies. As in a macroscopic circulating fluidised bed, the solid circulating velocity in a micro-circulating fluidised bed increases with liquid velocity in two distinct zones, increasing sharply first then levelling off at higher inlet fluid velocities. The determined transition velocities from solid circulation rate versus velocity plots are comparable to the particle terminal velocity, i.e. the normalised transition velocity is approximately 1 in line with previous studies. The transition velocity is strongly influenced by solid inventory, i.e. it decreases with solid inventory before levelling off at high enough solid inventory. Finally, a weak increase in the normalised transition velocity with particle size was observed, which is probably due the wall effects (higher particle to bed ratio).

Chapter 6. Influence of circulating fluidised bed geometry on the hydrodynamics of liquid-solid flow in microchannel

6.1 Introduction

As the component of a solid-liquid Circulating fluidised bed include two columns the storage vessel or down comer and the riser with continuous particle circulation between the two columns, the flow characteristics and solid circulating velocity in the circulating fluidised bed system can be considerably influenced by the bed geometry, especially in large scale systems. Solid feed pipe is one of the most influential components of the circulating fluidised bed geometry. As the solid feeding pipe structure changes, the fluidisation characteristics in the system may not remain similar [99, 108, 247].

Although there have been many reported studies on the hydrodynamics of liquid-solid circulating fluidised beds, there are limited published articles on the importance of the solid feed pipe diameter on the circulating fluidised bed hydrodynamics. Most reported experimental investigation were carried out without modifying the diameter of the solid feed pipe, the main reason is that changing the solids feed pipe structure using traditional fabrication method used to manufacture these type of liquid-solid processing equipment are costly, labour-intensive, and cause time wastage when making a change in the design. Therefore, in the present research investigation an attempt was made to study the effect of these important parameters in the solid-liquid micro-circulating fluidised bed flow behaviour.

A number of experimental studies has been done to determine the influence of solid feeding pipe structure on the hydrodynamics of circulating fluidised beds. Zheng and Zhu [116] investigated the solid circulation rate in a liquid-solid circulating fluidised bed by changing the solid feeding pipe diameter, and reported that the solid circulation rate is depended on the solid feeding pipe structure. Feng et al. [114] experimentally investigated the influence of solid feeding pipe system on the solid circulation rate and concluded that the solid feeding pipe diameter strongly influence the flow characteristics of the liquid-solid circulating fluidised bed system. Natarajan et al. [36, 104] studied the effect of the diameter of the solids feed pipe on the hydrodynamic behaviour of the liquid-solid circulating fluidised bed hydrodynamics, particularly the solid circulation rate by using five different solids feed pipes of 9, 12, 22, 25, and 30 mm inner diameter size. In their report they concluded that the solid circulation rate

increases with increase solid feed pipe diameter and the particles input to the circulating fluidised beds riser is dependent on the diameter of solid feed pipe.

6.2 Experimental details

Here we are presenting the first experimental study on the effect of circulating fluidised bed geometry (the ratio between the diameter of solid feed pipe and riser and also the angle between solid feed pipe and riser) on the hydrodynamics of liquid-solid circulating fluidised beds (LSCFB) at the micro-scale. Additive manufacturing technology, digital light processing (Miicraft+ printer) and stereolithography (Form2 printer) were used to fabricate a novel micro-circulating fluidised bed. Compared with other fabrication techniques such as lithography, additive manufacturing technology allowed us to rapidly fabricate a reliable micro-circulating fluidised bed using low cost material and most importantly, the solid feed pipe structure such as the diameter and angle of the solid feed pipe can be easily be modified.

For this experimental study, new solids feed pipe designs were suggested. The idea is that by changing the size of the solid feed pipe diameter and the angle between the solid feed pipe and the riser can have a major influence on the internal recycling of particles in the riser column, and eventually on the system hydrodynamics. The micro-circulating fluidised bed used for this experimental investigation is schematically illustrated in figure 75. The bed consist of a riser column of 2mm square cross-section and 100 mm in height, a solid-liquid separator, a down comer acting as a particle reservoir, a solid return pipe, and a solid feeding pipe. At the base of the riser is the distributor (a two layer of parallel array pillars of 150 µm diameter and 100 µm spacing which prevents particles leaving the bed at the bottom and provides uniform flow distribution and stable fluidisation.

The first experiment were carried out using three different solid feed pipe of 1, 1.5 and 2 mm square cross section as shown in figure 75, and the second experiment were done using three different angles (angle between the solid feed pipe and the riser) of 30, 50, and 60° as displayed in figure 76 to explain the importance of the solid feed pipe cross section and the angle between the solid feed pipe and the riser on the flow behaviour.

In this experimental investigation the bed particles were lime glass micro-particles (Whitehouse Scientific Ltd, UK) of two different diameters, $d = 165 \pm 15\ \mu m$ *and* $d = 196 \pm 16\ \mu m$ whose density is $\rho_p = 2500\ kg/m^3$ were used as the fluidised solid and tap water as the fluidising liquid. The above microsphere glass particles were chosen for this experimental

study because the liquid distributor was not able to support any particle of diameter below 150 µm.

In the current research investigation, particle imaging velocimetry (PIV) software PIVlab [200-202], was employed to determine the solid circulating velocity in the micro-circulating fluidised bed. This measurement technique was chosen because of its simplicity and ease of implementation in microfluidics when compared with others measurement methodologies already mentioned in chapter 3. The critical transition velocity, the superficial liquid velocity from conventional to circulating fluidised bed regime was identified by the solid circulation rate method.

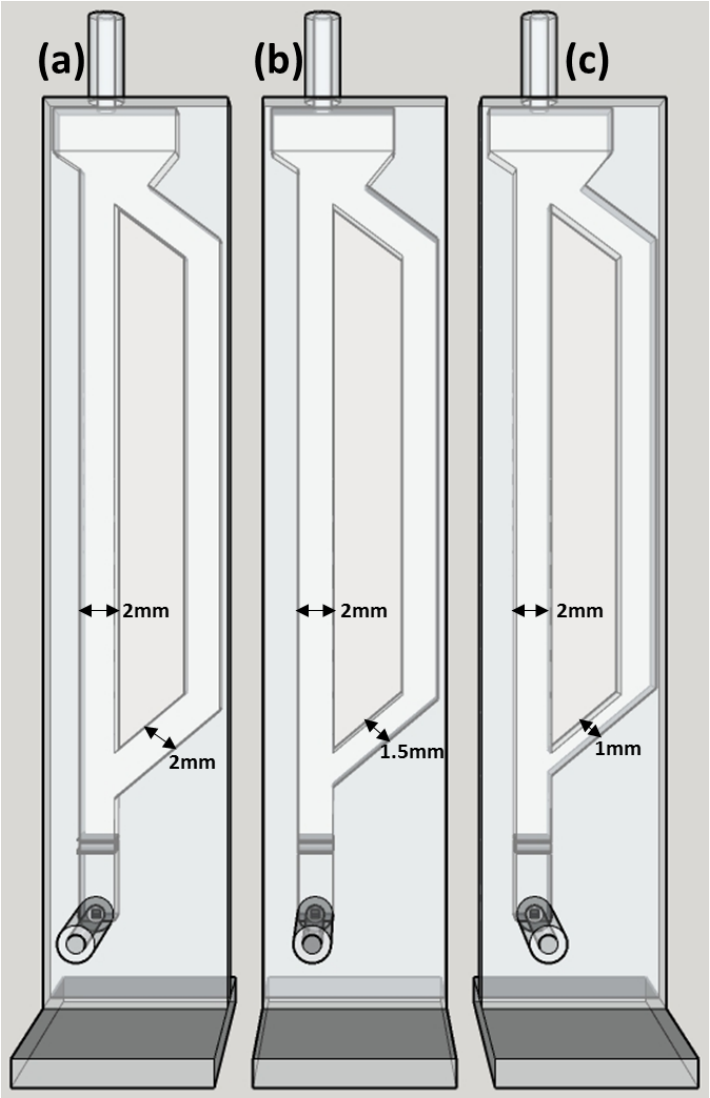

Figure 75. Schematic of the three systems used to study the influence of solid feed pipe cross section on the flow behaviour of a liquid-solid micro-circulating fluidised bed system: (a) shows a system with 2mm cross section solid feed pipe, (b) shows system with a 1.5 mm cross sectional solid feed pipe, and (c) show a system with a 1mm cross sectional solid feed pipe

Figure 76. Schematic of the three system used to study the influence of the angle between the riser and solid feed pipe on the liquid-solid flow behaviour in a micro-circulating fluidised bed system. (a) With a 60°angle between the riser and solid feed pipe, (b) with a 50°angle between the riser and solid feed pipe, and (c) with a 30°angle between the riser and solid feed pipe

6.3 Results and discussion

In solid-liquid micro-circulating fluidised beds, particle motion is controlled by changing the inlet superficial liquid flow rate and the solid feed pipe structure. The solid circulating velocity for the three types of solid feed pipe are different in the current experimental investigation. Figure 77 displays the influence of the ratio between the cross section of the solid feed pipe and riser on the hydrodynamics of liquid-solid micro-circulating fluidised bed, specifically

solid circulating velocity for glass (165 and 196 µm) particles as determined by digital PIV analysis described in chapter 3.

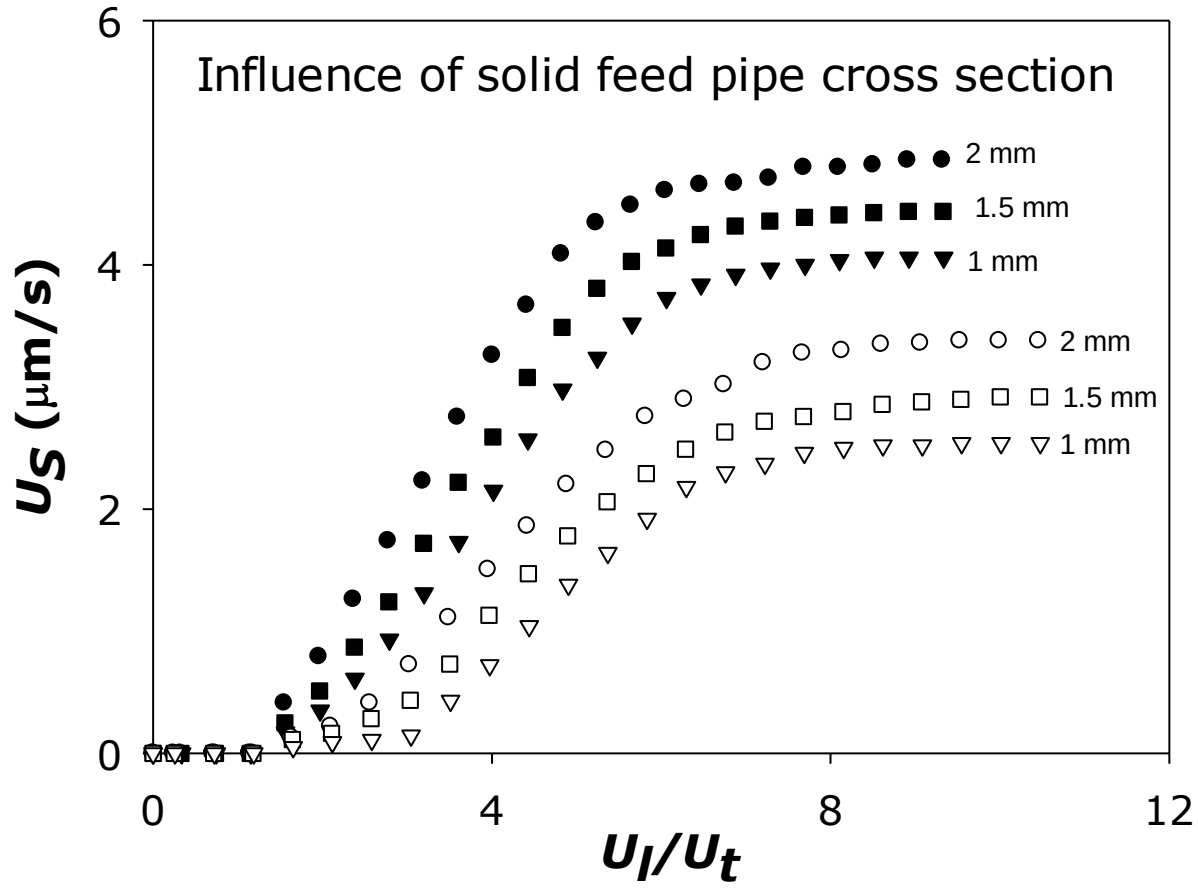

Figure 77. particle circulating velocity as a function of normalised velocity (U_l/U_t) for both 165µm glass particle in black and 196 µm glass particle in white colour. The angle between the riser and solid feed pipe is 60°.

First there is a trend of increased solid circulating velocity with an increase in the solid feed pipe cross section. For the three types of solid feed pipe (1, 1.5 and 2mm), it was observed that the solid circulating velocity is highest for the circulating fluidised bed with a cross section solid feed pipe of 2 mm and lowest for solid feed pipe of 1 mm cross section. It can be said that as the solid feed pipe cross section increases, the solid circulating velocity in the system also increases. The increment in the solid circulating velocity with an increase in the cross section of solid feed pipe indicates an increase in the amount of particles reintroduction from the downcomer to the riser. This was predicted because as the solid feed pipe cross section increases so does the area of the pipe and consequently a higher amount of solids being

reintroduced to the rise. The increment in solid circulating velocity with increased solid feed pipe cross section could also be attributed to the wall effect as shown in our previous research study [234]. As in microscopic circulating fluidised bed, the change in solid circulating velocity with superficial liquid flow rate indicates two zones. The first zone (initial circulating fluidisation zone) where solid circulating velocity increases rapidly with increasing superficial liquid flow rate and the second zone (fully developed zone) where solid circulating velocity insignificantly varies with increasing superficial liquid velocity.

The experimental results also show that the maximum value in the solid circulating velocity is directly proportional to the cross sectional size of the solid feed pipe. For the three types of solid feed pipe (1, 1.5 and 2mm), it was notice that the maximum value in the solid circulating velocity is higher for the 2mm cross section solid feed pipe and lower for the solid feed pipe of 1mm cross section. These trend was the same for both the 165 and 196 µm glass particles. Additional, it was also found that the maximum value in superficial liquid flow rate increases with solid feed pipe cross section size. The bigger the solid feed pipe cross section is, the higher the maximum superficial liquid flow rate is. These observations are similar to those reported by Natarajan *et al.* [104], the solid circulating velocity in the liquid-solid circulating fluidised bed system is influenced by the superficial liquid flow rate and the solid feed pipe cross section.

Figure 78 shows the critical transition velocity for the three different solid feed pipe structure. It can be notice that the critical transition velocity (U_{cr}) which demarcate the transition from conventional to circulating fluidised bed regime is dependent upon the solid feed pipe cross section size. The critical transition velocity is higher for the 1 mm cross section solid feed pipe and lower for the system with solid feed pipe of 2 mm cross section, it can be concluded that the critical transition velocity increases with a reduction in the solid feed pipe cross section size. In general, for both particles (165 and 196µm) the critical transition velocity is roughly equal to the particle terminal velocity, and the normalised transition velocity, U_{cr}/U_t in all consider cases is close to 1, varies from 1.13 to 1.187. These observations are similar to those reported by Liang et al. [4], the critical transition velocity depends on the bed geometry, liquid and particles properties but is slightly different from the observation reported by Zheng and Zhu as their reported onset velocity (U_{cf}) which gives the lowest critical transition velocity from the conventional to circulating fluidised bed regime was found to be independent of the bed geometry. Their proposed (U_{cf}) was found using the emptying bed methodology which was carried out by measuring the time needed to empty the particles in the bed by varying the liquid velocity. The *Ucf* was defined as the inflection point in the emptying time plot as a function of

the liquid velocities and was found out to be approximately equal to the particle terminal velocity *Ut*. They suggested that *Ucr* is the actual transition from conventional to circulating fluidised bed regime and *Ucf* represents the lowest transition from conventional to circulating fluidised bed regime. From figure 78, it can also be noticed a trend of increased normalised critical transition velocity with an increase in particle size which is probably because of increased wall effects which are not usually present in large circulating fluidised beds.

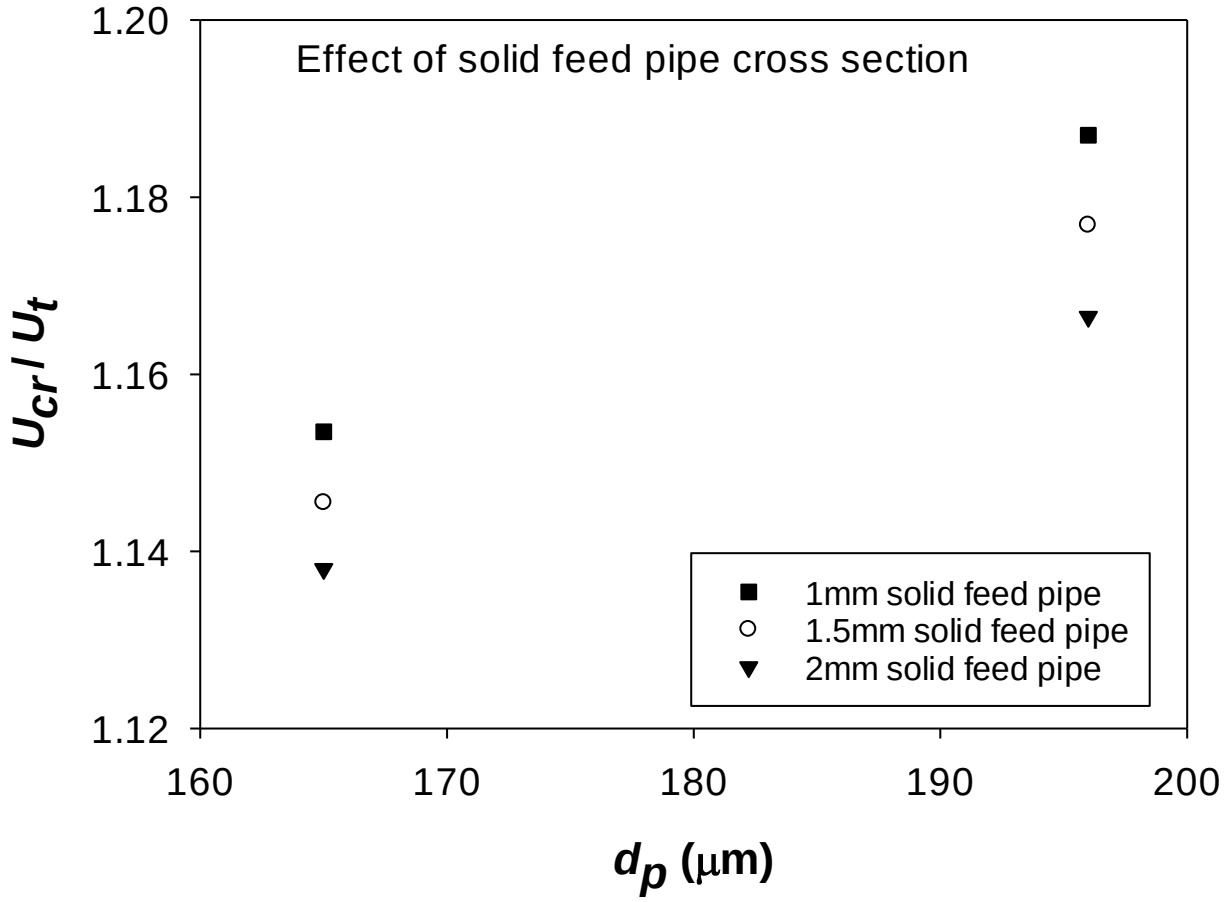

Figure 78. Importance of solid feed pipe on the normalised transition velocity for both 165 and 196 m glass particle. The angle between the riser and solid feed pipe is 60°

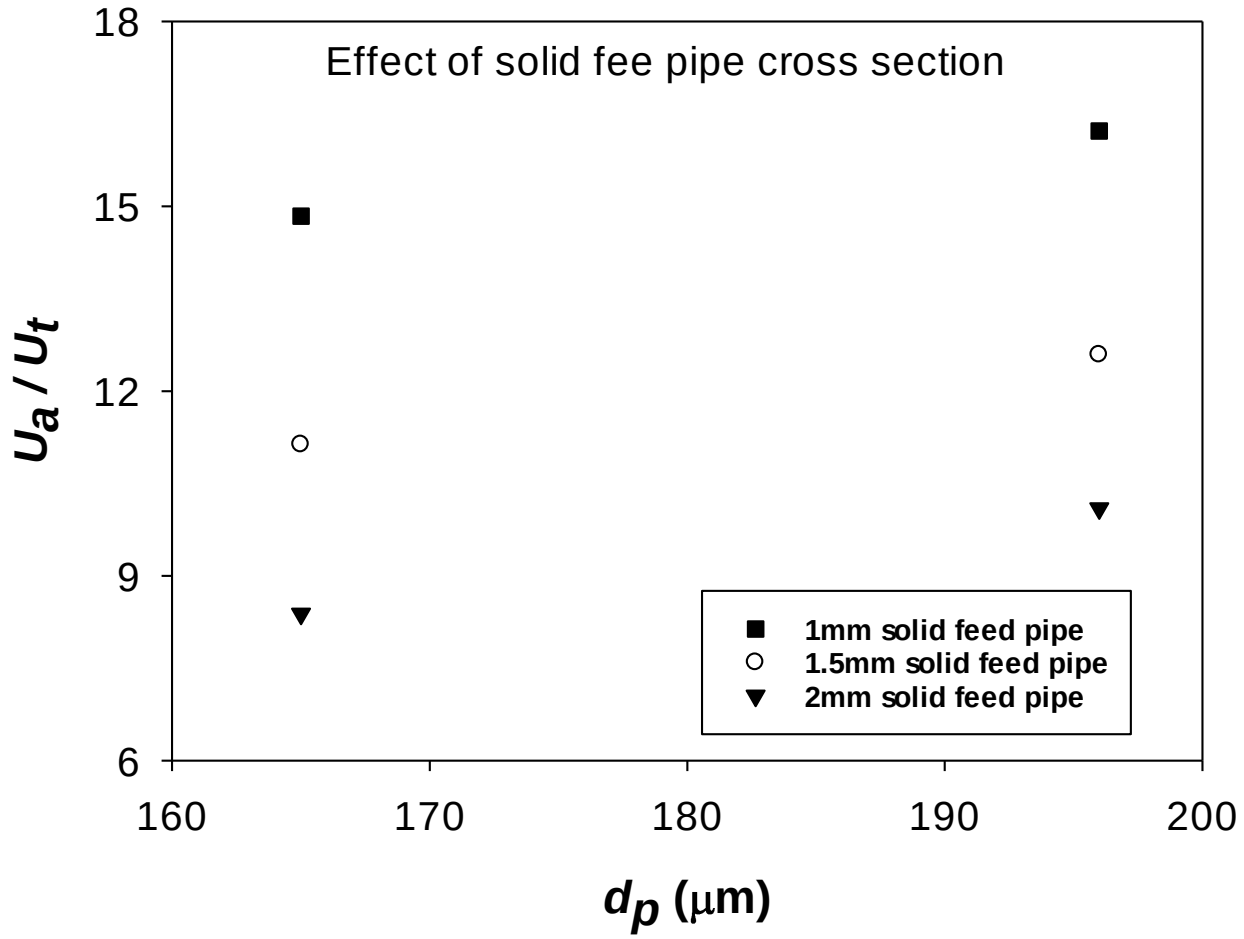

Figure 79. Importance of solid feed pipe on the transition velocity from circulating fluidised bed regime to transport regime for both 165 and 196 m glass particle. The angle between the riser and solid feed pipe was 60°

Figure 79 shows the transition velocity from circulating fluidised bed regime to transport regime for the three different solid feed pipe structure. It can also be notice that the transition velocity, U_a, from circulating fluidisation to transport regime is also dependent upon the solid feed pipe cross section size. The transition velocity U_a, is higher for the 1 mm cross section solid feed pipe and lower for the system with solid feed pipe of 2 mm cross section, it can be concluded that the transition velocity U_a, from circulating fluidised bed regime to transport regime increases with a reduction in the solid feed pipe cross section size. The increase in the transition velocity from circulating fluidisation regime to transport regime is due to the wall effects which are not usually present in large circulating fluidised beds.

To my knowledge, the influence of the angle between the riser and solid feed pipe has never been investigated. The flow behaviour in liquid-solid circulating fluidised bed system depends on several hydrodynamics parameters in the flow, one of these crucial parameter is the angle between the riser and solid feed pipe. With a change in the angle between the riser and the solids feed pipe, the fluidisation characteristics in the liquid-solid circulating fluidised bed system such as solid circulating velocity, critical transition velocity from conventional to circulating fluidised bed regime main not remain the same. Here, three cases of different angle, type 1 (30°), type 2 (50°) and type 3 (60°) were investigated to explain their influence on the fluidisation characteristics. The three system used for this experiment had a riser and solid feed pipe of 2mm square cross section

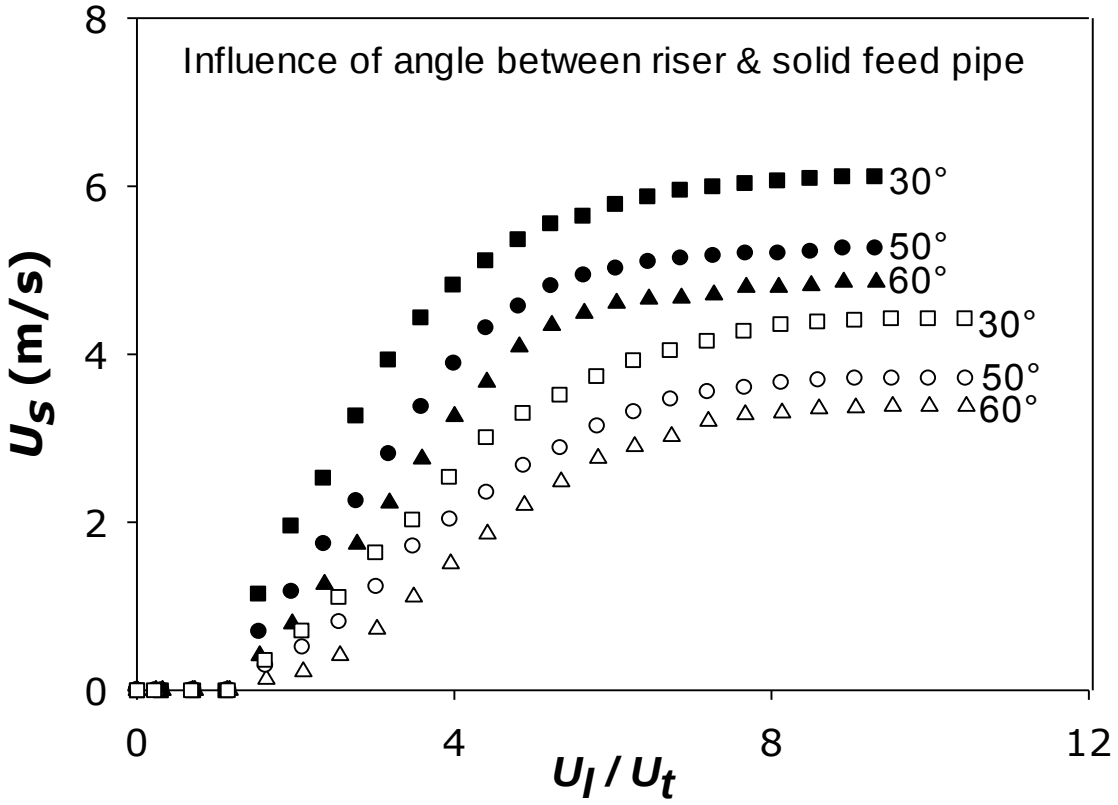

Figure 80: Influence of the angle between the riser and solid feed effect on the flow behaviour for both 165µm glass particle in black and 196 µm glass particle in white colour. The micro-circulating fluidised bed employed for this experiment had a riser and solid feed pipe of 2mm square cross section.

From Figure 80 it is observed that there is a trend of increased solid circulating velocity with reduction in the angle between the riser and solid feed pipe. The solid circulating velocity is higher for the type 1 system and lower for type 3 circulating fluidised bed system. This strongly

suggests that the angle between the riser and solid feed pipe is influencing the flow behaviour as would be expected. This influence could be caused by the hydrodynamics forces acting on the particle. From chapter 3, the importance of surface force and wall effect on the hydrodynamics of liquid-solid micro-fluidised beds, it was found that flow behaviour in the liquid-solid micro-fluidised bed can be determined by the balance of hydrodynamics force such as adhesion, gravitational, drag, and buoyant force acting on the particle. Since the solid feed pipe inclination angle for type 1, 2, and 3 systems is not the same as shown in figure 76, the net hydrodynamics forces such as drag and buoyancy forces acting on the particles are also not the same. In other words, as the solid feed pipe inclination angle changes, so does the net force acting on the particles, and this change plays a major influence on the hydrodynamics flow behaviour such as solid circulating velocity and transition from one regime to another.

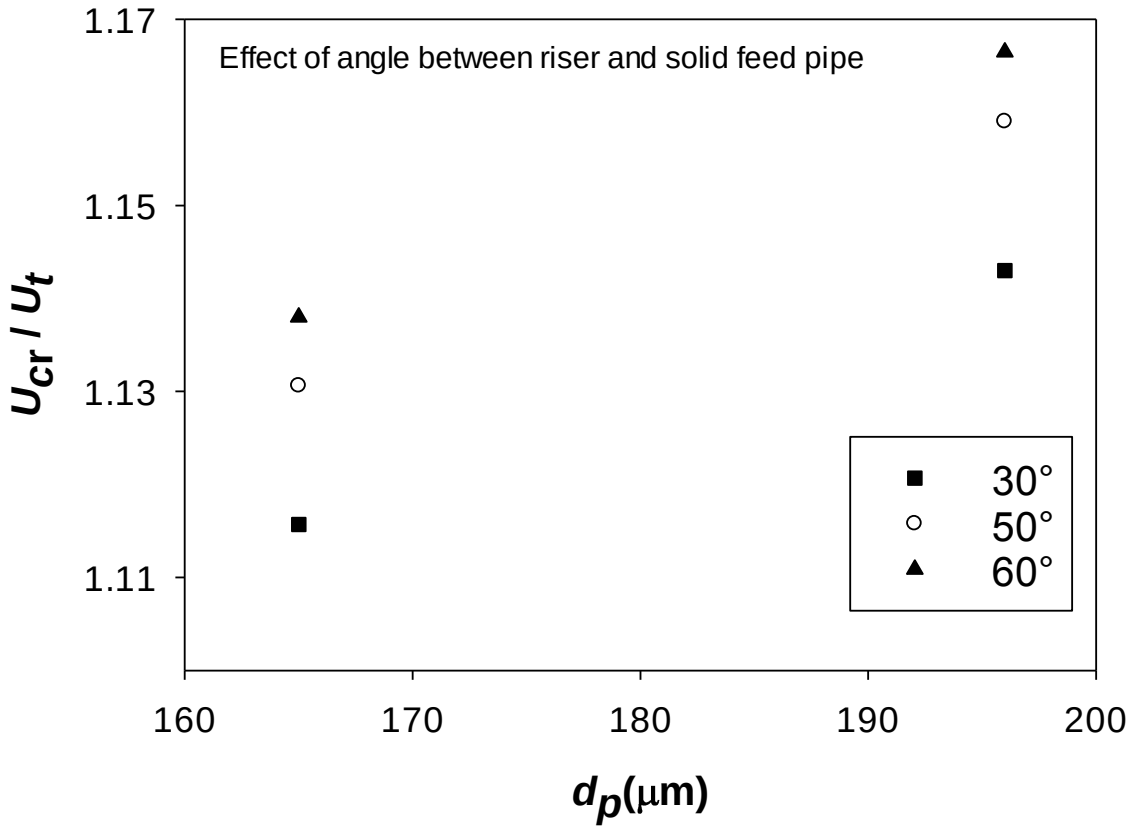

Figure 81. Effect of angle between riser and solid feed pipe on the normalised transition velocity for both 165 and 196 m glass particle. The micro-circulating fluidised bed employed for this experiment had a riser and solid feed pipe of 2mm square cross section.

It was also found that the critical transition velocity, *Ucr*, from conventional to circulating fluidised bed regime increases with an increase in the angle between the riser and solid feed

pipe looking at figure 81. For particles with the same size and density, U_{cr} is higher for type 3, and smaller for type 1 system. This is due to the difference in the net hydrodynamics force acting on the particle. The difference in the net hydrodynamics force due to the difference in the solid feed pipe inclination angle clearly affects the flow behaviour and postpone the critical transition velocity from conventional to circulating fluidised bed regime.

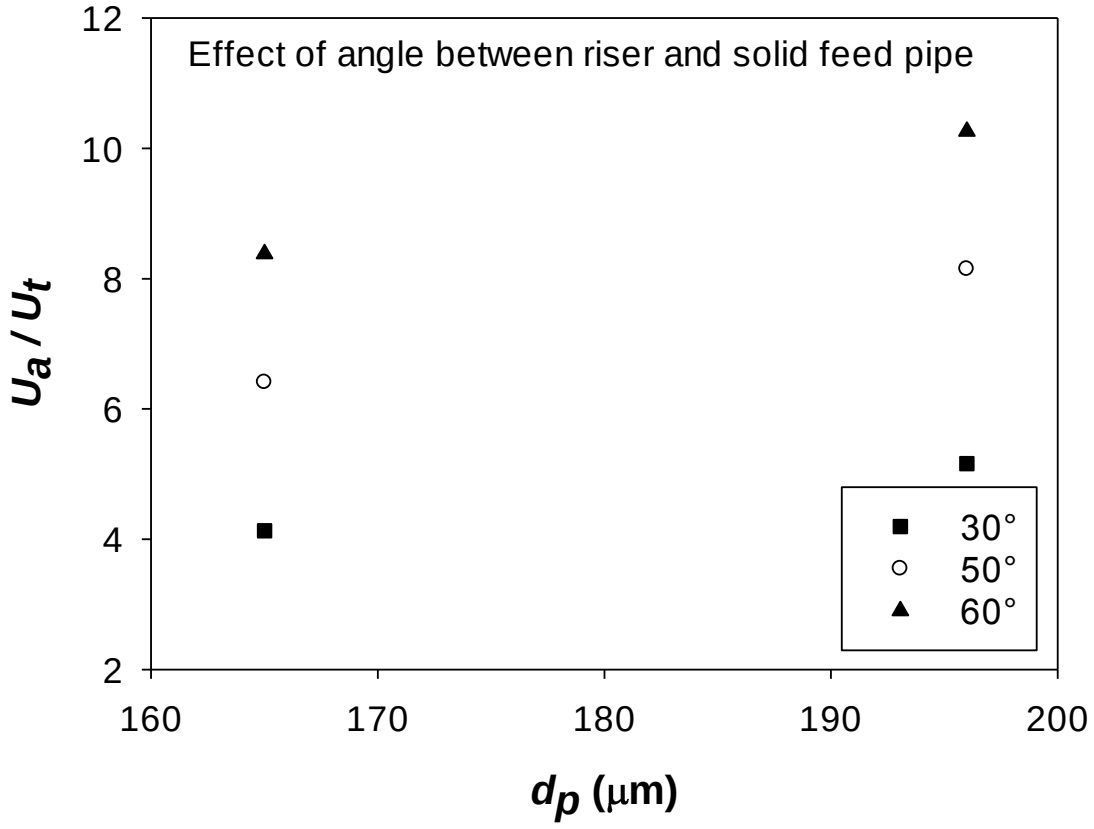

Figure 82. Effect of angle between riser and solid feed pipe on the transition velocity from circulating fluidised bed regime to transport regime for both 165 and 196 μm glass particle using a circulating fluidised bed with 2mm cross section feed pipe and riser.

From figure 82 it can be notice that the transition velocity U_a, from circulating fluidised bed regime to transport regime increases with an increase in the angle between the riser and solid feed pipe. For particles with the same size and density, the transition velocity from circulating fluidised bed regime to transport regime is higher for the system with 60° angle between riser and solid feed pipe system and lower for the 30° system. This is due to the difference in the net hydrodynamics force acting on the particle as explained above.

6.4 Conclusion

We presented the first investigation study on the importance of solid feed pipe and riser ratio, and the influence of the angle between the riser and solid feed pipe on the hydrodynamics of liquid-solid micro-circulating fluidised system, with a special interest on the flow behaviour and solid circulating velocity. For the first time, additive manufacturing technology, digital light processing (Miicraft+ printer) and stereolithography (Form2 printer) were used to fabricate a micro-circulating fluidised bed. The results indicate that the flow behaviour and solid circulating velocity in liquid –solid micro-circulating fluidised bed channel depends on the solid feed pipe. The solid circulating velocity increases with increased solid feed pipe cross section. This was predicted because as the solid feed pipe cross section increases so does the area of the pipe and consequently a higher amount of solids are reintroduced to the rise. As in macroscopic circulating fluidised the maximum value in the particle velocity and superficial liquid flow rate increases with solid feed pipe cross section. The critical transition velocity increases with a reduction in the solid feed pipe cross section size.

Additionally, the solid circulating velocity and the critical transition velocity from conventional to circulating fluidised bed regime in liquid-solid micro-circulating fluidised beds is also dependent on the angle between the riser and solid feed pipe. The solid circulating velocity increases with a reduction in the angle between the riser and solid feed pipe, and the critical transition velocity from conventional to circulating fluidised bed regime reduces with reducing the angle between the riser and solid feed pipe which is probably due to the difference in the net hydrodynamics force acting on the particle. The reduction in the angle between the riser and solid feed pipe reduces the particle–wall friction forces which in turn increases the mobility of the fluidised particles and this reduces the critical transition velocity hence circulating fluidised bed regime started early. The increase in the solid circulating velocity with a reduction in the angle between the riser and solid feed pipe could also be attributed to the increased effective gravity. The reduction in the riser and solid feed pipe angle increased the effective gravity, which in turn increased the mobility of the fluidised particles therefore the critical transition velocity started at lower superficial liquid velocity.

Chapter 7. Influence of liquid viscosity in liquid-solid micro-fluidised beds

7.1 Introduction

In most industrial processes where solid-liquid circulating fluidised beds are employed as a solid-liquid processing equipment, highly viscous liquid is often required as a processing fluid [248]. The flow behaviour in liquid-solid circulating fluidised bed system depends on several hydrodynamics parameters in the flow, one of these crucial parameters is the viscosity of the fluidising media which is not explore in detail as others parameters such as particle diameter, particle-fluid density difference and temperature [249]. With changes in the liquid viscosity, the fluidisation characteristics in the liquid-solid circulating fluidised bed system such as minimum fluidisation velocity, solid flux, critical transition velocity from conventional and circulating fluidised bed regime may not remain the same.

A number of experimental studies has been done to determine the influence of liquid viscosity on the minimum fluidisation velocity. Vijaya *et al.* [250] experimentally studied the importance of liquid viscosity on the minimum fluidisation velocity. Tap water and carboxy methyl cellulose (0.1, 0.2, and 0.3 %) were used as the liquid mixture. They found a decrease in the minimum fluidisation velocity with increasing liquid viscosity. The experimental results of minimum fluidisation velocity were compared with predicted minimum fluidisation velocity using Ergun equation and were in good agreement. Qui *et al.* [251] investigated the influence of viscous liquid on the minimum fluidisation velocity. Their experimental study was carried out using tape water, and 9 different concentrations of aqueous glycerol solution with liquid viscosity ranging from 7 to 1400 cp as the liquid mixture. They also reported a reduction in the minimum fluidisation velocity with increased liquid viscosity. Their experimental minimum fluidisation velocity data agrees with calculated minimum fluidisation velocity by Ergun Equation.

Although the importance of solid-liquid density difference, pressure, temperature, and diameter of particles on the flow behaviour have been previous determined, there is still a limited knowledge of the influence of liquid viscosity on the flow characteristic. The influence of liquid viscosity on the hydrodynamics of a liquid-solid circulating fluidised bed has been reported previously by various researchers. Zheng [252] experimentally studied the flow behaviour in a liquid-solid circulating fluidised bed system with varying liquid viscosity. The carrier liquid employed in their investigation was water and glycerol solutions (20% v/v and 30% v/v). They

concluded that the flow structure was less vigorous and more uniform in a viscous system, and the non-uniform particles distribution in the radial direction is reduced with liquid viscosity. Cho *et al.* [253] investigated the radial dispersion behaviour of viscous liquid in liquid-solid circulating fluidised bed system. The liquid medium employed in their experimental studies was water and carboxymethylcellulose solution. They also found the radial distribution was more uniform in a viscous system. Vidyasagar [108] investigated the influence of liquid viscosity on the critical transition velocity, solid circulation rate, axial and average particles holdup in a liquid-solid circulating fluidised bed. Tape water and glycerol of different concentrations (10, 20, and 40 vol. % aqueous glycerol) were used as the liquid mixture. They observed a decrease in the critical transition velocity with increasing liquid viscosity. Gnanasundaram investigated the influence of liquid viscosity on the hydrodynamics characteristics of a liquid-solid circulating fluidised bed. Their experimental study was carried out using tap water and glycerol at different concentration (5% and 15% (v/v) [99] and also 10% and 20% (v/v) aqueous glycerol [254]. They found an increase in solid circulation rate and solid holdup with increasing liquid viscosity, and a decrease in slip velocity with increased liquid viscosity. They observed a uniform axial particles distribution in the flow structure for a viscous system, and also reported a decrease in the critical transition velocity from conventional to circulating fluidisation regime with increases in the fluidising liquid viscosity.

It is believed that the influence of viscous liquid on the hydrodynamics of micro-circulating fluidised bed has never been investigated, and to date most of the publish literature on liquid-solid circulating fluidised bed hydrodynamics at macroscale considered water as the liquid medium. Therefore, an attempt was made to investigate the importance of viscous liquid on the hydrodynamics, particularly on the solid circulation rate and minimum fluidisation velocity of a liquid-solid circulating fluidised bed. For the first time, the influence of liquid viscosity on the hydrodynamics of liquid-solid micro-circulating fluidised bed is presented.

7.2 Experimental procedure

Two different groups of particles were used as fluidised solid: (1) soda lime glass microspheres of five different diameters, d = 26 ± 1.5 μm, 30 ± 1.5 μm, 35 ± 3 μm, 58 ± 5 μm, 82 ± 6 μm, 98 ± 8 μm, 115 ± 9 μm, *165 ± 15 μm*, *196 ± 16 μm* μm whose density is ρ_p = 2500 kg/m^3 and (2) PMMA particles of five different diameters, d = 23 ± 3.5 μm, 35 ± 3 μm, 41 ± 3.5 μm, 58 ± 5 μm, and 115 ± 9 μm whose density is ρ_p = 1200kg/m^3. Tap water and glycerol of different concentration (5, 10, and 15 vol. % aqueous glycerol) were used as the liquid mixture. More viscous mixture could not be studied due to limitation of the setup, the syringe pump could not pump very viscous liquid. The fluidising liquid density and viscosity is listed in table 14. All experiments were performed at room temperature of average 18 ± 2 ºC.

Table 14: Density and viscosity of fluidising liquid

Fluidising liquid	Density (kg/m^3)	Viscosity (mPa·s)
Tape water	1000	1
5% v/v glycerol	1011	1.085
10% v/v glycerol	1022	1.17
15% v/v glycerol	1036	1.36

To investigate the dependency of fluidisation behaviour on the liquid viscosity, two experimental investigation was conducted. The first experiment was carried in a micro-fluidised bed to study the importance of viscous liquid in the minimum fluidisation velocity, and the second experiment were conducted in a micro-circulating fluidised bed to investigate the influence of fluidised liquid viscosity on the solid flux and critical transition velocity from conventional to circulating fluidised bed regime in a liquid-solid circulating fluidised bed at micro-scale.

As in the previous experimental investigation in chapter 4 (the importance of surface force and wall effect on the minimum fluidisation velocity), here the minimum fluidisation velocity required to achieve fluidisation were obtained by observing visually the bed height expansion and also by extrapolation of linear relationship between the superficial liquid velocity and ratio of bed expansion as measuring pressure drop is difficult due to the very fine resolution required (the pressure drop is only of the order of several Pa). ImageJ [237], an image processing and analysis computer programme was used for off-line analysis to determine the bed height as a function of superficial liquid velocity. Minimum fluidisation velocity values were obtained from the plot of bed height expansion vs superficial liquid velocity. The point of intersection

of the expansion line with vertical line for packed bed height was taken as minimum fluidisation velocity. Typical plots of relative bed height for water and 3 glycerol solutions as a function of superficial fluid velocity are given in figure 83. The Ergun equation (equation 12, in chapter 2) [255] was used to predict the minimum fluidisation velocity with an estimated initial packed bed voidage of $\varepsilon_{mf} = 0.40 \pm 0.01$ in line with previous experiments [59] and trend of rectangular packed bed voidage with particle-to-bed ratios lower than 0.15 [256]. The calculated minimum fluidisation velocity for glass and PMMA particles is summarised in table 15 and 16 respectively and the experimental minimum fluidisation velocity for PMMA and glass particles is given in table 17 and 18 respectively. The experimental minimum fluidisation velocities were compared with minimum fluidisation velocity results obtained by the Ergun equation.

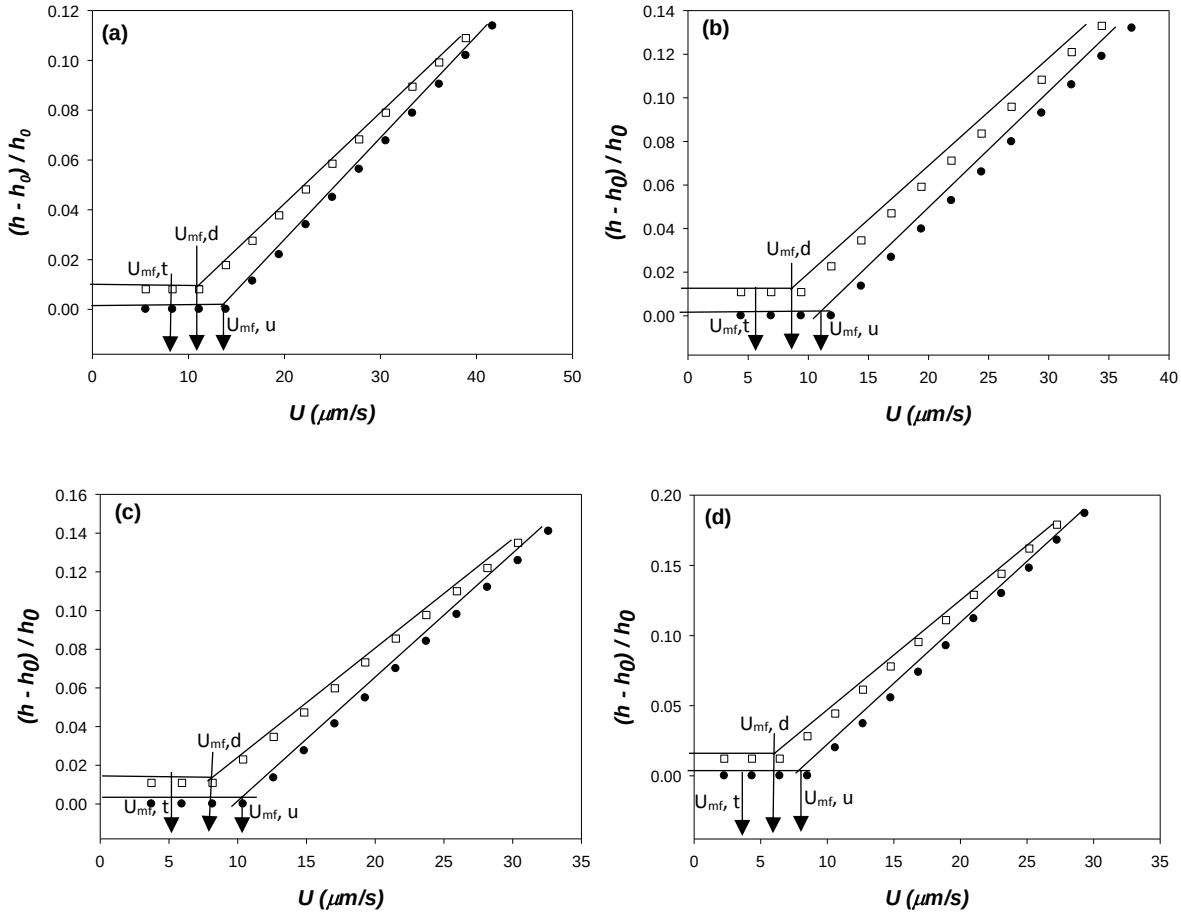

Figure 83. Relative bed height as a function of superficial liquid velocity, *U*, with increasing liquid velocity ($U_{mf,u}$), and decreasing liquid velocity ($U_{mf,d}$) for (a) water, (b) 5% v/v glycerol, (c) 10% v/v glycerol (d) 15% v/v glycerol solution as the fluidising liquid in 1 mm^2 micro-fluidised bed using 26μm glass particles. Errors are not visible in the graph as they are smaller than the symbols.

Table 15. The theoretical minimum fluidisation velocity for PMMA particle using Ergun equation from chapter 2

d_p (μm)	U_{mf} (μm/s)			
	water	5 % (v/v) glycerol	10 % (v/v) glycerol	15 % (v/v) glycerol
23	0.75	0.65	0.57	0.45
35	1.66	1.44	1.26	0.998
41	2.33	2.03	1.77	1.40
58	4.55	3.96	3.46	2.74
115	18.03	15.70	13.72	10.87

Table 16. The theoretical minimum fluidisation velocity for glass particle using Ergun equation mentioned in chapter 2.

d_p (μm)	U_{mf} (μm/s)			
	water	5 % (v/v) glycerol	10 % (v/v) glycerol	15 % (v/v) glycerol
26	7.01	6.27	5.77	4.92
30	9.05	8.35	7.68	6.55
35	12.10	11.36	10.46	8.91
58	33.97	31.20	28.72	24.47
82	68.15	62.35	57.40	48.91
98	97.34	89.06	81.98	69.86
115	134.70	123.69	113.86	97.03
165	275.75	252.31	232.28	197.96
196	388.87	355.85	327.62	279.25

Table 17. The Experimental minimum fluidisation velocity for PMMA particles obtained from the plot of bed height expansion as a function of superficial liquid velocity

d_p (μm)	water	5%	10%	15%
23	16.79	13.58	11.31	8.33
35	25.25	20.26	15.86	11.13
41	30.80	23.98	18.68	12.73
58	46.62	35.05	24.39	15.21
115	139.73	98.14	56.23	23.92

Table 18. The Experimental minimum fluidisation velocity for glass particles obtained from the plot of bed height expansion as a function of superficial liquid velocity

d_p (μm)	U_{mf} (μm/s)			
	water	0.05	0.1	0.15
26	13.81	11.91	10.39	8.51
30	16.74	14.52	12.83	10.34
35	19.97	17.61	15.27	12.39
58	48.58	41.18	35.90	27.65
82	89.96	74.82	65.43	50.87
98	120.70	100.63	86.08	64.97
115	157.60	131.11	108.17	81.51
165	303.32	244.74	195.11	142.53
196	396.65	313.15	242.44	170.34

As discussed in chapter 4, the major difference between micro-fluidised beds and macro-fluidised bed flows is the importance of surface forces which can prevent fluidisation [61]. Here the Dupree equation using acid-base theory developed by Oss, Chaudhury and Good [183] (equation 19, chapter 3) was used to predict the free interaction energy, ΔG_{1w2}, between two different solid surfaces submerged in a liquid. The surface tension parameters for the fluid (water and glycerol), glass, PMMA particles and PMMA walls used in the micro-fluidised bed study are shown in table 19. The free interaction energy between glass, PMMA particles and PMMA walls in water were obtained using all combinations of values in table 19. Given the surface energy obtained from the acid and base approach using surface tension components for liquid-solids given in table 19, the adhesion force was found using the Derjaguin approximation [183], (equation 21, chapter 3) and the drag force was determined from the buoyant weight of particles as shown in equation 24 from chapter 3. When ΔG_{1w2} value is negative, particles have the propensity to adhere to the walls of the micro-fluidised bed in the presence of liquid phase, and when ΔG_{1w2} value is positive, the interaction between the particle and bed wall is repulsive. The Eberhart relation [257, 258], equation 28, was used to determine the surface tension of the aqueous glycerol solution (5% v/v, 10% v/v and 15% v/v).

$$\gamma_{mix} = X_1\gamma_1 + X_2\gamma_2 \qquad (28)$$

where, γ_{mix} is the theoretical surface tension of the liquid mixture, γ_1 and γ_2 are the surface tension of water and glycerol, X_1 and X_2 are the volume fractions of water and glycerol respectively.

Table 19. Liquid and solid surface tension components

Material	γ	γ^{LW}	γ^{AB}	γ^{+}	γ^{-}	Reference
Glycerol	64	34	30	3.92	57.4	Janczuk *et al*.[259]
Water	72.8	21.8	51	25.5	25.5	Van Oss [183]
5 % v/v glycerol	72.36	22.41	49.95	23.02	27.01	
10 % v/v glycerol	71.92	23.02	48.90	20.84	28.69	
15 % v/v glycerol	71.48	23.63	47.85	18.90	30.29	
Glass	59.8	42	17.8	1.97	40.22	Freitas & Sharma [186]
	64.37	42.3	22.07	2.9	42	Clint & Wicks [185]
	51.7	33.7	18	1.3	62.2	Van Oss [183]
PMMA	44.65	42	2.65	0.55	3.2	Della Volpe *et al.* [187]
	44.58	41.2	3.38	0.38	7.5	Clint & Wicks [185]
	40.6	40.6	0	0	12	Van Oss [183]
	39.21	36.68	2.53	0.16	10.02	Zdziennicka [188]

In the current research investigation, particle imaging velocimetry (PIV) software PIVlab [200-202], was employed to determine the solid flux in the micro-circulating fluidised bed. The experimental procedure was described early in chapter 3. This solid flux measurement technique was chosen because of its simplicity and easy to implement in microfluidics when compared with others measurement methodology. The critical transition velocity, the superficial liquid velocity from conventional to circulating fluidised bed regime was identified by the solid circulation rate method.

7.3 Result discussion

7.3.1 Adhesion force prediction

Here eight different cases of free energy of interaction, ΔG_{1w2} involving four liquids (water, 5 v/v aqueous glycerol, 10 v/v aqueous glycerol and 15 v/v aqueous glycerol solution), and two solids (Glass and PMMA) were determined :

1st case: involves a glass particle and PMMA wall with water as the fluidising liquid

2nd case: Glass particle and PMMA wall with 5% volume aqueous glycerol as the fluidising liquid

3rd case: Glass particle and PMMA wall with 10% vol. aqueous glycerol solution as the fluidising liquid

4th case: Glass particle and PMMA wall with 15% vol. aqueous glycerol solution as the fluidising liquid

5th case: PMMA particle and PMMA wall with water as the fluidised liquid

6th case: PMMA particle and PMMA wall with 5% vol. aqueous glycerol solution as the fluidised liquid

7th case: PMMA particle and PMMA wall with 10% vol. aqueous glycerol as the fluidised liquid

8th case: PMMA particle and PMMA wall with 15% vol. aqueous glycerol as the fluidised liquid

In the first to fourth case, the majority of the combination values estimated that the free energy of interaction acting between glass particles and PMMA walls with water, and glycerol (*5% v/v, 10% v/v, and 15% v/v*) solution as the fluidising liquid is attractive, only when Van Oss glass surface tension components were used with PMMA components excluding Della Volpe and Siboni a positive free interaction energy was obtained (3/12 combination). Overall the average free energy of interaction obtained from the 12 parameter combinations between glass particle and PMMA walls in the first, second, third and fourth case are negative as shown in table 20. This indicates that the glass micro-particles have a small propensity to adhere to a PMMA walls surface in the presence of water and glycerol solution (*5% v/v, 10% v/v, and 15% v/v*). The free energy of interaction acting between the PMMA micro fluidised bed walls and

the glass particles is attractive, and the adhesion tendency decreases with addition of glycerol as can be seen in Table 20 by decreasing value of the free energy of interactions.

Table 20. Free energy of interaction (mJ/m^2) acting between glass particles and PMMA walls with water, and glycerol (*5% v/v, 10% v/v, and 15% v/v*) solution as the fluidising liquid.

Surface1	Surface2	Liquid	ΔG_{1w2}	$\sigma(\Delta G)$	$(\Delta G)_{min}$	$(\Delta G)_{max}$	Interaction
Glass	PMMA	water	-4.62	9.28	-19.21	12.38	attractive
Glass	PMMA	5% v/v glycerol	-3.53	8.29	-17.24	14.62	attractive
Glass	PMMA	10% v/v glycerol	-2.41	7.69	-14.76	17.06	attractive
Glass	PMMA	15% v/v glycerol	-1.07	7.19	-11.92	19.85	attractive

In the fifth, sixth, seventh and eighth case involving PMMA particle and PMMA wall with water and aqueous glycerol solution (*5% v/v, 10% v/v, and 15% v/v*) as the fluidising liquid, the free energies of interaction, ΔG_{1w2} obtained using the 16 surface tension components combination of PMMA were significantly less than zero with an average free energy of interaction of -47.22, -43.13, -42.91, and -40.45, for water, 5% v/v, 10% v/v, and 15% v/v aqueous glycerol solution system respectively as shown in table 21. Therefore, like for the glass particles there is a decrease in the free energy of interaction values with increase of glycerol volume fraction indicating slight decrease in the adhesion tendency. However, the values are much higher than for glass particle case indicating that PMMA particles have a significant tendency to adhere to PMMA micro-fluidised bed surface when water and glycerol solution (*5% v/v, 10% v/v, and 15% v/v*) are used as the fluidising liquid

Table 21. Free energy of interaction (mJ/m^2) acting between PMMA particles and PMMA walls with water, and glycerol (*5% v/v, 10% v/v, and 15% v/v*) solution as the fluidising liquid.

Surface1	Surface2	Liquid	ΔG_{1w2}	$\sigma(\Delta G)$	$(\Delta G)_{min}$	$(\Delta G)_{max}$	Interaction
PMMA	PMMA	water	-47.22	7.49	-62.76	-37.83	attractive
PMMA	PMMA	5% v/v glycerol	-45.13	6.73	-60.54	-35.71	attractive
PMMA	PMMA	10% v/v glycerol	-42.91	6.18	-57.95	-33.12	attractive
PMMA	PMMA	15% v/v glycerol	-40.45	5.70	-54.82	-30.04	attractive

7.3.2 Influence of liquid viscosity on the minimum fluidisation velocity

From figure 83 and 84, the importance of viscous liquid on the minimum fluidisation velocity of a liquid-solid fluidisation in a micro-fluidised bed, it can clearly be notice that there is a trend of reduction in the minimum fluidisation velocity with increased liquid viscosity. Here, four cases of different liquid medium, type 1 (water), type 2 (5% v/v aqueous glycerol), type 3 (10% v/v aqueous glycerol), and type 4 (15% v/v aqueous glycerol), were investigated to explain their influence on the minimum fluidisation velocity. The minimum fluidisation velocity is much higher for type 1 system, and lower for type 4 system. This trend was the same for both Glass and PMMA particles. This strongly suggests that the liquid viscosity is influencing the superficial liquid velocity where fluidisation is achieved. These observations are similar to those reported by Vijaya *et al.[250]* and Qiu *et al*.[251]. In Their experimental studies, they explained that in solid-liquid fluidisation system, the minimum fluidisation velocity reduces with an increase in the viscosity of the fluidised liquid due to the fact that viscosity enhances the shearing stress acting on particle, consequently, this increased the drag force acting on the particles and as a result the minimum fluidisation velocity was achieved at lower superficial liquid velocity when the fluidising liquid viscosity was increased.

Figure 84 and 85 also shows that the normalised minimum fluidisation velocity is considerably higher for PMMA particles when compared to glass particles of the same size. This is probable due to difference in surface properties with PMMA particles being hydrophobic while glass particles hydrophilic. For glass particle the experimental minimum fluidisation velocity is about two times bigger when compared to the theoretical prediction using the Ergun equation, and For PMMA particles the experimental minimum fluidisation velocity is about 4-23 times higher than the theoretical prediction depending on the size of the particle. This was anticipated since the Ergun equation used to predict the minimum fluidisation in the present study does not consider the surface forces among particles and bed wall. Consequently, for both PMMA and glass particles the proportional increments in the minimum fluidisation velocity is much higher for the smallest particles.

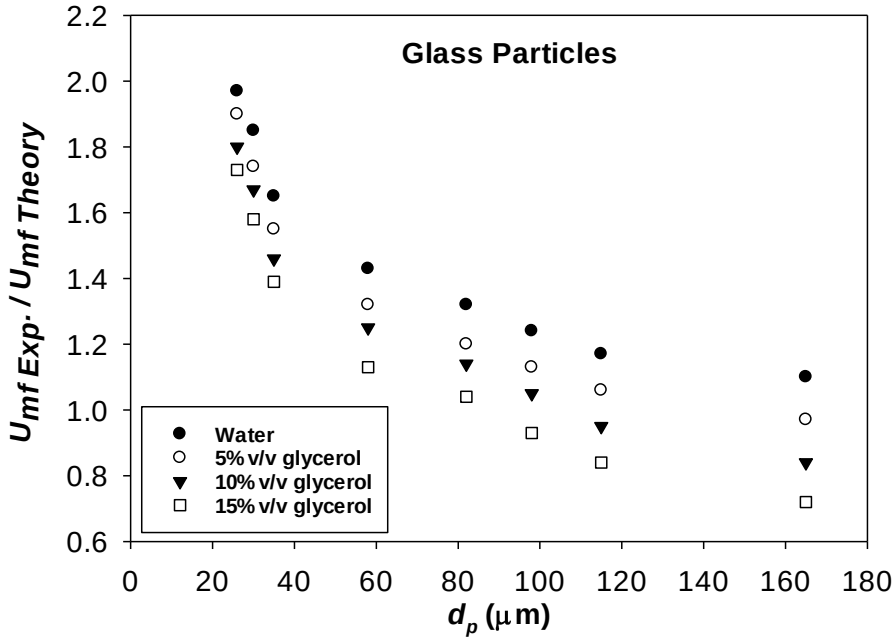

Figure 84. Experimentally determined minimum fluidisation velocity over the theoretical calculated values using the Ergun equation as a function of particle diameter four different liquid medium, tape water, 5% aqueous glycerol, 10% aqueous glycerol and 15% aqueous glycerol solution, with glass as the fluidised particle

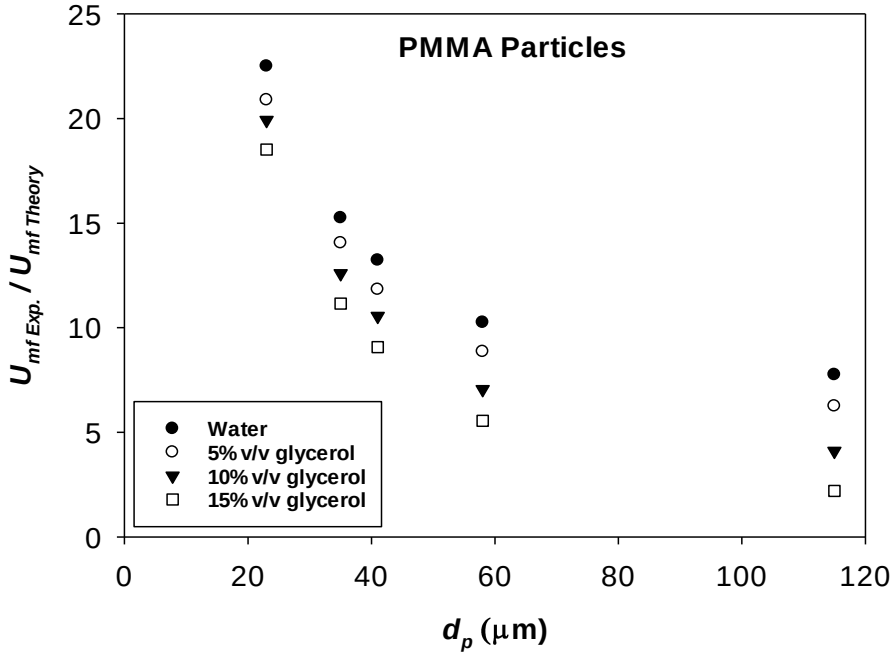

Figure 85. Experimentally determined minimum fluidisation velocity over the theoretical calculated values using the Ergun equation as a function of particle diameter four different liquid medium, tape water, 5% aqueous glycerol, 10% aqueous glycerol and 15% aqueous glycerol solution, with PMMA as the fluidised particle

7.3.3 Influence of particle density on the on minimum fluidisation velocity

From figure 86 and 87, the influence of particle density on the minimum fluidisation velocity, it can be notice that the minimum superficial liquid velocity at which particle fluidisation is achieved for both PMMA and glass particles is almost the same even though glass particles have a higher density compare to PMMA particles (2500 and 1200 kg/m^3 respectively). Based on theory, the theoretical minimum fluidisation velocity based on Ergun equation for glass microparticles should be 8 times bigger than for PMMA particle of the same size for the particle size range of 23-115µm as used in this study. However, our recent research study [234] found that in solid-liquid micro fluidised bed system, surface forces strongly influences the minimum superficial liquid velocity at which particle fluidisation is achieved.

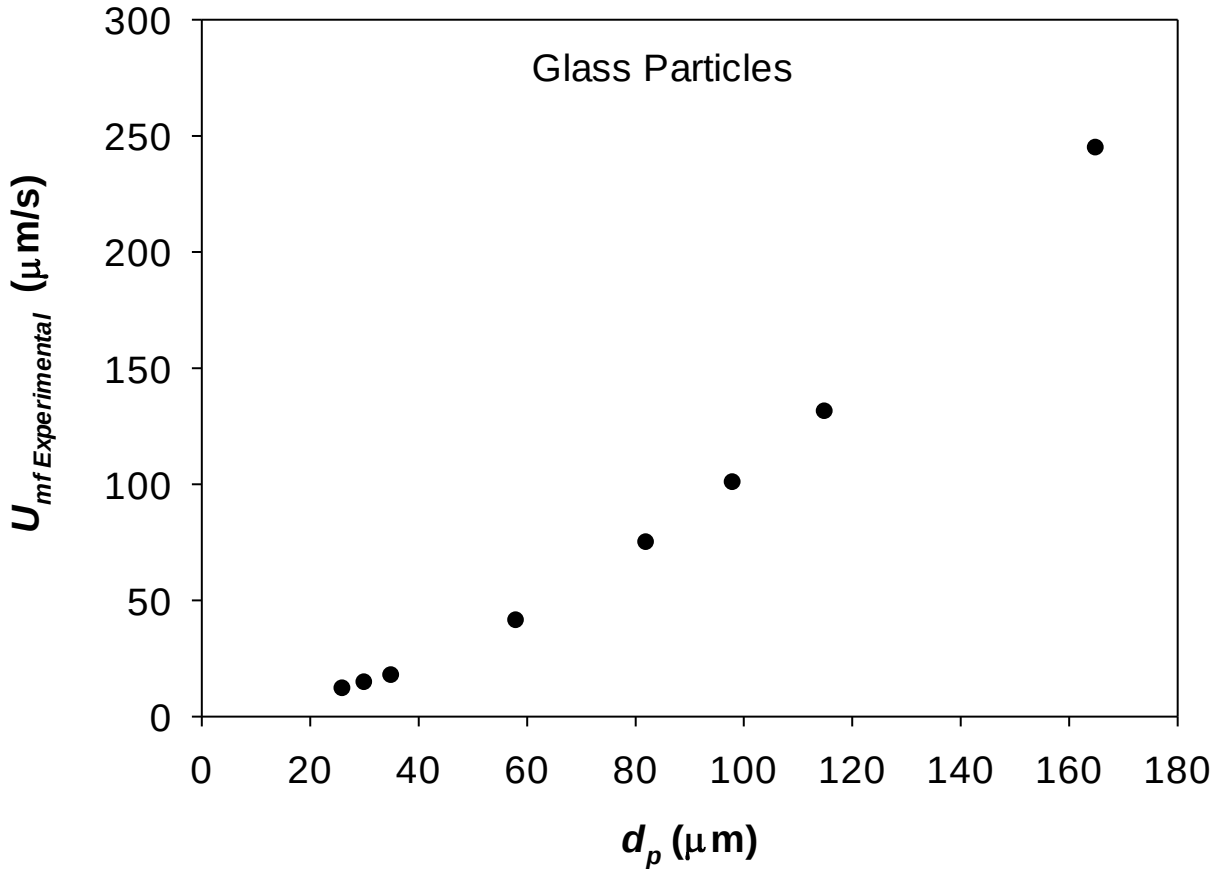

Figure 86. Experimental minimum fluidisation velocity as a function of particle size for glass particle with 5% v/v aqueous glycerol as the fluidising liquid.

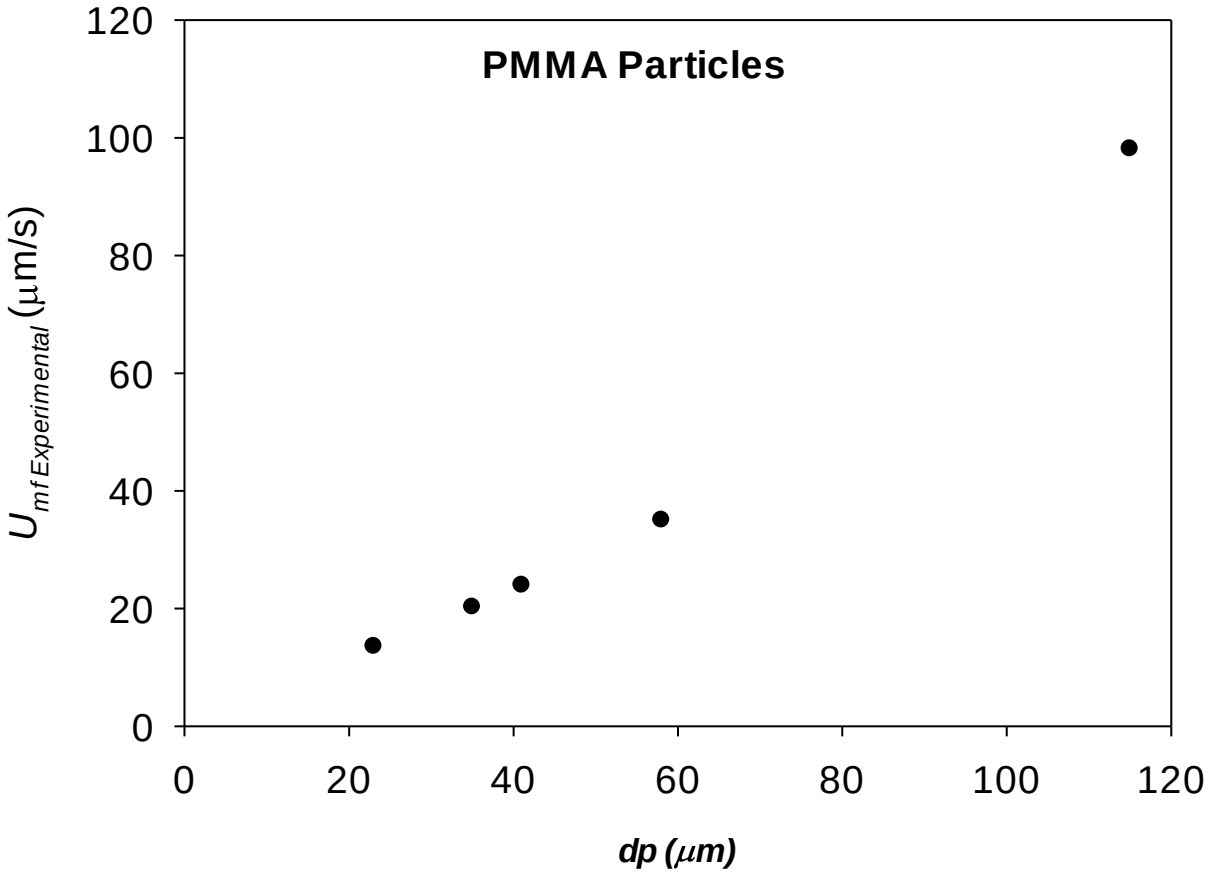

Figure 87. Experimental minimum fluidisation velocity as a function of particle size for PMMA particle with 5% v/v aqueous glycerol as the fluidising liquid.

For PMMA particles the transitional region from fixed state to fluidised state was considerable extensive when compare to glass particles. This is probably due to difference in surface properties with PMMA particles being hydrophobic while glass particles hydrophilic. PMMA particles are extremely hard to fluidise at a lower superficial liquid velocity as the cohesive forces (capillary, electro static and van der walls forces) present in the particles are relative higher than the gravitational and drag force exerted on the particles. These cohesive forces which are present in PMMA particles and not in glass particle increases particle size as a result of agglomeration which strongly influences the point of fluidisation and beyond as shown in Figure 89. In some cases, PMMA particles were fluidised in the form of agglomerates at superficial liquid velocity twenty times higher than the predicted minimum fluidisation velocity.

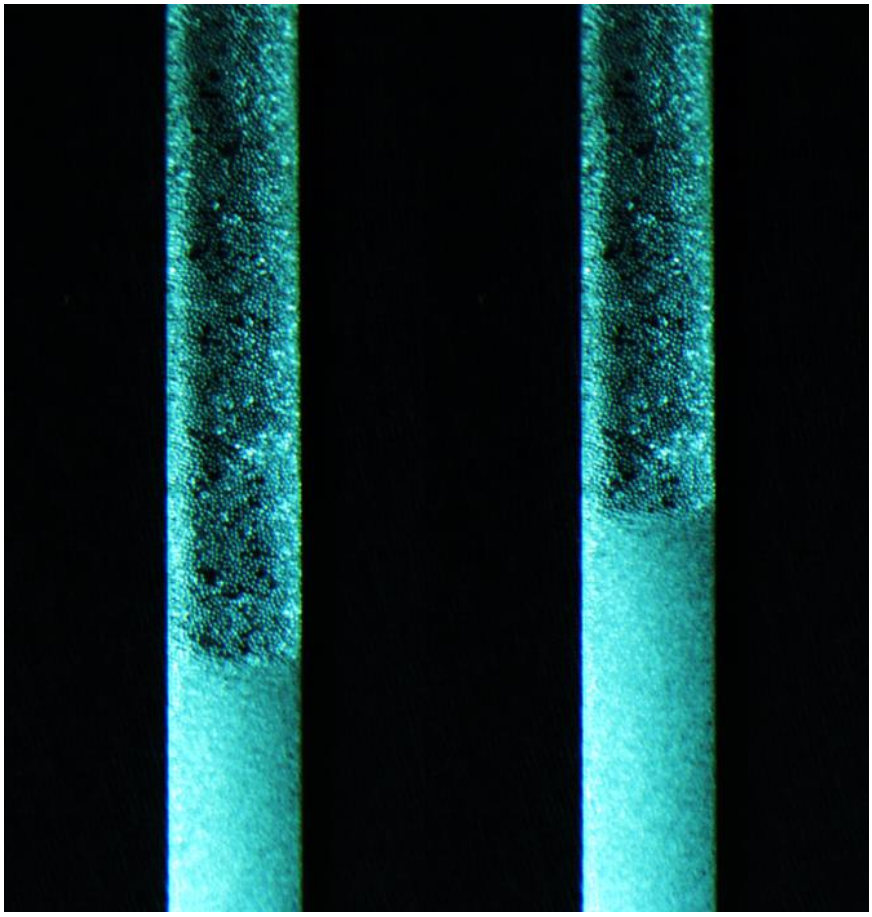

Figure 88. Optical Microscope illustrating adhesion of 35 µm PMMA particle inside 1mm^2 micro-fluidised bed with water as the fluidising liquid.

Figure 89. Optical Microscope illustrating agglomeration of 35 µm PMMA particle inside 1mm^2 micro-fluidised bed with water as the fluidising liquid.

7.3.4 Surface force magnitude for glycerol mixtures

Even though the free interaction energy helps to predict particle tendency for adhesion to the walls of micro-fluidised beds and its absence, the adhesion to drag force ratio is needed to determine if particle adhesion to the bed wall will in fact happen. For this experimental investigation tap water, 5 % glycerol, 10% glycerol, and 15% glycerol solution were used as the liquid phase. Adhesion to drag force ratios was plotted as function of particle size for both glass and PMMA particles as shown in figure 90 and 91 respectively. The adhesion forces scale up with particle diameter, whilst the drag force scales with the cube of diameter. Figure 90 and 91 shows that the adhesion/drag forces ratio reduces with increasing fluidising liquid viscosity. This is in a way direct consequence of the fact that the adhesion tendency (force) is decreasing with increase in volume fraction of glycerol for both glass and PMMA particles.

The ratio of adhesion to drag force is the highest for water system and the lowest for 15% glycerol solution system. In the cases of PMMA micro-particles fluidized by water in a PMMA micro-fluidized bed, adhesion forces are some 3 to 5 orders of magnitude larger than the estimated drag forces, indicating particle adhesion to the bed walls is highly likely to influence the fluidization process.

For glass particle fluidised in water, because they have a higher particle density and weaker adhesion forces, the adhesion to drag force ratio is only 1-3 orders of magnitude larger. For both PMMA and glass particles fluidised by 5% glycerol, 10 glycerol and, 15% glycerol aqueous solution the influence of adhesion forces when compared to the gravitational and buoyancy forces was relatively lower than the particles fluidised by water, and particle fluidisation was achieved at superficial liquid velocity comparable to theoretical prediction. It was understood that the adhesion/drag force ratio in the liquid solid micro-fluidised bed system decreases with increasing the viscosity of the fluidising liquid, consequently, this decreased the friction forces between particles and increased the mobility of the fluidised particles resulting in a decrease of the minimum fluidisation velocity in our experiment. This clearly indicates that in addition to the adhesion/drag force ratio, the liquid viscosity influences the postponement of incipient fluidization.

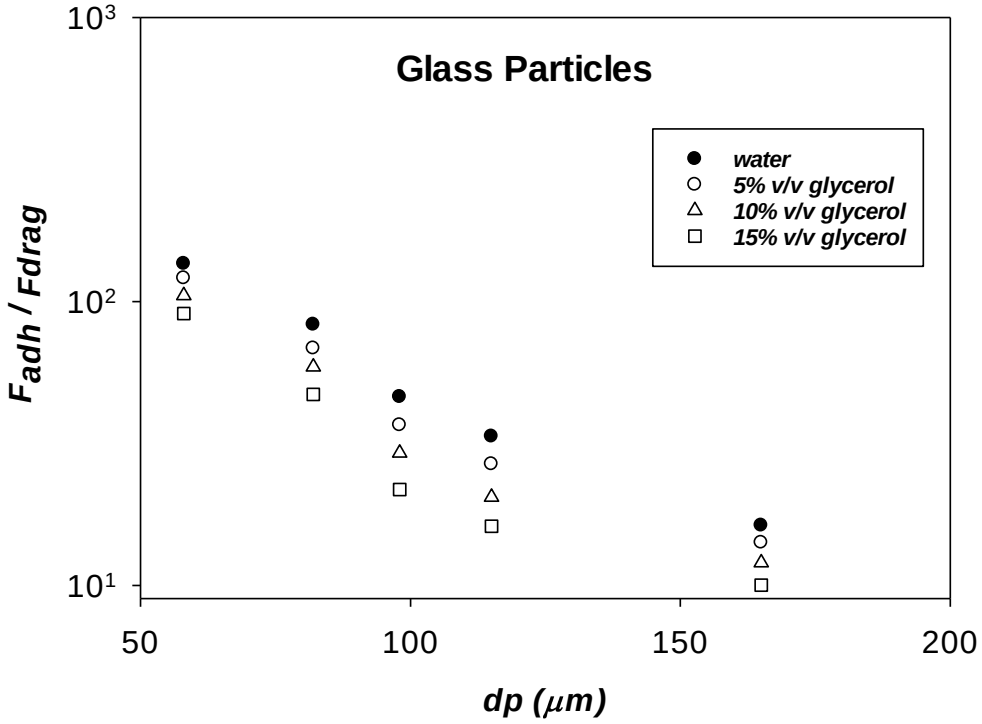

Figure 90. Adhesion to drag forces ratio as a function of particle diameter for glass micro-particles with water and aqueous glycerol solution (5% v/v, 10% v/v, and 15% v/v) as the fluidising liquid in 1 mm^2 micro-fluidised bed.

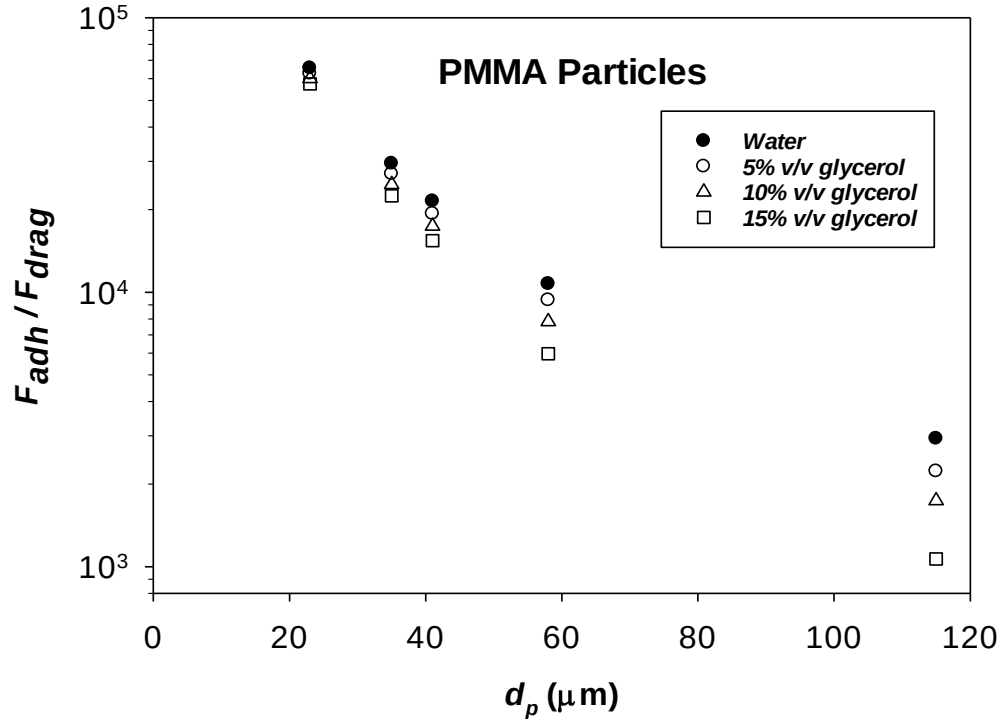

Figure 91. Adhesion to drag forces ratio as a function of particle diameter for glass micro-particles with water and aqueous glycerol solution (5% v/v, 10% v/v, and 15% v/v) as the fluidising liquid in 1mm^2 micro-fluidised bed.

Looking at figure 92 and 93 it is evident that there is a trend of decreased experimental minimum fluidisation velocity with an increased fluidised liquid viscosity. It was observed that the experimental minimum fluidisation velocity is higher for water system in comparison with glycerol solution system. This is most likely due to the fact that viscous systems have a lower adhesion/drag force ratio, hence the minimum fluidisation velocity starts at comparatively even lower superficial liquid velocity when the viscosity of the fluidised liquid is increased. For both types of particles, glass and PMMA, the minimum fluidisation velocity at which particles are fluidised is postponed, but the proportional increment in the minimum fluidisation velocity is much higher for PMMA particles. It can also be noticed that the ratio of experimental minimum fluidisation velocity over the predicted minimum fluidisation velocity using Ergun equation is higher for smaller particles when compared to large particles for both PMMA and glass, that could be due to the ratio of adhesion to drag force, as smaller particles have a higher ratio of adhesion to drag force than large particles, hence the surface force effect on the minimum fluidisation velocity is higher for smaller particles as shown in Figure 92 and 93.

Looking at the data for glass particles, it can be observed that for low force ratio, U_{mf} for water system is almost at the theoretical values (first 3 point), indicating small influence of adhesion forces on fluidization behaviour as already discussed in chapter 4 (Influence of surface forces and wall effects on the minimum fluidization velocity of liquid-solid micro-fluidized bed). In this case it is clear that due to viscosity influence U_{mf} measured is much smaller in line with previous studies. In the case of other points, the force ratio is higher and the U_{mf} is increased due to adhesion issues like for water system. However, if we compare the points for glycerol solutions to the fitting for water system, we can see clearly that deviation from the line is bigger for the more viscous system, once again confirming the liquid viscosity influence. On contrary, seems like increase in viscosity decrease U_{mf}, looking at beginning points, we have U_{mf} smaller than theoretical prediction. From fitting line in graph 92 and 93, it can be seen that for e.g. 5% glycerol deviation from water line is small (within experimental error), especially for the top points, but it is bigger for 10 and the biggest for 15 volume fraction of glycerol, indicating that viscosity is also influencing U_{mf} in addition to dominant adhesion forces influence.

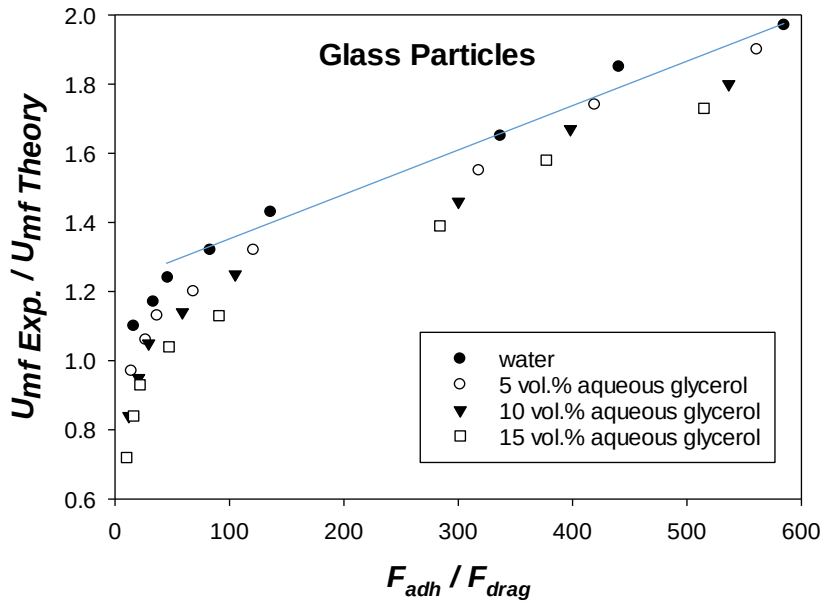

Figure 92. Experimentally determined minimum fluidisation velocity over the theoretical calculated values using the Ergun equation as a function of adhesion/drag force ratios for four different liquid medium, tape water, 5% aqueous glycerol, 10% aqueous glycerol and 15% aqueous glycerol solution.

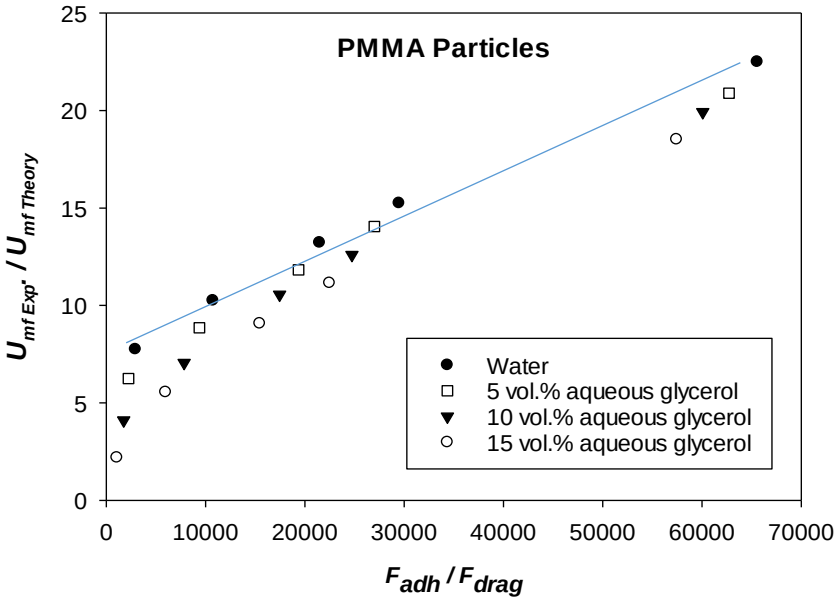

Figure 93. Experimentally determined minimum fluidisation velocity over the theoretical calculated values using the Ergun equation as a function of adhesion/drag force ratios for four different liquid medium, tape water, 5% aqueous glycerol, 10% aqueous glycerol and 15% aqueous glycerol solution.

7.3.5 Influence of liquid viscosity on solid circulating velocity

Even though there are few published studies on the importance of liquid viscosity on the solid circulating velocity as outline above, here for the first time, the influence of the fluidising liquid viscosity on the solid circulating velocity and critical transition velocity from conventional to circulating fluidisation regime of a liquid solid circulating fluidised bed at micro scale will be discussed.

Figure 94-97 displays the variation of solid circulating velocity with normalised transition velocity as determined by digital PIV analysis described in chapter 3 (additional figures 122 to 132 are given in appendix). Here four different fluidising liquids were studied:

- type 1- water
- Type 2 - 5 vol.% aqueous glycerol
- Type 3 - 10 vol.% aqueous glycerol
- Type 4 - 15 vol.% aqueous glycerol

Like in the water system in chapter 5, the change in solid circulating velocity with superficial liquid flow rate indicates two zones. The first zone (initial circulating fluidisation zone) is where solid circulating velocity increases rapidly with increasing superficial liquid flow rate and the second zone (fully developed zone) where solid circulating velocity insignificantly varies with increasing superficial liquid velocity as reported by Nirmala [249].

From figures 94 to 97 it can also be seen that there is a trend of increased solid circulating velocity with an increased in the viscosity of the fluidised liquid. The solid circulating velocity is the highest for the most viscous type 4 system (15%v/v glycerol) and the lowest for type 1 system (pure water). This was predicted since viscous system have a lower particle terminal velocity than water, and the particle terminal velocity decreases with increased fluidised liquid viscosity. As the particle terminal velocity decreases so does the critical transition velocity from conventional to fluidised bed regime resulting in an earlier circulating fluidised bed regime for type 4 system. This trend was the same for both Glass and PMMA particles. These observation are similar to those reported by Gnanasundaram [248]

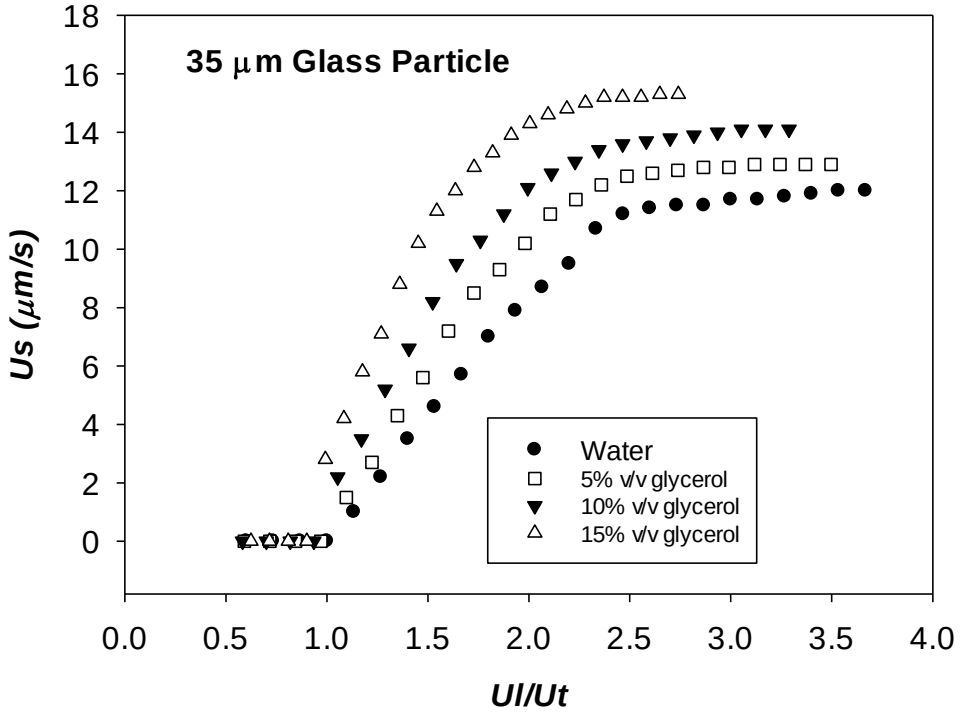

Figure 94. Influence of fluidising liquid viscosity on the particle circulating speed for 35 μm glass particle

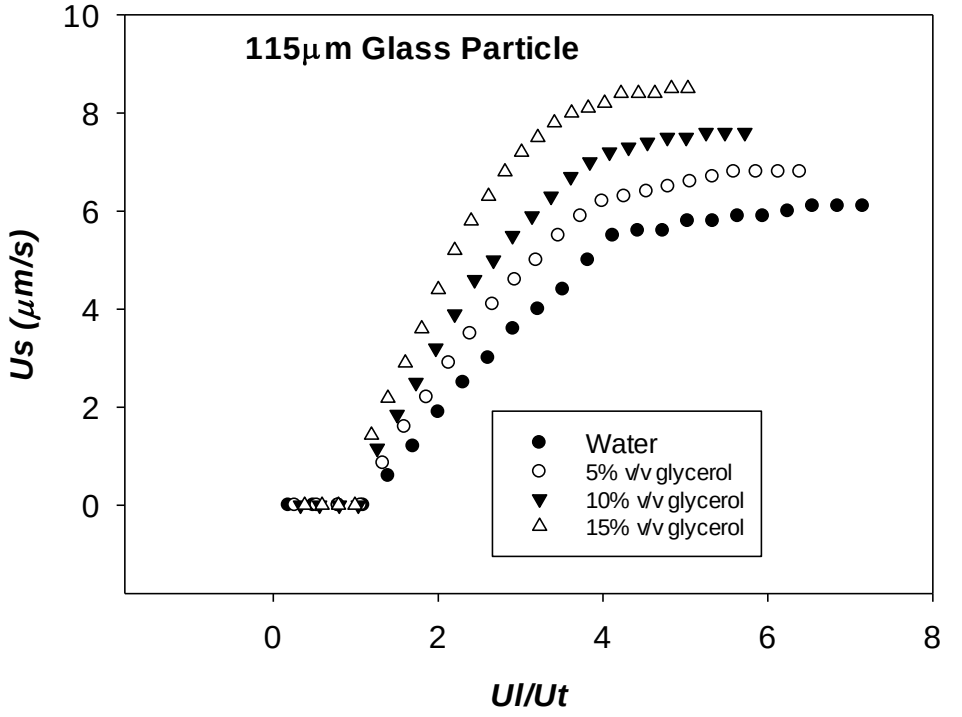

Figure 95. Influence of fluidising liquid viscosity on the particle circulating speed for 115 μm glass particle

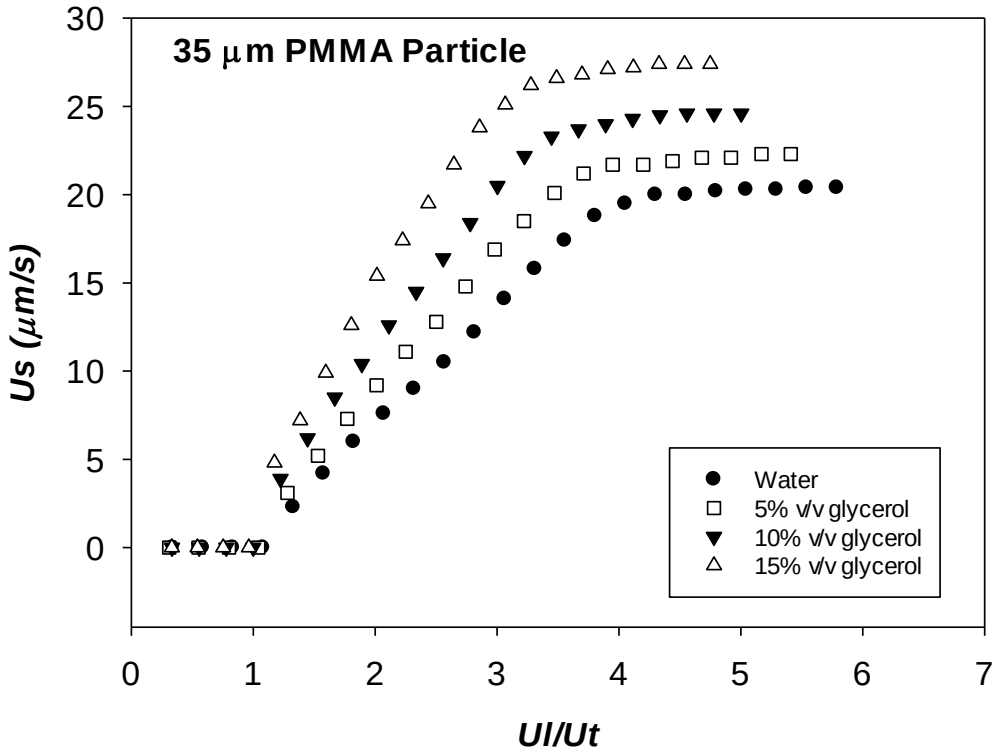

Figure 96. Influence of fluidising liquid viscosity on the particle circulating speed for 35μm PMMA particle

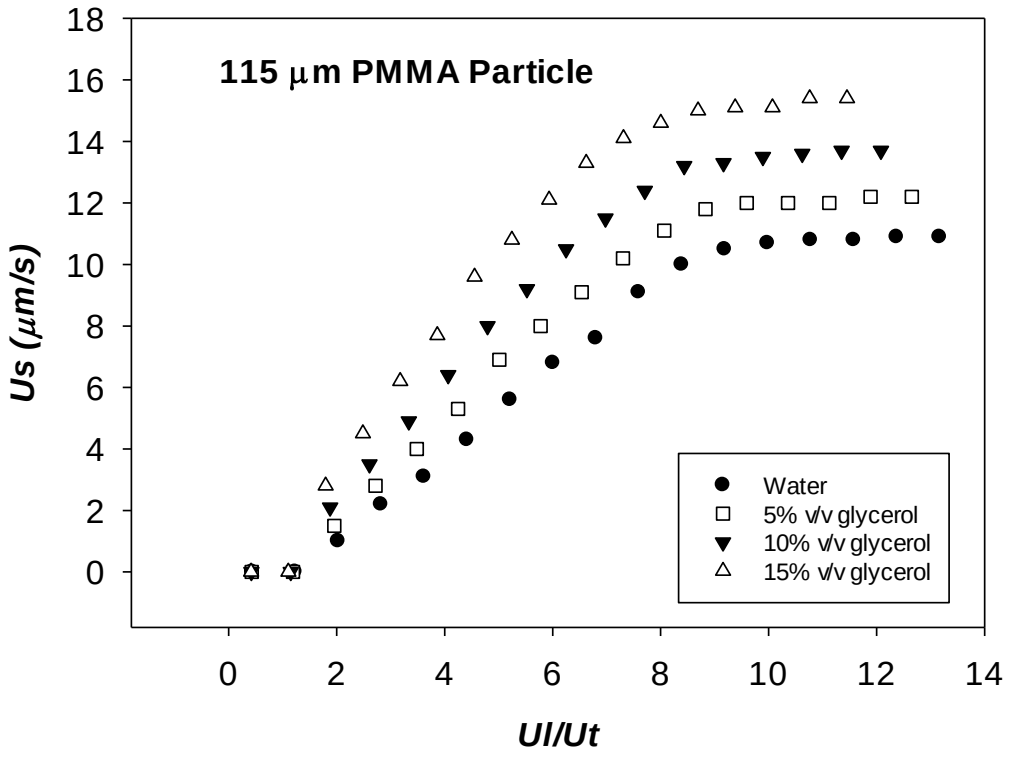

Figure 97. Influence of fluidising liquid viscosity on the particle circulating speed for 115μm PMMA particle

7.3.6 Influence of liquid viscosity on the critical transition velocity

As previously mentioned, solid-liquid circulating fluidised beds system have different operating regimes as a function of liquid velocity. In order to understand their hydrodynamics characteristics, it is crucial to identify the transition from one regime to another such as the critical transition velocity which delineates the transition from conventional to circulating fluidised bed regime.

Figures 98 and 99 shows the normalised transition velocity as a function of particle size for type 1, 2, 3, and 4 system and glass and PMMA as the fluidised particles. First there is a trend of increased normalised transition velocity with a decreased fluidising liquid viscosity. The critical transition velocity from conventional to circulating fluidised bed regime is the lowest for the most viscous system (15% vol glycerol) system and the highest for pure water system due to the fact that viscous liquids have a lower particle terminal velocity than water as explained above. These observations are similar to those reported by Gnanasundaram [28] and Nirmala [27]. It is also evident from the figure 98 and 99 that the normalised critical transition velocity increases with increased particle size which is probably because of increased wall effects which are not usually present in large circulating fluidised beds. In addition to wall effect, large particles have a higher particle terminal velocity than smaller particle which in turn increases the critical transition velocity and consequently postpone the circulating fluidised bed regime. Similar to the water system in chapter 5, it can also be observed that the normalised transition velocity (U_{cr}/U_t) is considerably higher for PMMA particles compared to glass particles of the same size. This is probably due to the difference in surface properties with PMMA particles being hydrophobic while glass particles are hydrophilic. Particle agglomeration due to cohesion was visually observed for PMMA as was some particle adhesion to the walls. Cohesion increases particle size as a result of agglomeration and that may postpone the critical transition velocity (U_{cr}) from conventional to circulating fluidised bed regime and the wall adhesion present in the downcomer will also contribute to postponing transition.

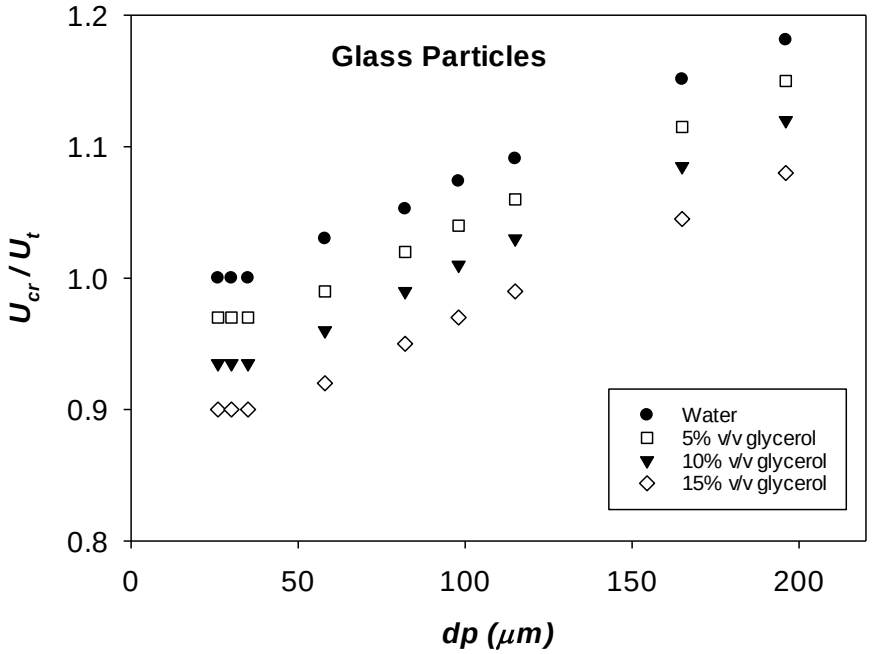

Figure 98. Influence of liquid viscosity on the critical transition velocity from conventional to circulating fluidised bed regime for glass particles

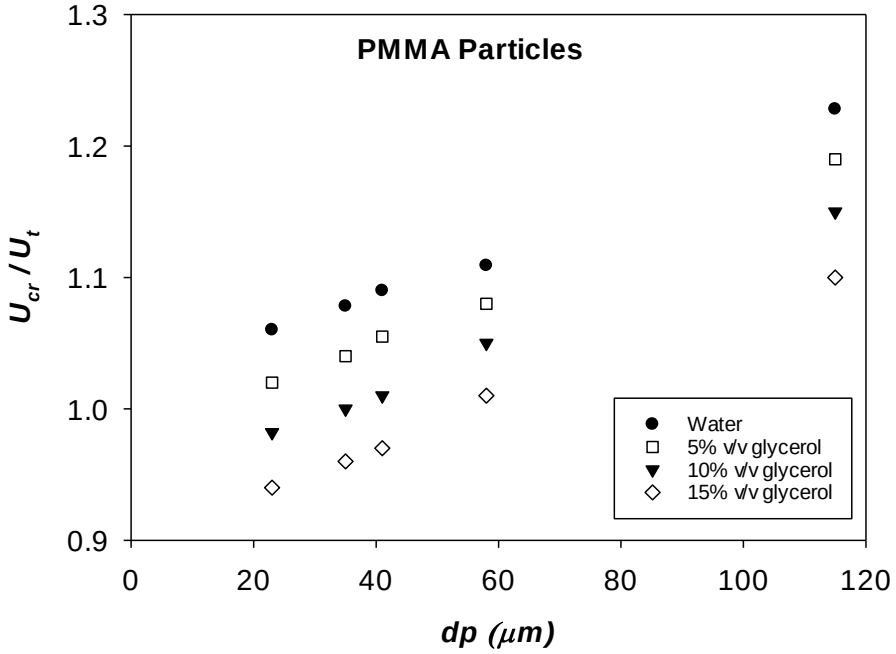

Figure 99. Influence of liquid viscosity on the critical transition velocity from conventional to circulating fluidised bed regime for glass particles

7.3.7 Influence of liquid viscosity on the transition velocity U_a, from circulating fluidised bed to transport regime

Figures 100 and 101 shows the normalised transition velocity as a function of particle size for water, 5% volume aqueous glycerol, 10% volume aqueous glycerol, and 15% volume aqueous glycerol solution system with glass and PMMA as the fluidised particles. From figure 100 and 101 it can be observed that the normalised transition velocity U_a/U_t reduces with increasing liquid viscosity, the normalised transition velocity U_a/U_t, is highest for water system and lowest for 15% volume aqueous glycerol solution system. The decline in the normalised transition velocity U_a/U_t, with increased liquid viscosity is due to the fact that viscosity enhances the shearing stress acting on particle, subsequently, this increased the drag force acting on the particles resulting in a decrease of the normalised transition velocity U_a/U_t. Transport regime started at lower superficial liquid velocity when the fluidising liquid viscosity was increased.

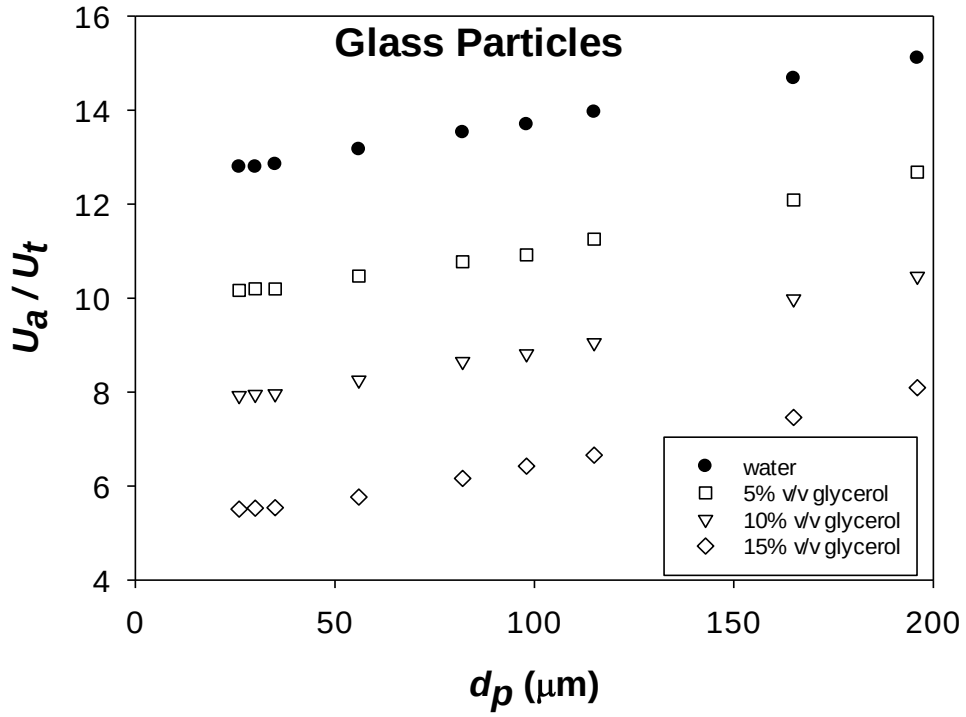

Figure 100. Influence of liquid viscosity on the transport velocity from circulating fluidised bed regime to transport regime for glass particles

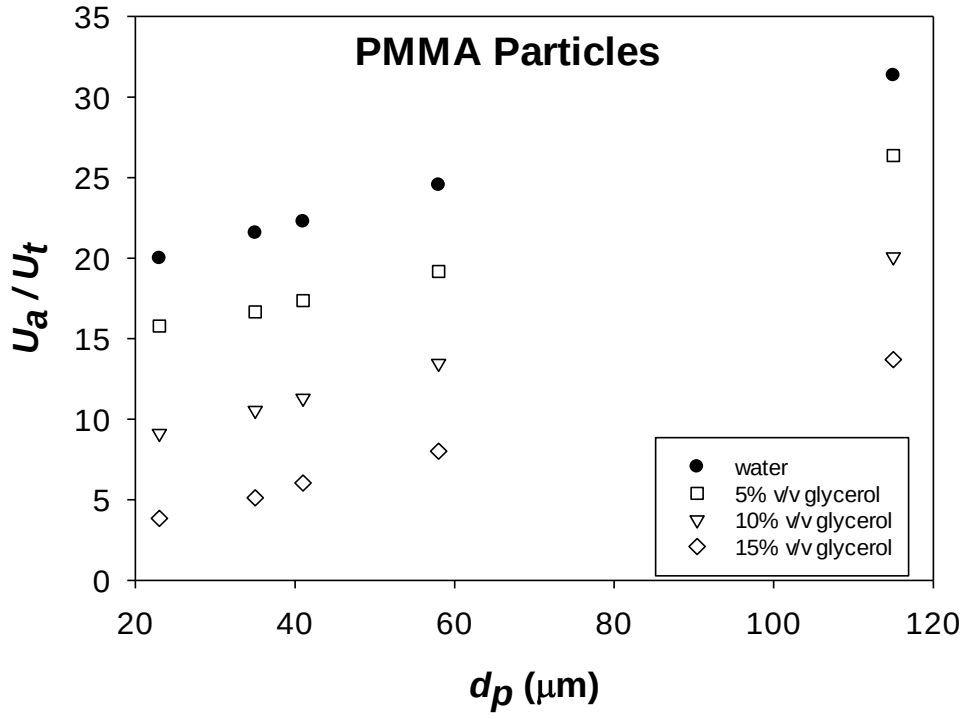

Figure 101. Influence of liquid viscosity on the transport velocity from circulating fluidised bed regime to transport regime for PMMA particles

7.4 Conclusions

The importance of fluidising liquid viscosity on the hydrodynamics of liquid-solid micro-circulating fluidised system, with special interest on the minimum fluidisation velocity, critical transition velocity and solid circulating velocity was studied for the first time. It was found that the minimum superficial liquid velocity at which particles fluidisation is achieve decreases with increasing liquid viscosity. The reduction in the minimum fluidisation velocity with an increase in the liquid viscosity is mostly due to the fact that viscous systems have a lower ratio of adhesion to drag force but seems like this cannot explain the whole reduction. Similar to the water system, for the same glycerol solutions, the minimum fluidization velocity was found to be linearly scaling with the ratio of adhesion to drag force.

Like in water system, the change in solid circulating velocity with superficial liquid flow rate indicates two zones. The first zone where solid circulating velocity increases rapidly with increasing superficial liquid flow rate and the second zone where solid circulating velocity insignificantly varies with increasing superficial liquid velocity. The solid circulating velocity in a micro-circulating fluidised bed is influenced by the viscosity of the fluidised liquid, the solid circulating velocity in the system increases with an increase in the liquid viscosity. The

critical transition velocity from conventional to circulating fluidised bed regime declines with increasing liquid viscosity. The reduction in the normalised critical transition velocity is due to the fact particle terminal velocity reduces with increasing liquid viscosity, therefore the critical transition from convention to circulating fluidised bed regime decreases resulting in an earlier circulating fluidisation regime.

Chapter 8. Flow regime mapping of a liquid-solid micro-circulating fluidised bed

8.1 Introduction

Solid-liquid circulating fluidised beds systems have different operating regimes as a function of liquid velocity [106]. The performance of these systems as solid-liquid processing equipment is influenced by flow regime. The fluidisation characteristics differ from one regime to another [106]. The rates of mixing in liquid-solid circulating fluidised beds are different in each flow regime [107] . Different fluidisation regimes produce different liquid-solid mixing. Hence knowledge on the fluidisation regime is crucial for the design and optimisation of the liquid-solid circulating fluidised bed [107].

Fluidisation regimes identification have attracted lots of attention due to rapid advance in fluidisation research. The operation regime map in a solid-liquid circulating fluidised bed has been reported previously by various researchers. *Liang et al.* [106] carried out an experimental investigation to define the fluidisation characteristics of liquid-solid circulating fluidised beds and suggested a liquid-solid circulating fluidised bed regime map which is identical to the fluidisation regime map proposed by Grace [38] for gas-solid circulating fluidised beds. They classified the circulating fluidized bed into four operating regimes: fixed bed, conventional fluidisation, circulating fluidisation and the transport regime. Zheng and Zhu [116] also studied the flow characteristics in a solid-liquid circulating fluidised bed. In their experiments they suggested an onset velocity (U_{cf}) which gives the lowest value of U_{cr}, critical transition velocity from the conventional to circulating fluidised bed regime and is independent of system geometry and operating conditions. Zheng et al.[107] studied the flow regime map of liquid-solid circulating fluidised bed and reported two existing zone in the circulating fluidised bed regime. The first zone (initial circulating fluidisation zone) where solid flux increases rapidly with increasing superficial liquid flow rate and the second zone (fully developed zone) where solid flux insignificantly varies with increasing superficial liquid velocity. Shilapuram *et al.* [33].conducted an experimental study to investigate the fluidisation regime in liquid-solid circulating fluidise beds using three different experimental methodologies and found that the critical transition velocity which indicates the transition velocity from conventional to circulating fluidisation regime was not the same for these three operational methodology. Natarajan et al. [98] also studied the flow regime map for a liquid-solid circulating fluidised bed. Their observations are similar to those reported by Zheng et al. [107], where there exists

two regions within the circulating fluidised bed regime, the initial circulating fluidised bed region and the fully developed region.

In the current research investigation, a new fluidisation regime, the solid-liquid micro circulating fluidisation regime, will be mapped for the solid-liquid fluidisation system based upon different particles sizes and materials (Polymethylmethacrylate (PMMA) and soda lime glass microspheres). The operation regime map is a function of liquid velocity inherently related to particle terminal velocity which is a function of solid-particle density and size, liquid density and viscosity. Previous studies showed that liquid density and viscosity have very little effect on the solid circulating rate, particle velocity and pressure drop, once taken into account in the particle terminal velocity [260]. Therefore, a new liquid-solid micro-circulating fluidisation regime will be studied primarily as a function of superficial liquid velocity for different sizes and densities of particles and bed sizes. The operation regime map in the micro-circulating fluidised bed is expected to be similar to the solid-liquid circulating fluidised bed regime map proposed by Liang and co-workers [260]. The major differences from their macro-scale counterparts are expected to be the surface forces, which can prevent fluidisation, and inevitably the wall effects due to small bed size [61].

8.2 Results and discussion

8.2.1 Observation

Solid-liquid fluidisation in a micro circulating fluidised bed is reasonably uniform. In the circulating fluidisation regime with increasing liquid flow rate, a difference could be observed in the liquid flow rate in the riser, with higher liquid flow rate at the centre of the riser and lower liquid flow rate near the walls.

In the middle section of the riser, particles were carried up to the top of the column riser by a higher liquid flow, while a small downwards flow of particles occurred near the wall of the riser as shown in figure 102. However, this downwards flow of particles near the wall of the riser column was insignificant and did not have an effect on regime transition. These observations are similar to that reported by Zheng and Zhu [116] and Liang *et al* [106]. Agglomeration of particles which was caused by the presence of bubbles in the system was also observed, special with the PMMA particles which were extremely hard to separate using the solid-liquid separator, as these particle-bubble agglomerates usually float to the top of the solid-liquid-separator.

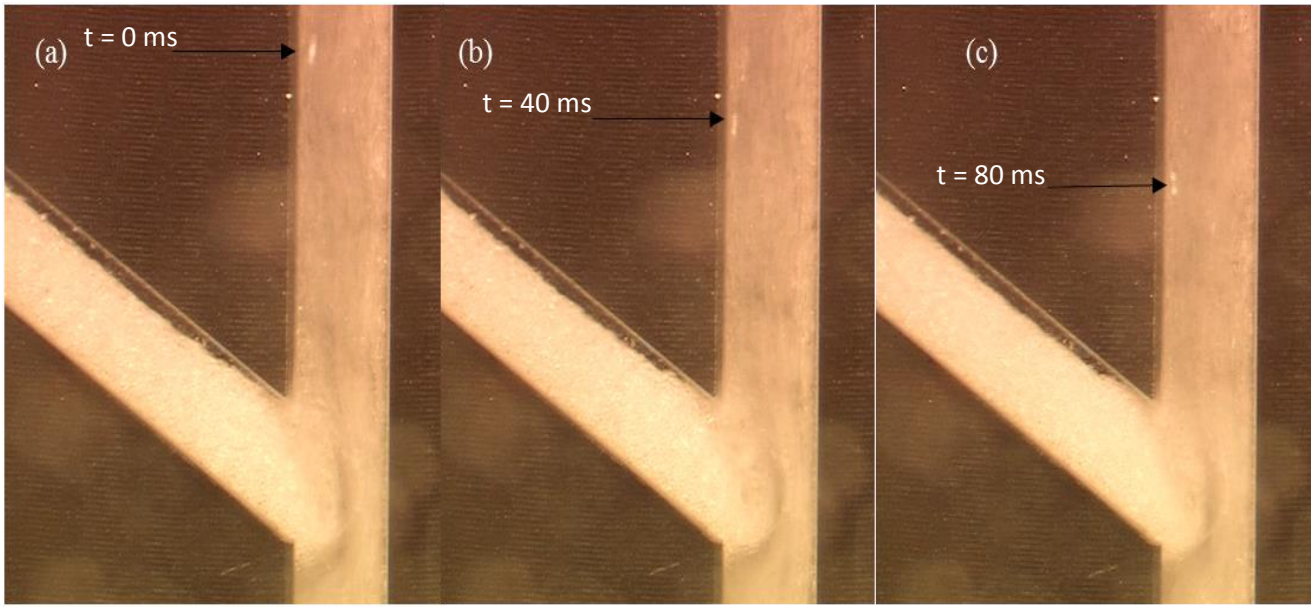

Figure 102. The time sequenced images extracted from the movie of circulating fluidized bed using 38 µm soda lime glass microsphere particle at 1.5 mm/s. the arrows show small downwards flow of particles close to the riser wall. The letters a, b and c show three consecutive images of downwards flow of particles taken in a short time interval (0, 40, and 80 milliseconds respectively)

8.2.2 Transition from circulating fluidisation regime to transport regime

To facilitate the comparison between different particle size and density, the transition velocity, U_a, which demarcate the transition from circulating fluidised bed regime to transport regime was normalised by dividing the corresponding particle terminal velocities U_t.

Figure 103 shows the normalised transition velocity, U_a / U_t as a function of particle diameter for both glass and PMMA particle respectively. One can notice that U_a is influenced by particle size and density. Firstly, for glass and PMMA particles, the normalised transition velocity, U_a/U_t was found to increase with particle size which is probably because of increased wall effects. Once again, one can also observe that U_a/U_t is also perceptibly higher for PMMA particles, compared to glass particles of the same size, even though PMMA particles density are lighter than glass particle (1200 and 2500 kg/m3 respectively). This is due to differences in surface properties as already discussed.

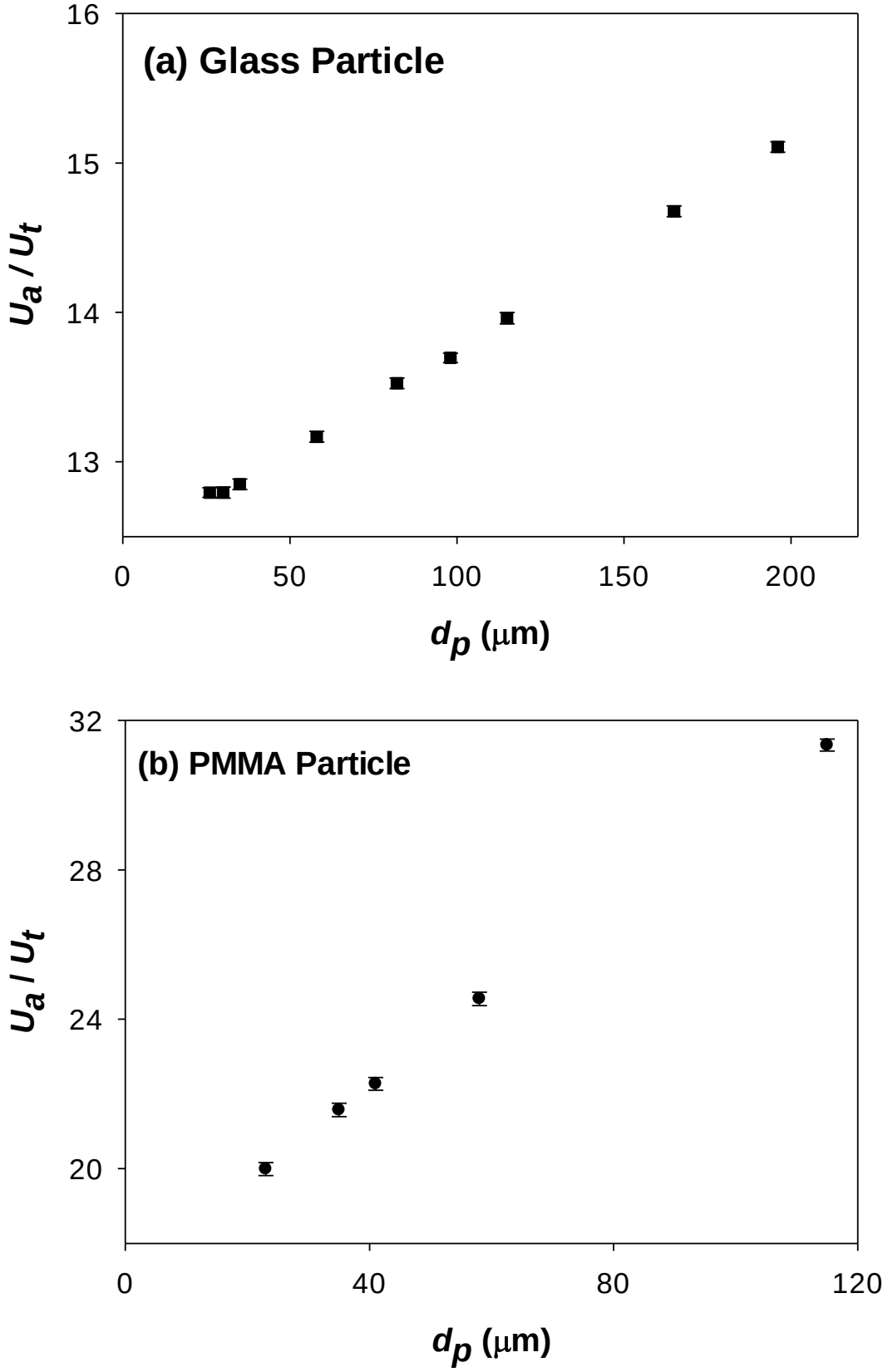

Figure 103. Transition velocity from circulating fluidised bed regime to transport regime for (a) glass and (b) PMMA particles with solid inventory in the range of 10 – 25%.

8.2.3 Flow regime map

Based on this experiment and our previous experiments in the simple micro-fluidised bed [234], the fluidisation regime map is constructed for both PMMA and glass particles as shown in figure 104. Both experimental results were plotted on the same plot using non-dimensional quantities of dimensionless liquid velocity, U_l^* and dimensionless particle diameter d_p^* as introduced by Liang, Zhang [106]:

$$U_l^* = U_l \left(\frac{\rho_f^2}{\mu g \Delta \rho} \right)^{1/3} \qquad (29)$$

$$d_p^* = d_p \left(\frac{\rho_f g \Delta \rho}{\mu^2} \right)^{1/3} \qquad (30)$$

The most striking trend of the plot is that the minimum fluidisation velocity ($U_{mf,\,exp.}$) at which particle fluidisation is achieved for both PMMA and glass particles deviates strongly from the theoretical prediction of the Ergun equation, with proportionally higher deviation for the PMMA particles. This is due to the strong influence of surface forces on the minimum superficial liquid velocity at which particle fluidisation is achieved as found in our recent study [234]. For PMMA particles fluidised by water in a PMMA micro fluidised bed, adhesion forces are 3–5 orders of magnitude higher than the drag forces, while for glass particles adhesion forces are only 1–3 orders of magnitude higher than the predicted drag force due to weaker adhesion forces and larger particle densities. These particle–wall adhesion forces are transferred as frictional forces to the particle ensemble inside the bed [261, 262]. Consequently, this increased wall friction force results in an increase of the experimental minimum fluidisation velocity [71].

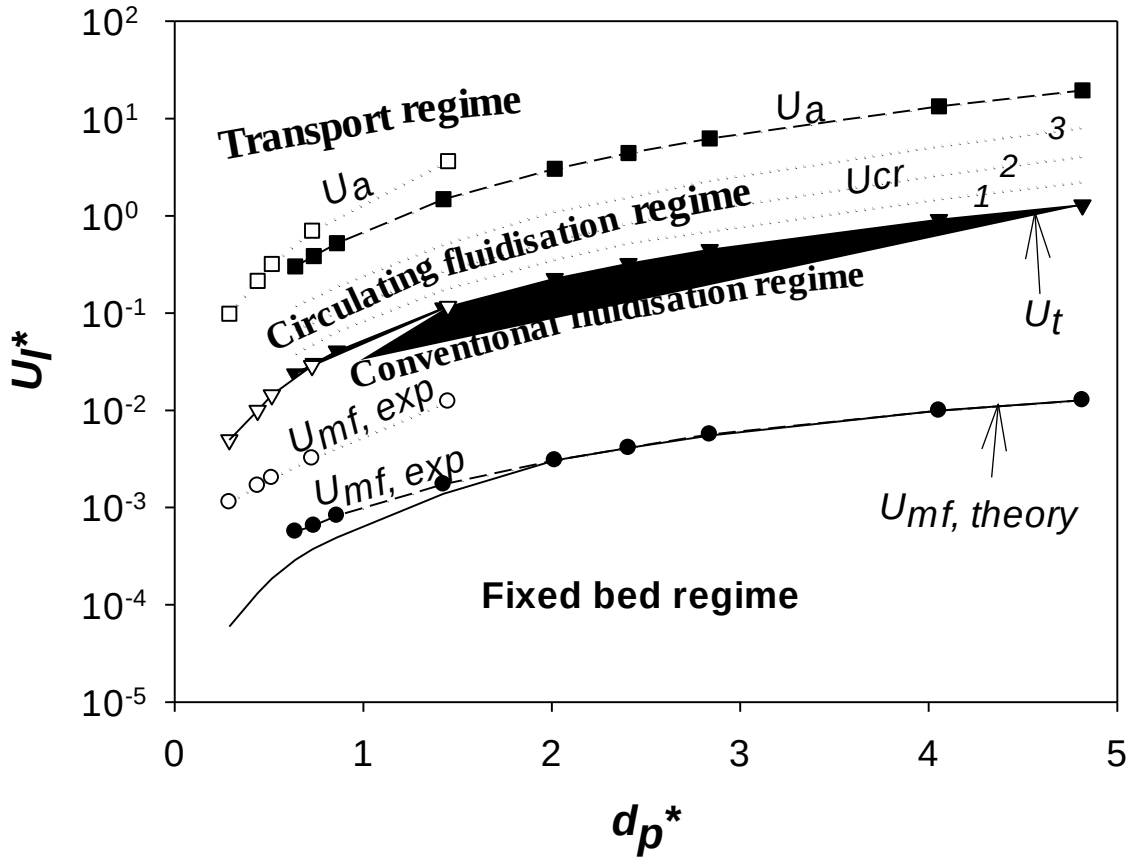

Figure 104. Flow regime map of solid–liquid micro–circulating fluidised bed for glass (filled symbols) and PMMA (empty symbols) particles with water as fluidizing liquid. The solid lines are the theoretical prediction for minimum fluidisation velocity and terminal velocity. The dashed (glass particles) and dotted (PMMA particles) lines connecting experimental points for the minimum fluidisation velocity (circles), the critical transitional velocity (triangles) and the transport transition velocity (squares) are a guide for the eye only. Three dotted lines labeled 1, 2 and 3 are U_{cr} of glass particles at solid inventories of 8%, 6% and 3% respectively.

The minimum fluidization is postponed for both types of particles, but the proportional increase is much bigger for PMMA micro–particles (8–20 times bigger experimental U_{mf} to the theoretical prediction depending on the size of particles) in comparison with glass beads (only about 2 times bigger experimental U_{mf} compared to the theoretical prediction for the smallest size particles). Our experimental data show that the increase in the minimum velocity scales linearly with the product of the adhesion/drag force and particle–to–bed diameter ratios [234], but mostly is influenced by the surface forces. Therefore, the proportional increase is the highest for the smallest particles of both glass and PMMA, decreasing with the increase in particle size, and becoming unity for the biggest glass particles as can be seen in the plot.

However, the surface forces did not have a major influence on the critical transition velocity (U_{cr}) which demarcates the transition from conventional to circulating fluidised bed regime as shown in figure 104. For both types of particles, the normalised transition velocity, U_{cr}/U_t, is roughly 1, at solid loading above 10%, with a weak increased U_{cr}/U_t, with an increase in particle size which is probably because of increased wall effect as already discussed. In addition, the relative transition velocity is slightly higher for PMMA particles due to influence of cohesion which forms bigger agglomerates and wall adhesion observed in the downcomer. This is not visible in the plot as the increased transition velocity is only 5 to 10% (smaller than the symbol used). Three additional dotted lines labelled on the plot as 1, 2 and 3 shows the U_{cr} of glass beads at solid inventories of 8%, 6% and 3% respectively. These show that the solid loading influences significantly this transitional velocity further limiting the operating range of velocities for the circulating fluidized bed at the micro-scale. This is not given for PMMA particles due to clarity reasons, but similar trends are also present.

The transport transition velocities, U_a from circulating fluidized bed to transport regime are very similar in magnitude for PMMA and glass particles of the same size which indicate it might be a property of the system geometry only for a given particle size. Therefore, there are two distinctive lines on the map as the relative transition velocity for PMMA particles is around 20 times particle terminal velocity while it is only 10 times for the glass beads which indicates that transition to the transport regime is influenced by cohesion. Further study is needed to elucidate this further.

8.2.4 Flow regime map for liquid-solid micro-circulating fluidised bed system with change in liquid viscosity

Fluidisation regime map was constructed for glass and PMMA particles using four kinds of fluidising liquid, water, 5% volume aqueous glycerol, 10% volume aqueous glycerol, and 15% volume aqueous glycerol solution as shown in figure 105.

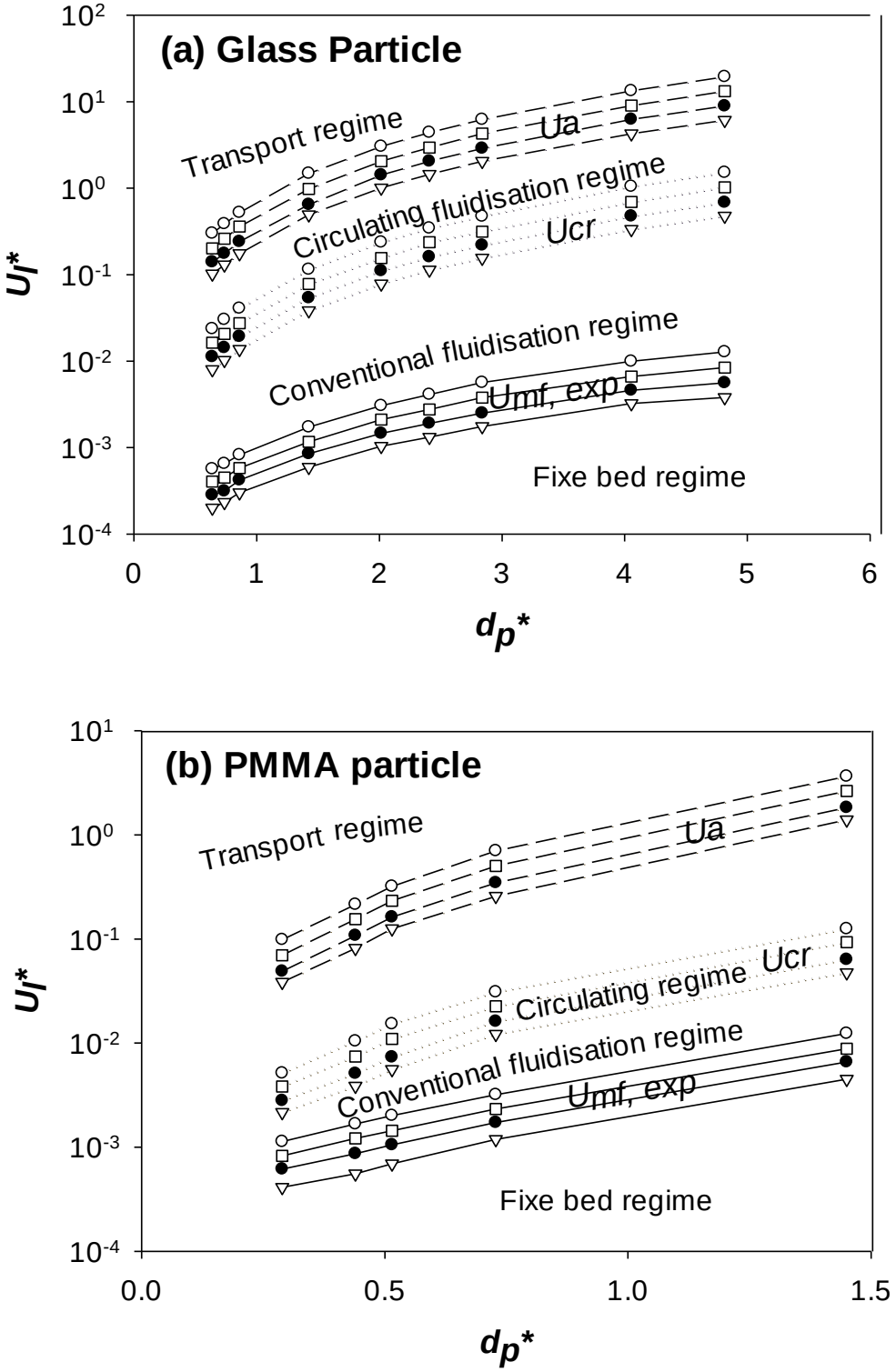

Figure 105. Flow regime map of solid–liquid micro–circulating fluidised bed for (a) Glass particles and (b) PMMA particles with water (empty circle), 5% volume aqueous glycerol (empty square), 10% volume aqueous glycerol solution (filled circle) and 15% volume aqueous glycerol solution (empty triangle) as fluidising liquid. The solid lines are experimental minimum fluidisation velocity, the dotted lines connecting experimental points for the critical transition velocity, and the dashed lines are the transport transition velocity

Based on the experimental results a new flow regime map of solid-liquid micro-circulating fluidised bed for glass and PMMA particles with water, glycerol (5% v/v, 10% v/v, and 15% v/v) solution as the fluidising liquid is presented in figure 103a & 103b.

The experimental data in figure 105a and 105b shows that, the liquid viscosity have a major influence on the fluidisation behaviour of a liquid-solid micro-circulating fluidised bed system. The experimental minimum fluidisation velocity U_{mf}, critical transition velocity U_{cr}, and transport velocity U_a decreased with increased fluidising liquid viscosity. The experimental U_{mf}, U_{cr}, and U_a was higher for water system in comparison with glycerol solution system. The reduction in the experimental minimum fluidisation velocity U_{mf}, critical transition velocity U_{cr}, and transport velocity U_a, with increased fluidised liquid viscosity is due to the fact that viscosity enhances the shearing stress acting on particle, consequently, this increased the drag force acting on the particles resulting in a decrease of the minimum fluidisation velocity, critical transition velocity, and transport velocity. Hence, conventional fluidisation regime, circulating fluidisation regime, and transport regime started earlier for viscous system, but the size of each regime is approximately the same regardless of liquid viscosity.

8.2.5 Flow regime map for liquid-solid micro-circulating fluidised bed system with change in solid feed pipe geometry

Fluidisation regime map was constructed for 165 µm and 196µm glass particles using three solid feed pipe of 1, 1.5 and 2 mm square cross section. The difference in the solid feed pipe cross section size did not have any major influence on the transition velocity from fixed bed regime to conventional fluidised bed regime as shown in figure 106. The minimum fluidisation velocity was the same for three types of system (1mm, 1.5 mm, and 2mm cross section solid feed pipe).

The critical transition velocity U_{cr}, from conventional to circulating fluidised bed regime and transport transition velocities U_a, from circulating fluidised bed regime to transport regime was affected by the change in the solid feed pipe cross section size. The critical transition velocity U_{cr}, and transport transition velocity U_a, increases with a reduction in the solid feed pipe cross section size due to the wall effects which are not usually present in large circulating fluidised beds. Hence, the circulating fluidised bed regime and transport regime start at lower superficial liquid with increasing solid feed pipe cross section. The fluidisation regime, and transport

regime started much earlier for the 2 mm cross section solid feed pipe system and was much later for the system with solid feed pipe of 1 mm cross section. However, the size of each regime seems unchanged by this geometry of the bed.

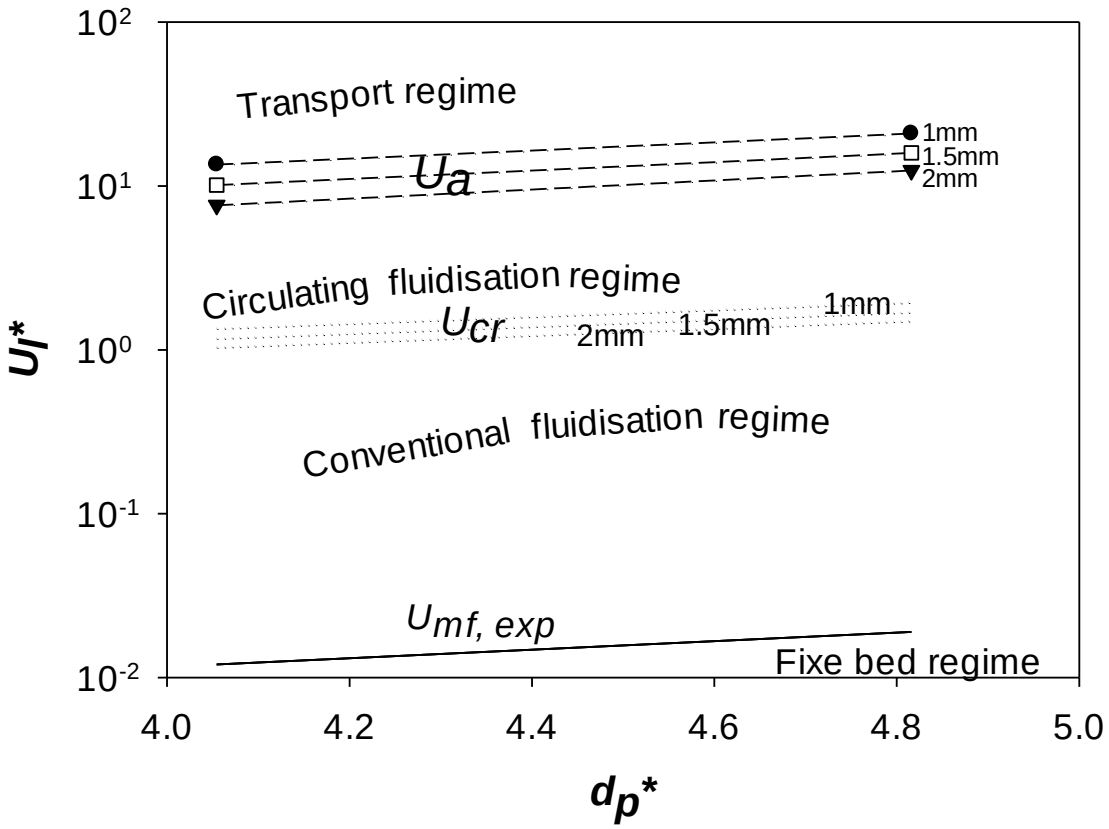

Figure 106. Flow regime map of solid–liquid micro–circulating fluidised bed with change in the solid feed pipe cross section size. Three different solid feed pipe structure of 1mm, 1.5mm, and 2mm cross section were used construct the fluidisation regime map for 165 and 196µm glass particles with water as fluidising liquid. The angle between the riser and solid feed pipe was 60°. The solid lines are experimental minimum fluidisation velocity, the dotted lines connecting experimental points for the critical transition velocity, and the dashed lines are the transport transition velocity.

8.2.6 Flow regime map for liquid-solid micro-circulating fluidised bed system with change in the angle between riser and solid feed pipe

Fluidisation regime was mapped for 165µm and 196µm glass particles using three kinds of angle between the riser and solid feed pipe of 30, 50, and 60°. The variation in the angle between the riser and solid feed pipe did not have any major influence on the transition velocity from fixed bed regime to conventional fluidised bed regime as shown in figure 107. The

minimum superficial liquid velocity at which particle fluidisation was achieved was the same for the three types of system (30°, 50°, and 60°).

However, the critical transition velocity U_{cr}, from conventional to circulating fluidised bed regime and transport transition velocity U_a, from circulating fluidised bed regime to transport regime is dependent upon the angle between the riser and solid feed pipe. The critical transition velocity U_{cr}, and transport transition velocity U_a, increases with an increase in the angle between the riser and solid feed due to the difference in the net hydrodynamics force acting on the particle. Therefore, the circulating fluidised bed regime and transport regime started at much lower superficial liquid for the system with 30° angle between the riser and solid feed pipe and was much late for the system with 60° angle between riser and solid feed pipe.

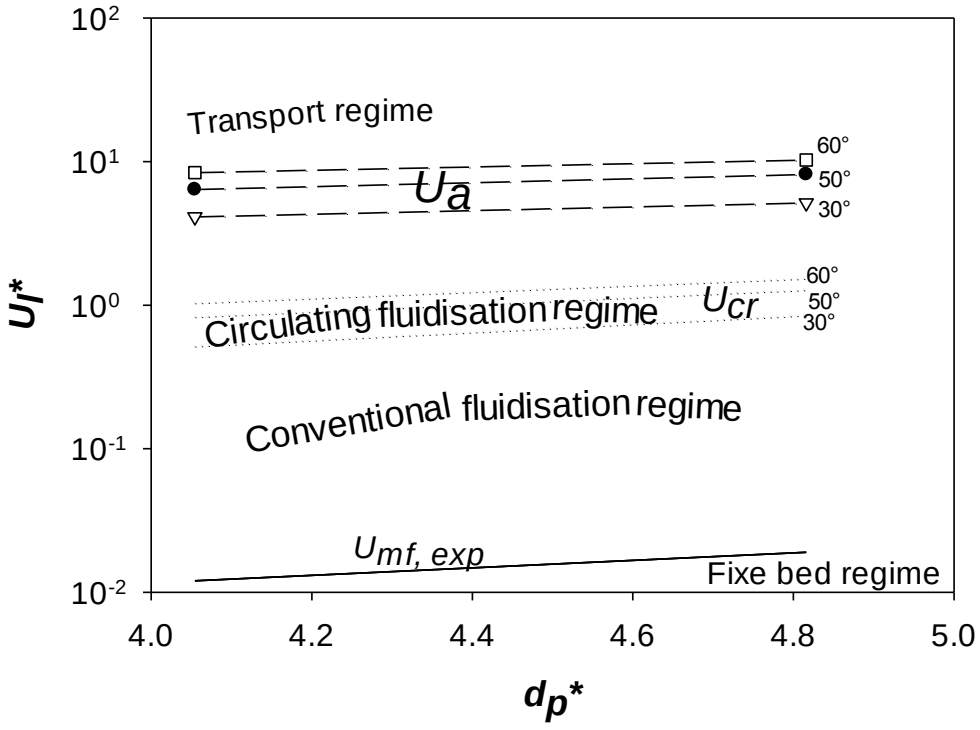

Figure 107. Flow regime map of solid–liquid micro–circulating fluidised bed with change in the angle between the riser and the solid feed pipe. Three different angles of 30°, 50°, and 60°were used to construct the fluidisation regime map for 165 and 196µm glass particles with water as fluidising liquid. The micro-circulating fluidised bed employed for this experiment had a riser and solid feed pipe of 2mm square cross section. The solid lines are experimental minimum fluidisation velocity, the dotted lines connecting experimental points for the critical transition velocity, and the dashed lines are the transport transition velocity.

8.3 Conclusions

A research investigation on solid-liquid fluidisation in a micro circulating fluidised bed was performed to map different regimes with a special interest in the transition from a conventional fluidised bed to circulating fluidised bed regime. The results indicate that fluidisation in a solid-liquid micro circulating fluidised bed system could be categorised in to four operating regimes: fixed bed, conventional fluidisation, circulating fluidisation, and transport regime, with the critical transition velocity roughly equal to the particle terminal velocity. The surface forces influence strongly the minimum fluidisation velocity which can be up to 20 times bigger for the smallest PMMA microparticles while the increase is only minor for glass particle (less than 2 times for the same size smallest glass microparticles). As in a macroscopic circulating fluidised bed, the transition velocity from conventional to circulating fluidised bed decreases with solid inventory before levelling off at high enough solid inventory. The transition velocity is comparable to the particle terminal velocity, i.e. the normalised transition velocity is approximately 1 in line with previous macroscopic studies. However, there was a weak increase in the normalized transition velocity with particle size which is probably due the wall effects (higher particle to bed ratio). In addition the normalised velocity is slightly higher for PMMA particles due to stronger adhesion and cohesion forces but influence is minimal in comparison with influence on the minimum fluidisation velocity. Finally it seems that transition to the transport regime is influenced by cohesion so the relative transition velocity for PMMA particles is around 20 times particle terminal velocity while it is only 10 times for the glass beads. Consequently, the conventional regime is proportionally bigger for the glass beads in comparison with PMMA particles, whist the situation is opposite for circulating fluidisation regime as it is bigger for PMMA particles.

Chapter 9. Conclusions

A research study on fluidisation of glass and PMMA microparticles in a micro-circulating fluidised bed was performed. The investigation confirmed that liquid-solid fluidisation in micro-circulating fluidised bed system is strongly influenced by surface force and wall effect. For both particles, some adhesion was observed to the fluidised bed walls as predicted by the Acid-based theory developed by Oss, Chaudhury and Good. For PMMA particles the adhesion forces were 3-5 order of magnitude higher than the drag forces, indicating particle adhesion to the bed walls is highly likely to influence the fluidization process. while for glass particles adhesion forces are only 1-3 order of magnitude higher than the predicted drag force due weaker adhesion forces and large particle density. These adhesion forces are transferred as frictional forces to the particle ensemble inside the bed. Consequently, this increased wall friction force results in an increase of the experimental minimum fluidisation velocity and beyond. For both PMMA and glass particles surface force is more important for smaller particle as adhesion force scale up with particle diameter while drag force scales with the cube of diameter.

The experimental fluidisation was postponed in comparison with theoretical minimum fluidisation velocity predicted by Ergun equation. The minimum fluidization velocity was influenced by both surface force and wall effects. The minimum fluidisation velocity can be up to 23 times bigger for the smallest PMMA microparticles while the increase is only minor for glass particle (less than 2 times for the same size smallest glass microparticles).

The digital PIV analysis using PIVlab and MATLAB was used to determine the solid circulating velocity in a micro-circulating fluidised bed. The use of PIVlab and MATLAB codes to estimate the average particle velocity seems promising, and the results looks relevant when compared with previous reported studies. As in a macroscopic circulating fluidised bed, the average particle velocity in a micro-circulating fluidised bed increases with liquid velocity in two distinct zones, increasing sharply first then levelling off at higher inlet fluid velocities. The determined transition velocities are comparable to the particle terminal velocity, i.e. the normalised transition velocity is approximately 1 in line with previous studies. The transition velocity is strongly influenced by solid inventory, i.e. it decreases with solid inventory before levelling off at high enough solid inventory. A weak increase in the normalised transition velocity with particle size was observed, which is probably due the wall effects (higher particle to bed ratio).

The study also confirms that fluidisation behaviour in liquid-solid micro-circulating fluidised bed system is also influenced by bed geometry such as cross section size of solid feed pipe and the angle between the riser and solid feed pipe. The average particle velocity increases with increased solid feed pipe cross section while the critical transition velocity increases with a reduction in the solid feed pipe cross section size. Furthermore, the average solid velocity increases with decreased angle between the riser and solid feed pipe, and the critical transition velocity from conventional to circulating fluidised bed regime increases with increased angle between the riser and solid feed pipe due to the difference in the net hydrodynamics force acting on the particle.

The solid circulating velocity in a micro-circulating fluidised bed is influenced by the viscosity of the fluidised liquid. The minimum superficial liquid velocity at which particles fluidisation is achieve decreases with increasing liquid viscosity. The reduction in the minimum fluidisation velocity with an increase in the liquid viscosity is mostly due to the fact that viscous systems have a lower ratio of adhesion to drag force. Similar to the water system, for the same glycerol solutions, the minimum fluidization velocity was found to be linearly scaling with the ratio of adhesion to drag force. The solid circulating velocity in the system increases with an increase in the liquid viscosity. The critical transition velocity from conventional to circulating fluidised bed regime declines with increasing liquid viscosity. The reduction in the normalised critical transition velocity is due to the fact particle terminal velocity reduces with increasing liquid viscosity, therefore the critical transition from convention to circulating fluidised bed regime decreases resulting in an earlier circulating fluidisation regime.

Finally, a new fluidisation regime, the solid-liquid micro-circulating fluidisation regime, was mapped for the solid-liquid fluidisation systems of different particles size and materials (Polymethylmethacrylate (PMMA) and soda lime glass microspheres). The result indicates that fluidisation in a solid-liquid micro circulating fluidised bed system could be categorised in to four operating regimes: fixed bed, conventional fluidisation, circulating fluidisation, and transport regime, with the critical transition velocity roughly equal to the particle terminal velocity.

Chapter 10. Future work

An interesting idea of practical application of developed micro-fluidized bed system is to study heat transfer and hydrodynamics in inverse micro- circulating fluidised bed system. The motivation for this work is as follows. In the last four decades high heat flux electronic cooling has become an important technology in the power electronics and micro-electronics industry for the manufacture of various electronics equipment such as high power computer micro-chips, medical X-ray, electronic radar, laser diodes [263, 264]. For a successful and reliable operation of these electronic equipment, temperature control within a certain range is extremely vital as high heat flux (1000-2000 W/cm^2) produced by these micro-processor devices causes malfunction, shortened life and equipment failure [265, 266]. For that reason, it is important to remove the large amount of heat generated in these micro-processor devices. Conventional cooling solutions such as air system, vapour chamber, thermoelectric cooling, and heat pipes which have long been used for the cooling of computer chip in the micro-electronic and power electronic industry have either reached their practical application limits or are soon to become impractical for recently emerging electronics components as they are not capable of removing high heat fluxes of 1000-2000 W/cm^2 [267, 268]. Hence, higher heat flux removal in today's emerging micro-electronic device continues to be one of the major challenge facing the micro-electronics industry [268]. Efforts to improve the reliability of electronic computers are as important as efforts to improve their speed and storage capacity [268]. Solid-liquid micro-circulating fluidised beds are considered to be a potential high flux technology, their unique thermal transport properties make them prime contenders for the next generation of coolers for high power computer chips [269, 270]. They have a better and efficient heat removal capabilities when comparing to most conventional cooling solutions, as they are capable of removing very high heat flux (1000-2000 W/cm^2) from micro-processor equipment such as computer chips and telecom devices while keeping the equipment temperature low and steady, reduced power consumption and enhance the system efficiency [271, 272]. Although the influence of angles on micro-circulating fluidised bed hydrodynamics was not studied at the present research investigation, many studies have concluded that when the misalignment is less than 5 degree, the influence on the hydrodynamics variables is small and easy to control [273-277]. Furthermore, the cooling device is not projected to be used for laptops and such devices, mostly envision for huge data centres (cluster computers) where position is easy to control.

Furthermore, micro-encapsulated phase change materials (PCM) can be used as the fluidised particles in the recommended experimental studies. PCM are latent heat storage materials, they absorbs energy when melts, and release energy when solidifies enabling them to act as heat storage media [278]. PCM particles have the capability to store and release high amount of heat while maintaining a uniform temperature, which is essential for processes where temperature uniformity is required to achieve higher conversion efficiency [279, 280]. The particles would be encapsulated PCM, ie. there is a shell which would not go through phase transition, pcm would be inside so not possible to go outside and cause any agglomeration [281, 282]. Microencapsulated phase change materials are very stable, e.g. they are been used in building applications as construction material to improve thermal comfort and to save energy consumption in buildings (commercially available from e.g. BASF) [283, 284], and in the textile applications for the manufacturing of smart textile product such as space suits to protect astronauts from cold and heat during space mission, and sensor baby vest to monitor babies body temperature [285, 286].

Hence PCM particles are ideal for the recommended study. Since PCM particles have a density lower than water (around 800 kg/m^3), a novel inverse micro-circulating fluidised bed is required in this case as particles will be fluidised by a downwards flow of the liquid. Study on heat transfer along with hydrodynamics of inverse micro-circulating fluidised bed will offer important parameters for design a micro-fluidised bed cooler capable to fulfil the needs of cooling high power computer micro-chips and others micro-electronics component.

The second idea for future work is to use fast design-manufacture cycle provided by additive manufacturing technology (3D printing) to study non-conventional bed geometries. 3D printing will allow to rapidly fabricate a reliable micro-circulating fluidised bed using low cost material and most importantly, the bed geometry can easily be modified. Specifically, Miicraft+ printer and Form2 printer can be used in future experimental studies to design and construct the micro-circulating fluidised bed of different bed cross-sectional geometry like circular, square geometries (used in my study), hexagonal (other polygons can be considered), semi-circle shaped micro-fluidized bed. The liquid-solid fluidisation characteristics such as minimum fluidisation velocity, critical transition velocity, transport transition velocity, solid circulation rate, in circular and hexagonal cross section shaped channels can be studied and the results obtained will be compared with corresponding ones in a square shaped bed channel. It would be interesting to find polygon shape which resembles the most circular geometry as the

most common big scale fluidized bed geometry while still having the flat surface important for easy of visualization studies like used in this study.

Since the liquid-solid circulating fluidised bed consist of two columns, the riser and downcomer with continuous particle circulation between the two columns. The angle of the solid return pipe, the liquid-solid separator structure, and riser-downcomer diameter ratio could potentially influence the hydrodynamic parameters in the liquid-solid micro-circulating fluidised bed system, particularly the solid circulation rate, critical transition velocity U_{cr} from conventional to circulating fluidised bed regime, and transport transition velocity U_a from circulating fluidised to transport regime. Therefore, future experimental studies also include the influence of circulating fluidised bed geometry (riser-downcomer diameter ratio, solid return pipe angle, and the structure of liquid-solid), on the hydrodynamic variables such as solid circulating velocity, critical transition velocity from conventional to circulating fluidise bed regime, and transport transition velocity from circulating fluidised bed to transport regime. The idea is that by changing the liquid-solid separator structure, solid return pipe angle, and riser-downcomer ratio can have an influence on the internal recycling of particles in the riser and eventually on the system hydrodynamics. 3D printing will be used to fabricate the micro-circulating fluidised. This will allow to rapidly fabricate a reliable fluidised bed and most importantly, the structure of solid-liquid separator can easily be modified.

Future experimental studies should also include the hydrodynamics study of gas-solid micro-circulating fluidised bed as the gas-fluidized beds have much wider application on a macro scale in comparison with liquid-solid fluidized beds. The study aim would be to investigate the influence of hydrodynamics of the system and the influence of surface forces, wall effect, minimum fluidisation velocity, critical transition velocity, transport transition velocity in a gas-solid micro-circulating fluidised bed system, and a new fluidisation regime, the gas-solid micro-circulating fluidisation regime, will be mapped for the gas-solid fluidisation systems of different particles size and materials.

Chapter 11. Appendix

11.1 Calibration

Before the experimental procedure, flowrates were calibrated in the range of fluidization velocities with and without particles inside the bed in order to estimate the systematic error and showed a good linear relationship from the pump reading as shown in figure 108.

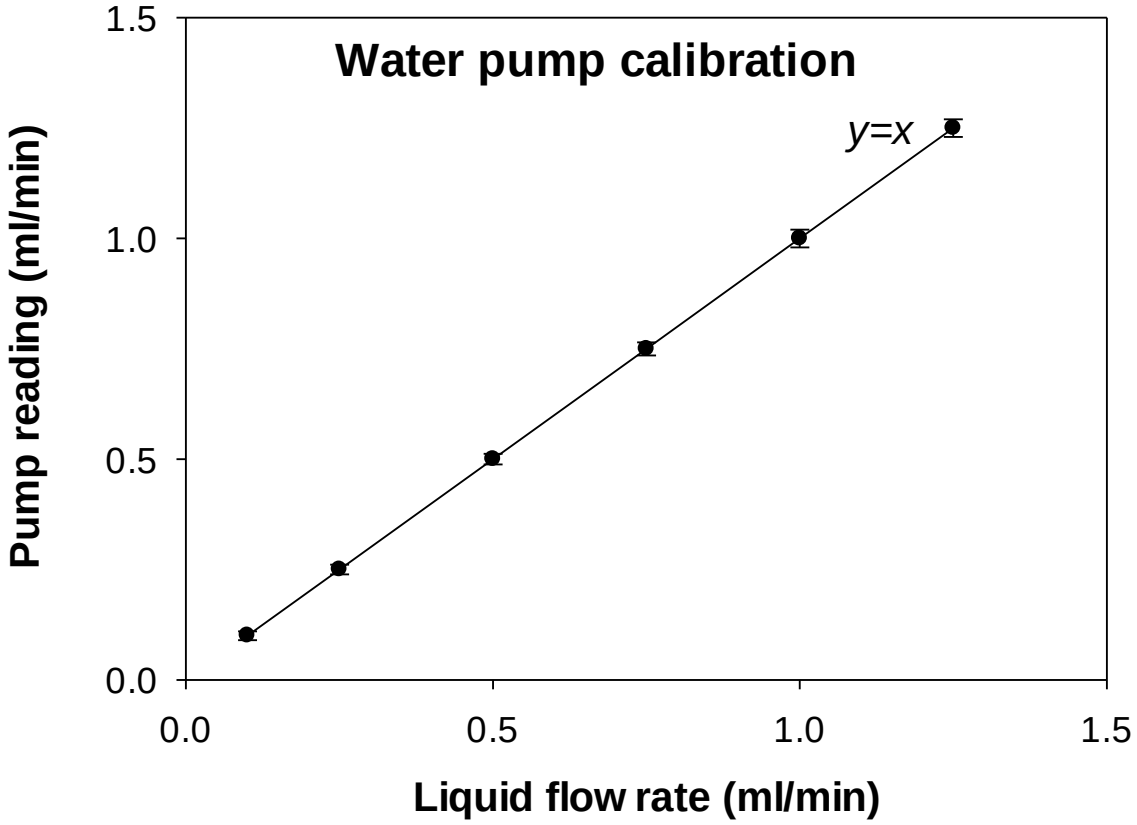

Figure 108. Liquid calibration

11.2 Minimum fluidization experiments results

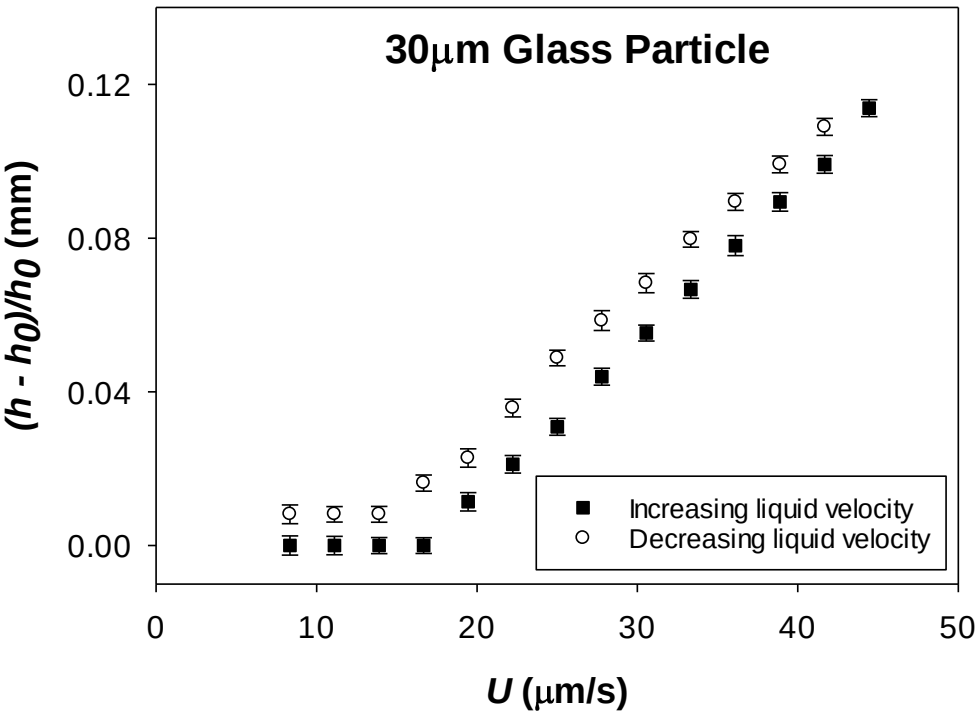

Figure 109. Relative bed height as a function of liquid velocity for 30μm glass particle in 1mm micro-fluidised bed with water as the fluidised particles.

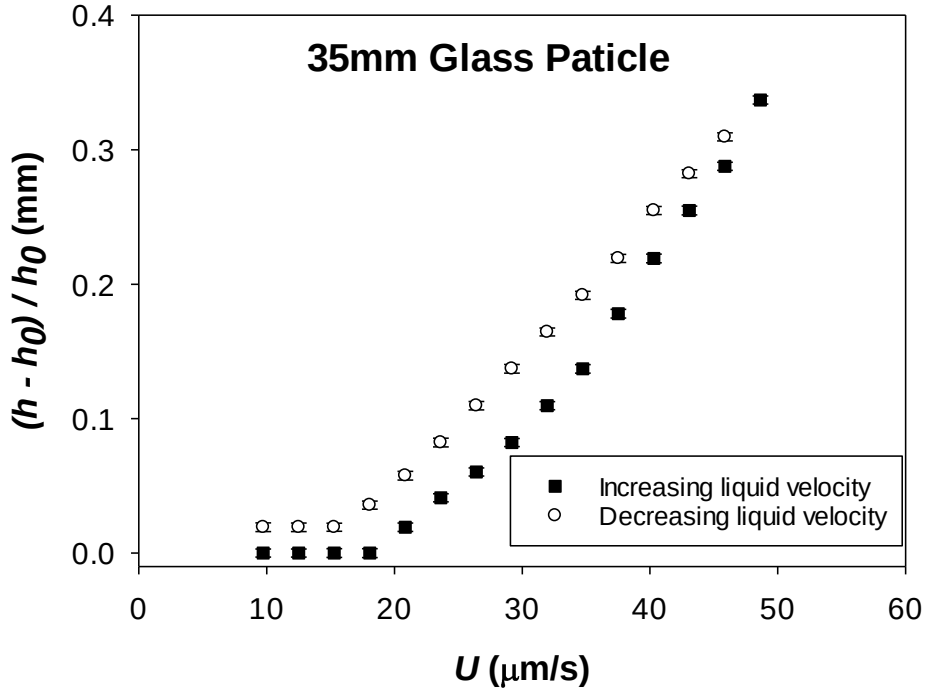

Figure 110. Relative bed height as a function of liquid velocity for 35μm glass particle in 1mm micro-fluidised bed with water as the fluidised particles.

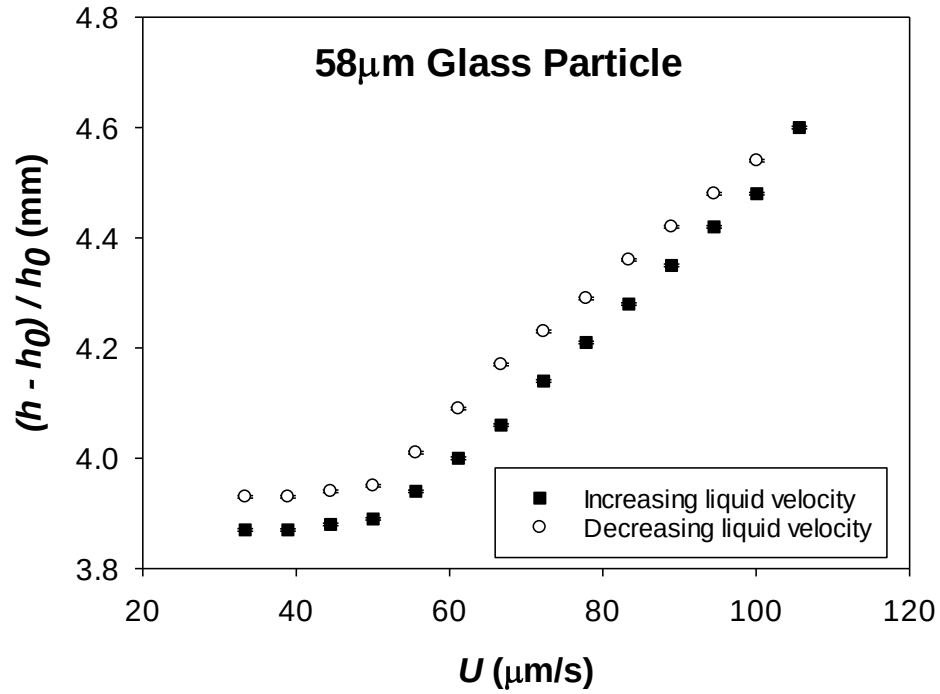

Figure 111. Relative bed height as a function of liquid velocity for 58μm glass particle in 1mm micro-fluidised bed with water as the fluidised particles.

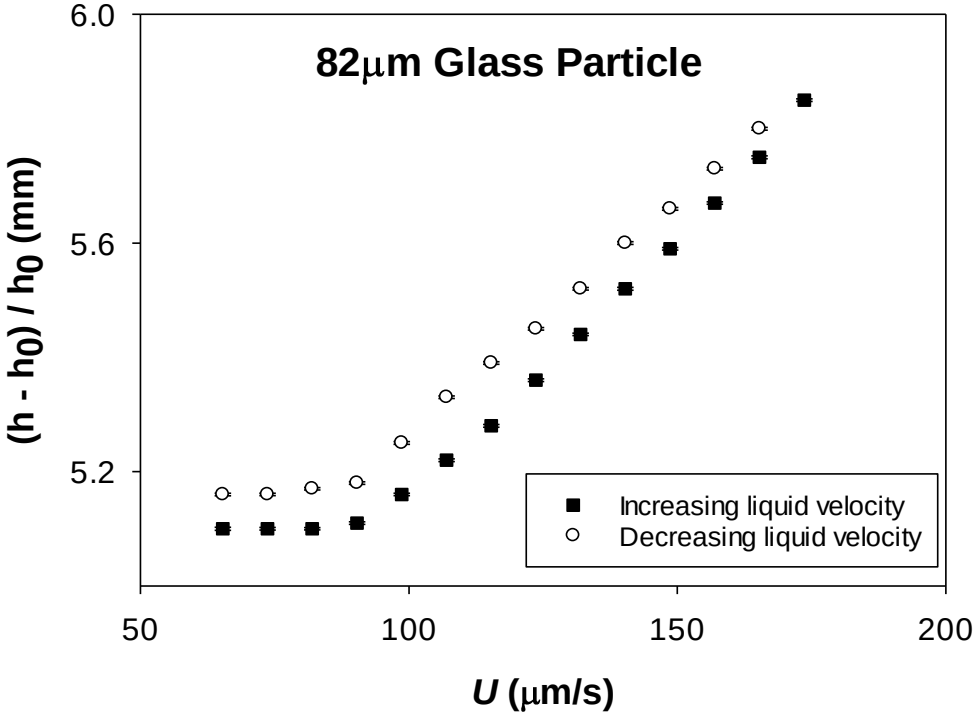

Figure 112. Relative bed height as a function of liquid velocity for 82μm glass particle in 1mm micro-fluidised bed with water as the fluidised particles.

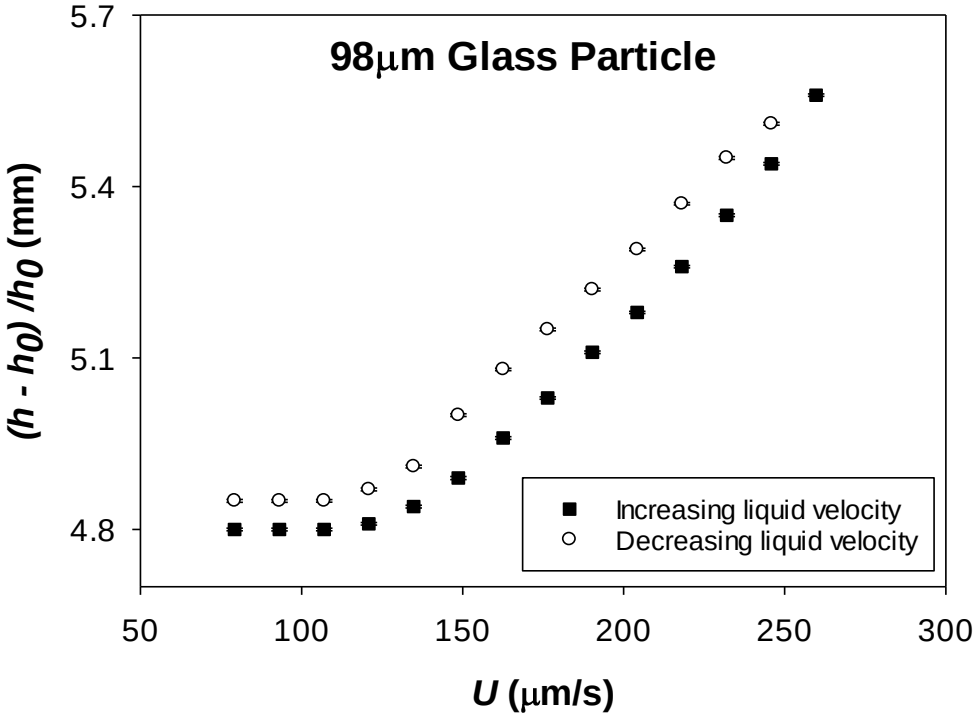

Figure 113. Relative bed height as a function of liquid velocity for 98μm glass particle in 1mm micro-fluidised bed with water as the fluidised particles.

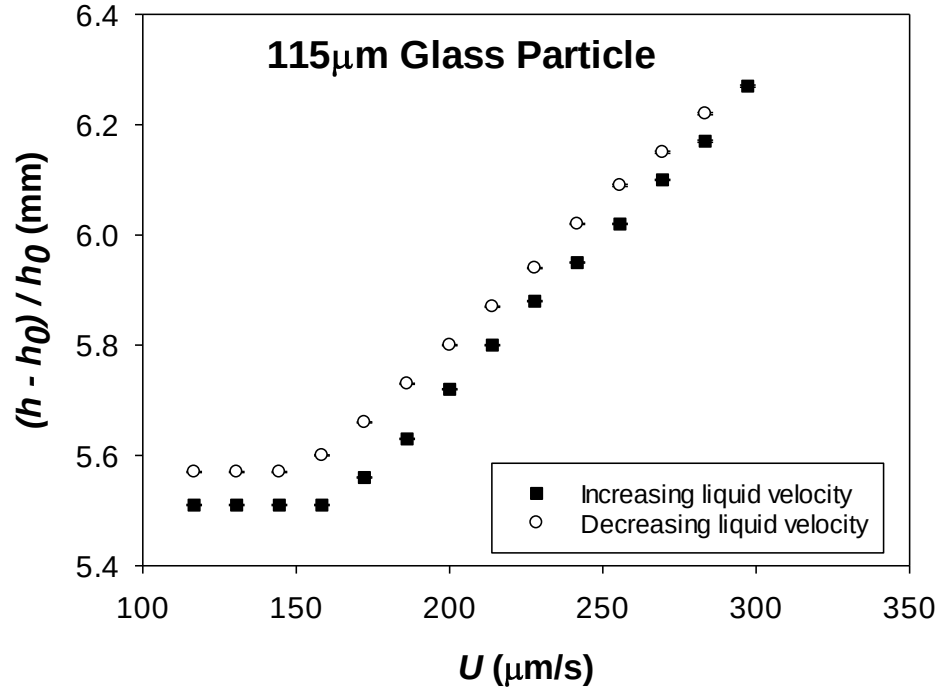

Figure 114. Relative bed height as a function of liquid velocity for 115μm glass particle in 1mm micro-fluidised bed with water as the fluidised particles.

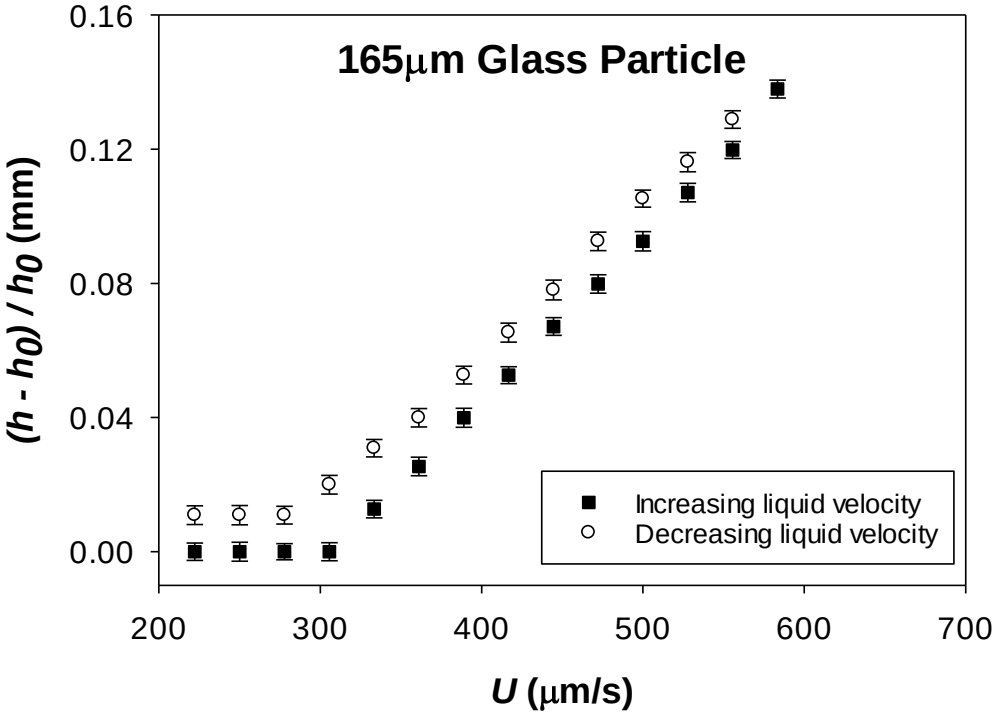

Figure 115. Relative bed height as a function of liquid velocity for 165μm glass particle in 1mm micro-fluidised bed with water as the fluidised particles.

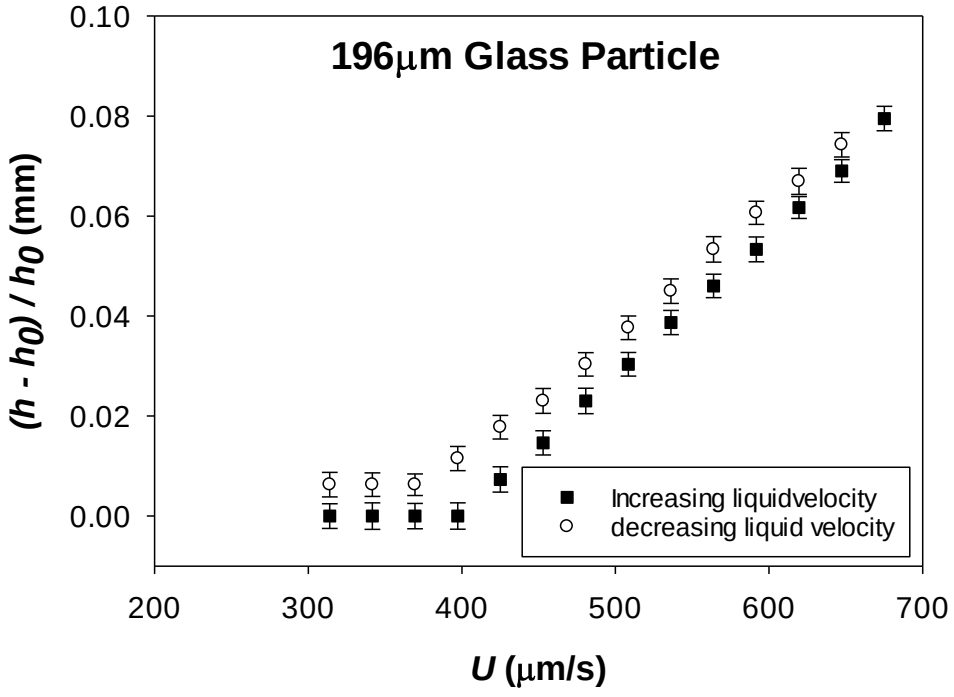

Figure 116. Relative bed height as a function of liquid velocity for 196μm glass particle in 1mm micro-fluidised bed with water as the fluidised particles.

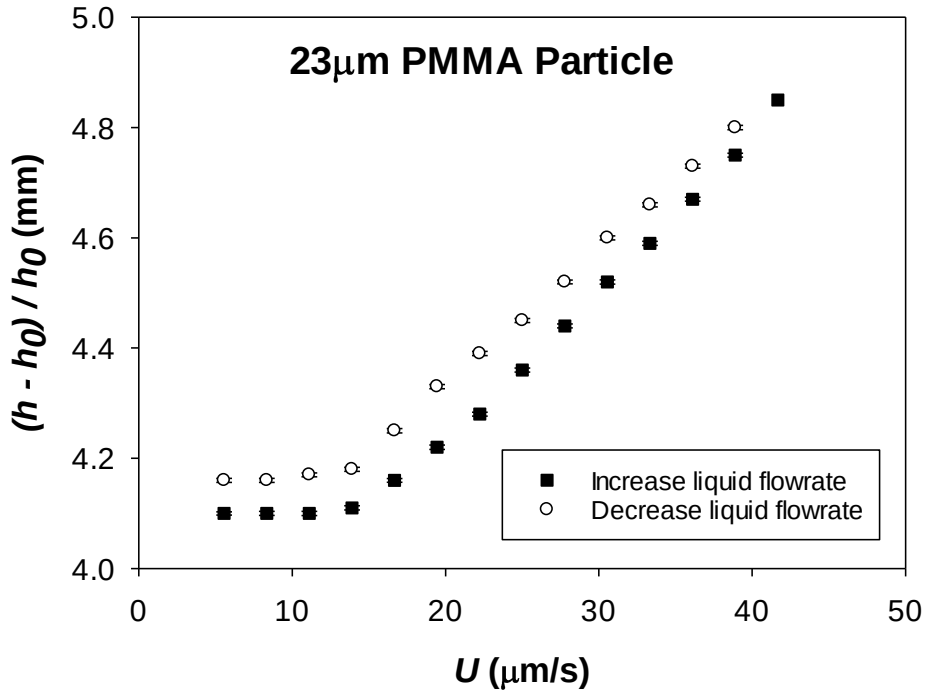

Figure 117. Relative bed height as a function of liquid velocity for 23μm PMMA particle in 1mm micro-fluidised bed with water as the fluidised particles.

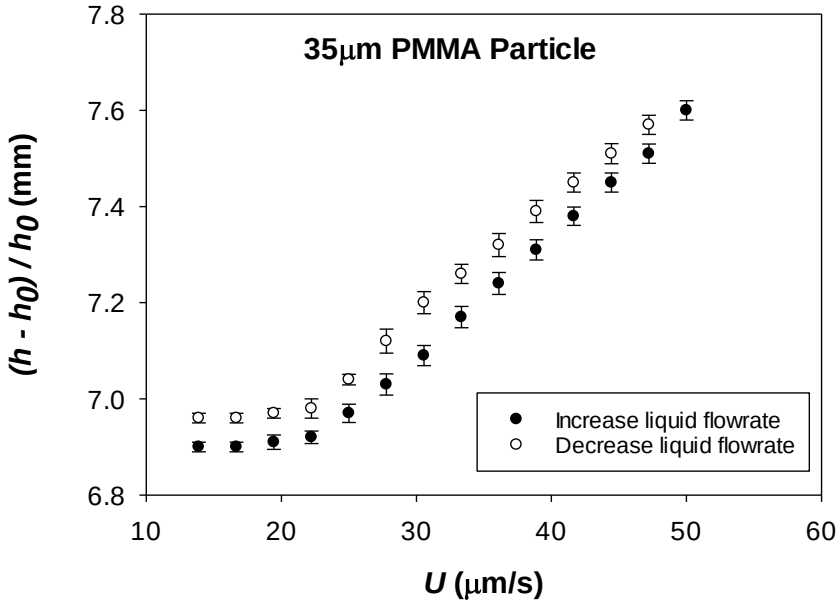

Figure 118. Relative bed height as a function of liquid velocity for 35μm PMMA particle in 1mm micro-fluidised bed with water as the fluidised particles.

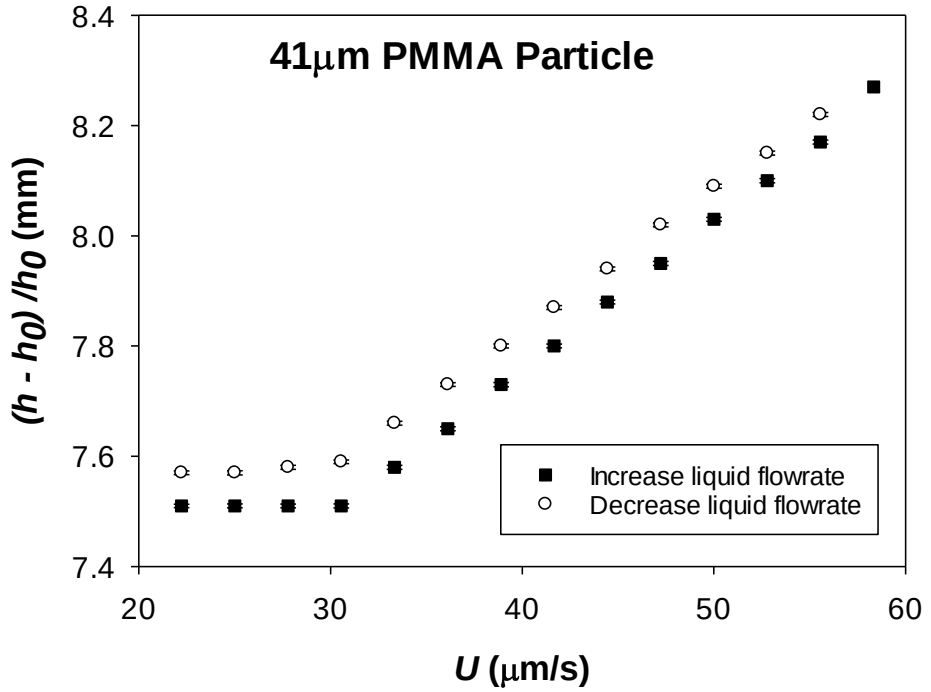

Figure 119. Relative bed height as a function of liquid velocity for 41μm PMMA particle in 1mm micro-fluidised bed with water as the fluidised particles.

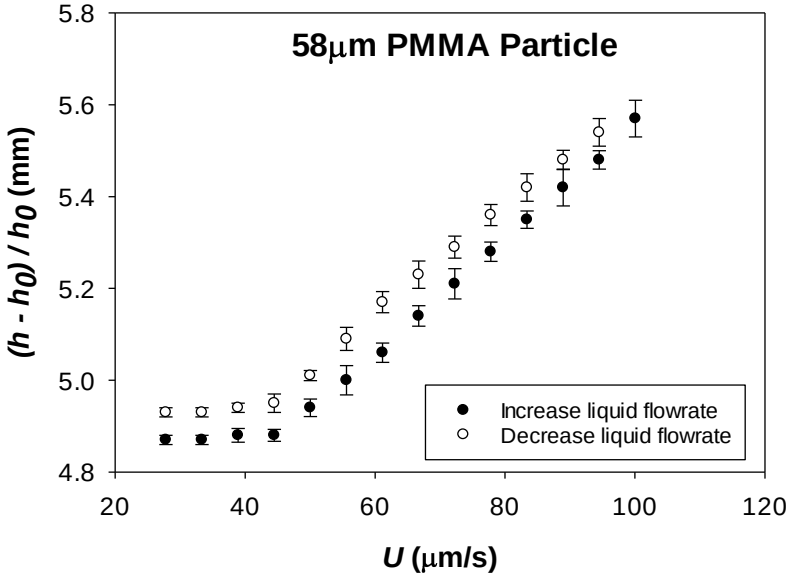

Figure 120. Relative bed height as a function of liquid velocity for 58μm PMMA particle in 1mm micro-fluidised bed with water as the fluidised particles.

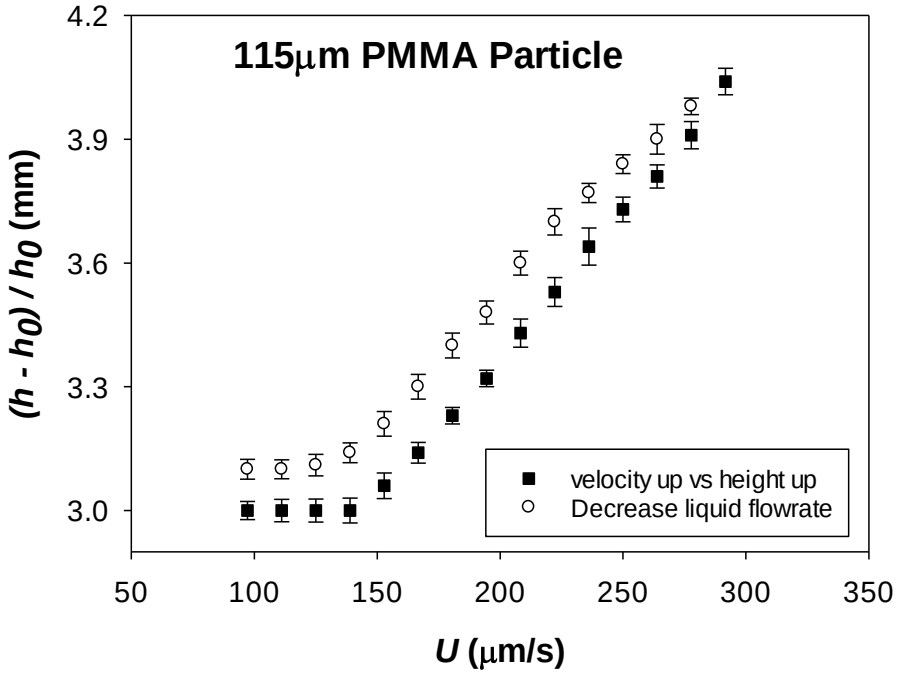

Figure 121. Relative bed height as a function of liquid velocity for 115μm PMMA particle in 1mm micro-fluidised bed with water as the fluidised particles.

11.3 Solid circulation rate conversion to solid circulating velocity

$$U_s = \frac{G_s}{\rho_s}$$

Where U_s is the solid circulating velocity, ρ_s solid density, and G_s the solid circulation rate

When

$G_s = 1.14 \times 10^{-2}$ kg/m^2. s

$\rho_s = 2500$ kg/m^3

$$U_s = \frac{1.04 \times 10^{-2}}{2500} = 4.17 \times 10^{-6}\ m/s$$

11.4 Influence of fluidising liquid viscosity on the solid flux

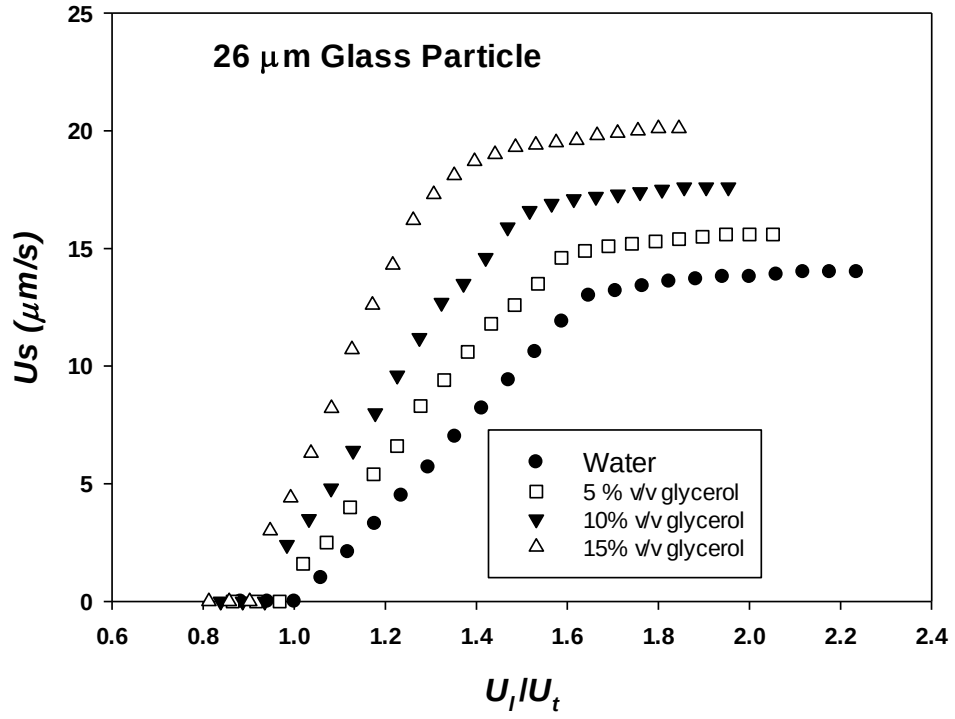

Figure 122. Particle circulating speed for 26μm glass particle as function of normalized liquid velocity for water and glycerol mixtures.

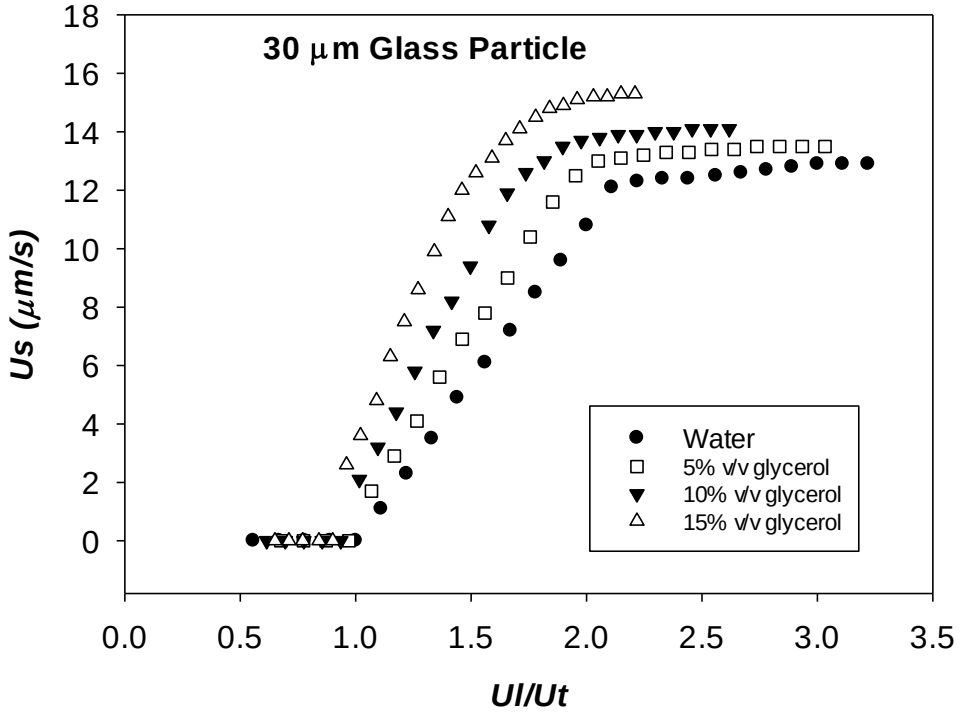

Figure 123. Particle circulating speed for 30μm glass particle as function of normalized liquid velocity for water and glycerol mixtures.

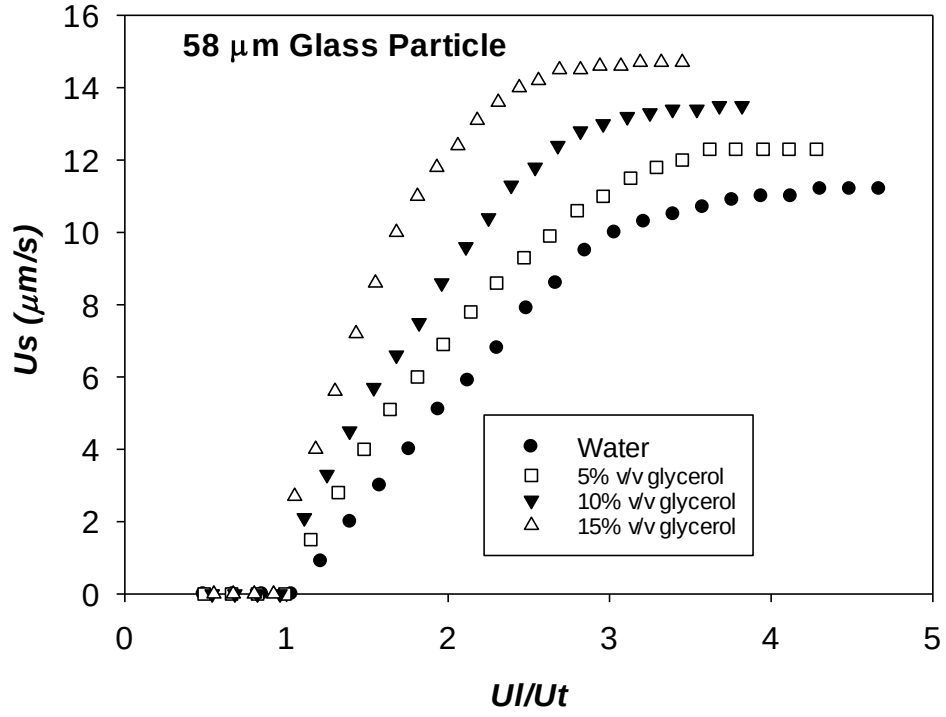

Figure 124. Particle circulating speed for 58μm glass particle as function of normalized liquid velocity for water and glycerol mixtures.

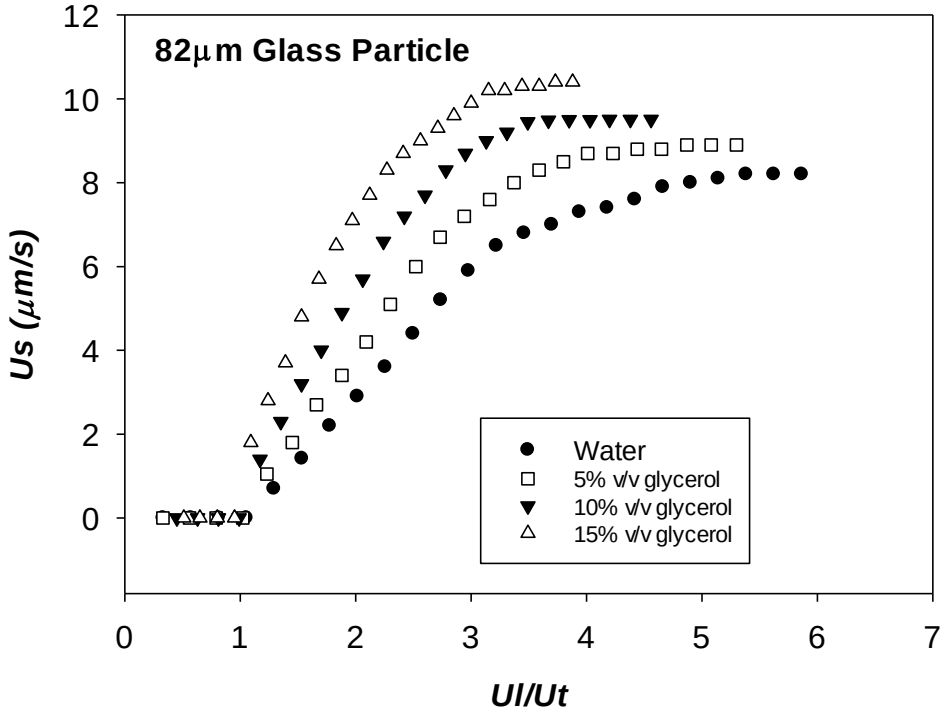

Figure 125. Particle circulating speed for 82μm glass particle as function of normalized liquid velocity for water and glycerol mixtures.

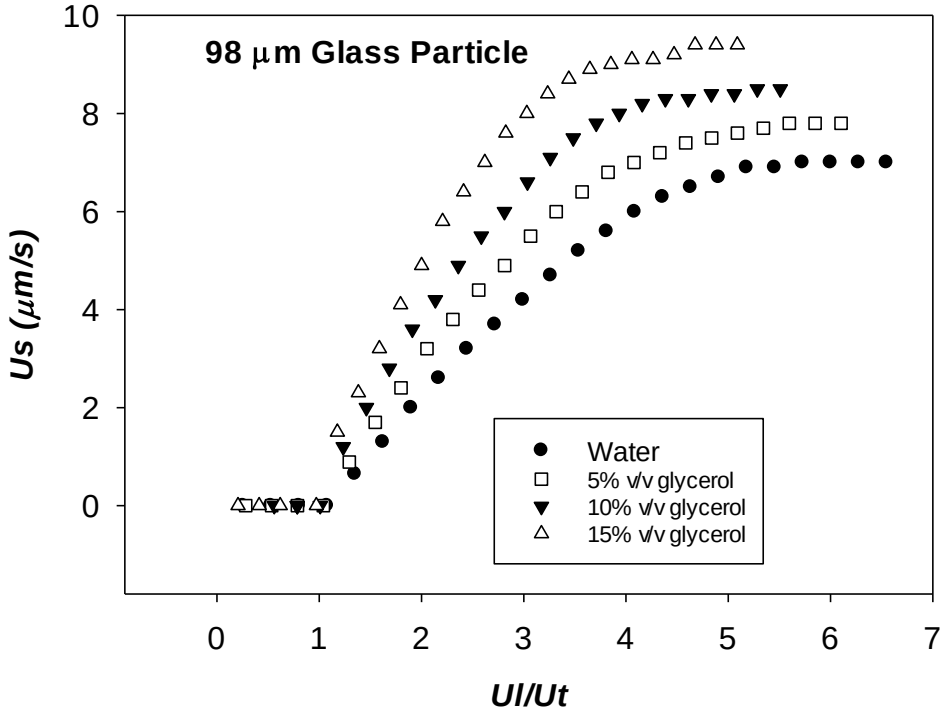

Figure 126. Particle circulating speed for 98µm glass particle as function of normalized liquid velocity for water and glycerol mixtures.

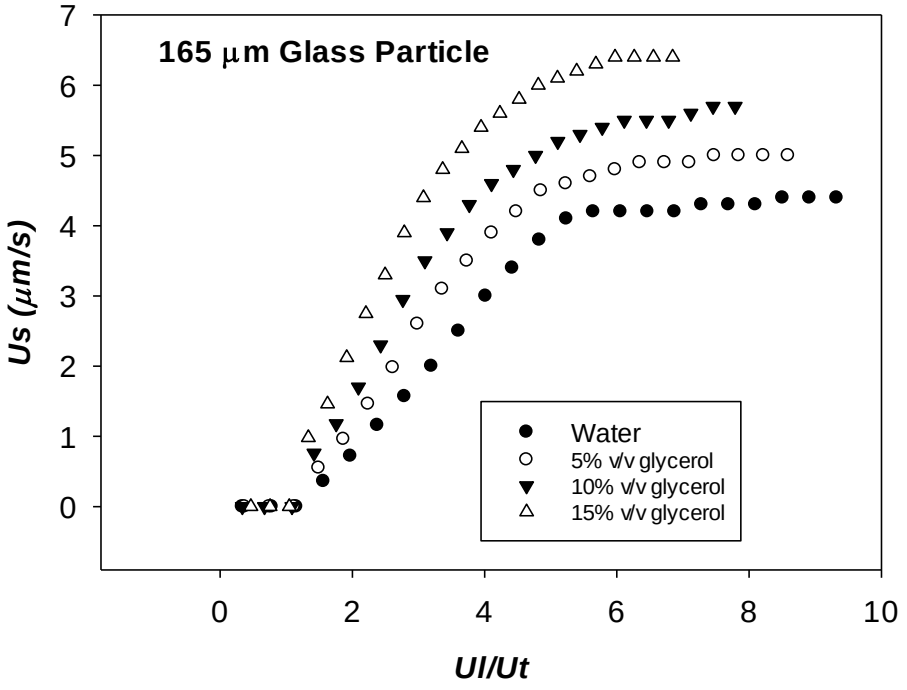

Figure 127. Particle circulating speed for 165µm glass particle as function of normalized liquid velocity for water and glycerol mixtures.

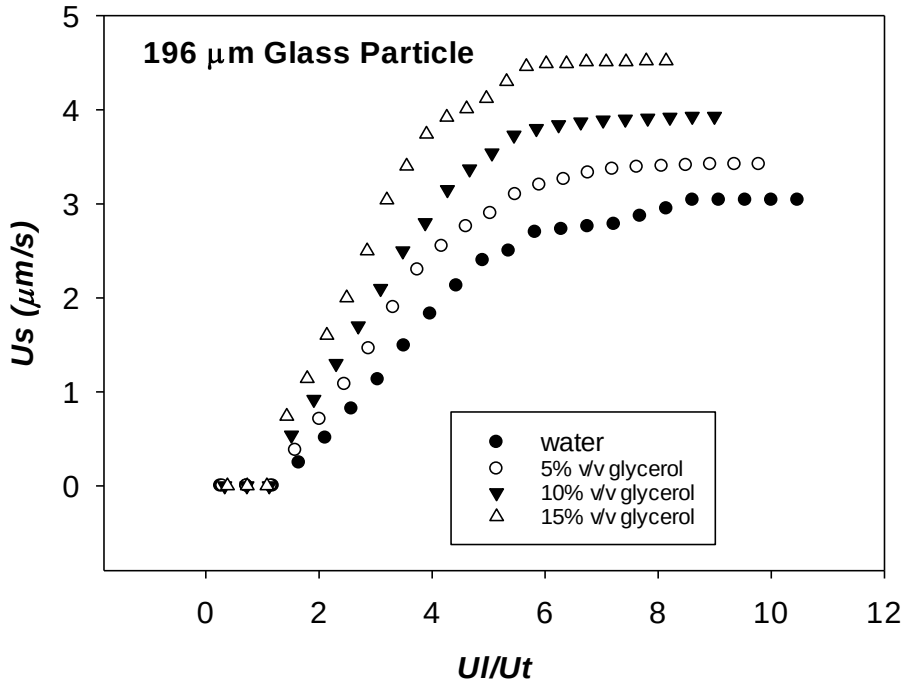

Figure 128. Particle circulating speed for 196μm glass particle as function of normalized liquid velocity for water and glycerol mixtures.

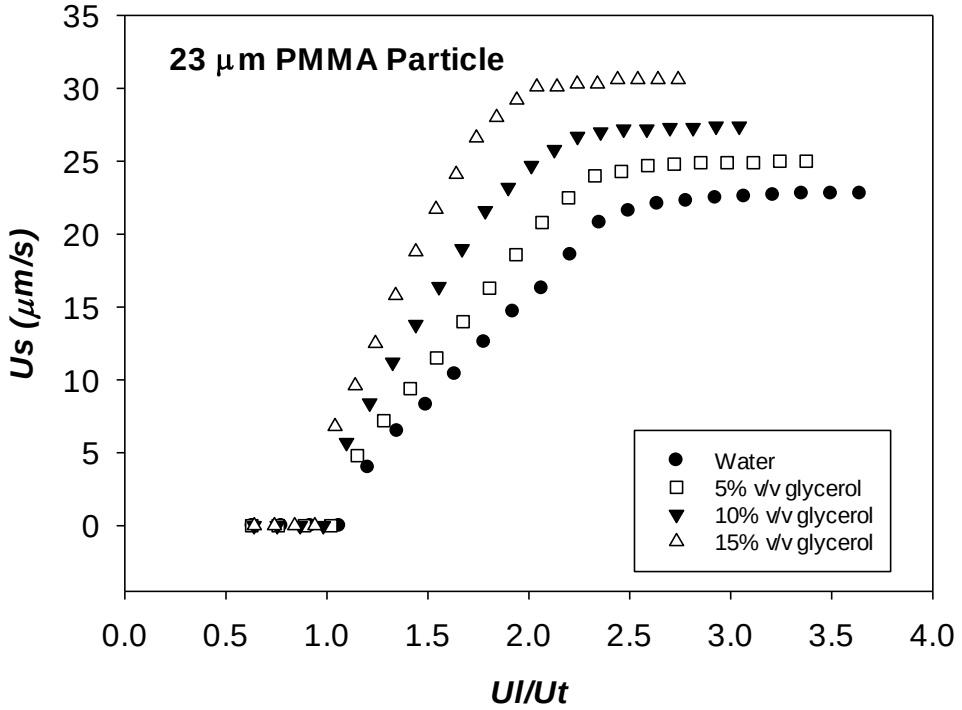

Figure 129. Particle circulating speed for 23μm PMMA particle as function of normalized liquid velocity for water and glycerol mixtures.

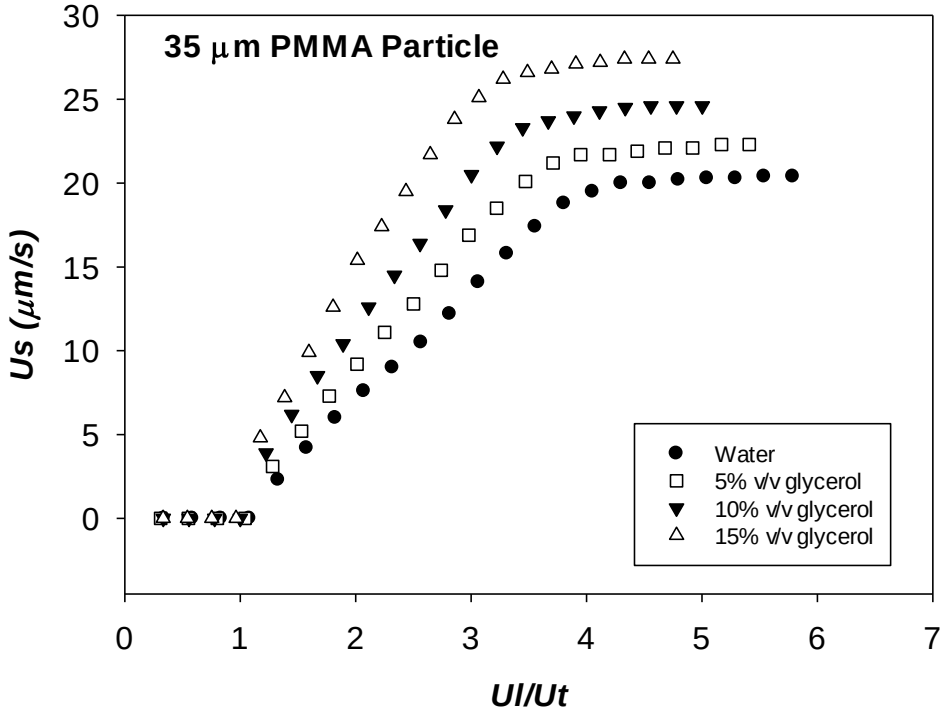

Figure 130. Particle circulating speed for 35μm PMMA particle as function of normalized liquid velocity for water and glycerol mixtures.

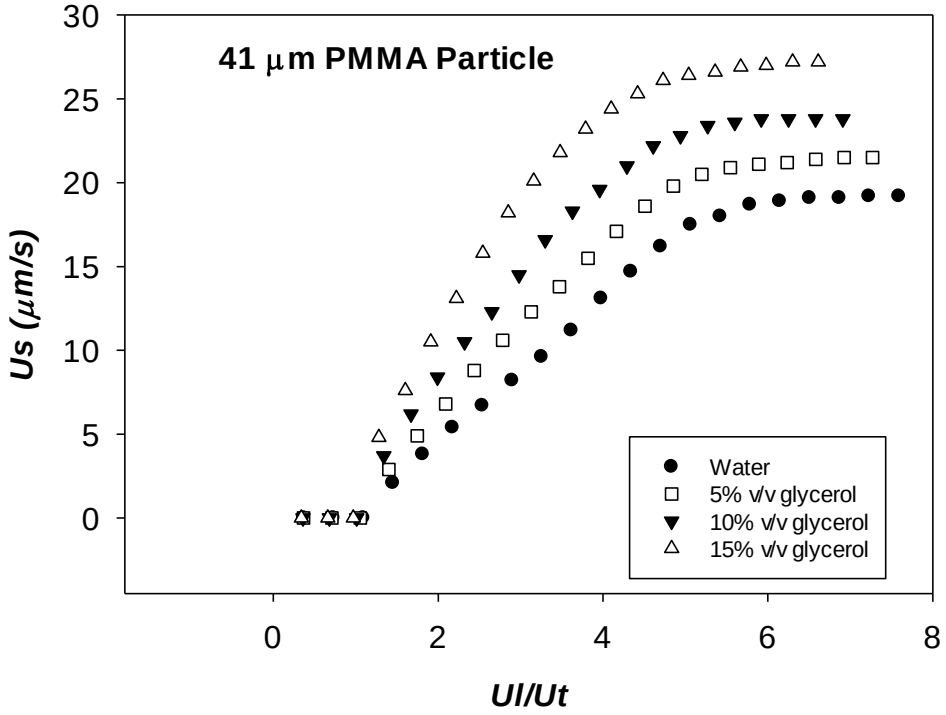

Figure 131. Particle circulating speed for 41μm PMMA particle as function of normalized liquid velocity for water and glycerol mixtures.

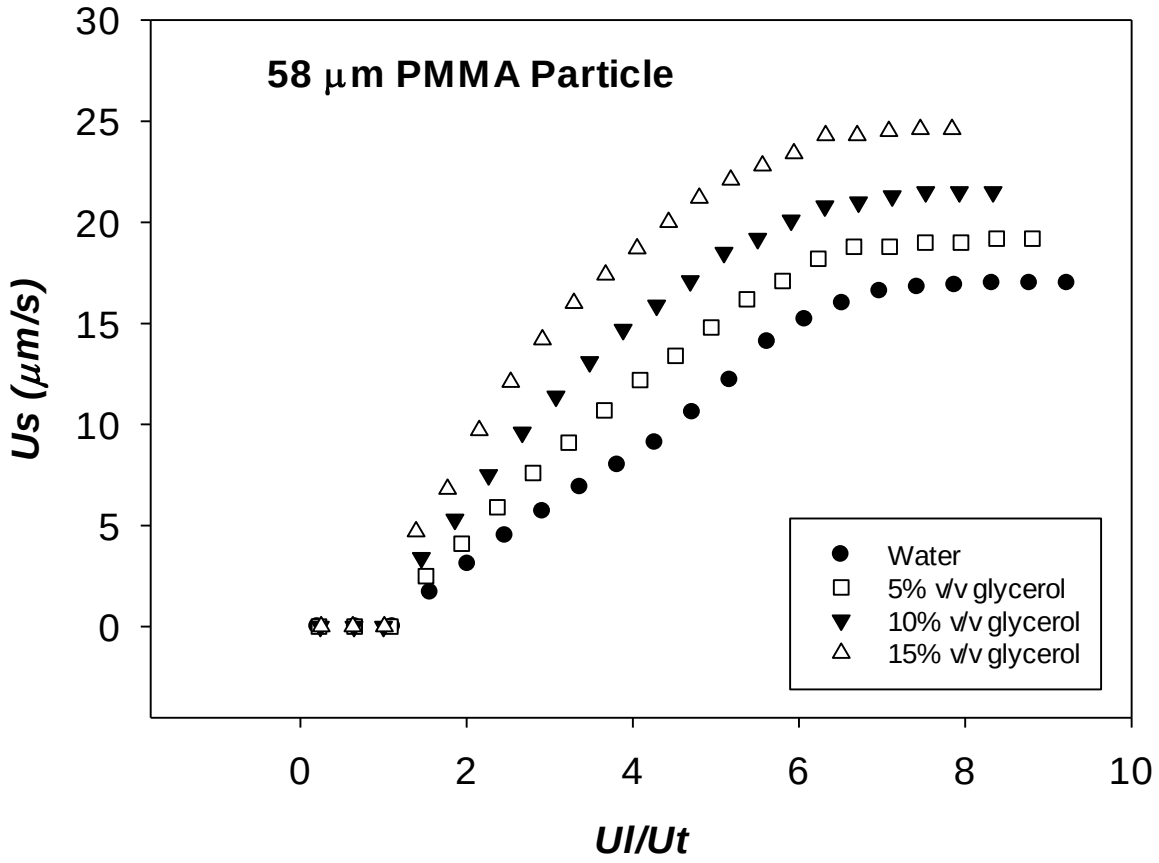

Figure 132. Particle circulating speed for 58μm PMMA particle as function of normalized liquid velocity for water and glycerol mixtures.

Reference

1. Kunii, D. and O. Levenspiel, *Fluidization Engineering, 1991Butterworth–Heinemann*. 1991, Boston.
2. Fueyo, N. and C. Dopazo, *Fluidization fundamentals*, in *Pressurized Fluidized Bed Combustion*. 1995, Springer. p. 38-79.
3. Pell, M., *Gas fluidization*. 2012: Elsevier.
4. Howard, J.R., *Fluidized bed technology: principles and applications*. 1989: Adam Hilger.
5. Ullah, A., W. Wang, and J. Li, *"Generalized Fluidization" Revisited.* Industrial & Engineering Chemistry Research, 2013. **52**(33): p. 11319-11332.
6. Asif, M., N. Kalogerakis, and L.A. Behie, *Hydrodynamics of liquid fluidized beds including the distributor region.* Chemical engineering science, 1992. **47**(15): p. 4155-4166.
7. Juma, A.K.A. and J.F. Richardson, *Particle segregation in liquid-solid fluidised beds.* Chemical Engineering Science, 1979. **34**(1): p. 137-143.
8. Carlos, C.R. and J.F. Richardson, *Solids movement in liquid fluidised beds—I Particle velocity distribution.* Chemical Engineering Science, 1968. **23**(8): p. 813-824.
9. Carlos, C.R. and J.F. Richardson, *Solids movement in liquid fluidised beds—II Measurements of axial mixing coefficients.* Chemical Engineering Science, 1968. **23**(8): p. 825-831.
10. Kang, Y. and S.D. Kim, *Solid flow transition in liquid and three-phase fluidized beds.* Particulate science and technology, 1988. **6**(2): p. 133-144.
11. Golriz, M., J. Grace, and H. Bi, *Handbook of Fluidization and Fluid-Particle Systems*. 2003.
12. Jahnig, C.E., D.L. Campbell, and H.Z. Martin, *History of Fluidized Solids Development at Exxon*, in *Fluidization*, J.R. Grace and J.M. Matsen, Editors. 1980, Springer US: Boston, MA. p. 3-24.
13. Vogt, E.T.C. and B.M. Weckhuysen, *Fluid catalytic cracking: recent developments on the grand old lady of zeolite catalysis.* Chemical Society Reviews, 2015. **44**(20): p. 7342-7370.
14. Jiang, X.M., X.X. Han, and Z.G. Cui, *New technology for the comprehensive utilization of Chinese oil shale resources.* Energy, 2007. **32**(5): p. 772-777.
15. Davidson, J.F., R. Clift, and D. Harrison, *Fluidization.* 1985.
16. Grace, J.R., *High-velocity fluidized bed reactors.* Chemical Engineering Science, 1990. **45**(8): p. 1953-1966.
17. Dewettinck, K. and A. Huyghebaert, *Fluidized bed coating in food technology.* Trends in Food Science & Technology, 1999. **10**(4): p. 163-168.
18. Anthony, E.J., *Fluidized bed combustion of alternative solid fuels; status, successes and problems of the technology.* Progress in Energy and Combustion Science, 1995. **21**(3): p. 239-268.
19. Vanecek, V., et al., *Fluidized bed drying*. 1966: Leonard Hill London.
20. Cooke, R.B., M.J. Goodson, and A.N. Hayhurst, *The Combustion of Solid Wastes as Studied in a Fluidized Bed.* Process Safety and Environmental Protection, 2003. **81**(3): p. 156-165.
21. Si, C. and Q. Guo, *Fluidization Characteristics of Binary Mixtures of Biomass and Quartz Sand in an Acoustic Fluidized Bed.* Industrial & Engineering Chemistry Research, 2008. **47**(23): p. 9773-9782.
22. Babu, S.P., B. Shah, and A. Talwalkar. *Fluidization correlations for coal gasification materials-minimum fluidization velocity and fluidized bed expansion ratio*. in *AIChE Symp. Ser*. 1978.
23. Baskakov, A.P., G.A. Malykh, and Shishko, II, *SEPARATION OF MATERIALS IN EQUIPMENT WITH A FLUIDIZED-BED AND WITH CONTINUOUS CHARGING AND DISCHARGING.* INTERNATIONAL CHEMICAL ENGINEERING, 1975. **15**(2): p. 286-289.
24. Kaljuvee, T., et al., *FLUIDIZED-BED COMBUSTION OF OIL SHALE RETORTING SOLID WASTE*.* Oil Shale, 2004. **21**(3): p. 237.
25. Mukherjee, A.K., B.K. Mishra, and R.V. Kumar, *Application of liquid/solid fluidization technique in beneficiation of fines.* International Journal of Mineral Processing, 2009. **92**(1): p. 67-73.

26. Shin, K.S., et al., *Heat-transfer coefficient in viscous liquid–solid circulating fluidized beds.* AIChE journal, 2005. **51**(2): p. 671-677.
27. Li, J. and M. Kwauk, *Exploring complex systems in chemical engineering—the multi-scale methodology.* Chemical Engineering Science, 2003. **58**(3): p. 521-535.
28. Wasmund, B. and J.W. Smith, *Wall to fluid heat transfer in liquid fluidized beds. I.* Canadian Journal of Chemical Engineering, 1967. **45**(3): p. 156-&.
29. Yang, J. and A. Renken, *Intensification of mass transfer in liquid fluidized beds with inert particles.* Chemical Engineering and Processing: Process Intensification, 1998. **37**(6): p. 537-544.
30. Tournie, P., C. Laguerie, and J.P. Couderc, *Correlations for mass transfer between fluidized spheres and a liquid.* Chemical Engineering Science, 1979. **34**(10): p. 1247-1255.
31. Garside, J. and J.W. Mullin, *Crystallization of aluminium potassium sulphate: a study in the assessment of crystallizer design data. III: Growth and dissolution rates.* Transactions of the Institution of Chemical Engineers, 1968. **46**: p. 11-18.
32. Parkin, G.F. and R.E. Speece, *Anaerobic biological waste treatment.* Chem. Eng. Prog.;(United States), 1984. **80**(12).
33. Shilapuram, V., K. Krishnaiah, and P.S.T. Sai, *Comparison of macroscopic flow properties obtained by three methods of operation in a liquid–solid circulating fluidized bed.* Chemical Engineering and Processing: Process Intensification, 2009. **48**(1): p. 259-267.
34. Haribabu, K. and V. Sivasubramanian, *Treatment of Wastewater in Fluidized Bed Bioreactor Using Low Density Biosupport.* Energy Procedia, 2014. **50**: p. 214-221.
35. Gòdia, F. and C. Solà, *Fluidized-Bed Bioreactors.* Biotechnology Progress, 1995. **11**(5): p. 479-497.
36. Natarajan, P., R. Velraj, and R.V. Seeniraj, *Effect of various parameters on the solid circulation rate in a liquid–solid circulating fluidized bed.* Asia-Pacific Journal of Chemical Engineering, 2008. **3**(4): p. 459-470.
37. Geldart, D., *Gas fluidization technology.* 1986.
38. Grace, J.R., A.A. Avidan, and T.M. Knowlton. *Circulating Fluidized Beds*. 1996; Available from: http://dx.doi.org/10.1007/978-94-009-0095-0.
39. Andreux, R., et al., *New description of fluidization regimes.* AIChE Journal, 2005. **51**(4): p. 1125-1130.
40. Kunii, D. and O. Levenspiel, *Fluidization engineering*. 2013: Elsevier.
41. Botton, R.J. *Gas-solid contacting in fluidized beds*. in *Chem. Engng. Progr. Symp. Series*. 1970.
42. Lanneau, K.P., *Gas-solids contacting in fluidized beds.* Trans. Inst. Chem. Eng, 1960. **38**: p. 125-137.
43. Bi, H.T. and J.R. Grace, *Flow regime diagrams for gas-solid fluidization and upward transport.* International Journal of Multiphase Flow, 1995. **21**(6): p. 1229-1236.
44. Didwania, A.K. and G.M. Homsy, *Flow regimes and flow transitions in liquid fluidized beds.* International Journal of Multiphase Flow, 1981. **7**(6): p. 563-580.
45. Fiege, A. and A. Zippelius, *Liquid Fluidized Beds of Granular Particles.* Journal of Physics: Conference Series, 2016. **759**: p. 012001.
46. Zhou, D., et al., *Minimum fluidization velocity of a three-phase conical fluidized bed in comparison to a cylindrical fluidized bed.* Industrial & Engineering Chemistry Research, 2008. **48**(1): p. 27-36.
47. Jing, S., et al., *Fluidization of coarse particles in gas–solid conical beds.* Chemical Engineering and Processing: Process Intensification, 2000. **39**(4): p. 379-387.
48. Toyohara, H. and Y. Kawamura, *Fluidization of a tapered fluidized-bed of a binary particle-mixture.* Int. Chem. Eng, 1992. **32**(1): p. 164-171.
49. Webster, G.H. and J.J. Perona. *The effect of taper angle on the hydrodynamics of a tapered liquid-solid fluidized bed*. in *AI Ch. E. Symp. Ser.* 1990.

50. Liu, S., et al., *Investigation of square fluidized beds using capacitance tomography: preliminary results.* Measurement Science and Technology, 2001. **12**(8): p. 1120.
51. Wang, H., et al., *Application of process tomography in gas–solid fluidised beds in different scales and structures.* Measurement Science and Technology, 2018. **29**(4): p. 044001.
52. Bouillard, J.X., R.W. Lyczkowski, and D. Gidaspow, *Porosity distributions in a fluidized bed with an immersed obstacle.* AIChE Journal, 1989. **35**(6): p. 908-922.
53. Promvonge, P., et al., *Drying characteristics of peppercorns in a rectangular fluidized-bed with triangular wavy walls.* International Communications in Heat and Mass Transfer, 2011. **38**(9): p. 1239-1246.
54. Jianmin, D. and R. Lyczkowski, *Three-dimensional kinetic theory modeling of hydrodynamics and erosion in fluidized beds.* Powder Technology, 1992. **73**(2): p. 127-138.
55. Mills, P.L., D.J. Quiram, and J.F. Ryley, *Microreactor technology and process miniaturization for catalytic reactions—A perspective on recent developments and emerging technologies.* Chemical Engineering Science, 2007. **62**(24): p. 6992-7010.
56. Reay, D., C. Ramshaw, and A. Harvey, *Process Intensification: Engineering for efficiency, sustainability and flexibility*. 2013: Butterworth-Heinemann.
57. Potic, B., et al., *Fluidization with hot compressed water in micro-reactors.* Chemical Engineering Science, 2005. **60**(22): p. 5982-5990.
58. Zivkovic, V., M.J. Biggs, and Z.T. Alwahabi, *Experimental study of a liquid fluidization in a microfluidic channel.* AIChE Journal, 2013. **59**(2): p. 361-364.
59. Tang, C., M. Liu, and Y. Li, *Experimental investigation of hydrodynamics of liquid–solid mini-fluidized beds.* Particuology, 2015.
60. Wang, F. and L.-S. Fan, *Gas− Solid Fluidization in Mini-and Micro-channels.* Industrial & Engineering Chemistry Research, 2011. **50**(8): p. 4741-4751.
61. Zivkovic, V. and M.J. Biggs, *On importance of surface forces in a microfluidic fluidized bed.* Chemical Engineering Science, 2015. **126**: p. 143-149.
62. Geng, S., et al., *Gas back-mixing in micro fluidized beds.* Chem. Eng. J, 2013. **64**: p. 867-876.
63. Kivikero, N., et al., *Microscale granulation in a fluid bed powder processor using electrostatic atomisation.* European Journal of Pharmaceutics and Biopharmaceutics, 2009. **71**(1): p. 130-137.
64. Kivikero, N., et al., *Rapid formulation screening with a Multipart Microscale Fluid bed Powder processor.* Pharmaceutical Development and Technology, 2011. **16**(4): p. 358-366.
65. Zeng, X., et al., *Micro fluidized bed reaction analysis and its application to coal char gasification kinetics.* CIESC Journal, 2013. **1**: p. 031.
66. Xu, Y. and X. Yue, *Fluidization Characteristics in Micro-Fluidized Beds of Various Inner Diameters.* Chemical engineering & technology, 2009. **32**(12): p. 1992-1999.
67. Yu, J., et al., *Biomass pyrolysis in a micro-fluidized bed reactor: Characterization and kinetics.* Chemical engineering journal, 2011. **168**(2): p. 839-847.
68. Yu, J., et al., *Kinetics and mechanism of solid reactions in a micro fluidized bed reactor.* AICHE journal, 2010. **56**(11): p. 2905-2912.
69. Doroodchi, E., et al., *Fluidisation and packed bed behaviour in capillary tubes.* Powder Technology, 2012. **223**: p. 131-136.
70. Liu, X., G. Xu, and S. Gao, *Micro fluidized beds: Wall effect and operability.* Chemical Engineering Journal, 2008. **137**(2): p. 302-307.
71. Rao, A., et al., *The effect of column diameter and bed height on minimum fluidization velocity.* AIChE Journal, 2010. **56**(9): p. 2304-2311.
72. Li, X., M. Liu, and Y. Li, *Bed expansion and multi-bubble behavior of gas-liquid-solid micro-fluidized beds in sub-millimeter capillary.* Chemical Engineering Journal, 2017. **328**: p. 1122-1138.
73. Li, Y., M. Liu, and X. Li, *Flow regimes in gas-liquid-solid mini-fluidized beds with single gas orifice.* Powder Technology, 2018. **333**: p. 293-303.

74. Li, X., et al. *Influence of oblique angle on hydrodynamics of gas-solid fluidization in micro fluidized bed*. in *2017 Chinese Automation Congress (CAC)*. 2017.
75. Yang, Z., M. Liu, and C. Lin, *Photocatalytic activity and scale-up effect in liquid–solid mini-fluidized bed reactor.* Chemical Engineering Journal, 2016. **291**: p. 254-268.
76. Li, X., M. Liu, and Y. Li, *Hydrodynamic behavior of liquid–solid micro-fluidized beds determined from bed expansion.* Particuology, 2018. **38**: p. 103-112.
77. Pereiro, I., et al., *A new microfluidic approach for the one-step capture, amplification and label-free quantification of bacteria from raw samples.* Chemical Science, 2017. **8**(2): p. 1329-1336.
78. Pereiro, I., et al., *Magnetic fluidized bed for solid phase extraction in microfluidic systems.* Lab on a Chip, 2017. **17**(9): p. 1603-1615.
79. Jensen, K.F., *Microreaction engineering—is small better?* Chemical Engineering Science, 2001. **56**(2): p. 293-303.
80. Berruti, F., et al., *Hydrodynamics of circulating fluidized bed risers: a review.* The Canadian Journal of Chemical Engineering, 1995. **73**(5): p. 579-602.
81. Zhu, J.X.J., et al., *(Gas-) liquid-solid circulating fluidized beds and their potential applications to bioreactor engineering.* The Canadian Journal of Chemical Engineering, 2000. **78**(1): p. 82-94.
82. Lim, K.S., J.X. Zhu, and J.R. Grace, *Hydrodynamics of gas-solid fluidization.* International Journal of Multiphase Flow, 1995. **21, Supplement**: p. 141-193.
83. Adams, C.K., *Gas mixing in fast fluidized beds*, in *Circulating Fluidized Bed Technology II*. 1988, Pergamon Press Oxford. p. 299-306.
84. Pitié, F., et al., *Circulating fluidized bed heat recovery/storage and its potential to use coated phase-change-material (PCM) particles.* Applied Energy, 2013. **109**: p. 505-513.
85. Zhang, H.L., et al., *The convection heat transfer coefficient in a Circulating Fluidized Bed (CFB).* Advanced Powder Technology, 2014. **25**(2): p. 710-715.
86. Zenz, F.A., *Two-Phase Fluid-Solid Flow.* Industrial & Engineering Chemistry, 1949. **41**(12): p. 2801-2806.
87. Yerushalmi, J., D.H. Turner, and A.M. Squires, *The Fast Fluidized Bed.* Industrial & Engineering Chemistry Process Design and Development, 1976. **15**(1): p. 47-53.
88. Li, Y. and M. Kwauk, *The dynamics of fast fluidization*, in *Fluidization*. 1980, Springer. p. 537-544.
89. Sguires, A.M., *1. Origins of the Fast Fluid Bed.* Fast Fluidization, 1994. **20**: p. 1.
90. Wen, C.Y. and Y.H. Yu, *A generalized method for predicting the minimum fluidization velocity.* AIChE Journal, 1966. **12**(3): p. 610-612.
91. Geldart, D., *Types of gas fluidization.* Powder technology, 1973. **7**(5): p. 285-292.
92. Abrahamsen, A.R. and D. Geldart, *Behaviour of gas-fluidized beds of fine powders part I. Homogeneous expansion.* Powder technology, 1980. **26**(1): p. 35-46.
93. Stewart, P.S.B. and J.F. Davidson, *Slug flow in fluidised beds.* Powder Technology, 1967. **1**(2): p. 61-80.
94. Yerushalmi, J. and N.T. Cankurt, *Further studies of the regimes of fluidization.* Powder Technology, 1979. **24**(2): p. 187-205.
95. Schnitzlein, M.G. and H. Weinstein, *Flow characterization in high-velocity fluidized beds using pressure fluctuations.* Chemical engineering science, 1988. **43**(10): p. 2605-2614.
96. Perales, J.F., et al., *On the transition from bubbling to fast fluidization regimes*. 1991: Pergamon Press: Oxford, UK.
97. Horio, M., H. Ishii, and M. Nishimuro, *On the nature of turbulent and fast fluidized beds.* Powder Technology, 1992. **70**(3): p. 229-236.
98. Natarajan, P., R. Velraj, and R.V. Seeniraj, *Studies on Regime Transition, Operating Range and System Stability in a Liquid-Solid Circulating Fluidized Bed.* Chemical engineering & technology, 2009. **32**(4): p. 572-579.

99. Nirmala, G.S. and L. Muruganandam, *An Experimental Study of Liquid-Solid Flow in a Circulating Fluidized Bed of Varying Liquid Viscosity.* Journal of Applied Fluid Mechanics, 2015. **8**(1): p. 95-101.
100. Gnanasundaram, N., M. Loganathan, and K. Perumal, *Solid holdup in liquid solid circulating fluidized bed with viscous liquid medium.* Alexandria Engineering Journal, 2014. **53**(4): p. 959-968.
101. Roy, S. and M.P. Dudukovic, *Flow mapping and modeling of liquid-solid risers.* Industrial & engineering chemistry research, 2001. **40**(23): p. 5440-5454.
102. Natarajan, P., R. Velraj, and R.V. Seeniraj, *Hydrodynamic similarity in liquid–solid circulating fluidized bed risers.* Powder Technology, 2014. **264**: p. 166-176.
103. Chavan, P.V., D.V. Kalaga, and J.B. Joshi, *Solid− Liquid Circulating Multistage Fluidized Bed: Hydrodynamic Study.* Industrial & Engineering Chemistry Research, 2009. **48**(9): p. 4592-4602.
104. Natarajan, P., R. Velraj, and R.V. Seeniraj, *Hydrodynamics of a Liquid–Solid Circulating Fluidized Bed: Effect of Solid Feed Pipe Diameter.* Indian Chemical Engineer, 2015. **57**(1): p. 67-81.
105. Lan, Q., et al., *Continuous protein recovery with a liquid–solid circulating fluidized-bed ion exchanger.* AIChE Journal, 2002. **48**(2): p. 252-261.
106. Liang, W., et al., *Flow characteristics of the liquid–solid circulating fluidized bed.* Powder Technology, 1997. **90**(2): p. 95-102.
107. Zheng, Y., et al., *The axial hydrodynamic behavior in a liquid-solid circulating fluidized bed.* The Canadian Journal of Chemical Engineering, 1999. **77**(2): p. 284-290.
108. Vidyasagar, S., K. Krishnaiah, and P.S.T. Sai, *Macroscopic properties of liquid–solid circulating fluidized bed with viscous liquid medium.* Chemical Engineering and Processing: Process Intensification, 2011. **50**(1): p. 42-52.
109. Sang, L. and J. Zhu, *Experimental investigation of the effects of particle properties on solids holdup in an LSCFB riser.* Chemical engineering journal, 2012. **197**: p. 322-329.
110. Hashizume, K., et al., *Pressure drop in liquid–solid circulating fluidized beds.* Heat Transfer—Asian Research, 2009. **38**(4): p. 248-261.
111. Grbavčić, Ž.B., et al., *Hydrodynamic modeling of vertical liquid-solids flow.* Powder Technology, 1992. **72**(2): p. 183-191.
112. Capes, C.E. and K. Nakamura, *Vertical pneumatic conveying: A theoretical study of uniform and annular particle flow models.* The Canadian Journal of Chemical Engineering, 1973. **51**(1): p. 39-46.
113. Liang, W., et al., *Flow characteristics and mixing properties in a high velocity liquid—solid loop reactor.* The Chemical Engineering Journal and the Biochemical Engineering Journal, 1996. **63**(3): p. 181-188.
114. Feng, X., et al., *The hydrodynamic behavior of the liquid–solid circulating fluidized bed ion exchange system for cesium removal.* Powder technology, 2003. **134**(3): p. 235-242.
115. Liang, W., et al., *Synthesis of linear alkylbenzene in a liquid–solid circulating fluidized bed reactor.* Journal of Chemical Technology and Biotechnology, 1995. **62**(1): p. 98-102.
116. Zheng, Y. and J.X. Zhu, *The onset velocity of a liquid-solid circulating fluidized bed.* Powder Technology, 2001. **114**(1): p. 244-251.
117. Ergun, S., *Fluid flow through packed columns.* Chem. Eng. Prog., 1952. **48**: p. 89-94.
118. DiFelice, R., et al., *Particle mixing in a circulating liquid fluidized bed*. 1988. Medium: X; Size: Pages: (17 p).
119. Bourgeois, P. and P. Grenier, *The ratio of terminal velocity to minimum fluidising velocity for spherical particles.* The Canadian Journal of Chemical Engineering, 1968. **46**(5): p. 325-328.
120. Vatanakull, M., Y. Zheng, and M. Couturier, *Flow Characterization of a Three-Phase Circulating Fluidized Bed Using an Ultrasonic Technique.* The Canadian Journal of Chemical Engineering, 2003. **81**(6): p. 1121-1129.

121. Fan, L.-S., *Gas-liquid-solid fluidization engineering.* 1989.
122. Liang, W., et al., *The phase holdups in a gas—liquid—solid circulating fluidized bed.* The Chemical Engineering Journal and the Biochemical Engineering Journal, 1995. **58**(3): p. 259-264.
123. Brenner, H., *Gas-Liquid-Solid Fluidization Engineering*. 2013: Butterworth-Heinemann.
124. Bhatia, V.K. and N. Epstein, *Three phase fluidization: a generalized wake model.* Fluidization and its Applications, 1974: p. 380-392.
125. Razzak, S.A., S. Barghi, and J.X. Zhu, *Electrical resistance tomography for flow characterization of a gas–liquid–solid three-phase circulating fluidized bed.* Chemical Engineering Science, 2007. **62**(24): p. 7253-7263.
126. Wang, T., et al., *Bubble behavior in gas–liquid–solid three-phase circulating fluidized beds.* Chemical Engineering Journal, 2001. **84**(3): p. 397-404.
127. Razzak, S.A., et al., *Phase holdup measurement in a gas–liquid–solid circulating fluidized bed (GLSCFB) riser using electrical resistance tomography and optical fibre probe.* Chemical Engineering Journal, 2009. **147**(2): p. 210-218.
128. Yang, W.G., et al., *Liquid-phase flow structure and backmixing characteristics of gas–liquid–solid three-phase circulating fluidized bed.* Chemical engineering science, 1999. **54**(21): p. 5293-5298.
129. Jin, Y., W.G. Liang, and Z.Q. Yu, *Synthesis of linear alkylbenzene using liquid-solids circulating fluidized bed reactors.* Chinese Patent, 1994. **94**: p. 105.
130. Liang, W., et al., *Hydrodynamics of a gas-liquid-solid three phase circulating fluidized bed.* The Canadian Journal of Chemical Engineering, 1995. **73**(5): p. 656-661.
131. Karamanev, D.G. and L.N. Nikolov, *Bed expansion of liquid-solid inverse fluidization.* AIChE journal, 1992. **38**(12): p. 1916-1922.
132. Karamanev, D.G. and L.N. Nikolov, *Application of inverse fluidization in wastewater treatment: From laboratory to full-scale bioreactors.* Environmental progress, 1996. **15**(3): p. 194-196.
133. Nikolov, L. and D. Karamanev, *Experimental study of the inverse fluidized bed biofilm reactor.* The Canadian Journal of Chemical Engineering, 1987. **65**(2): p. 214-217.
134. Fan, L.-S., K. Muroyama, and S.-H. Chern, *Hydrodynamic characteristics of inverse fluidization in liquid—solid and gas—liquid—solid systems.* The Chemical Engineering Journal, 1982. **24**(2): p. 143-150.
135. Abgrall, P. and A.-M. Gué, *Lab-on-chip technologies: making a microfluidic network and coupling it into a complete microsystems: a review.* Journal of Micromechanics and Microengineering, 2007. **17**(5): p. R15.
136. Chiu, D.T., et al., *Small but Perfectly Formed? Successes, Challenges, and Opportunities for Microfluidics in the Chemical and Biological Sciences.* Chem, 2017. **2**(2): p. 201-223.
137. Haeberle, S. and R. Zengerle, *Microfluidic platforms for lab-on-a-chip applications.* Lab on a Chip, 2007. **7**(9): p. 1094-1110.
138. Ho, C.M.B., et al., *3D printed microfluidics for biological applications.* Lab on a Chip, 2015. **15**(18): p. 3627-3637.
139. Au, A.K., et al., *3D-printed microfluidic automation.* Lab on a chip, 2015. **15**(8): p. 1934-1941.
140. Yazdi, A.A., et al., *3D printing: an emerging tool for novel microfluidics and lab-on-a-chip applications.* Microfluidics and Nanofluidics, 2016. **20**(3): p. 1-18.
141. Waheed, S., et al., *3D printed microfluidic devices: enablers and barriers.* Lab on a Chip, 2016. **16**(11): p. 1993-2013.
142. Lee, J.M., M. Zhang, and W.Y. Yeong, *Characterization and evaluation of 3D printed microfluidic chip for cell processing.* Microfluidics and Nanofluidics, 2016. **20**(1): p. 5.
143. Sharma, A., et al., *3D printing: It's microfluidic functions and environmental impacts.* International Journal of Precision Engineering and Manufacturing-Green Technology, 2017. **4**(3): p. 323-334.

144. Guerra, M.G., et al., *Photogrammetric measurements of 3D printed microfluidic devices.* Additive Manufacturing, 2018. **21**: p. 53-62.
145. He, Y., et al., *Developments of 3D Printing Microfluidics and Applications in Chemistry and Biology: a Review.* Electroanalysis, 2016. **28**(8): p. 1658-1678.
146. Patrick, W.G., et al., *DNA assembly in 3D printed fluidics.* PloS one, 2015. **10**(12): p. e0143636.
147. McDonald, J.C., et al., *Prototyping of Microfluidic Devices in Poly(dimethylsiloxane) Using Solid-Object Printing.* Analytical Chemistry, 2002. **74**(7): p. 1537-1545.
148. Moore, J.L., et al., *Behavior of capillary valves in centrifugal microfluidic devices prepared by three-dimensional printing.* Microfluidics and Nanofluidics, 2011. **10**(4): p. 877-888.
149. Anderson, K.B., et al., *A 3D printed fluidic device that enables integrated features.* Analytical chemistry, 2013. **85**(12): p. 5622-5626.
150. Lee, W., et al., *On-Demand Three-Dimensional Freeform Fabrication of Multi-Layered Hydrogel Scaffold With Fluidic Channels.* Biotechnol. Bioeng., 2010. **105**: p. 1178.
151. Munshi, A.S. and R.S. Martin, *Microchip-based electrochemical detection using a 3-D printed wall-jet electrode device.* Analyst, 2016. **141**(3): p. 862-869.
152. Saggiomo, V. and A.H. Velders, *Simple 3D Printed Scaffold-Removal Method for the Fabrication of Intricate Microfluidic Devices.* Advanced Science, 2015. **2**(9): p. 1500125-n/a.
153. Gowers, S.A.N., et al., *3D Printed Microfluidic Device with Integrated Biosensors for Online Analysis of Subcutaneous Human Microdialysate.* Analytical Chemistry, 2015. **87**(15): p. 7763-7770.
154. He, Y., et al., *Printing 3D microfluidic chips with a 3D sugar printer.* Microfluidics and Nanofluidics, 2015. **19**(2): p. 447-456.
155. Rogers, C.I., et al., *3D printed microfluidic devices with integrated valves.* Biomicrofluidics, 2015. **9**(1): p. 016501.
156. Shallan, A.I., et al., *Cost-Effective Three-Dimensional Printing of Visibly Transparent Microchips within Minutes.* Analytical Chemistry, 2014. **86**(6): p. 3124-3130.
157. Gaal, G., et al., *Simplified fabrication of integrated microfluidic devices using fused deposition modeling 3D printing.* Sensors and Actuators B: Chemical, 2017. **242**: p. 35-40.
158. Lee, H., et al., *A high-speed, high-performance on-chip integrated reverse transcription (RT)-microchip.* Biomedical Microdevices, 2013. **15**(1): p. 9-15.
159. Bonyár, A., et al., *3D Rapid Prototyping Technology (RPT) as a powerful tool in microfluidic development.* Procedia Engineering, 2010. **5**: p. 291-294.
160. Kitson, P.J., et al., *Configurable 3D-Printed millifluidic and microfluidic 'lab on a chip' reactionware devices.* Lab Chip, 2012. **12**: p. 3267.
161. Erkal, J.L., et al., *3D printed microfluidic devices with integrated versatile and reusable electrodes.* Lab on a Chip, 2014. **14**(12): p. 2023-2032.
162. Hwang, Y., O.H. Paydar, and R.N. Candler, *3D printed molds for non-planar PDMS microfluidic channels.* Sensors and Actuators A: Physical, 2015. **226**: p. 137-142.
163. Capel, A.J., et al., *Design and additive manufacture for flow chemistry.* Lab on a Chip, 2013. **13**(23): p. 4583-4590.
164. Zhao, C., et al., *Three dimensional (3D) printed electrodes for interdigitated supercapacitors.* Electrochemistry Communications, 2014. **41**: p. 20-23.
165. Neils, C., et al., *Combinatorial mixing of microfluidic streams.* Lab on a Chip, 2004. **4**(4): p. 342-350.
166. Das, D., et al., *Hydrodynamics of a multi-stage counter-current fluidized bed reactor with down-comer for amine impregnated activated carbon particle system.* Advanced Powder Technology, 2017. **28**(3): p. 854-864.
167. Al-Akaishi, A., et al., *CFD Analysis of the Fluidised Bed Hydrodynamic Behaviour inside an Isothermal Gasifier with different Perforated Plate Distributors.* Energy Procedia, 2017. **142**: p. 835-840.

168. Kulkarni, A.V. and J.B. Joshi, *Design and selection of sparger for bubble column reactor. Part I: Performance of different spargers.* Chemical Engineering Research and Design, 2011. **89**(10): p. 1972-1985.
169. Kulkarni, A.V. and J.B. Joshi, *Design and selection of sparger for bubble column reactor. Part II: Optimum sparger type and design.* Chemical Engineering Research and Design, 2011. **89**(10): p. 1986-1995.
170. Sánchez-Prieto, J., et al., *The effect of temperature on the distributor design in bubbling fluidized beds.* Powder Technology, 2014. **261**: p. 176-184.
171. Sobrino, C., N. Ellis, and M. de Vega, *Distributor effects near the bottom region of turbulent fluidized beds.* Powder Technology, 2009. **189**(1): p. 25-33.
172. Basu, P., et al., *Fluidized bed boilers : design and application.* 1984.
173. Richardson, J.F., J.F. Davidson, and D. Harrison, *Fluidization*. 1971. 26.
174. Zivkovic, V. and M.J. Biggs, *On importance of surface forces in a microfluidic fluidized bed.* Chemical Engineering Science, 2015. **126**(0): p. 143-149.
175. do Nascimento, O., D.A. Reay, and V. Zivkovic, *Influence of surface forces and wall effects on the minimum fluidization velocity of liquid-solid micro-fluidized bed.* Powder Technology, 2016.
176. Jensen, K.F., *Microreaction engineering -- is small better?* Chemical Engineering Science, 2001. **56**(2): p. 293-303.
177. Yang, W.C., *Handbook of Fluidization and Fluid-Particle Systems*. 2003: Taylor & Francis.
178. MiiCraft. *MiiCraft+ Overview*. 2014; Available from: http://www.miicraft.com/product/miicraft/.
179. Li, J., et al., *Minimum and terminal velocity in fluidization of coal gasification materials and coal blending of gasification under pressure.* Fuel, 2013. **110**: p. 153-161.
180. Briens, L.A., et al., *Minimum liquid fluidization velocity in gas-liquid-solid fluidized beds of low-density particles.* Chemical engineering science, 1997. **52**(21): p. 4231-4238.
181. Charpentier, J.C., *Process Intensification by Miniaturization.* Chemical Engineering & Technology, 2005. **28**(3): p. 255-258.
182. Zivkovic, V., M.N. Kashani, and M.J. Biggs. *Experimental and theoretical study of a micro-fluidized bed*. in *POWDERS AND GRAINS 2013: Proceedings of the 7th International Conference on Micromechanics of Granular Media*. 2013. AIP Publishing.
183. van Oss, C.J., *Chapter Two-The Apolar and Polar Properties of Liquid Water and Other Condensed-Phase Materials.* Interface science and technology, 2008. **16**: p. 13-30.
184. Van Oss, C.J., *Interfacial forces in aqueous media. 1994.* New York: Marcel Decker Inc, 2005.
185. Clint, J.H. and A.C. Wicks, *Adhesion under water: surface energy considerations.* International journal of adhesion and adhesives, 2001. **21**(4): p. 267-273.
186. Freitas, A.M. and M.M. Sharma, *Effect of surface hydrophobicity on the hydrodynamic detachment of particles from surfaces.* Langmuir, 1999. **15**(7): p. 2466-2476.
187. Della Volpe, C. and S. Siboni, *Troubleshooting of surface free energy acid-base theory applied to solid surfaces: The case of Good, van Oss and Chaudhury theory.* Acid-base interactions: relevance to adhesion science and technology. VSP, Utrecht, The Netherlands, 2000: p. 55-91.
188. Zdziennicka, A., *The wettability of polytetrafluoroethylene and polymethylmethacrylate with regard to interface behaviour of Triton X-165 and short chain alcohol mixtures: I. Critical surface tension of wetting and adhesion work.* Colloids and Surfaces A: Physicochemical and Engineering Aspects, 2010. **367**(1): p. 108-114.
189. Rhodes, M., H. Mineo, and T. Hirama, *Particle motion at the wall of a circulating fluidized bed.* Powder Technology, 1992. **70**(3): p. 207-214.
190. Kumara, W.A.S., et al., *Comparison of Particle Image Velocimetry and Laser Doppler Anemometry measurement methods applied to the oil–water flow in horizontal pipe.* Flow measurement and Instrumentation, 2010. **21**(2): p. 105-117.

191. Sveen, J.K., *14 - Laser Doppler anemometry (LDA) and particle image velocimetry (PIV) for marine environments A2 - Watson, John*, in *Subsea Optics and Imaging*, O. Zielinski, Editor. 2013, Woodhead Publishing. p. 353-379e.
192. Wu, W., et al., *A device for measuring solids flowrate in a circulating fluidized bed.* Powder Technology, 2001. **120**(3): p. 151-158.
193. Heertjes, P.M., J. Verloop, and R. Willems, *The measurement of local mass flow rates and particle velocities in fluid—solids flow.* Powder Technology, 1970. **4**(1): p. 38-40.
194. Roy, S., et al., *A method for estimating the solids circulation rate in a closed-loop circulating fluidized bed.* Powder technology, 2001. **121**(2): p. 213-222.
195. White, D., W. Take, and M. Bolton, *Soil deformation measurement using particle image velocimetry (PIV) and photogrammetry.* Geotechnique, 2003. **53**(7): p. 619-631.
196. Pudasaini, S.P., et al., *Rapid flow of dry granular materials down inclined chutes impinging on rigid walls.* Physics of Fluids, 2007. **19**(5): p. 053302.
197. Eckart, W. and J.M.N.T. Gray, *Particle image velocimetry (PIV) for granular avalanches on inclined planes*, in *Dynamic Response of Granular and Porous Materials under Large and Catastrophic Deformations*. 2003, Springer. p. 195-218.
198. De Jong, J., et al., *Development and validation of a novel digital image analysis method for fluidized bed particle image velocimetry.* Powder technology, 2012. **230**: p. 193-202.
199. Boutelier, D., *TecPIV—A MATLAB-based application for PIV-analysis of experimental tectonics.* Computers & geosciences, 2016. **89**: p. 186-199.
200. Thielicke, W. and E. Stamhuis, *PIVlab–towards user-friendly, affordable and accurate digital particle image velocimetry in MATLAB.* Journal of Open Research Software, 2014. **2**(1).
201. Sarno, L., et al., *A reliable PIV approach for measuring velocity profiles of highly sheared granular flows.* ENERGY, ENVIRONMENTAL AND STRUCTURAL ENGINEERING SERIES, 2014.
202. Tebianian, S., et al., *Investigation of particle velocity in FCC gas-fluidized beds based on different measurement techniques.* Chemical Engineering Science, 2015. **127**: p. 310-322.
203. Keane, R.D. and R.J. Adrian, *Theory of cross-correlation analysis of PIV images.* Applied Scientific Research, 1992. **49**(3): p. 191-215.
204. Senatore, C., et al., *Design and implementation of a particle image velocimetry method for analysis of running gear–soil interaction.* Journal of Terramechanics, 2013. **50**(5-6): p. 311-326.
205. Sarno, L., et al., *Measuring the velocity fields of granular flows – Employment of a multi-pass two-dimensional particle image velocimetry (2D-PIV) approach.* Advanced Powder Technology, 2018. **29**(12): p. 3107-3123.
206. Jahanger, Z.K., J. Sujatha, and S.J. Antony, *Local and Global Granular Mechanical Characteristics of Grain–Structure Interactions.* Indian Geotechnical Journal, 2018. **48**(4): p. 753-767.
207. Jahanger, Z.K., et al., *Interaction of a rigid beam resting on a strong granular layer overlying weak granular soil: Multi-methodological investigations.* Journal of Terramechanics, 2018. **79**: p. 23-32.
208. Thielicke, W., *The Flapping Flight of Birds e Analysis and Application. University of Groningen*. 2014.
209. Raffel, M., C.E. Willert, and J. Kompenhans, *Particle image velocimetry: a practical guide*. 2007: Springer Science & Business Media.
210. Vidyasagar, S., K. Krishnaiah, and P.S.T. Sai, *Hydrodynamics of a liquid–solid circulating fluidized bed: Effect of dynamic leak.* Chemical Engineering Journal, 2008. **138**(1–3): p. 425-435.
211. Vatanakul, M., et al., *Regime transition in a gas–liquid–solid fluidized bed.* Chemical Engineering Journal, 2005. **108**(1–2): p. 35-45.
212. Squires, T.M. and S.R. Quake, *Microfluidics: Fluid physics at the nanoliter scale.* Reviews of modern physics, 2005. **77**(3): p. 977.

213. Stone, H.A., A.D. Stroock, and A. Ajdari, *Engineering flows in small devices: Microfluidics towards lab-on-a-chip.* Annual Review of Fluid Mechanics, 2004. **36**(1): p. 381-411.
214. Whitesides, G.M., *The origins and the future of microfluidics.* Nature, 2006. **442**(7101): p. 368-373.
215. Sun, J. and X. Jiang, *15 - Microfluidic devices for viral detection*, in *Microfluidic Devices for Biomedical Applications*, X. Li and Y. Zhou, Editors. 2013, Woodhead Publishing. p. 527-556.
216. Safdar, M., J. Jänis, and S. Sanchez, *Microfluidic fuel cells for energy generation.* Lab on a Chip, 2016. **16**(15): p. 2754-2758.
217. Jiang, L. and N.S. Korivi, *13 - Microfluidics: technologies and applications*, in *Nanolithography*, M. Feldman, Editor. 2014, Woodhead Publishing. p. 424-443.
218. Malhotra, B.D. and M.A. Ali, *Chapter 9 - Microfluidic Biosensor*, in *Nanomaterials for Biosensors*, B.D. Malhotra and M.A. Ali, Editors. 2018, William Andrew Publishing. p. 263-293.
219. Franssila, S., et al., *Chapter 27 - Microfluidics and BioMEMS in Silicon*, in *Handbook of Silicon Based MEMS Materials and Technologies (Second Edition)*, M. Tilli, et al., Editors. 2015, William Andrew Publishing: Boston. p. 565-581.
220. Dittrich, P.S., K. Tachikawa, and A. Manz, *Micro Total Analysis Systems. Latest Advancements and Trends.* Analytical Chemistry, 2006. **78**(12): p. 3887-3908.
221. Manz, A., N. Graber, and H.M. Widmer, *Miniaturized total chemical analysis systems: A novel concept for chemical sensing.* Sensors and Actuators B, 1990. **1**(1-6): p. 244-248.
222. West, J., et al., *Micro Total Analysis Systems: Latest Achievements.* Analytical Chemistry, 2008. **80**(12): p. 4403-4419.
223. Melin, J. and S.R. Quake, *Microfluidic Large-Scale Integration: The Evolution of Design Rules for Biological Automation.* Annual Review of Biophysics and Biomolecular Structure, 2007. **36**(1): p. 213-231.
224. Charpentier, J.-C., *Four main objectives for the future of chemical and process engineering mainly concerned by the science and technologies of new materials production.* Chemical engineering journal, 2005. **107**(1): p. 3-17.
225. Haswell, S.J., *Chemical technology: All together now.* Nature, 2006. **441**(7094): p. 705-705.
226. Dudukovic, M.P., *Frontiers in Reactor Engineering.* Science, 2009. **325**(5941): p. 698-701.
227. Zivkovic, V., M.N. Kashani, and M.J. Biggs, *Experimental and theoretical study of a micro-fluidized bed.* AIP Conference Proceedings, 2013. **1542**(1): p. 93-96.
228. Tang, C., M. Liu, and Y. Li, *Experimental investigation of hydrodynamics of liquid–solid mini-fluidized beds.* Particuology.
229. Derveaux, S., et al., *Synergism between particle-based multiplexing and microfluidics technologies may bring diagnostics closer to the patient.* Analytical and Bioanalytical Chemistry, 2008. **391**(7): p. 2453-2467.
230. Lim, C.T. and Y. Zhang, *Bead-based microfluidic immunoassays: The next generation.* Biosensors and Bioelectronics, 2007. **22**(7): p. 1197-1204.
231. Biggs, M.J., et al., *Importance of surface forces in a micro-fluidized bed.* Chemeca 2012: Quality of life through chemical engineering: 23-26 September 2012, Wellington, New Zealand, 2012: p. 698.
232. Hartman, R.L. and K.F. Jensen, *Microchemical systems for continuous-flow synthesis.* Lab on a Chip, 2009. **9**(17): p. 2495-2507.
233. Gunther, A. and K.F. Jensen, *Multiphase microfluidics: from flow characteristics to chemical and materials synthesis.* Lab on a Chip, 2006. **6**(12): p. 1487-1503.
234. do Nascimento, O.L., D.A. Reay, and V. Zivkovic, *Influence of surface forces and wall effects on the minimum fluidization velocity of liquid-solid micro-fluidized beds.* Powder Technology, 2016. **304**(Supplement C): p. 55-62.

235. van Oss, C.J., *Chapter Two The Apolar and Polar Properties of Liquid Water and Other Condensed-Phase Materials*, in *Interface Science and Technology*, J.v.O. Carel, Editor. 2008, Elsevier. p. 13-30.
236. Richardson, J.F. and W.N. Zaki, *Sedimentation and fluidisation: Part I.* Chemical Engineering Research and Design, 1997. **75**(1 SUPPL.): p. S82-S99.
237. Schneider, C.A., W.S. Rasband, and K.W. Eliceiri, *NIH Image to ImageJ: 25 years of image analysis.* Nat Meth, 2012. **9**(7): p. 671-675.
238. Goldman, D.I. and H.L. Swinney, *Signatures of glass formation in a fluidized bed of hard spheres.* Physical review letters, 2006. **96**(14): p. 145702.
239. Dietrich, F., et al., *Comparison of Four Different Methods for Measuring the Solids Circulation Rate in Circulating Fluidized Beds.* 2013.
240. Guío-Pérez, D.C., et al., *Estimation of solids circulation rate through magnetic tracer tests.* Powder Technology, 2017. **316**: p. 650-657.
241. Masuda, H. and K. Iinoya, *Electrification of particles by impact on inclined metal plates.* AIChE Journal, 1978. **24**(6): p. 950-956.
242. Hensler, T., et al., *Non-invasive investigation of the cross-sectional solids distribution in CFB risers by X-ray computed tomography.* Powder Technology, 2016. **297**: p. 247-258.
243. Wang, S., et al., *Application of Electrical Capacitance Tomography to Flow Modelling within a Circulating Fluidized Bed.* Particle & Particle Systems Characterization, 1998. **15**(1): p. 51-55.
244. Monazam, E.R., R. Panday, and L.J. Shadle, *Estimate of solid flow rate from pressure measurement in circulating fluidized bed.* Powder Technology, 2010. **203**(1): p. 91-97.
245. Lech, M., *Mass flow rate measurement in vertical pneumatic conveying of solid.* Powder Technology, 2001. **114**(1-3): p. 55-58.
246. Kuramoto, M., D. Kunii, and T. Furusawa, *Flow of dense fluidized particles through an opening in a circulation system.* Powder Technology, 1986. **47**(2): p. 141-149.
247. Nirmala , G.S. and L. Muruganandam, *Hydrodynamics Studies in a Liquid Solid Circulating Fluidized Bed of Varying Liquid Viscosity.* Journal of The Institution of Engineers (India): Series E, 2013. **94**(2): p. 73-78.
248. Gnanasundaram, N., M. Loganathan, and K. Perumal, *Viscosity Effects on Solid Circulation Rate in a Liquid Solid Circulating Fluidized Bed.* Journal of Applied Sciences, 2014. **14**(10): p. 1037-1042.
249. Nirmala, G.S. and L. Muruganandam, *Hydrodynamics Studies in a Liquid Solid Circulating Fluidized Bed of Varying Liquid Viscosity.* Journal of The Institution of Engineers (India): Series E, 2013. **94**(2): p. 73-78.
250. Vijaya Lakshmi, A.C., et al., *Minimum fluidization velocity and friction factor in a liquid-solid inverse fluidized bed reactor.* Bioprocess Engineering, 2000. **22**(5): p. 461-466.
251. Qiu, O., H. Li, and H. Tong, *Effect of Fluid Viscosity on Liquid− Solid Fluidization.* Industrial & engineering chemistry research, 2004. **43**(15): p. 4434-4437.
252. Zheng, Y., *Radial Particle Profiles in a Liquid-Solid CFB with Varying Viscosity.* Chemical Engineering & Technology, 2004. **27**(7): p. 769-776.
253. Cho, Y., et al., *Liquid radial dispersion in liquid-solid circulating fluidized beds with viscous liquid medium.* Chem. Eng. Comm., 2005. **192**(3): p. 257-271.
254. Gnanasundaram, N., et al., *Effect of Liquid Viscosity and Solid Inventory on Hydrodynamics in a Liquid - solid Circulating Fluidized Bed*. Vol. 10. 2017. 267-274.
255. Ergun, S., *Fluid flow through packed columns.* Chemical Engineering Progress, 1952. **48**: p. 89-94.
256. Navvab Kashani, M., et al., *A new method for reconstruction of the structure of micro-packed beds of spherical particles from desktop X-ray microtomography images. Part A. Initial structure generation and porosity determination.* Chemical Engineering Science, 2016. **146**: p. 337-345.

257. Saxena, M., P. Dubey, and A. Tripathi, *Surface Tension of Binary Liquid Mixture.* Asian Journal of Chemistry, 2011. **23**(3): p. 1411.
258. Eberhart, J., *The Surface Tension of Binary Liquid Mixtures1.* The Journal of Physical Chemistry, 1966. **70**(4): p. 1183-1186.
259. Jańczuk, B., W. Wójcik, and A. Zdziennicka, *Determination of the components of the surface tension of some liquids from interfacial liquid-liquid tension measurements.* Journal of colloid and interface science, 1993. **157**(2): p. 384-393.
260. Liang, W., et al., *Flow characteristics of the liquid–solid circulating fluidized bed.* Powder Technology, 1997. **90**(2): p. 95-102.
261. Mabrouk, R., J. Chaouki, and C. Guy, *Wall surface effects on particle–wall friction factor in upward gas–solid flows.* Powder Technology, 2008. **186**(1): p. 80-88.
262. Oke, O., P. Lettieri, and L. Mazzei, *An investigation on the mechanics of homogeneous expansion in gas-fluidized beds.* Chemical Engineering Science, 2015. **127**(Supplement C): p. 95-105.
263. Kandlikar, S.G., *High flux heat removal with microchannels—a roadmap of challenges and opportunities.* Heat Transfer Engineering, 2005. **26**(8): p. 5-14.
264. Agostini, B., et al., *State of the art of high heat flux cooling technologies.* Heat Transfer Engineering, 2007. **28**(4): p. 258-281.
265. Kun-Quan, M. and L. Jing, *Heat-driven liquid metal cooling device for the thermal management of a computer chip.* Journal of Physics D: Applied Physics, 2007. **40**(15): p. 4722.
266. Chu, R.C., et al., *Review of cooling technologies for computer products.* IEEE Transactions on Device and Materials Reliability, 2004. **4**(4): p. 568-585.
267. Ebadian, M.A. and C.X. Lin, *A Review of High-Heat-Flux Heat Removal Technologies.* Journal of Heat Transfer, 2011. **133**(11): p. 110801-110801.
268. Ma, K. and J. Liu, *Liquid metal cooling in thermal management of computer chips.* Frontiers of Energy and Power Engineering in China. **1**(4): p. 384-402.
269. Weilin, Q. and I. Mudawar. *Thermal design methodology for high-heat-flux single-phase and two-phase micro-channel heat sinks*. in *Thermal and Thermomechanical Phenomena in Electronic Systems, 2002. ITHERM 2002. The Eighth Intersociety Conference on*. 2002.
270. Zhang, W., et al., *Correlation of critical heat flux for flow boiling of water in mini-channels.* International Journal of Heat and Mass Transfer, 2006. **49**(5–6): p. 1058-1072.
271. Agostini, B., et al., *High heat flux flow boiling in silicon multi-microchannels – Part III: Saturated critical heat flux of R236fa and two-phase pressure drops.* International Journal of Heat and Mass Transfer, 2008. **51**(21–22): p. 5426-5442.
272. Agostini, B., et al., *High heat flux flow boiling in silicon multi-microchannels – Part I: Heat transfer characteristics of refrigerant R236fa.* International Journal of Heat and Mass Transfer, 2008. **51**(21–22): p. 5400-5414.
273. Ramesh, K., K.S. Chandra, and K.A. Kumar, *Flow Regime Mapping of Liquid-Solid Inclined Fluidized Beds.* International Journal of Engineering and Applied Sciences, 2016. **3**.
274. Yakubov, B., et al., *The dynamics and structure of a liquid–solid fluidized bed in inclined pipes.* Chemical Engineering Journal, 2007. **128**(2-3): p. 105-114.
275. Chiang, Y.-C., et al., *Circulating inclined fluidized beds with application for desiccant dehumidification systems.* Applied energy, 2016. **175**: p. 199-211.
276. Yakubov, B., et al., *The effect of pipe inclination on a liquid-solid fluidized bed.* HAIT J. Sci. Eng. B, 2005. **3**: p. 1-19.
277. Aguilar-Corona, A., et al., *The effect of column tilt on flow homogeneity and particle agitation in a liquid fluidized bed.* International Journal of Multiphase Flow, 2017. **92**: p. 50-60.

278. Zhao, C.Y. and G.H. Zhang, *Review on microencapsulated phase change materials (MEPCMs): Fabrication, characterization and applications.* Renewable and Sustainable Energy Reviews, 2011. **15**(8): p. 3813-3832.
279. Feczkó, T., L. Trif, and D. Horák, *Latent heat storage by silica-coated polymer beads containing organic phase change materials.* Solar Energy, 2016. **132**: p. 405-414.
280. Sarwar, J. and B. Mansoor, *Characterization of thermophysical properties of phase change materials for non-membrane based indirect solar desalination application.* Energy Conversion and Management, 2016. **120**: p. 247-256.
281. Cao, V.D., et al., *Rheological and thermal properties of suspensions of microcapsules containing phase change materials.* Colloid and polymer science, 2018. **296**(5): p. 981-988.
282. Giro-Paloma, J., et al., *Types, methods, techniques, and applications for microencapsulated phase change materials (MPCM): A review.* Renewable and Sustainable Energy Reviews, 2016. **53**: p. 1059-1075.
283. Konuklu, Y., et al., *Review on using microencapsulated phase change materials (PCM) in building applications.* Energy and Buildings, 2015. **106**: p. 134-155.
284. Souayfane, F., F. Fardoun, and P.-H. Biwole, *Phase change materials (PCM) for cooling applications in buildings: A review.* Energy and buildings, 2016. **129**: p. 396-431.
285. Salaün, F., *Microencapsulation technology for smart textile coatings*, in *Active Coatings for Smart Textiles*. 2016, Elsevier. p. 179-220.
286. Keyan, K., et al., *Microencapsulation of PCMs in textiles: a review.* Journal of Textile and Apparel, Technology and Management, 2012. **7**(3).